
Design, synthesis and study of molecular probes for diagnostic and therapeutic applications in Alzheimer's disease

A Thesis Submitted for the Degree of

Doctor of Philosophy

By

Kolla Rajasekhar



**Bioorganic Chemistry Laboratory, New Chemistry Unit
Jawaharlal Nehru Centre for Advanced Scientific Research**

(A Deemed University)

Bengaluru-560064, India

November 2017

Dedicated to my Parents



TABLE OF CONTENTS

Certificate	i
Declaration	iii
Acknowledgements	v
Preface	vii
Chapter 1: Introduction	1
1.1 A β processing	5
1.2 A β aggregation	6
1.3 A β toxicity	9
1.4 Diagnosis	13
1.5 Therapy	15
1.5.1 Modulators of A β aggregation	16
1.5.1.1 Peptide-based modulators	16
1.5.1.2 Small molecule-based modulators	19
1.5.2 Metal chelators	22
1.5.3 Enzyme inhibitors	25
1.5.4 Immunotherapy	27
1.5.5 Autophagy activators	28
1.6 Objective	29
1.7 References	30
Chapter 2: Diagnostic probes	41
<i>2A. A thiazole-coumarin based high-affinity red fluorescence and colorimetric probe for amyloid β aggregates</i>	43
2.1 Design of hemicyanine probes	45
2.2 Photophysical and molecular docking studies of TC with A β fibrillar aggregates	46
2.3 Calculation of binding parameters	51
2.4 TC selectivity towards A β fibrillar aggregates	52
2.5 Binding site determination and FRET studies of TC bound to A β fibrillar aggregates	53
2.6 Conclusion	58

2B. Aβ plaque-selective NIR fluorescence probe to differentiate Alzheimer's disease from tauopathies	61
2.7 Photophysical and molecular docking studies of CQ with A β fibrillar aggregates	63
2.8 CQ selectivity towards A β fibrillar aggregates	65
2.9 Calculation of binding parameters, binding site determination and FRET studies of CQ bound to A β fibrillar aggregates	67
2.10 Determination of stability and BBB permeability of CQ	71
2.11 Selective detection of A β plaques in human brain tissue	72
2.12 Conclusion	75
2.13 Experimental section	75
2.14 References	81
Chapter 3: Peptidomimetics as Aβ modulators	85
3A. A Rationally Designed Peptidomimetic Modulators of Aβ Toxicity in Alzheimer's Disease	87
3.1. Design strategy for Peptidomimetics	90
3.2 Studying inhibition and dissolution efficiency by thioflavin assay and CD measurements	91
3.3 TEM Analysis	97
3.4 Blood plasma and proteolytic stability for peptidomimetics	99
3.5 Designed peptidomimetics nullify A β toxicity in an autophagy-dependent manner	100
3.6 Conclusion	103
3.7 Experimental section	103
3B. Synthesis of hybrid cyclic peptoids and identification of autophagy enhancer	113
3.8. Design and synthesis	115
3.9. Characterization of cyclic hybrid peptoids	119
3.10. Hydrogen bonding interaction in cyclic hybrid peptoids	121
3.11. Cyclic hybrid peptoids as autophagy enhancers	123
3.12. Experimental methods	125
3C. Natural tripeptide-based inhibitor of multifaceted Aβ toxicity	149
3.13. Design Strategy	153

3.14. Inhibition of A β 42 Fibrillar Aggregates	153
3.15. Inhibition of A β Oligomeric Aggregates	157
3.16. Metal Ion Sequestration from the A β 42-Cu ²⁺ Complex	159
3.17. Antioxidant Properties of P6	162
3.18. DNA Cleavage	164
3.19. Serum Stability	166
3.20. Cell Toxicity	166
3.21. Conclusion	169
3.22. Experimental methods	170
3.23. References	175
Chapter 4: Small molecule based amyloid modulators	183
<i>4A. Clioquinol synthetic derivatization to obtain nontoxic and multifunctional modulators for Aβ toxicity in Alzheimer's disease</i>	185
4.1 Design strategy	187
4.2 Inhibition of A β aggregation and Cu ²⁺ induced A β aggregation	189
4.3 Molecular interactions of HMMs with A β 42 aggregates	191
4.4 Cu ²⁺ chelation and antioxidant properties of HMMs	193
4.5 Protein Oxidation	196
4.6 Cellular Toxicity	197
4.7 Prevention of Mitochondrial Damage	199
4.8 Conclusion	201
<i>4B. Synthesis of naphthalene monoimide derivatives as effective modulators of toxicity in Alzheimer's and Parkinson disease</i>	203
4.9 Design strategy	204
4.10 Inhibition of A β 42 fibrillar aggregates	205
4.11 NMI derivatives rescue of neuronal cells from amyloid toxicity	207
4.12 Structure-activity relationship	208
4.13 TGR63 and TGR64 as therapeutic agents in Parkinson disease	210
4.14 Conclusion	211
<i>4C. Non-toxic Berberine derivative to rescue cells from multifactorial Aβ toxicity</i>	213

4.15 Synthesis and comparative cytotoxicity of berberine derivative	214
4.16 Inhibition of metal independent and dependent A β aggregation	216
4.17 Molecular docking studies	217
4.18 Metal independent antioxidant assays	219
4.19 Metal dependant antioxidant assays	221
4.20 DNA damage and protein oxidation	223
4.21 Cellular Toxicity	226
4.22 Molecular pathway for protection of neuronal cell from A β toxicity	226
4.23 Conclusion	228
4.24 Experimental methods	229
4.25 References	252
Chapter 5: The cellular localization of Aβ16 and implications in Aβ toxicity	257
5.1 Design and synthesis	258
5.2 A β 16 cellular permeability	259
5.3 A β 16 cellular localization	260
5.4 Conclusion	262
5.5 Experimental methods	262
5.6 References	264
<i>List of publications</i>	267

CERTIFICATE

I hereby certify that the work described in this thesis entitled “**Design, synthesis and study of molecular probes for diagnostic and therapeutic applications in Alzheimer’s disease**” has been carried out by **Mr. K. Rajasekhar** under my supervision at the Bioorganic Chemistry Laboratory, New Chemistry Unit, Jawaharlal Nehru Centre for Advanced Scientific Research, Bengaluru, India and that it has not been submitted elsewhere for the award of any degree or diploma.

Prof. T. Govindaraju
(Research Guide)



DECLARATION

I hereby declare that the matter embodied in the thesis entitled “**Design, synthesis and study of molecular probes for diagnostic and therapeutic applications in Alzheimer’s disease**” is the resultant of the investigations carried out by me at the Bioorganic Chemistry Laboratory, New Chemistry Unit, Jawaharlal Nehru Centre for Advanced Scientific Research, Bengaluru, India under the supervision of **Prof. T. Govindaraju** and that it has not been submitted elsewhere for the award of any degree or diploma.

In keeping with the general practice in reporting the scientific observations, due acknowledgement has been made whenever the work described is based on the findings of other investigators. Any omission that might have occurred due to oversight or error in judgement is regretted.

K. Rajasekhar
(Int. PhD Student)



ACKNOWLEDGEMENTS

First and foremost, I would like to express my sincere gratitude to my research supervisor Prof. T. Govindaraju, Bioorganic Chemistry Laboratory, New Chemistry Unit, JNCASR, for his continuous support, motivation, infinite patience and guidance throughout my Int. PhD tenure. It has been a great privilege and honor to be associated with him.

I would like to thank Prof. C. N. R. Rao, FRS, the Chairman, New Chemistry Unit for being the source of inspiration, generous support and encouragement throughout my stay in JNCASR. I also thank him for providing the infrastructure and facilities to carry out my research work.

I would like to thank my collaborators Dr. Ravi Manjithaya, Dr. Arul Murugan, Prof. Kavita Shah, Prof. HyoungGon Lee, Prof. Hans Ågren, Mr. S. N. suresh, Mr. Keith Viccaro, Mr. Guanglin Kuang for fruitful discussions.

I am thankful to my wonderful lab mates Dr. Maity, Dr. Avinash, Mr. Pandu, Dr. Shivaprasad, Ms. Suseela, Ms. Malabika, Mr. Sourav, Mr. Debasis, Mr. Sumon, Mr. Biswanath, Mr. Sathyajit, Mr. Harshit, Mr. Madhu, Dr. Atul, Dr. Madhu, Dr. Chandrasekhar, Dr. Abhaya, Dr. Pardhasaradhi, Dr. Shadab, Dr. Bappa, Dr. Mahesh, Mr. vardaman, Ms. Manju, Ms. Shilpa, Mr. Anand, Mr. Sandeepa, Mr. Manjunath, Mr. Sarkar for their help and friendly environment in lab. I would like to thank summer trainees, Vikram, Chaithra and kavita for helping me in my work.

I am thankful to Prof. H. Ila, prof. Aloknath Chakraborty, Prof. S. Balasubramanian, Prof. G. U. Kulkarni, Prof. A. Sundaresan, Prof. Chandrabhas Narayana, Dr. Tapas. K. Maji, Dr. Eswaramoorthy, Dr. Govindaraju, Dr. Jayanta Halder, Dr. Subi J. George, Dr. Ujjal Gautam, Dr. Ranjani Viswanatha and Dr. Sebastian C. Peter for their valuable courses.

I would like to thank all my Integrated Ph.D-2010 friends Arkamita, Chandan Kumar, Chandan De, Sisir, Anirban, Ram Kumar and Koushik for extending their help and cooperation throughout my stay in JNCASR.

I would like to thank Academics, Administration and NCU Office staff for their constant help.

It is indeed a great pleasure to express my sincere thanks to St. Xavier degree collage, Kurnool for the most memorable moments of life.

I thank JNCASR Library, Comp Lab, Hostel, and Health Center for providing and maintaining the various facilities that have helped me immensely.

Finally and most importantly, I am grateful to my family, especially my parents (Balarangaiah and Pushpavathi) and sister (Madhavi) for their love, moral support and constant encouragement throughout my life. Their love, blessings and affection made me what I am today. This thesis is dedicated to my parents for their love and support.

PREFACE

This Ph.D thesis has been categorized into five chapters, *Chapter 1* provides introduction to Alzheimer's disease (AD) and various molecular mechanism underlying the pathogenesis of the disease especially protein processing, misfolding and aggregation of peptides and proteins which are consider to be the main causative factors. The discussion also encompasses the physiological role of amyloid beta (A β) and its role in multifaceted toxicity found in AD. Recent developments related to diagnostic agents and techniques, and therapeutic molecules that directly or indirectly interfere with A β -induced toxicity are presented in detail.

Chapter 2 comprises of two subchapters. Herein, we outline the design, synthesis and application of red and near-infrared (NIR) fluorescence probes as diagnostic tools for AD. The first subchapter present **TC** as a potential probe for the detection of toxic A β 42 aggregates through switch-on red fluorescence and characteristic colorimetric output. **TC** exhibits selectivity and nanomolar binding affinity towards aggregates. The binding sites of **TC** on A β fibrils was revealed from FRET and molecular docking studies. In the second subchapter, a turn-on NIR fluorescence probe **CQ** for selective detection of A β 42 aggregates and staining AD-human brain tissue is discussed. **CQ** selectively binds to A β 42 aggregates over other biomacromolecules and toxic protein aggregates (tau, α -Syn and IAPP). It is nontoxic to neuronal cells and shows significant blood brain barrier permeability. Remarkably, **CQ** specifically stains A β plaques in human brain tissue over co-existing tau aggregates and neurofibrillary tangles (NFTs), which are associated with AD and tauopathies. This is a highly desirable attribute to distinguish AD from tau pathology and mixed dementia.

Chapter 3 consists of three subchapters. In first sub chapter we present peptidomimetic inhibitors of A β aggregation designed based on the recognition motif KLVFF (**P1**) of A β peptide by introducing multiple hydrogen bond donor-acceptor moieties and incorporating sarcosine units at alternate positions of **P1** (**P4** and **P5**). **P5** showed good A β aggregation inhibition and dissolution activity. Moreover, **P4** and **P5** could rescue yeast cells from A β toxicity and A β aggregates were cleared through autophagy process. In second subchapter discuss our methodology for the synthesis of six (α N-alkyl) and twelve (α N-acyl) member cyclic hybrid peptoids from N-(2-aminoethyl)glycine monomers through intra- and intermolecular cyclization, respectively.

Screening of the collection of cyclic hybrid peptoids resulted in the identification of an autophagy enhancer, which will have implications in developing effective candidates for elimination of intracellular pathogens and neurodegenerative protein aggregates. In third subchapter we present a multifunctional peptidomimetic inhibitor (**P6**) developed based on natural metal chelating tripeptide (GHK) and the aggregation inhibitor (**P5**). **P6** interact with A β and prevent the formation of toxic oligomeric species and fibrillar aggregates. **P6** sequester Cu²⁺ from the A β -Cu²⁺ complex and maintained it in a redox-dormant state to prevent ROS generation and DNA damage. Moreover, **P6** prevent PC12 cells from multifaceted A β toxicity.

Chapter 4 comprises of three subchapters. Herein, we present multifunctional small molecule based modulators for multifaceted A β toxicity in AD. In first subchapter, we present synthetic modifications of clioquinol (TGR86, TGR87 and TGR88) to obtain cell viable, metal chelating, antioxidant A β aggregation modulators to target multifaceted A β toxicity in vitro and in cellulo. TGR86 improves cellular viability by preventing mitochondrial damage caused by A β aggregates. In second subchapter, we report synthesis of a series of naphthalene monoimide derivatives as amyloid aggregation modulators in AD and Parkinson disease. TGR63 and TGR64 showed good A β and α -synuclein (α -Syn) aggregation inhibition activity and rescue PC12 cells from A β - and α -Syn-toxicity. In third subchapter we report a natural product berberine-derived (Ber-D) compound as a nontoxic, antioxidant and multifunctional modulator for A β toxicity in AD. Ber-D prevents both normal and metal induced A β cellular toxicity in PC12 cells. Mechanism of Ber-D protection against A β involves preventing mitochondrial damage, cytochrome C and caspase 3 production. *Chapter 5* deals with understanding the role of A β 42 in cellular toxicity using fluorescently tagged A β fragment (FAM-A β), and its interaction with metal and overall localization in cells.

In summary, the proposed thesis presents an overview of AD, current status of diagnostic and therapeutic strategies and objective of the work in the introduction chapter. The second chapter describes the development of NIR fluorescence diagnostic probes, for selective detection of A β 42 aggregates in human brain tissue to distinguish AD from mixed dementia. The third and fourth chapter deals with developing peptidomimetic and small molecule based therapeutic molecules for AD. Fifth chapter present our efforts in understanding the role of specific A β fragment of A β 42 (A β 16) in cellular localization and cytotoxicity.

Chapter 1

Introduction

The process of protein misfolding and aggregation has been a prime subject of research. This process is identified in the main pathological event involved in several diseases like Alzheimer's disease (AD), Parkinson disease (PD), Huntington disease (HD), Type II diabetes (T2D) and prion-related disorders among others.¹⁻³ AD is the most prevalent form of neurodegenerative diseases causing progressive attrition of cognition, task performance ability, mood, speech, behaviour and memory.^{4,5,6} A recent report from the National Center for Health Statistics (NCHS), USA suggests that deaths caused by diseases like ischemic heart disease, brain stroke, AIDS (acquired immune deficiency syndrome) and cancer have decreased significantly, while deaths caused by AD is on a constant rise.⁷ Alarmingly, in the next decade AD is likely to become particularly devastating for the poor and developing countries, severely affecting their public health and economy.⁸ For this reason, both scientific and clinical research community is putting tremendous efforts into understanding the disease to develop molecular tools for early diagnosis and cure. AD involves two major types of misfolded protein aggregates: intracellular aggregates of the microtubule-associated tau protein (called neurofibrillary tangles - NFT) and extracellular peptide aggregates known as senile plaques, mainly composed of amyloid β ($A\beta$) peptides.⁹ $A\beta$ peptides are transmembrane peptides produced by incorrect processing of the integral membrane protein called amyloid precursor protein (APP).¹⁰ The physiological function of $A\beta$ peptide in normal brain is not completely understood, although it is said to be playing a vital role in neurogenesis and modulation of synaptic plasticity.¹¹ Excess production or dysfunctioning of $A\beta$ clearing pathways leads to their deposition, which deleteriously affects a large number of vital pathways like the lipid metabolism, the intracellular signalling, autophagy regulation

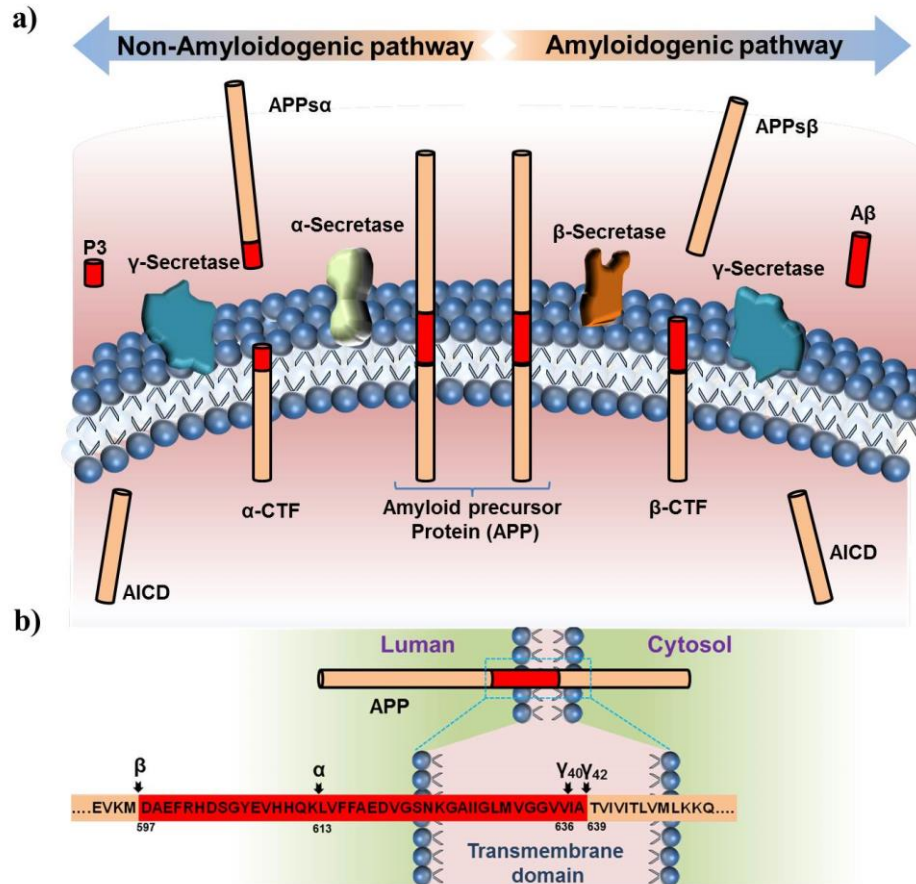


Figure 1. Proteolytic processing of APP. a) In non-amyloidogenic pathway, cleavage occurs when α -secretase acts on APP to liberate APPs α and α -CTF, the latter being cleaved by γ -secretase to generate P3 and intracellular C-terminal fragment (AICD) (left). Amyloidogenic cleavage by β -secretase liberates APPs β , and the residual peptide (β -CTF) is cleaved by γ -secretase to produce A β and AICD (right). b) The schematic structure of APP is shown with the A β domain shaded in red and enlarged. The major sites of cleavage by α , β and γ -secretase are indicated along with A β numbered from N-terminal.

neurotransmitter release and synaptic function ultimately resulting in neuronal death.¹² A β toxicity is attributed to the toxic oligomeric and fibrillar species formed through its aggregation (amyloid cascade hypothesis). Therefore, targeting fibrillogenesis of A β or activating pathways like autophagy or activating neuronal signalling for maintaining neuronal homeostasis that are blocked by toxic A β aggregates have been taken up as therapeutic strategies for preventing or curing AD.¹³ The molecular pathways, which

drive the formation of A β oligomers and fibrils, and their interdependence for existence is not well understood. Recent studies indicate that once the certain concentration of fibrils is deposited, they, in turn, catalyse the formation of toxic oligomeric species from soluble A β monomers and the process is termed as secondary nucleation.¹⁴ Therefore, targeting secondary nucleation mechanism also could be an effective therapeutic strategy. Molecules ranging from peptides to small synthetic and natural compounds have been extensively studied, and proven to be helpful in modulating the A β aggregation. Metal ions (Cu²⁺, Zn²⁺ and Fe²⁺) have been reported to play a vital role in accelerating and stabilizing A β oligomers (the toxic form of A β). Therefore, targeting metal ions using metal chelators is a promising therapeutic tool in decreasing A β toxicity.^{14,15} Targeting the proteolytic enzymes (β - and γ -secretase) involved in the APP processing (amyloidogenic pathway) is a potential strategy in decreasing the amyloid deposits in the brain.¹⁶ Developing A β -specific antibody, upregulating A β clearing pathways and activating autophagy are few other therapeutic routes for tackling AD.^{17,18}

1.1 A β processing

A β is the key component involved in the progression of the AD.¹¹ A β peptides with sequence length ranging from 36-43 are derived from the proteolytic cleavage of an integral membrane protein called APP (Figure 1). APP is a type 1 transmembrane glycoprotein (695 amino acids) expressed on both intra- and extracellular membranes and had various physiological functions.¹⁹ Production of A β in the amyloidogenic pathway involves sequential cleavage of APP by proteolytic enzymes β -secretase (β -site APP-cleaving enzyme 1 - BACE 1, which is an integral membrane protease) and γ -secretase (membrane-bound enzyme).²⁰ In the case of the non-amyloidogenic pathway, a third

secretase (α -secretase) cleaves within the A β sequence and prevents its production (Figure 1). In amyloidogenesis, APP is first cleaved by β -secretase producing APPs β and β -CTF (β C-terminal fragment). Successive action by γ -secretase on the transmembrane domain produces A β and AICD (amyloid precursor protein intracellular domain) (Figure 1).¹⁰ In non-amyloidogenic pathway, α -secretase cleaves the ectodomain of APP resulting in the formation of the APPs α fragment and α -CTF. Then the γ -secretase cleaves the α -CTF releasing the so-called P3 peptide and AICD (Figure 1). The imperative role of BACE 1 and γ -secretase in A β production make them obvious therapeutic targets for AD.^{16,21}

1.2 A β aggregation

Unraveling the structure and mechanistic insights on the higher order A β aggregates has been an important area of research because of its relevance to the AD. Nearly 80% of the A β in normal human brain constitutes of A β 40 whereas in the diseased condition excess A β 42 is produced and predominantly accumulated as amyloid plaques. The A β 42 has severe neurotoxicity and possesses faster aggregation kinetics compared to A β 40.²² A natively unfolded state of A β shows slow transformation into a partially folded state (β -sheet).²³ The rate of transformation is slower therefore, an initial lag in aggregation is observed. The external addition of higher-order aggregates (seeding effect) results in fast aggregation, suggesting a nucleation-growth mechanism.²⁴ Further, partially folded units associate with each other through hydrophobic interaction and hydrogen bonding to form paranucleus, which then self-associate to form higher-order structures called protofibrils (Figure 2a). The protofibrils are further self-assembled through the elongation phase and form the long fibrillar aggregates.²⁴ To understand the elongation mechanism Stultz *et al.*

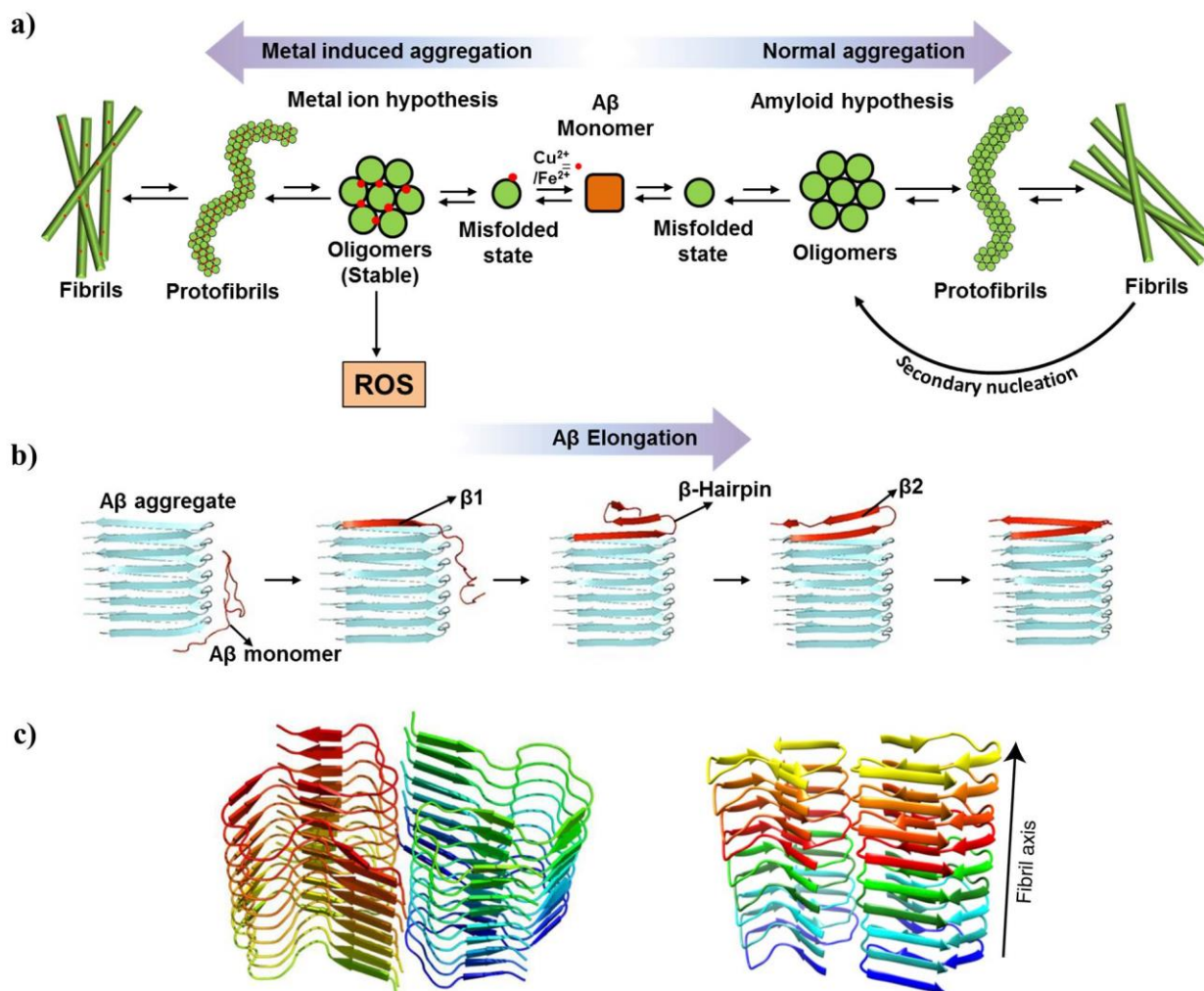


Figure 2. Aβ aggregation and structure. a) Schematic illustration for Aβ peptide aggregation in normal pathway representing amyloid cascade hypothesis (right) and metal-induced Aβ aggregation to stable toxic oligomers and fibrils representing metal ion hypothesis (left). b) Schematic for different energy minimized states for Aβ peptide interacting with Aβ aggregate during elongation process. c) atomic resolution structure of Aβ15–42 amyloid fibrils derived from over 500 ¹³C–¹³C, ¹³N distance and backbone angle structural constraints obtained from high field magic angle spinning NMR spectra, (right) A ribbon-based cartoon of the Aβ42 fibrils showing nine molecules of Aβ42 along the fibril axis.

recently performed a detailed molecular dynamic (MD) simulation suggesting that during elongation the N-terminal associates with the core Aβ fibril through intermolecular hydrogen bonding (β1) (Figure 2b).²⁵ This is followed by the formation of the bent β-hairpin structure and association of β2 strand of the monomer with β1 strand through intramolecular hydrogen bonding; this unit finally associates with the full Aβ fibril. β-

Hairpin stabilization enhances aggregation rate and appears to be one of the possible targets for designing drugs. The A β fibril formation includes oligomers as the intermediate state and oligomers existence depends on the A β monomer concentration (primary nucleation). Recently, Knowles *et al.* have shown that existence of the A β oligomers depends on the concentration of both monomers and fibrils.¹⁴ Initially, A β monomers undergo aggregation to form fibrils through primary nucleation with oligomers as the intermediates. Once a certain concentration of the fibrils is reached (10 nM) they catalyse the formation of the oligomers on their surface (secondary nucleation). Thus, a new concept has been introduced which implies that the A β oligomer formation is initially guided by primary nucleation and subsequently enriched by secondary nucleation on the surface of the A β fibrils.

A native unfolded A β peptide can also undergo off-pathway self-association to form stable oligomeric aggregates.²⁶ The oligomers are shown to be the most toxic form of A β , and they are considered to exist in the lag phase of the fibril formation.²⁴ These oligomers can act as nucleation centres in the brain for the creation of new oligomers and higher-ordered aggregates as well. Metal (Cu²⁺) coordination with A β has shown enhanced aggregation rates, stabilization of oligomeric state and reactive oxygen species (ROS) generation (metal ion hypothesis) (Figure 2a).¹⁴ A β oligomers are highly unstable and determining their structure is difficult. Hydrophobic regions (residues 10–21 and 30–40) attain a conformation similar to the fibrils, while the turn region (residues 22–29, involving a salt bridge) and the N-terminal (residues 1–9 are more flexible in oligomers) are different. Oligomers exhibit structural similarity with corresponding protofibrils whereas protofibrils share less similarity with their fibrils.²⁷⁻²⁹ Indicating the possible

conversion of intramolecular hydrogen bonds to intermolecular hydrogen bonds during the structural transition from A β protofibrils to the corresponding matured fibrils. This mechanistic and structural analysis of toxic oligomers and matured aggregates provides a handle in designing potential molecules to modulate the A β aggregation.

1.3 A β toxicity

The progression of the AD and its mechanism of toxicity is not very well understood.³⁰ There are many hypotheses proposed, remarkable to note that A β is the key player in all the proposed hypotheses. This has understandably raised immense interest in comprehending its origin and means of toxicity.³¹ In the following sections, different means of A β toxicity have been discussed (Figure 3).

1.3.1 Oxidative stress. Accumulation of A β peptide coordinated with redox active metals has been hypothesized to induce oxidative stress.³² However, the exact causative mechanism for stress generation by A β is still a matter of debate. Redox-active copper ions have been found accumulated in amyloid plaques which form Cu-A β complexes and catalyse the production of ROS. A β can reduce Cu²⁺ to Cu⁺ or Fe³⁺ to Fe²⁺, and these reduced metal ions can react with O₂ to produce superoxide anion which further takes up 2H⁺ ions and generates H₂O₂. H₂O₂ react with another reduced metal ion to produce the toxic HO \cdot radicals through Fenton reaction (Figure 4).³³ These radical species are said to be involved in lipid and protein peroxidation and finally leading to neuronal death. Metal reduction in the Fenton cycle is said to be mediated by methionine (M35) whose sulfide group can oxidize and easily donate electrons, although recent studies indicate that absence of M35 does not prevent A β toxicity.^{34,35} A β has also been known to induce T10 intermolecular cross-linking to promote the formation of toxic oligomeric species.³⁶ The

N-terminal region of A β has a metal binding domain, and amino acid residues D1, H6, H13 and H14 are proposed to be involved in metal chelation. Cu²⁺ coordinates through D1, H6 and H13 or H14, while Cu⁺ coordinates through H13 and H14. Large structural rearrangement occurs in the copper coordination during electron transfer (redox reaction) indicating the presence of an intermediate state involved in ROS generation. Recently, Collin *et al.* showed the existence of the intermediate transition state through mass spectroscopy where copper coordinates with A1, H13 and H14 residues whereas H6 has to break its bond with Cu²⁺ to initiate the redox reaction.³⁷ ¹³C and ¹⁵N NMR studies have supported the contention that such major rearrangement in the copper binding site occurs during the redox cycle of ROS production.³⁸ Metal binding elongates in the lag phase of

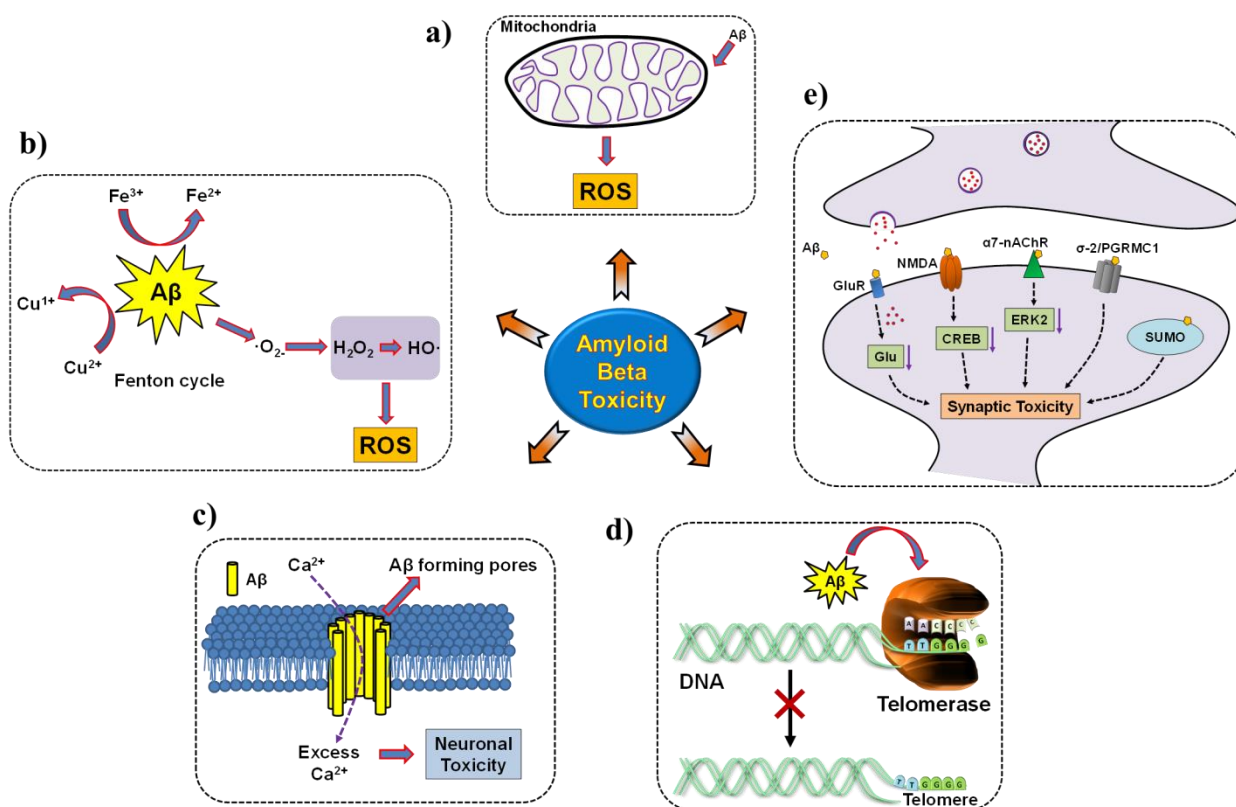


Figure 3. A β toxicity. a) A β causes mitochondrial dysfunction leading to ROS generation. b) Oxidative stress caused by A β oligomers. c) Cell membrane disruption by A β aggregates. d) Telomerase inhibition. e) A β , interfere with signalling pathways causing synaptic toxicity.

fibril formation or stabilizes the oligomeric state.³⁹ Cu^{2+} with $\text{A}\beta$ forms toxic oligomeric species whereas Zn^{2+} forms amorphous non-fibrillar aggregates with reduced neurotoxicity. The impact of Zn^{2+} on $\text{A}\beta$ -Cu complex in altering ROS production is minimal.⁴⁰ Matured $\text{A}\beta$ aggregates are said to be less toxic, but Cu^{2+} -induced $\text{A}\beta$ fibrillar aggregates retain their redox activity and can produce hydroxyl radical from H_2O_2 .⁴¹

1.3.2 Synaptic dysfunction. Synaptic loss is better correlated with cognitive impairment of AD rather than with the amount of $\text{A}\beta$ plaques.⁴² Disturbances of synaptic transmission occur long before the development of the hallmark $\text{A}\beta$ deposits. Therefore the mechanism by which $\text{A}\beta$ disturb the synaptic transmission is not completely understood. $\text{A}\beta$ oligomers bind to neural receptors on the synaptic cleft and hinder their function, thus leading to synaptic dysfunction and cognitive decline.⁴² $\text{A}\beta$ oligomers and not their fibrillar aggregates are considered to be responsible for synaptic dysfunction. $\text{A}\beta$ oligomers bind to essential synaptic receptors like glutamate receptors (GluR), NMDA receptor (N-methyl-D-aspartate receptor), AMPA receptor (α -amino-3-hydroxy-5-methyl-4-isoxazolepropionic acid receptor) and deregulate synaptic plasticity, memory formation and learning (Figure 3).⁴³ $\text{A}\beta$ has high-affinity binding to the $\alpha 7$ - nicotinic receptors which has a significant role in the internalization and intracellular accumulation of $\text{A}\beta$ in neuronal cells.⁴⁴ Small ubiquitin-like modifier (SUMO) molecules acting through post-translational modification are required for normal synaptic and cognitive function. SUMOylation is involved in long-term potentiation (LTP) and hippocampal-dependent learning. The $\text{A}\beta$ oligomers are involved in impairment and inhibition of SUMOylation leading to cognitive decline.⁴⁵ Catalano *et al.* have shown that sigma-2/PGRMC1 (progesterone receptor membrane component 1) is involved in $\text{A}\beta$ oligomer binding and

inducing toxicity. It indicates that sigma-2/PGRMC1 plays a key role in pathogenesis of AD and can act as a disease modifying therapeutic target.⁴⁶

1.3.3 Membrane interaction. Interaction of A β aggregates with the cellular membrane leads to pore formation causing the abnormal flow of ions, in and out of the neuronal cells. These pores facilitate Ca²⁺ entry disturbing its active regulation, which leads to cellular damage and neuronal death (Figure 3).^{47,48} The mechanism of pore formation in the cell membrane by the A β oligomers is similar to that of antibacterial agents killing bacteria through pore formation in the bacterial membrane by different mechanisms.⁴⁹

1.3.4 Telomerase dysfunction. Telomerase is a ribonucleoprotein enzyme that adds DNA sequence repeats (TTAGGG) to the 3' end of DNA strands in the telomere regions which are found at the ends of eukaryotic chromosomes and are essential for cell survival. Telomere length is related to biological aging and its shortening is observed in many age-related diseases.⁵⁰ Recent studies have revealed that telomere shortening can play a major role in the AD pathological process. Upregulation of telomerase activity is also being considered as a therapeutic strategy in treating the AD. Recently, Qu *et al.* found that the A β aggregates could inhibit telomerase activity both in *vitro* and *in vivo*. A β oligomers bind to the DNA-telomerase complex (DNA-RNA complex) and block the elongation of telomeric DNA. Telomerase inhibition might be one of the reasons for A β cytotoxicity (Figure 3).⁵¹

1.3.5 Apoptosis. It is the process of programmed cell death and is implicated in neuronal loss in AD patients. It is triggered by the shutdown of mitochondrial function and the mechanism behind it is still not fully understood (Figure 3).⁵² Recent studies show that A β induce the activation of I κ B α /NF- κ B pathway which decreases the expression of

cytochrome c oxidase subunit (COXIII) and inhibits COX activity leading to mitochondria dysfunction.⁵³ In another report, high levels of apoptosis signal-regulating kinase 1–interacting (ASK1-interacting) protein-1 (AIP1) was observed in the brain of AD Tg2576 mice.⁵⁴ Interaction of A β with AIP1 initiates a cascade of pathways inducing apoptosis in the neuronal cells. Khanday *et al.* reported that the A β causes the phosphorylation of MKK6 at S207, T211 and Y219 residues.⁵⁵ Then phosphorylated MKK6 interacts with P66sch and forms MKK6-P66shc complex, which is involved in phosphorylation of p66shc at S36 and ROS production triggering apoptosis in cells and finally leading to cell death. Further efforts are required to understand the exact mechanistic role of A β in initiating the apoptotic pathway and subsequent neuronal death.

1.4 Diagnosis

It is widely accepted that presence of A β plaques precedes the clinical symptoms of AD, therefore A β aggregates are ideal biomarker for early diagnosis of AD.⁵⁶ The current available clinical diagnosis for AD is mainly based on family (for genetic inheritance) and patients medical history as well as cognition ability. Thus, the diagnosis is often not reliable. Confirmative AD diagnosis is possible only through the examination of patient's brain during post-mortem for A β plaques. There is a great urgency to develop non-invasive and selective probes for A β plaques in diagnosis of AD. Such probes will also be useful in understanding the disease progression and develop effective therapeutics for AD. Significant advances have been made in recent times for the design of molecular probes for specific, selective detection and imaging of A β plaques both *in vitro* and *in vivo*.⁵⁷ Various imaging techniques have been adopted, which include positron emission tomography (PET), single photon emission computed tomography (SPECT), magnetic resonance imaging (MRI), and optical imaging techniques

(mainly fluorescence based). MRI based approaches suffer from low resolution and moreover, they lack selectivity.⁵⁸ When compared with MRI, PET and SPECT probes are sensitive towards broad range of A β plaques.⁵⁹ Many probes, such as [¹¹C]PIB, [¹¹C]SB-1329, [¹⁸F]FPIB, [¹⁸F]AV-45 and [¹²³I]IMPY, are currently undergoing clinical trials. Three PET probes [¹⁸F]FPIB (VizamyITM), [¹⁸F]AV-45 (AmyvidTM) and [¹⁸F]AV-1 (NeuraceqTM) are recently approved PET probes by the FDA.⁶⁰ The clinical utility of these imaging agents is limited as they cannot be used for the confirmative diagnose of AD. Moreover, PET probes are limited by high cost and narrow availability, since generation of these probes needs specialized facilities.

In contrast to the imaging techniques mentioned above optical imaging is inexpensive, nonradioactive, can be used in real-time imaging, they have wide availability, non-hazardous, and high-resolution imaging can be performed. For *in vivo* applications, to avoid absorption and background autofluorescence, and scattering of biological molecules, probe fluorescence emission wavelength in the red and near-infrared (NIR) region between 600 and 900 nm is advantageous so that we obtain an optimal penetration depth and high sensitivity.⁶¹ Therefore, NIR fluorescence imaging has emerged as an attractive alternative to PET/SPECT and MRI techniques and may provide a solution for the early diagnosis of AD. Recent, developments in developing NIR probes is being detailed in chapter 2. Even though a large number of NIR probes have been reported in the literature, they lack the key property for being an ideal diagnostic probe that is selectivity. Most of the reported fluorescence probes can bind to any hydrophobic aggregates and exhibit turn-on fluorescence. This particular problem could lead to the wrong diagnosis, as many of neurodegenerative diseases involve the presence of various hydrophobic aggregates. In the current work, we developed red and NIR fluorescence probes (Chapter 2) to selectively detect A β plaques in the brain tissue in the presence of protein aggregates which are

implicated in other neurodegenerative diseases and coexist in case of mixed dementia. Our fluorescence probes will find applications in academic research, to understand disease pathology in AD models (zebra fish, mice etc.) and in vitro staining and imaging of AD brain tissues to correlate amyloid load and disease progression. Such information is useful in understanding disease pathways at molecular level and drug development. Among all the imaging agents only PET probes have been approved by FDA for imaging amyloid plaques, however lack of selectivity hampered their application as diagnostic tools. There is a immense scope to synthetically modify our probes to PET-ready probes by incorporating radioactive tracer which make them practically viable diagnostic tools for AD.

5. Therapy

The prominent role played by $A\beta$ in the AD makes it an obvious therapeutic target. In this section, various therapeutic strategies and recent developments in preventing $A\beta$ -induced toxicity will be discussed (Figure 5).

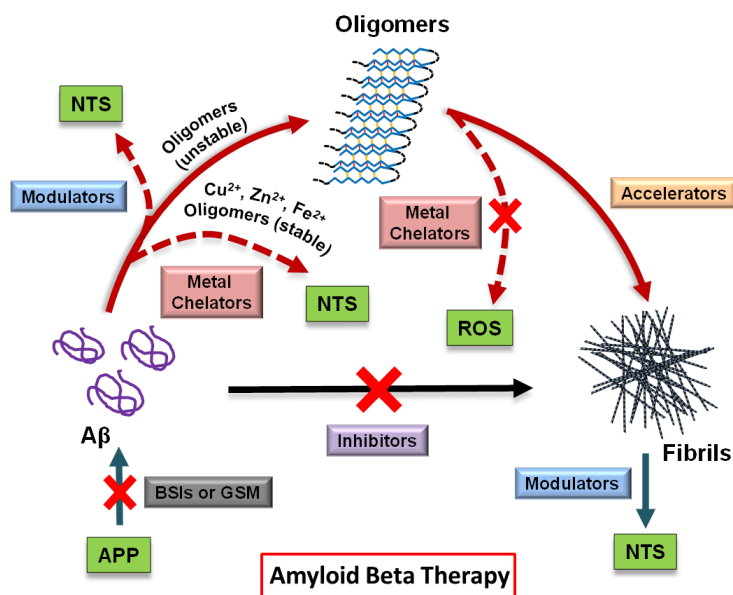


Figure 5. Schematic illustration of different therapeutic targets, which are explored to prevent $A\beta$ toxicity. NTS (nontoxic species), BSIs (β -secretase inhibitors), GSM (γ -secretase modulators).

1.5.1 Modulators of A β aggregation

The amyloid hypothesis suggests a direct correlation of AD with A β aggregates; hence targeting A β aggregation is considered an effective therapeutic strategy. A β peptide switches from a non-toxic α -helical state to a toxic β -sheet conformation. Molecules that can (i) block the β -sheet formation (ii) prevent the fibrillogenesis (iii) dissolve A β aggregates to non-toxic species (iv) destabilize A β oligomers (v) accelerate conversion of A β oligomers to A β aggregates are considered as modulators of A β aggregation.⁶² This section has been organized into peptide-based modulators and small molecule-based modulators depending upon their chemical structure.

1.5.1.1 Peptide-based modulators. Peptide-based inhibitors (sequence of 5-15 natural or unnatural amino acids) are a minor class of molecules designed upon the understanding of β -sheet-driven self-assembly involved in the aggregation of A β peptide (Figure 6). The hydrophobic core (KLVFF) of the A β plays a central role in the initiation of A β aggregation, and it acts as a recognition unit for their elongation to fibrillar aggregates.⁶³ For the past two decades, KLVFF has been the basis for designing most of the peptide-based modulators of the A β aggregation. Hydrophobic peptides like KLVFF (**1**) and LPFFD (**2**) have been screened and reported to be effective in the inhibition of A β fibrillogenesis both *in vitro* and *in vivo*.^{64,65} Recently, Xu *et al.* developed a recognition unit based peptide H102 (HKQLPFFEED, **3**) which could inhibit the A β aggregation, decrease expression of p-tau, inflammatory and apoptosis factors, and enhance cognitive ability in mice. H102 undergoes rapid metabolism by proteolytic enzymes. Therefore, chemical modifications are necessary to enhance its proteolytic stability.⁶⁶ Peptide-based drugs are very specific and efficient, but their poor bioavailability and protease stability

limits their use as potential therapeutic agents.⁶⁷

Several modification strategies such as incorporating unnatural amino acids (peptidomimetics), functionalizing the N- or C- terminal with various organic moieties and cyclization of modified peptides have been reported in the literature to enhance bioavailability, protease stability and therapeutic values. Similar modifications have been adopted in developing peptide-based modulators of the A β aggregation in AD. Peptoids are an important class of peptidomimetics made of N-methyl glycine units, which can be effectively used in designing A β inhibitors and are protease-resistant. Once bound to A β they can inhibit the elongation process as the peptoid backbone lacks the amide protons.⁶⁸ Servoss *et al.* designed a peptoid-based mimic of KLVFF, JPT1 (**4**) which exhibited a α -helix state in solution and had an enhanced aromatic interaction with the A β . JPT1 showed a decrease in lag time of A β 40 fibrillar aggregation and reduction in the level of A β 40 fibrillar aggregates when compared to its parent peptide KLVFF.⁶⁹ In recent years cyclic peptides (CP) have emerged as a new class of powerful and specific amyloid modulators.⁷⁰ CP is metabolized slowly than their non-cyclic analogues and hence display higher bioavailability. Kanai *et al.* showed that cyclization of the recognition moiety (cyclo-D-[KLVFF]) enhanced its inhibition efficiency by three-fold compared to its linear analogue. Further, by understanding the structure-activity relationship (SAR) of the phenyl group in the inhibition of A β aggregates, a phenyl group at β -position of F4 (**5**) was introduced leading to enhanced inhibition efficiency and neuroprotective property.

The A β aggregation to toxic polymorphic forms and A β -Cu²⁺ catalysed ROS generation are two important aspects of neuronal toxicity observed in AD.¹⁴ The toxicity exhibited by A β has to impose for the development of multifunctional modulators.

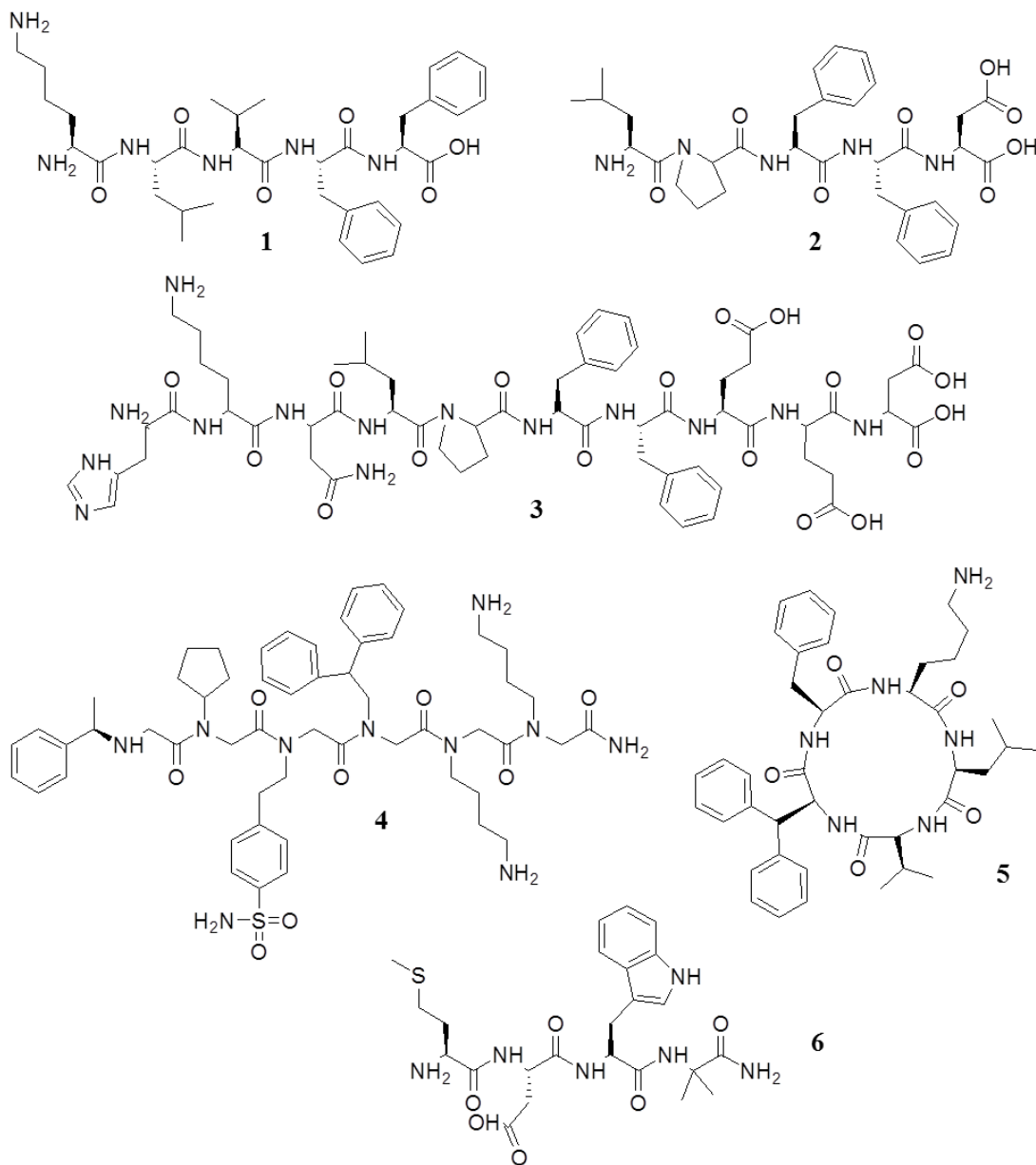


Figure 6. Peptide-based modulators of A β aggregation.

There is significant amount of literature available on small molecule-based multifunctional inhibitors, but they are only few reports on peptide or peptidomimetic based inhibitors targeting both A β aggregation and A β -metal toxicity.⁴ Faller *et. al* have used A β peptide fragment (A β 12-20), which has both aggregation modulating (KLVFF) and metal chelating (VHH) moiety. It showed aggregation inhibition, antioxidant property

by sequestering metal and significant protection against A β -Cu²⁺ induced cell toxicity in SH-SY5Y cells.⁷¹ On similar lines, Yuan *et. al.* have developed a bifunctional A β aggregation inhibitor GGHRYYAAFFARR (GR), in which RYYAAFFARR (RR) inhibit the aggregation of A β through the hydrophobic, electrostatic and hydrogen bonding interaction and GGH act as a metal chelator for Cu(II) preventing generation of ROS.⁷² GR reduced the toxicity induced by the A β -Cu²⁺ complex in PC12 cells, and the cell viability was improved to 88%, which was much higher than compared to peptide GGH and RR. Currently use of peptidomimetics as drug candidates are encouraged over natural amino acid based peptides. Quintanar *et. al.* have designed a bifunctional non-natural tetrapeptide (Met-Asp-D-Trp-Aib, **6**), with copper chelating and A β aggregation modulation properties.⁷³ In living systems, redox-active metal ions like Fe and Cu exist mostly in the complexed state with peptides or proteins. This chelating property of peptides and proteins has not been fully explored to develop peptide-derived metal chelators. In conclusion, although the serum stability and BBB crossing issues of peptide-based inhibitors can be overcome by using peptidomimetics their inhibition efficiencies are still low compared to small molecule-based inhibitors. Selectivity and biocompatibility are key factors that have kept researchers active in developing peptide-based disease modifying therapeutics for the AD.

1.5.1.2 Small molecule-based modulators. Modulation of A β aggregation using small molecules has been reported to be a highly efficient approach (Figure 7).⁷⁴ Most of the modulators control the fibrillogenesis of A β through blocking hydrophobic interactions. Natural products like curcumin (**7**) (IC₅₀ ~ 13.3 μ M), resveratrol (**8**) (IC₅₀ ~ 15.1 μ M), and epigallocatechin-3-gallate (**9**) (EGCG) (IC₅₀ ~ 2.4 \pm 0.4 μ M) have been shown to be effective in

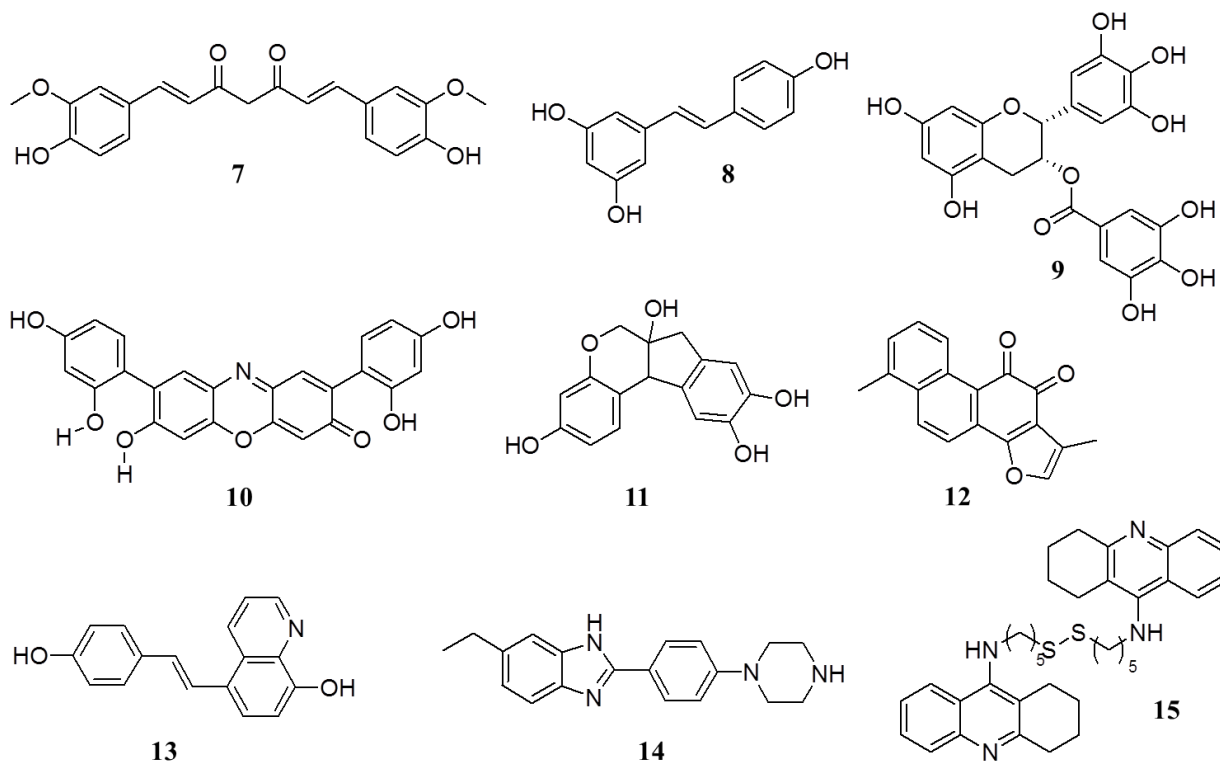


Figure 7. Small molecule-based modulators of Aβ aggregation.

decreasing the load of Aβ plaques in the brain through their antioxidant and aggregation inhibition properties.⁷⁵ Curcumin and resveratrol inhibit Aβ aggregation by binding to the N-terminal of the low molecular weight Aβ oligomers and prevent the formation of the more toxic, high molecular weight oligomers.⁷⁶ Wanker *et al.* showed that EGCG (in phase III clinical trial) is not just an antioxidant but also perturbs the aggregation propensity of Aβ by binding to its monomeric state and rendering it into non-toxic species.⁷⁷ The same research group also reported orcein, a natural product-based molecule (**10**) which accelerates the formation of Aβ₄₂ fibrillar aggregates from highly toxic Aβ₄₂ oligomeric species. Orcein was found to bind parallel to the long axis of Aβ₄₂ aggregates are targeting the hydrophobic region of spherical oligomeric Aβ₄₂ species. Once bound, it nucleated the formation of less toxic higher order Aβ₄₂ fibrillar aggregates.⁷⁸ Brazilin

(11) a natural product obtained from *Caesalpinia sappan* inhibited A β 42 aggregation and also remodelled the A β 42 aggregates to prevent them from acting as secondary nucleation centres for further fibrillogenesis.⁷⁹ Molecular docking studies suggest that brazilin binds to A β 42 through hydrophobic interactions and interferes with the intermolecular salt bridge of D23-K28 via hydrogen bonding to induce a pathway for the formation of non-toxic aggregates. Therefore targeting salt bridge formation (D23-K28) in the loop region of the A β can modulate A β aggregation and is a promising therapeutic strategy.⁸⁰ Zheng *et al.* reported tanshinone (TS1, 12) obtained from the Chinese herb danshen, as an efficient and natural inhibitor of A β aggregation.⁸¹ These natural products could inhibit A β 42 fibrillogenesis and also dissolve preformed A β 42 fibrillar aggregates. Gazit *et al.* reported 1,4-naphthoquinon-2-yl-L-tryptophan (NQTrp) as an A β aggregation inhibitor. Recently, a detailed MD simulation of NQTrp and its analogues was performed to understand the mechanism of inhibition, binding modes, and to design efficient and improved inhibitors.⁸² Based on the multiple target ligand approach Li *et al.* designed an inhibitor (E)-5-(4-hydroxystyryl)quinoline-8-ol (13) which is a combination of clioquinol, a well-known inhibitor for both normal and copper-induced A β fibrillar aggregates toxicity, and resveratrol.⁸³ Inhibitor 13 showed higher inhibition and dissolution efficiency for copper-guided A β 42 aggregates, antioxidant property and BBB permeability compared to its constituent elements clioquinol and resveratrol. Recently, Oya *et al.* have synthesized a series of benzimidazole derivatives as multifunctional agents for the AD. Modulator 14 exhibited BChE inhibitory activity, anti-aggregating activity, cytotoxicity, and neuroprotective properties. Tacrine is a well-known acetylcholinesterase inhibitor and A β aggregation modulator. Jose *et al.* have designed

and synthesized a series of tacrine homo and hetero dimers with antioxidant properties. **15** have shown 19 fold enhancement in acetylcholinesterase activity and improved aggregation inhibition properties.

1.5.2 Metal chelators

The metal ion hypothesis is a well-received pathway and contributes substantially to the neuropathogenesis involved in the AD. Presence of high concentrations of metal ions such as Cu^{2+} , Zn^{2+} and Fe^{2+} coordinated with the $\text{A}\beta$ peptide in senile plaques indicates their strong involvement in $\text{A}\beta$ aggregation and its toxicity.^{84,85} Metal binding to the $\text{A}\beta$ stabilizes the toxic oligomeric form which is indeed involved in ROS generation and causes synaptic breakdown, finally leading to neuronal cell death.¹⁴ Sequestration of physiologically relevant metal ions by $\text{A}\beta$ disturbs metal ion homeostasis in the brain.⁸⁶ Disruption of $\text{A}\beta$ -metal interactions via metal chelators has been tried in order to reduce neurotoxicity initiated by $\text{A}\beta$ -metal complex and to refurbish metal ion homeostasis in the brain (Figure 8).⁸⁷ Desferrioxamine B was the first metal chelator used to dissolve metal-directed $\text{A}\beta$ aggregates and enhance cognitive ability in a mouse model. However, its use was constrained by its poor BBB permeability and fast *in vivo* degradation in combination with other adverse side effects. In the past few years 8-hydroxyquinoline-based molecules have gained tremendous interest as metal chelators and aggregation modulators.⁸⁸ In this context, Lindquist *et al.* have shown that the 8-hydroxyquinoline-based molecule clioquinol (**16**) exhibited a prominent role in perturbing the aggregation of $\text{A}\beta$ in the presence and absence of metal, and also restored the endocytic function in a yeast model of AD (Figure8).⁸⁹ However, the presence of mutagenic di-iodo form of clioquinol barred its usage and it has also failed in phase II clinical trials.⁹⁰ However in the presence of mutagenic

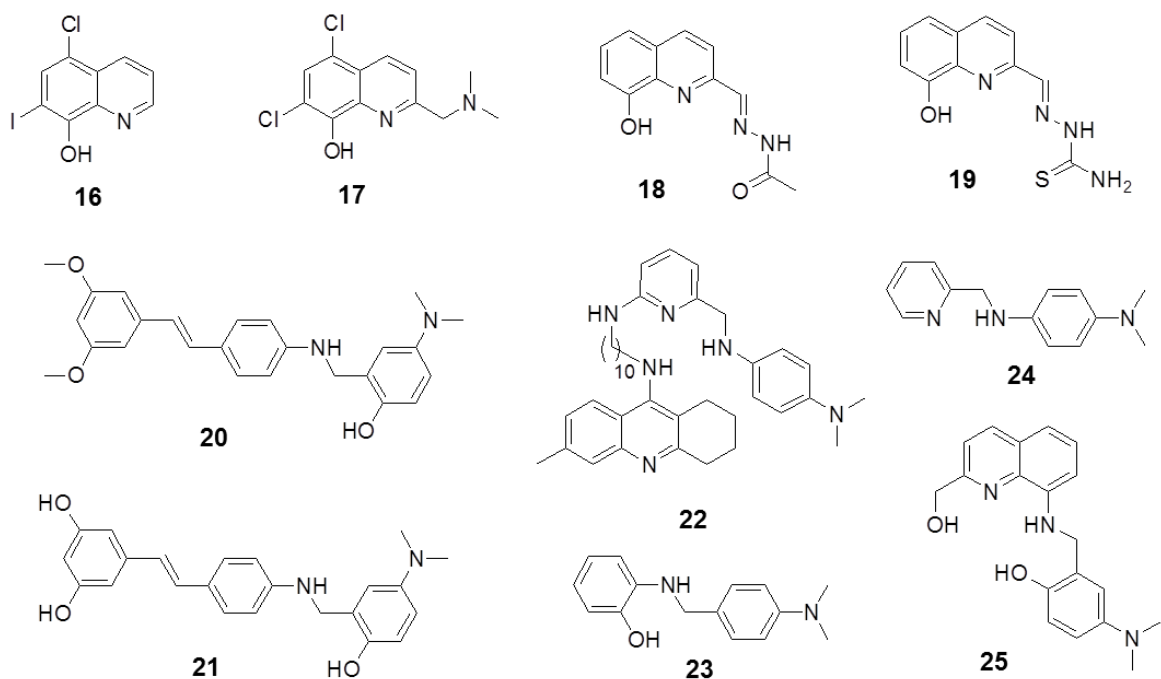


Figure 8. Metal chelators for inhibiting metal guided A β aggregation and toxicity.

di-iodo form of clioquinol (impurity) barred its usage, and it also failed in phase II clinical trials.¹²⁰ Later PBT2 (**17**), Iyer *et al.* have appended hydroxyquinoline to polyfluorene (PF-HQ), which forms nano co-aggregates with toxic amyloid intermediates to non-toxic aggregates and displays inhibitory activity toward A β fibrillation and amyloid cytotoxicity. An acetohydrazone (**18**) and thiosemicarbazone (**19**) derivative of 8-hydroxyquinoline have shown Cu²⁺ and Zn²⁺ sequestration from A β -Cu²⁺/Zn²⁺ oligomers while the metal-free aggregation pathway of A β was unaffected. **18** (TEAC = ~1.5) and **19** (TEAC = ~1.2) showed decent antioxidant property in the Trolox equivalent antioxidant capacity (TEAC) assay.⁸⁸ Li *et al.* designed a series of MFLs (Multifunctional ligands) based on clioquinol and the well-known antioxidant resveratrol (**20** and **21**).⁹¹ Ligands **20** (A β , IC₅₀ = 7.56 μ M) and **21** (A β , IC₅₀ = 6.51 μ M) showed remarkable efficiency towards A β . The docking studies show that these ligands interact mainly at the C-terminal of A β peptide through hydrogen bonding and hydrophobic interactions.

Oxygen radical absorbance capacity (ORAC-FL) assay showed good antioxidant property for **20** (4.72 ± 0.14) and **21** (4.70 ± 0.57), and enhanced BBB permeability compared to their parent molecules. Similarly, 6-chlorotacrine an AChE inhibitor derivatized with Cu^{2+} and Zn^{2+} chelating ligands led to the hybrid 6-chlorotacrine–metal– $\text{A}\beta$ modulator (**22**) with inhibition and dissolution ability for both self- and metal-guided $\text{A}\beta$ aggregation and AChE inhibition.⁹² Lim *et al.* designed a bifunctional ligand L2NO (**23**) derived from $\text{A}\beta$ imaging agent *p*-stilbene (recognition moiety) and clioquinol (chelation moiety).⁹³ **23** showed preferential and efficient inhibition activity in case of Cu^{2+} -directed $\text{A}\beta_{40}$ aggregation over Zn^{2+} -mediated or self-aggregated $\text{A}\beta_{40}$. Phenanthrene and *p*-stilbene-derived MFL, L2-b (**24**) targets $\text{A}\beta_{40}\text{-Cu}^{2+}/\text{Zn}^{2+}$ complex, a process which was thoroughly analysed by ion mobility mass spectroscopy (IM-MS).⁹⁴ **28** acts by metal chelation, dissolving toxic $\text{A}\beta_{40}$ oligomeric species and also as an antioxidant (TEAC = 2.3 ± 0.2). *In vivo* studies have indicated that **24** can cross BBB, prevent cognitive decline and decreases the $\text{A}\beta$ load in the brain of 5XFAD mice model for AD. L2-b was further modified by linking it to 2-[(8-quinolinylamino)methyl]phenol to obtain ligand ML (**25**).⁹⁵ Ligand **25** accommodates copper in the distorted square-planar form preventing the copper redox cycle and has strong binding affinity with both $\text{A}\beta_{40}$ monomers (binds to F4, R5, V12, and Q15 amino acid residues of $\text{A}\beta$) and its aggregates (quinoline ring interact with F19 and dimethylamino group with I32 and L34 residues through van der Waals interactions). The docking studies showed that ligand **25** binds between the steric zipper of $\text{A}\beta_{40}$ distorting hydrogen bonding and its elongation to toxic aggregates. It also modulates toxic oligomer formation, exhibits superior antioxidant property (TEAC = 0.86 ± 0.10) and displays neuroprotective nature in the $\text{A}\beta_{40}/\text{A}\beta_{40}$ -metal treated

neuroblastoma cells. On similar lines, Mirica *et al.* designed MFL L1 and L2 with its core structure derived from ThT, o-vanillin (A β recognition) and N-(2-pyridylmethyl)amine (metal chelating moiety). ThT bound to A β aggregates was displaced by L1 (135 ± 25 nM) and L2 (36 ± 6 nM) showing their high binding affinity.⁹⁶ Inhibition and dissolution studies of A β showed prevention of fibril formation. Generally dissolution of fibrillar aggregates by the inhibitors or metal

chelators leads to the formation of non-toxic species. However, in the above case neurotoxic oligomeric species were obtained. Therefore, MFL should be carefully designed and studied *in vivo* to illustrate their non-toxic nature in both presence and absence of A β aggregates.

1.5.3 Enzyme inhibitors

There are large number of pathways guided by enzymes that affect the production and clearance of A β . In this section, we focus on enzyme inhibitors of β -secretase and γ -secretase, which are involved in APP processing to produce A β .

1.5.2.1 β -Secretase inhibitors. BACE1 (beta-site APP-cleaving enzyme 1) is a 501 amino acid type-I transmembrane aspartic protease. It controls nerve axonal myelination and muscle spindle formation via proteolytic processing of neuregulin 1. BACE1 cleavage of APP mostly occurs in endosomes with optimum protease activity at lower pH (pH = 5).⁹⁷ *In vivo* (mice) testing of β -secretase inhibitors (BSIs) have shown least effect on normal physiological functions implicating that BSIs use may have minimum side effects. In recent times, LY2886721, MK-8931 and E-2609 have completed phase 1 clinical trials and entered phase II trials.^{98,99} The inhibition of β -Secretase can cause many more adverse effects as, β -Secretase is involved in many other physiological functions of

cells.

1.5.2.2 γ -Secretase inhibitors. γ -Secretase is an intramembrane aspartyl protease composed of the subunits presenilins (PS), nicastrin, anterior pharynx defective 1 (APH-1), and presenilin enhancer 2 (PEN-2). Mutations in PS account for overproduction of amyloidogenic A β 42 and the majority of inherited forms responsible for early onset of AD. The role of γ -secretase in sequential cleavage of APP in the production of A β makes it an appealing therapeutic target for AD. Direct use of γ -secretase inhibitors has shown detrimental side effects as the enzyme is involved in many other critical functions like lymphocyte development and cell differentiation, among others. The concept of γ -secretase modulators (GSMs) was introduced to selectively modulate the APP cleaving site and prevent the production of neurotoxic A β 42 while still maintaining normal A β 40 concentration in the brain.²¹ Wood *et al.* performed high throughput screening to obtain sulfonamide based molecules as a novel GSM scaffold. Further, they performed structural optimization on the lead molecule to obtain a better modulator (**26**).¹⁰⁰ **26** showed improved cell potency, enhanced PKDM (pharmacokinetics and drug metabolism) and reduced A β 42 (IC₅₀ = 0.26 \pm 0.10 μ M) production in an *in vivo* model. Recently, Pettersson *et al.* introduced pyridopiperazine-1,6-dione ring into their previously designed GSM to enhance its ADME (absorption, distribution, metabolism and excretion) parameters like clearance, permeability and MDR efflux ratio.¹⁰¹ The outcome of such modification was molecule **27** which has shown reduced A β 42 levels (IC₅₀ = 101 nM) in guinea pig at 30 mg/kg dosed orally and its activity was directly linked with the binding to presenilin N-terminal fragment of γ -secretase complex.¹⁰² Based on a less potent GSM core structure an efficient anilinothiazole (**28**) GSM was optimized through varying spacer link

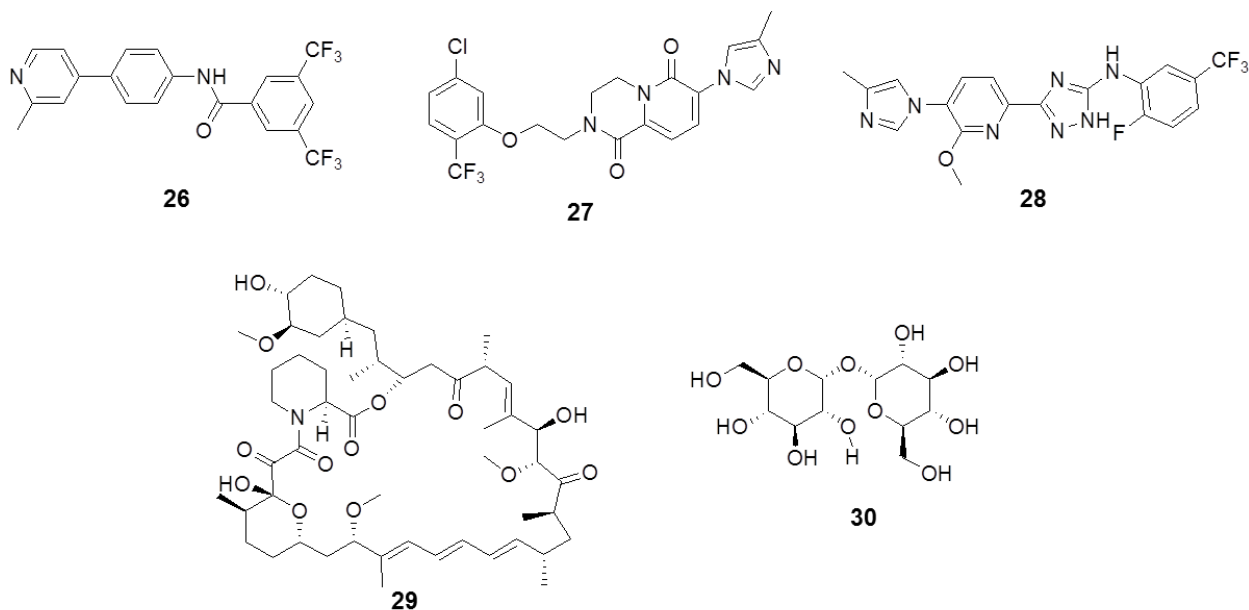


Figure 9. Secretase inhibitors and autophagy activators.

between the triazole ring and substituted aromatic ring. **28** displayed enhanced efficiency in reducing the A β 42 levels ($IC_{50} = 19$ nM) in both *in vitro* and *in vivo* models and had a superior ADME profile compared to its lead moiety.¹⁰³ Most of the recent works focus on designing GSM, but more efforts are needed to understand their mechanism of action on γ -secretase. The inhibition of γ -Secretase can cause many more adverse effects as, γ -Secretase is involved in many other physiological functions of cells.

1.5.4 Immunotherapy

The immune system of the body is capable of recognizing misfolded protein (A β or Tau) aggregates in the brain of AD patient. Immune system responds in two different forms of activation, innate and adaptive immunity. A β monomers are treated as normal by immune system with no immune response but once A β monomers aggregates to form large polymeric species, immune system is confused, which in turn activates immune cells as well as mass inflammation causing clearance of toxic A β aggregates. Immunotherapy is a therapeutic tool where antibodies are raised in a living organism against a specific

antigen. Antibodies are very specific and selective toward their targets making them efficient therapeutic tools for treating many pathological diseases. Most A β -directed immunotherapies are based on non-selective antibody that can bind to different forms of A β (monomers, oligomers and fibrils). Immunotherapy in AD patients is constrained by its poor brain penetration levels and non-specific binding to A β monomers and fibrils (high concentration in AD patient) over low concentration oligomers which are relevant in inducing toxicity.¹⁷ Immunotherapy becomes more relevant when oligomer-specific antibody is developed. Recently, Krafft *et al.* reported a selective; high affinity humanized antibody engineered into an IgG2 (ACU-193) for A β oligomeric (IC₅₀ = 17 nM) species. ACU-193 showed dose-dependent pharmacokinetics, biodistribution and the brain penetration in various AD models.¹⁰⁴ Similarly Pradier *et al.* developed SAR228810 humanized antibody engineered into an IgG4 which bound higher molecular weight soluble A β oligomers and fibrils with high affinity over monomeric A β and lower large molecular weight soluble A β oligomers.¹⁰⁵ Immunotherapy is a promising strategy but structure and BBB permeability has overshadowed their use as therapeutic drugs for the AD.

1.5.5 Autophagy activators

Autophagy is an intracellular degradation pathway involved in clearance of damaged organelles, misfolded proteins and recycling of cytosolic components during starvation condition.¹⁰⁶ In AD defective delivery of autophagosomes to lysosomes has been observed indicating down-regulation of autophagy (Figure 9).^{107, 108} Galvan *et al.* showed that inhibition of mTOR (regulate autophagy) by rapamycin (**29**) prevented AD-like cognitive deficits and lowered levels of A β 42 in the PDAPP transgenic mouse model.

These data indicate that inhibition of mTOR pathway may reduce A β 42 levels and hence, is a therapeutic target for AD.¹⁰⁹ Trehalose (**30**), a natural alpha-linked disaccharide has showed improvement in cognitive and learning ability, and A β deposit in hippocampus was reduced through upregulation of the autophagy process.¹¹⁰ Glycogen synthase kinase-3 (GSK) impairs lysosomal acidification and hinders autophagy. Treatment with L803-
mts a GSK inhibitor restored lysosomal acidification in 5XFAD mice brains. Inhibition of GSK enables clearance of A β and reactivation of mTOR.¹¹¹ Such upregulation of autophagy using small molecules is a promising approach for the elimination of misfolded protein aggregates. Therefore designing molecules that can upregulate autophagy for degrading deleterious A β aggregates is a useful and promising therapeutic strategy.

1.6 Objective

AD is most devastating illness that humankind is facing in the 21th century. Currently there are no reliable diagnostic tools to diagnosis the disease, because of which we are unable to treat patients in the early stage. Absence of appropriate techniques has hindered us from understanding the molecular mechanism of the disease progression in the patients, due to which we lack drugs that target core pathology involved in AD. Currently drugs available in market can only provide temporary relief, and not slow down or cure the disease. In this context, we designed and synthesized molecular probes as diagnostic tools for possible diagnosis of AD and therapeutic molecules (peptidomimetics, natural products and small molecules) targeting core pathology involved in AD (Figure 10).

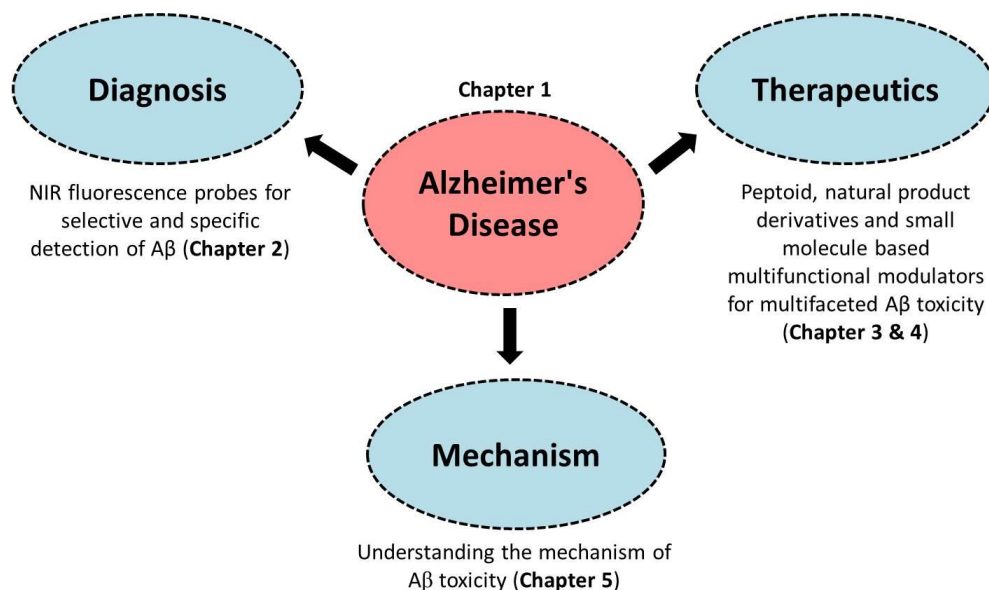


Figure 10. Thesis outline

1.7 References

- Selkoe, D. J., Folding proteins in fatal ways. *Nature* **2003**, *426*, 900-904.
- Aguzzi, A.; O'Connor, T., Protein aggregation diseases: pathogenicity and therapeutic perspectives. *Nat. Rev. Drug Discov.* **2010**, *9*, 237-248.
- DeToma, A. S.; Salamekh, S.; Ramamoorthy, A.; Lim, M. H., Misfolded proteins in Alzheimer's disease and type II diabetes. *Chem. Soc. Rev.* **2012**, *41*, 608-621.
- Rajasekhar, K.; Chakrabarti, M.; Govindaraju, T., Function and toxicity of amyloid beta and recent therapeutic interventions targeting amyloid beta in Alzheimer's disease. *Chem. Commun.* **2015**, *51*, 13434-13450.
- Brettschneider, J.; Tredici, K. D.; Lee, V. M. Y.; Trojanowski, J. Q., Spreading of pathology in neurodegenerative diseases: A focus on human studies. *Nat. Rev. Neurosci.* **2015**, *16*, 109-120.
- Ciechanover, A.; Kwon, Y. T., Degradation of misfolded proteins in neurodegenerative diseases: Therapeutic targets and strategies. *Exp. Mol. Med.* **2015**, *47*, e147.
- 2014 Alzheimer's disease facts and figures. *Alzheimer's & Dementia* **10**, e47-e92.
- Prince, M.; Bryce, R.; Albanese, E.; Wimo, A.; Ribeiro, W.; Ferri, C. P., The global prevalence of dementia: A systematic review and metaanalysis. *Alzheimer's & Dementia* **2013**, *9*, 63-75.
- Knowles, T. P. J.; Vendruscolo, M.; Dobson, C. M., The amyloid state and its association with protein misfolding diseases. *Nat. Rev. Mol. Cell Biol.* **2014**, *15*, 384-396.
- Thinakaran, G.; Koo, E. H., Amyloid Precursor protein trafficking, processing, and function. *J. Biol. Chem.* **2008**, *283*, 29615-29619.

11. Pearson, H. A.; Peers, C., Physiological roles for amyloid β peptides. *Journal of Physiology* **2006**, *575*, 5-10.
12. Jucker, M.; Walker, L. C., Self-propagation of pathogenic protein aggregates in neurodegenerative diseases. *Nature* **2013**, *501*, 45-51.
13. Karran, E.; Mercken, M.; Strooper, B. D., The amyloid cascade hypothesis for Alzheimer's disease: an appraisal for the development of therapeutics. *Nat. Rev. Drug Discov.* **2011**, *10*, 698-712.
14. Savelieff, M. G.; Lee, S.; Liu, Y.; Lim, M. H., Untangling amyloid β , Tau, and metals in Alzheimer's disease. *ACS Chem. Biol.* **2013**, *8*, 856-865.
15. Barnham, K. J.; Bush, A. I., Biological metals and metal-targeting compounds in major neurodegenerative diseases. *Chem. Soc. Rev.* **2014**, *43*, 6727-6749.
16. Yuan, J.; Venkatraman, S.; Zheng, Y.; McKeever, B. M.; Dillard, L. W.; Singh, S. B., Structure-Based Design of β -Site APP Cleaving Enzyme 1 (BACE1) Inhibitors for the treatment of Alzheimer's disease. *J. Med. Chem* **2013**, *56*, 4156-4180.
17. Wisniewski, T.; Goni, F., Immunotherapeutic approaches for Alzheimer's disease. *Neuron* **2015**, *85*, 1162-1176.
18. Bu, G., Apolipoprotein E and its receptors in Alzheimer's disease: pathways, pathogenesis and therapy. *Nat. Rev. Neurosci.* **2009**, *10*, 333-344.
19. Muller, U. C.; Zheng, H., Physiological functions of APP family proteins. *Cold Spring Harb Perspect Med.* **2012**, *2*, a006288.
20. Zheng, H.; Koo, E. H., Biology and pathophysiology of the amyloid precursor protein. *Mol. Neurodegener.* **2011**, *6*, 27.
21. Tate, B.; McKee, T. D.; Loureiro, R. M. B.; Dumin, J. A.; Xia, W.; Pojasek, K.; Austin, W. F.; Fuller, N. O.; Hubbs, J. L.; Shen, R.; Jonker, J.; Ives, J.; Bronk, B. S., Modulation of gamma-secretase for the treatment of Alzheimer's disease. *Int. J. Alzheimers Dis.* **2012**, *2012*, 210756.
22. Conicella, A. E.; Fawzi, N. L., The C-Terminal Threonine of A β 43 Nucleates toxic aggregation via structural and dynamical changes in monomers and protofibrils. *Biochemistry* **2014**, *53*, 3095-3105.
23. Roychaudhuri, R.; Yang, M.; Hoshi, M. M.; Teplow, D. B., Amyloid β -protein assembly and Alzheimer disease. *J. Biol. Chem.* **2009**, *284*, 4749-4753.
24. Hard, T., Amyloid fibrils: Formation, polymorphism, and inhibition. *J. Phys. Chem. Lett.* **2014**, *5*, 607-614.
25. Gurry, T.; Stultz, C. M., Mechanism of amyloid- β fibril elongation. *Biochemistry* **2014**, *53*, 6981-6991.

26. Marshall, K. E.; Marchante, R.; Xue, W.-F.; Serpell, L. C., The relationship between amyloid structure and cytotoxicity. *Prion* **2014**, *8*, 192-196.
27. Scheidt, H. A.; Morgado, I.; Huster, D., Solid-state NMR reveals a close structural relationship between amyloid- β protofibrils and oligomers. *J. Biol. Chem.* **2012**, *287*, 22822-22826.
28. Colvin, M. T.; Silvers, R.; Ni, Q. Z.; Can, T. V.; Sergeev, I.; Rosay, M.; Donovan, K. J.; Michael, B.; Wall, J.; Linse, S.; Griffin, R. G., Atomic resolution structure of monomorphic A β 42 amyloid fibrils. *J. Am. Chem. Soc.* **2016**, *138*, 9663-9674.
29. Wälti, M. A.; Ravotti, F.; Arai, H.; Glabe, C. G.; Wall, J. S.; Böckmann, A.; Güntert, P.; Meier, B. H.; Riek, R., Atomic-resolution structure of a disease-relevant A β (1-42) amyloid fibril. *Proc. Natl. Acad. Sci. U. S. A.* **2016**, *113*, E4976-E4984.
30. Hayden, E. Y.; Teplow, D. B., Amyloid β -protein oligomers and Alzheimer's disease. *Alzheimers Res. Ther.* **2013**, *5*, 60.
31. Carrillo-Mora, P.; Luna, R.; Colin-Barenque, L., Amyloid beta: Multiple mechanisms of toxicity and only some protective effects? *Oxidative Medicine and Cellular Longevity* **2014**, *2014*, 795375.
32. Bush, A. I., The metallobiology of Alzheimer's disease. *Trends Neurosci.* **2003**, *26*, 207-214.
33. Butterfield, D. A.; Swomley, A. M.; Sultana, R., Amyloid β -peptide (1-42)-induced oxidative stress in Alzheimer disease: Importance in disease pathogenesis and progression. *Antioxid. Redox Signal.* **2013**, *19*, 823-835.
34. Butterfield, D. A.; Sultana, R., Methionine-35 of A β (1-42): Importance for oxidative stress in Alzheimer disease. *J. Amino Acids* **2011**, *2011*, 10.
35. Maiti, P.; Lomakin, A.; Benedek, G. B.; Bitan, G., Despite its role in assembly, methionine 35 is not necessary for amyloid β -protein toxicity. *J. Neurochem.* **2010**, *113*, 1252-1262.
36. Al-Hilaly, Y. K.; Williams, T. L.; Stewart-Parker, M.; Ford, L.; Skaria, E.; Cole, M.; Bucher, W. G.; Morris, K. L.; Sada, A. A.; Thorpe, J. R.; Serpell, L. C., A central role for dityrosine crosslinking of Amyloid β in Alzheimer's disease. *Acta Neuropathol. Commun.* **2013**, *1*, 83.
37. Cassagnes, L.-E.; Herve, V.; Nepveu, F.; Hureau, C.; Faller, P.; Collin, F., The catalytically active copper-amyloid-beta state: Coordination Site responsible for reactive oxygen species production. *Angew. Chem. Int. Ed.* **2013**, *52*, 11110-11113.

38. Parthasarathy, S.; Yoo, B.; McElheny, D.; Tay, W.; Ishii, Y., Capturing a reactive state of amyloid aggregates: NMR-based characterization of copper-bound Alzheimer disease amyloid β -fibrils in a redox cycle. *J. Biol. Chem.* **2014**, *289*, 9998-10010.
39. Sharma, A. K.; Pavlova, S. T.; Kim, J.; Kim, J.; Mirica, L. M., The effect of Cu^{2+} and Zn^{2+} on the $\text{A}\beta_{42}$ peptide aggregation and cellular toxicity. *Metallomics* **2013**, *5*, 1529-1536.
40. Alies, B.; Sasaki, I.; Proux, O.; Sayen, S.; Guillon, E.; Faller, P.; Hureau, C., Zn impacts Cu coordination to amyloid- β , the Alzheimer's peptide, but not the ROS production and the associated cell toxicity. *Chem. Commun.* **2013**, *49*, 1214-1216.
41. Mayes, J.; Tinker-Mill, C.; Kolosov, O.; Zhang, H.; Tabner, B. J.; Allsop, D., β -Amyloid fibrils in Alzheimer disease are not inert when bound to copper ions but can degrade hydrogen peroxide and generate reactive oxygen species. *J. Biol. Chem.* **2014**, *289*, 12052-12062.
42. Tu, S.; Okamoto, S.-i.; Lipton, S. A.; Xu, H., Oligomeric $\text{A}\beta$ -induced synaptic dysfunction in Alzheimer's disease. *Mol. Neurodegener.* **2014**, *9*, 48.
43. Shankar, G. M.; Walsh, D. M., Alzheimer's disease: Synaptic dysfunction and $\text{A}\beta$. *Mol. Neurodegener.* **2009**, *4*, 48.
44. Ni, R.; Marutle, A.; Nordberg, A., Modulation of $\alpha 7$ nicotinic acetylcholine receptor and fibrillar amyloid- β interactions in Alzheimer's disease brain. *J. Alzheimer's Dis.* **2013**, *33*, 841-851.
45. Lee, L.; Dale, E.; Staniszewski, A.; Zhang, H.; Saeed, F.; Sakurai, M.; Fa, M.; Orozco, I.; Michelassi, F.; Akpan, N.; Lehrer, H.; Arancio, O., Regulation of synaptic plasticity and cognition by SUMO in normal physiology and Alzheimer's disease. *Sci. Rep.* **2014**, *4*, 7190.
46. Izzo, N. J.; Xu, J.; Zeng, C.; Kirk, M. J.; Mozzoni, K.; Silky, C.; Rehak, C.; Yurko, R.; Look, G.; Rishton, G.; Safferstein, H.; Cruchaga, C.; Goate, A.; Cahill, M. A.; Arancio, O.; Mach, R. H.; Craven, R.; Head, E.; LeVine, H.; Spires-Jones, T. L.; Catalano, S. M., Alzheimer's therapeutics targeting amyloid beta 1- 42 oligomers II: Sigma-2/PGRMC1 receptors mediate $\text{A}\beta_{42}$ oligomer binding and synaptotoxicity. *PLoS ONE* **2014**, *9*, e111899.
47. Kawahara, M.; Kuroda, Y., Molecular mechanism of neurodegeneration induced by Alzheimer's β -amyloid protein: channel formation and disruption of calcium homeostasis. *Brain Res. Bull.* **2000**, *53*, 389-397.
48. Zhao, L. N.; Long, H.; Mu, Y.; Chew, L. Y., The Toxicity of amyloid β oligomers. *Int. J. Mol. Sci.* **2012**, *13*, 7303-7327.
49. Tofoleanu, F.; Buchete, N.-V., Alzheimer $\text{A}\beta$ peptide interactions with lipid membranes: Fibrils, oligomers and polymorphic amyloid channels. *Prion* **2012**, *6*, 339-345.
50. Cai, Z.; Yan, L.-J.; Ratka, A., Telomere shortening and Alzheimer's disease. *NeuroMol. Med.* **2013**, *15*, 25-48.

51. Wang, J.; Zhao, C.; Zhao, A.; Li, M.; Ren, J.; Qu, X., New insights in amyloid beta interactions with human telomerase. *J. Am. Chem. Soc.* **2015**, *137*, 1213-1219.
52. Hedskog, L.; Zhang, S.; Ankarcrona, M., Strategic role for mitochondria in Alzheimer's Disease and cancer. *Antioxid. Redox Signal.* **2012**, *16*, 1476-1491.
53. Shi, C.; Zhu, X.; Wang, J.; Long, D., Intromitochondrial I κ B/NF- κ B signaling pathway is involved in amyloid β peptide-induced mitochondrial dysfunction. *J. Bioenerg. Biomembr.* **2014**, *46*, 371-376.
54. Wang, H.; Fan, L.; Wang, H.; Ma, X.; Du, Z., Amyloid β regulates the expression and function of AIP1. *J. Mol. Neurosci.* **2015**, *55*, 227-232.
55. Bashir, M.; Parray, A.; Baba, R.; Bhat, H.; Bhat, S.; Mushtaq, U.; Andrabi, K.; Khanday, F., β -Amyloid-evoked apoptotic cell death is mediated through MKK6-p66shc pathway. *NeuroMol. Med.* **2014**, *16*, 137-149.
56. Cuijpers, Y.; van Lente, H., Early diagnostics and Alzheimer's disease: Beyond 'cure' and 'care'. *Technol. Forecast. Soc. Change* **2015**, *93*, 54-67.
57. Adlard, P. A.; Tran, B. A.; Finkelstein, D. I.; Desmond, P. M.; Johnston, L. A.; Bush, A. I.; Egan, G. F., A review of β -amyloid neuroimaging in Alzheimer's disease. *Front. Neurosci.* **2014**, *8*.
58. Li, S.; He, H.; Cui, W.; Gu, B.; Li, J.; Qi, Z.; Zhou, G.; Liang, C.-m.; Feng, X.-y., Detection of A β plaques by a novel specific MRI probe precursor CR-BSA-(Gd-DTPA)_n in APP/PS1 transgenic mice. *Anat. Rec.* **2010**, *293*, 2136-2143.
59. Vlassenko, A. G.; Benzinger, T. L. S.; Morris, J. C., PET amyloid-beta imaging in preclinical Alzheimer's disease. *Biochim. Biophys. Acta* **2012**, *1822*, 370-379.
60. Marcus, C.; Mena, E.; Subramaniam, R. M., Brain PET in the diagnosis of Alzheimer's disease. *Clin. Nucl. Med.* **2014**, *39*, e413-e426.
61. Tong, H.; Lou, K.; Wang, W., Near-infrared fluorescent probes for imaging of amyloid plaques in Alzheimer's disease. *Acta Pharm. Sin. B* **2015**, *5*, 25-33.
62. Wang, C.; Yang, A.; Li, X.; Li, D.; Zhang, M.; Du, H.; Li, C.; Guo, Y.; Mao, X.; Dong, M.; Besenbacher, F.; Yang, Y.; Wang, C., Observation of molecular inhibition and binding structures of amyloid peptides. *Nanoscale* **2012**, *4*, 1895-1909.
63. Jarmuła, A.; Stępkowski, D., The β -sheet breakers and π -stacking. *J. Peptide Sci.* **2013**, *19*, 345-349.
64. Tjernberg, L. O.; Naslund, J.; Lindqvist, F.; Johansson, J.; Karlstrom, A. R.; Thyberg, J.; Terenius, L.; Nordstedt, C., Arrest of β -amyloid fibril formation by a pentapeptide ligand. *J. Biol. Chem.* **1996**, *271*, 8545-8548.

65. Soto, C.; Sigurdsson, E. M.; Morelli, L.; Asok Kumar, R.; Castano, E. M.; Frangione, B., β -sheet breaker peptides inhibit fibrillogenesis in a rat brain model of amyloidosis: Implications for Alzheimer's therapy. *Nat. Med.* **1998**, *4*, 822-826.
66. Lin, L.-x.; Bo, X.-y.; Tan, Y.-z.; Sun, F.-x.; Song, M.; Zhao, J.; Ma, Z.-h.; Li, M.; Zheng, K.-j.; Xu, S.-m., Feasibility of β -sheet breaker peptide-H102 treatment for Alzheimer's disease based on β -amyloid hypothesis. *PLoS ONE* **2014**, *9*, e112052.
67. Kaffy, J.; Brinet, D.; Soulier, J.-L.; Khemtamourian, L.; Lequin, O.; Taverna, M.; Crousse, B. t.; Ongeri, S., Structure-activity relationships of sugar-based peptidomimetics as modulators of amyloid β -peptide early oligomerization and fibrillization. *Eur. J. Med. Chem.* **2014**, *86*, 752-758.
68. Simon, R. J.; Kania, R. S.; Zuckermann, R. N.; Huebner, V. D.; Jewell, D. A.; Banville, S.; Ng, S.; Wang, L.; Rosenberg, S.; Marlowe, C. K., Peptoids: A modular approach to drug discovery. *Proc. Natl. Acad. Sci.* **1992**, *89*, 9367-9371.
69. Turner, J. P.; Lutz-Rechtin, T.; Moore, K. A.; Rogers, L.; Bhave, O.; Moss, M. A.; Servoss, S. L., Rationally designed peptoids modulate aggregation of amyloid-beta 40. *ACS Chem. Neurosci.* **2014**, *5*, 552-558.
70. Luo, J.; Abrahams, J. P., Cyclic peptides as inhibitors of amyloid fibrillation. *Chem. Eur. J* **2014**, *20*, 2410-2419.
71. Jensen, M.; Canning, A.; Chiha, S.; Bouquerel, P.; Pedersen, J. T.; Ostergaard, J.; Cuvillier, O.; Sasaki, I.; Hureau, C.; Faller, P., Inhibition of Cu-amyloid- β by using bifunctional peptides with β -sheet breaker and chelator moieties. *Chem. Eur. J.* **2012**, *18*, 4836-4839.
72. Zhang, Q.; Hu, X.; Wang, W.; Yuan, Z., Study of a bifunctional A β aggregation inhibitor with the abilities of anti-amyloid- β and copper chelation. *Biomacromolecules* **2016**, *17*, 661-668.
73. Marquez, M.; Blancas-Mejia, L. M.; Campos, A.; Rojas, L.; Castaneda-Hernandez, G.; Quintanar, L., A bifunctional non-natural tetrapeptide modulates amyloid-beta peptide aggregation in the presence of Cu(II). *Metallomics* **2014**, *6*, 2189-2192.
74. Doig, A. J.; Derreumaux, P., Inhibition of protein aggregation and amyloid formation by small molecules. *Curr. Opin. Struct. Biol.* **2015**, *30*, 50-56.
75. Ji, H.-f.; Zhang, H.-y., Multipotent natural agents to combat Alzheimer's disease. Functional spectrum and structural features. *Acta Pharmacol. Sin.* **2008**, *29*, 143-151.
76. Yanagisawa, D.; Ibrahim, N. F.; Taguchi, H.; Morikawa, S.; Hirao, K.; Shirai, N.; Sogabe, T.; Tooyama, I., Curcumin derivative with the substitution at C-4 position, but not curcumin, is effective against amyloid pathology in APP/PS1 mice. *Neurobiol. Aging* **2015**, *36*, 201-210.

77. Ehrnhoefer, D. E.; Bieschke, J.; Boeddrich, A.; Herbst, M.; Masino, L.; Lurz, R.; Engemann, S.; Pastore, A.; Wanker, E. E., EGCG redirects amyloidogenic polypeptides into unstructured, off-pathway oligomers. *Nat. Struct. Mol. Biol.* **2008**, *15*, 558-566.
78. Bieschke, J.; Herbst, M.; Wiglenda, T.; Friedrich, R. P.; Boeddrich, A.; Schiele, F.; Kleckers, D.; Lopez del Amo, J. M.; Gruning, B. A.; Wang, Q.; Schmidt, M. R.; Lurz, R.; Anwyl, R.; Schnoegl, S.; Fandrich, M.; Frank, R. F.; Reif, B.; Gunther, S.; Walsh, D. M.; Wanker, E. E., Small-molecule conversion of toxic oligomers to nontoxic β -sheet-rich amyloid fibrils. *Nat. Chem. Biol.* **2012**, *8*, 93-101.
79. Du, W.-J.; Guo, J.-J.; Gao, M.-T.; Hu, S.-Q.; Dong, X.-Y.; Han, Y.-F.; Liu, F.-F.; Jiang, S.; Sun, Y., Brazilin inhibits amyloid β -protein fibrillogenesis, remodels amyloid fibrils and reduces amyloid cytotoxicity. *Sci. Rep.* **2015**, *5*, 7992.
80. Sinha, S.; Lopes, D. H. J.; Du, Z.; Pang, E. S.; Shanmugam, A.; Lomakin, A.; Talbiersky, P.; Tennstaedt, A.; McDaniel, K.; Bakshi, R.; Kuo, P.-Y.; Ehrmann, M.; Benedek, G. B.; Loo, J. A.; Karner, F.-G.; Schrader, T.; Wang, C.; Bitan, G., Lysine-specific molecular tweezers are broad-spectrum inhibitors of assembly and toxicity of amyloid proteins. *J. Am. Chem. Soc.* **2011**, *133*, 16958-16969.
81. Wang, Q.; Yu, X.; Patal, K.; Hu, R.; Chuang, S.; Zhang, G.; Zheng, J., Tanshinones inhibit amyloid aggregation by amyloid- β peptide, disaggregate amyloid fibrils, and protect cultured cells. *ACS Chem. Neurosci.* **2013**, *4*, 1004-1015.
82. Scherzer-Attali, R.; Convertino, M.; Pellarin, R.; Gazit, E.; Segal, D.; Caflisch, A., Methylations of tryptophan-modified naphthoquinone affect its inhibitory potential toward A β aggregation. *J. Phys. Chem. B* **2013**, *117*, 1780-1789.
83. Mao, F.; Yan, J.; Li, J.; Jia, X.; Miao, H.; Sun, Y.; Huang, L.; Li, X., New multi-target-directed small molecules against Alzheimer's disease: a combination of resveratrol and clioquinol. *Org. Biomol. Chem.* **2014**, *12*, 5936-5944.
84. Budimir, A., Metal ions, Alzheimer's disease and chelation therapy. In *Acta Pharm.*, 2015; Vol. 61, pp 1-14.
85. Pramanik, D.; Ghosh, C.; Dey, S. G., Heme-Cu bound A β peptides: Spectroscopic characterization, reactivity, and relevance to Alzheimer's disease. *J. Am. Chem. Soc.* **2011**, *133*, 15545-15552.
86. Rosenberg, R. N., Metal chelation therapy for alzheimer disease. *Arch. Neurol.* **2003**, *60*, 1678-1679.
87. Hegde, M. L.; Bharathi, P.; Suram, A.; Venugopal, C.; Jagannathan, R.; Poddar, P.; Srinivas, P.; Sambamurthi, K.; Rao, K. J.; Scancar, J.; Messori, L.; Zecca, L.; Zatta, P., Challenges

associated with metal chelation therapy in Alzheimer's disease. *J. Alzheimers Dis.* **2009**, *17*, 457-468.

88. Gomes, L. M. F.; Vieira, R. P.; Jones, M. R.; Wang, M. C. P.; Dyrager, C.; Souza-Fagundes, E. M.; Da Silva, J. G.; Storr, T.; Beraldo, H., 8-Hydroxyquinoline schiff-base compounds as antioxidants and modulators of copper-mediated A β peptide aggregation. *J. Inorg. Biochem.* **2014**, *139*, 106-116.

89. Matlack, K. E. S.; Tardiff, D. F.; Narayan, P.; Hamamichi, S.; Caldwell, K. A.; Caldwell, G. A.; Lindquist, S., Clioquinol promotes the degradation of metal-dependent amyloid- β (A β) oligomers to restore endocytosis and ameliorate A β toxicity. *Proc. Natl. Acad. Sci.* **2013**, *111*, 4013-4018.

90. Mao, X.; Schimmer, A. D., The toxicology of clioquinol. *Toxicol. Lett.* **2008**, *182*, 1-6.

91. Lu, C.; Guo, Y.; Yan, J.; Luo, Z.; Luo, H.-B.; Yan, M.; Huang, L.; Li, X., Design, synthesis, and evaluation of multitarget-directed resveratrol derivatives for the treatment of Alzheimer's disease. *J. Med. Chem* **2013**, *56*, 5843-5859.

92. Kochi, A.; Eckroat, T. J.; Green, K. D.; Mayhoub, A. S.; Lim, M. H.; Garneau-Tsodikova, S., A novel hybrid of 6-chlorotacrine and metal-amyloid- β modulator for inhibition of acetylcholinesterase and metal-induced amyloid- β aggregation. *Chem. Sci.* **2013**, *4*, 4137-4145.

93. Savelieff, M. G.; Liu, Y.; Senthamarai, R. R. P.; Korshavn, K. J.; Lee, H. J.; Ramamoorthy, A.; Lim, M. H., A small molecule that displays marked reactivity toward copper-versus zinc-amyloid- β implicated in Alzheimer's disease. *Chem. Commun* **2014**, *50*, 5301-5303.

94. Beck, M. W.; Oh, S. B.; Kerr, R. A.; Lee, H. J.; Kim, S. H.; Kim, S.; Jang, M.; Ruotolo, B. T.; Lee, J.-Y.; Lim, M. H., A rationally designed small molecule for identifying an in vivo link between metal-amyloid- β complexes and the pathogenesis of Alzheimer's disease. *Chem. Sci.* **2015**, *6*, 1879-1886.

95. Lee, S.; Zheng, X.; Krishnamoorthy, J.; Savelieff, M. G.; Park, H. M.; Brender, J. R.; Kim, J. H.; Derrick, J. S.; Kochi, A.; Lee, H. J.; Kim, C.; Ramamoorthy, A.; Bowers, M. T.; Lim, M. H., Rational design of a structural framework with potential use to develop chemical reagents that target and modulate multiple facets of Alzheimer's disease. *J. Am. Chem. Soc.* **2014**, *136*, 299-310.

96. Sharma, A. K.; Pavlova, S. T.; Kim, J.; Finkelstein, D.; Hawco, N. J.; Rath, N. P.; Kim, J.; Mirica, L. M., Bifunctional compounds for controlling metal-mediated aggregation of the A β 42 peptide. *J. Am. Chem. Soc* **2012**, *134*, 6625-6636.

97. Vassar, R.; Kuhn, P.-H.; Haass, C.; Kennedy, M. E.; Rajendran, L.; Wong, P. C.; Lichtenthaler, S. F., Function, therapeutic potential and cell biology of BACE proteases: Current status and future prospects. *J. Neurochem.* **2014**, *130*, 4-28.

98. Menting, K. W.; Claassen, J. A. H. R., β -secretase inhibitor; a promising novel therapeutic drug in AD. *Front. Aging Neurosci.* **2014**, *6*, 1-9.
99. Rajendran, L.; Schneider, A.; Schlechtingen, G.; Weidlich, S.; Ries, J.; Braxmeier, T.; Schwille, P.; Schulz, J. B.; Schroeder, C.; Simons, M.; Jennings, G.; Knolker, H.-J.; Simons, K., Efficient Inhibition of the Alzheimer's Disease γ -Secretase by Membrane Targeting. *Science* **2008**, *320*, 520-523.
100. Chen, J. J.; Qian, W.; Biswas, K.; Yuan, C.; Amegadzie, A.; Liu, Q.; Nixey, T.; Zhu, J.; Ncube, M.; Rzasna, R. M.; Chavez Jr, F.; Chen, N.; DeMorin, F.; Rumfelt, S.; Tegley, C. M.; Allen, J. R.; Hitchcock, S.; Hungate, R.; Bartberger, M. D.; Zalameda, L.; Liu, Y.; McCarter, J. D.; Zhang, J.; Zhu, L.; Babu-Khan, S.; Luo, Y.; Bradley, J.; Wen, P. H.; Reid, D. L.; Koegler, F.; Dean Jr, C.; Hickman, D.; Correll, T. L.; Williamson, T.; Wood, S., Discovery of 2-methylpyridine-based biaryl amides as γ -secretase modulators for the treatment of Alzheimer's disease. *Bioorg. Med. Chem. Lett.* **2013**, *23*, 6447-6454.
101. Pettersson, M.; Johnson, D. S.; Humphrey, J. M.; am Ende, C. W.; Evrard, E.; Efremov, I.; Kauffman, G. W.; Stepan, A. F.; Stiff, C. M.; Xie, L.; Bales, K. R.; Hajos-Korcsok, E.; Murrey, H. E.; Pustilnik, L. R.; Steyn, S. J.; Wood, K. M.; Verhoest, P. R., Discovery of indole-derived pyridopyrazine-1,6-dione γ -secretase modulators that target presenilin. *Bioorg. Med. Chem. Lett.* **2015**, *25*, 908-913.
102. Pozdnyakov, N.; Murrey, H. E.; Crump, C. J.; Pettersson, M.; Ballard, T. E.; am Ende, C. W.; Ahn, K.; Li, Y.-M.; Bales, K. R.; Johnson, D. S., γ -Secretase modulator (GSM) photoaffinity probes reveal distinct allosteric binding sites on presenilin. *J. Biol. Chem.* **2013**, *288*, 9710-9720.
103. Velter, A. I.; Bischoff, F. o. P.; Berthelot, D.; De Cleyn, M.; Oehlich, D.; Jaroskova, L.; Macdonald, G.; Minne, G.; Pieters, S.; Rombouts, F.; Van Brandt, S.; Van Roosbroeck, Y.; Surkyn, M.; Trabanco, A. A.; Tresadern, G.; Wu, T.; Borghys, H.; Mercken, M.; Masungi, C.; Gijzen, H., Anilinothiazoles as potent gamma secretase modulators. *Bioorg. Med. Chem. Lett.* **2014**, *24*, 5805-5813.
104. Krafft, G.; Hefti, F.; Gouere, W.; Jerecic, J.; Iverson, K.; Walicke, P., ACU-193: A candidate therapeutic antibody that selectively targets soluble beta-amyloid oligomers. *Alzheimer's & Dementia* **2013**, *9*, P326.
105. Pradier, L.; Cohen, C.; Blanchard, V.; Debeir, T.; Barneoud, P.; Canton, T.; Menager, J.; Bohme, A.; Rooney, T.; Guillet, M.-C.; Cameron, B.; Shi, Y.; Naimi, S.; Ravetch, J.; Claudel, S.; Alam, J., SAR228810: An antiprotofibrillar beta-amyloid antibody designed to reduce risk of amyloid-related imaging abnormalities (ARIA). *Alzheimer's & Dementia* **2013**, *9*, P808-P809.
106. Zhu, X.-C.; Yu, J.-T.; Jiang, T.; Tan, L., Autophagy modulation for Alzheimer's disease therapy. *Mol. Neurobiol.* **2013**, *48*, 702-714.

107. Fleming, A.; Noda, T.; Yoshimori, T.; Rubinsztein, D. C., Chemical modulators of autophagy as biological probes and potential therapeutics. *Nat. Chem. Biol.* **2011**, *7*, 9-17.
108. Hochfeld, W. E.; Lee, S.; Rubinsztein, D. C., Therapeutic induction of autophagy to modulate neurodegenerative disease progression. *Acta Pharmacol. Sin.* **2013**, *34*, 600-604.
109. Spilman, P.; Podlitskaya, N.; Hart, M. J.; Debnath, J.; Gorostiza, O.; Bredesen, D.; Richardson, A.; Strong, R.; Galvan, V., Inhibition of mTOR by rapamycin abolishes cognitive deficits and reduces amyloid- β levels in a mouse model of Alzheimer's disease. *PLoS ONE* **2009**, *5*, e9979.
110. Du, J.; Liang, Y.; Xu, F.; Sun, B.; Wang, Z., Trehalose rescues Alzheimer's disease phenotypes in APP/PS1 transgenic mice. *J. Pharm. Pharmacol.* **2013**, *65*, 1753-1756.
111. Avrahami, L.; Farfara, D.; Shaham-Kol, M.; Vassar, R.; Frenkel, D.; Eldar-Finkelman, H., Inhibition of glycogen synthase kinase-3 ameliorates β -amyloid pathology and restores lysosomal acidification and mammalian target of rapamycin activity in the Alzheimer disease mouse model: In vivo and In vitro Studies. *J. Biol. Chem.* **2013**, *288*, 1295-1306.

Chapter 2

Diagnostic probes

Chapter 2A

**A thiazole-coumarin based high-affinity red fluorescence and
colorimetric probe for amyloid β aggregates**

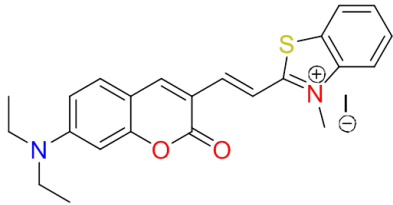
Accumulation of fibrillar aggregates (plaques) of A β peptides in the brain is one of the leading causes of Alzheimer's disease (AD).¹ The neurodegeneration and subsequent progressive deterioration in cognitive ability are hallmark symptoms of this incurable syndrome. The A β 42 peptide with 42 amino acids has been shown to be highly susceptible to aggregation and toxic behaviour among all the A β peptides (36-43).² Thus, A β 42 aggregate is an attractive biomarker to target for diagnosis and therapeutics of the AD. One of the biggest problems in the diagnosis of AD is the lack of effective methods for the selective detection of A β 42 aggregates.³ While diagnosis of AD is traditionally based on behavioral tests or cognition in patients, several imaging technologies such as positron emission tomography (PET),⁴ magnetic resonance imaging (MRI), and single-photon emission computed tomography (SPECT) have been developed for the detection of A β 42 aggregates.⁵ However, these technologies are still limited by several obstacles, like long data acquisition time, radioactive exposure, poor resolution and need of expensive equipment.⁶ Optical imaging using fluorescence and colorimetric probes has emerged as a potential alternative technique as it offers real-time, nonradioactive, high-resolution imaging for inexpensive diagnostics and screening of drugs for the AD. Thioflavin T (ThT) is the most extensively used fluorescence probe for the *in vitro* detection, and staining of A β aggregates.⁷ However, it suffers from poor selectivity and often leads to false detection.⁸ In the past few years, derivatives of oxazine,⁹ BODIPY,¹⁰ curcumin,¹¹ and benzothiazole¹² have been developed and used as fluorescence probes for A β aggregates.

An ideal fluorescence probe must exhibit certain characteristic properties to be used as a diagnostic probe for A β aggregates in AD viz., i) high specificity and strong binding affinity, ii) emission in the optical window of 500-750 nm with a large Stokes shift, and iii) switch-on fluorescence change upon binding with A β aggregates among other credentials. Further, mixed

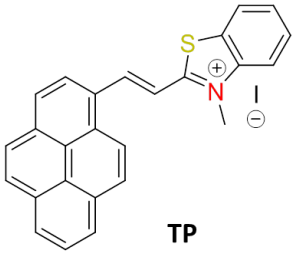
dementia is a condition in which abnormal characteristics of more than one type of dementia co-occur and, in such cases, determining the specific type of neurodegenerative disorder in the patient is very crucial. Therefore, there is an urgent need for developing probes which could selectively differentiate toxic aggregates responsible for the specific neurodegenerative disease. Unfortunately, there is a lack of studies on probes that selectively differentiate plaques responsible for any specific disorder. We lack fluorescence probes which selectively binds to specific aggregates, as most of them fluoresce upon binding to forced or artificially formed protein aggregates generally observed in all kinds of dementia.¹³ Recently, J. Yang *et al.* reported an amino naphthalene 2-cyanoacrylate based fluorescence probe, which discriminates between A β and Prion plaques by means of differential mode of binding attributed to microenvironments in the binding pockets.¹⁴ However, still, there is a need for many more probes which can selectively differentiate other important neurodegenerative disorders. Colorimetric detection of A β aggregates using antibodies has been demonstrated, but this technique is complicated and expensive. With this background, the need for developing selective fluorometric and colorimetric probes based on simple organic molecules which are easy to handle and offer quick detection is strongly indicated. In this context, we report a hemicyanine derivative as a high affinity, switch-on red fluorescence and colorimetric probe for A β 42 aggregates.

2.1 Design of hemicyanine probes

ThT has been extensively used to stain A β aggregates for the past few decades. This probe mainly consists of electron donating (*N,N*-dimethylaniline) and electron withdrawing (benzothiazole) moieties. The benzothiazole group is known to play a crucial role in the interaction of ThT on the surface of A β aggregates.^{15, 16} The major drawbacks of ThT and many other probes involve lack of selectivity and low affinity, which encouraged us to search for a the



TC



TP

Probe	Absorption maxima		Emission maxima		Molecular weight	logP	Hydrogen bond donor	Hydrogen bond acceptor
	without Aβ ₄₂	with Aβ ₄₂	without Aβ ₄₂	with Aβ ₄₂				
TC	537 nm	595 nm	638 nm	654 nm	391.14	3.2	3	1
TP	460 nm	462 nm	623 nm	626 nm	376.11	6.0	1	0

Figure 1. Molecular structures of probes **TC** [(benzo)thiazole-coumarin] and **TP** [(benzo)thiazole-pyrene] with their corresponding absorption and emission maxima in presence and absence Aβ₄₂ aggregates, and other properties.

new, more efficient fluorescence probe for Aβ aggregates based on the benzothiazole platform, with high selectivity and affinity. We chose to investigate the **TC** as a ‘fluorescence-ready’ probe for Aβ₄₂ aggregates (Figure 1). A benzothiazole conjugate with hydrophobic pyrene chromophore (TP) was also included in our studies (Figure 1). To our surprise, **TC** was found to exhibit highly enhanced fluorescence with superior selectivity and sensitivity for Aβ₄₂ aggregates with higher affinity compared to DNA. Furthermore, the **TC** and **TP** probes with molecular weights in the optimum range of ~350-550 Da, and possesses appropriate log P values and number of hydrogen bond donors and acceptors (Figure 1).¹⁷

2.2 Photophysical and molecular docking studies of TC with Aβ fibrillar aggregates

Initially, we studied the molecular interactions of **TC** and **TP** in the absence and presence of Aβ₄₂ aggregates through the absorption and emission measurements in PBS buffer (10 mM, pH = 7.4). Mature Aβ₄₂ fibrillar aggregates were prepared following the procedure reported in the

literature. **TC** and **TP** showed absorption bands at 537 nm and 460 nm, respectively, and very weak emissions at 638 nm and 623 nm, respectively, in the absence of A β 42 aggregates (Figure 2b and 1). In the presence of A β 42 aggregates (10 μ M), **TC** (2 μ M) showed a remarkable increase in the absorption maxima (hyperchromicity) with an enormous bathochromic shift ($\Delta\lambda_{\text{max}} \sim 59$ nm) relating to solution colour change from pale pink to purple. To elucidate the observed spectral changes of **TC**, we carried out concentration-dependent studies of A β 42 aggregates against a fixed concentration of **TC** (2 μ M). Initially, **TC** exhibited a decrease in absorption intensity in the concentration range 0-1 μ M of A β 42 aggregates. In addition, a shoulder band was observed for 0.8 μ M of A β 42 at 595 nm. Further, with increasing concentration of A β 42 aggregates (1 - 10 μ M) the shoulder band at 595 nm became more prominent with strong absorption (Figure 2a). The bathochromic shift in the absorption band of **TC**, in the presence of A β 42 aggregates, indicated their favourable interactions. The observed colorimetric change (pale pink to purple) as a consequence of binding of **TC** to A β 42 aggregates may be attributed to aggregate-induced changes in the intramolecular alignment and electronic structure of **TC**.^{18,19} In similar absorption studies with A β 42 aggregates; **TP** failed to exhibit any detectable change in absorption and in the colour of the solution.

In order to characterize the aggregate-specific shift in the absorption spectrum of **TC** and to propose its absorption maximum as a “colorimetric signature” for amyloidosis, its one photon absorption properties were computed by employing time-dependent density functional theory (at the B3LYP/TZVP level) in polar, nonpolar and fibril-like environments. In particular, the static and dynamic results were presented where the former one involves a single optimized geometry of **TC** in the specific solvent environments while the latter results are obtained as average over numerous configurations from Car-Parrinello QM/MM molecular dynamics. These models are

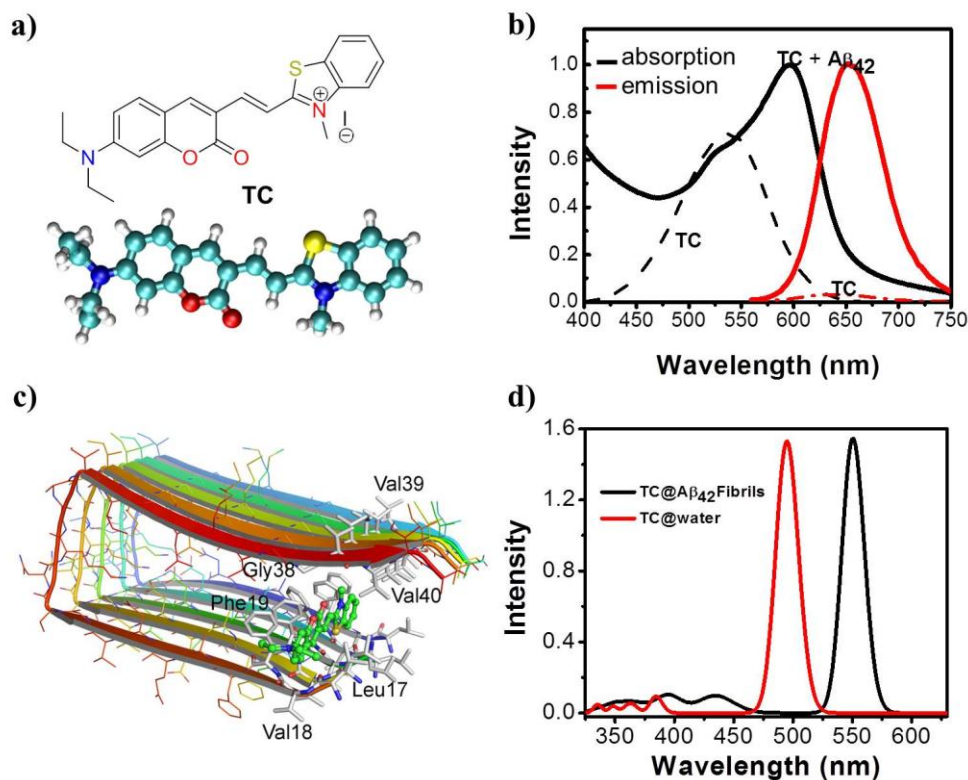


Figure 2. a) Molecular and energy minimized structures of probe TC. b) Absorption and emission (λ_{ex} = 537 nm) spectra of probe TC in presence and absence (dotted lines) of Aβ₄₂ fibrillar aggregates. c) The binding mode of TC in the entry site of the Aβ₄₂ fibril. The Aβ₄₂ fibril is shown in cartoon mode, the binding site residues in stick mode and TC in stick and ball mode (PyMol 1.3). d) The absorption spectra computed for TC@water and TC@ Aβ₄₂ fibril system using TD-DFT/MM models.

respectively referred to as TD-DFT/PCM and TD-DFT/MM.²⁰ The calculation only for the most stable binding mode of TC in fibril as shown in Figure 2c has been carried out.

The spectra computed only for dynamic models (by convoluting the absorption bands of six lowest energy excitations) are shown in Figure 2d. The absorption spectrum is characterized by a single dominant band in the visible region which is due to the lowest frequency excitation of π - π^* character. The absorption maximum (λ_{max}) for TC from the aforementioned models is listed in Table 1 along with the experimental results which show a red shift by 58 nm for the TC probe going into the fibril-like environment. The simplistic polarizable continuum model reproduces the trend of a red-shift in the absorption spectra of TC when going from water-like to non-polar

Table 1. The absorption maximum in nm (with oscillator strength shown in parenthesis) for **TC** in different micro-environment as predicted from TD-DFT/PCM, and TD-DFT/MM approaches.

Method	TC/chloroform	TC/fibril	TC/water	Shift, nm
Static (TD-DFT/PCM)	528(1.9)	-	514 (1.8)	14
Dynamic (TD-DFT/MM)	-	551 (1.6)	495 (1.5)	56
Experiment	561	595	537	58

chloroform environment even though the size of the shift is small (14 nm) when compared to experiment (24 nm). Based on this result, it can be suggested that the hydrophilic-like to hydrophobic-like change in the microenvironment may be a feasible mechanism for the fibril-induced red-shift in the absorption spectra of **TC**. The more sophisticated TD-DFT/MM approach which accounts for electrostatic and polarization interactions between **TC** and its fibril-like and aqueous environment also confirmed this and reproduced the red shift (56 nm) in excellent agreement with experiment. Usually, the change in the microenvironment alters the molecular structure and conformation of the probe which also significantly contributes to the shift in the spectra.²⁰ For this reason, we investigated the fibril-induced changes in conformation and molecular structure (along with the conjugation pathway) of **TC**, and interestingly this does not change significantly) and so only contributes to the shift by 4 nm. The absolute λ_{\max} is underestimated in our models, which refers to limitations of the QM model itself. Our motivation though is to explain the possible origin for the observed red shift due to change in environment (aqueous to fibril), something that is allowed by the excellent reproduction of the red shift by the

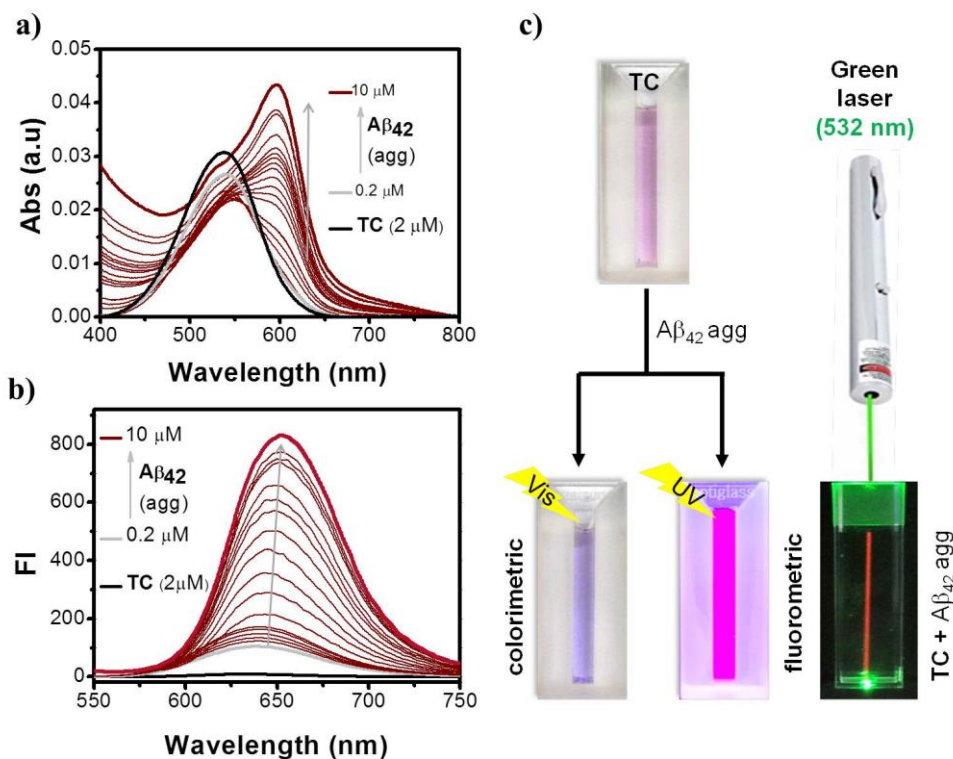


Figure 3. a) Absorption (Abs) spectra of probe **TC** ($2 \mu\text{M}$) with increasing concentration of $\text{A}\beta_{42}$ aggregates ($0.2, 0.4, 0.6, 0.8, 1.0, 1.2, 1.4, 1.6, 1.8, 2.0, 2.5, 3.0, 3.5, 4.0, 4.5, 5.0, 6.0, 7.0$ and $10.0 \mu\text{M}$). b) Emission (FI: fluorescence intensity) spectra ($\lambda_{\text{ex}} = 537 \text{ nm}$) of probe **TC** ($2 \mu\text{M}$) with increasing concentration of $\text{A}\beta_{42}$ fibrillar aggregates ($0.2, 0.4, 0.6, 0.8, 1.0, 1.2, 1.4, 1.6, 1.8, 2.0, 2.5, 3.0, 3.5, 4.0, 4.5, 5.0, 6.0, 7.0$ and $10.0 \mu\text{M}$). c) Photographs of **TC** and **TC** ($2 \mu\text{M}$) + $\text{A}\beta_{42}$ fibrillar aggregates ($15 \mu\text{M}$) samples illuminated under visible and UV light (365 nm), and **TC** ($2 \mu\text{M}$) + $\text{A}\beta_{42}$ fibrillar ($15 \mu\text{M}$) illuminated with a green laser (532 nm) shows a red beam in the sample solution.

more advanced TD-DFT/MM model. The characterization of the microenvironment of **TC** binding site clarifies its hydrophobic nature, and we can attribute the change in the hydrophilic-like to the hydrophobic-like environment around **TC** when it binds to the fibril as the responsible factor for the red shift.

Subsequently, we performed fluorescence titration experiments to probe the response of **TC** in the presence of $\text{A}\beta_{42}$ aggregates. The emission spectrum of **TC** ($2 \mu\text{M}$) exhibited a ~ 30 -fold fluorescence enhancement ($E_{\text{max}} = 654 \text{ nm}$), with a quantum yield of 40% upon binding to aggregates (Figure 3). Again, **TP** did not show any detectable change in the fluorescence

behaviour in the presence of A β 42 aggregates. The switch-on red fluorescence of **TC** is a typical behaviour of cyanine-based probes, which are known to form twisted intramolecular charge transfer (TICT) complexes in the excited state and exhibit fluorescence emission in response to a surrounding environment.²¹ **TC** probe alone is non-fluorescence in buffer due to internal non-radiative molecular twisting and self-aggregation whereas the intramolecular twisting is restricted upon binding to A β 42 aggregates leading to enhanced (~30-fold) red fluorescence.

2.3 Calculation of binding parameters

We calculated the binding constant by studying the fluorescence response with varying concentration of **TC** against a fixed concentration of A β 42 aggregates (dose-dependent saturation assay). The obtained standard saturation curve was fitted to a single-binding site, which gave a dissociation constant K_d of 58 ± 1.2 nM (The association constant was calculated to be $K_a = 1.72 \times 10^7$ M⁻¹ for 2 μ M of A β 42 aggregates) (Figure 4a). Notably, our recent study showed that AT-selective binding of **TC** to a DNA duplex generates a ~16-fold fluorescence enhancement and K_d in the micromolar range (10 μ M). Remarkably, the current study reveals a ~30-fold fluorescence enhancement of **TC** when it binds A β 42 aggregates with K_d in the nanomolar (58 nM) range indicating that a much higher binding affinity of **TC** towards A β 42 aggregates compared to DNA.²² To further evaluate high affinity of the probe **TC** towards A β 42 aggregates compared to DNA, we performed a competitive binding experiment. Notably, there is a clear difference in the absorption and emission maxima of **TC** bound to DNA and A β 42 aggregates. The competitive binding experiment is based on the fact that probe **TC** binding to either A β 42 aggregates or DNA show characteristic changes in both absorption and emission spectra corresponding to the probe and changes observed in each case is substantially different. First, probe **TC** was, saturated with excess DNA (calf thymus) which showed the characteristic

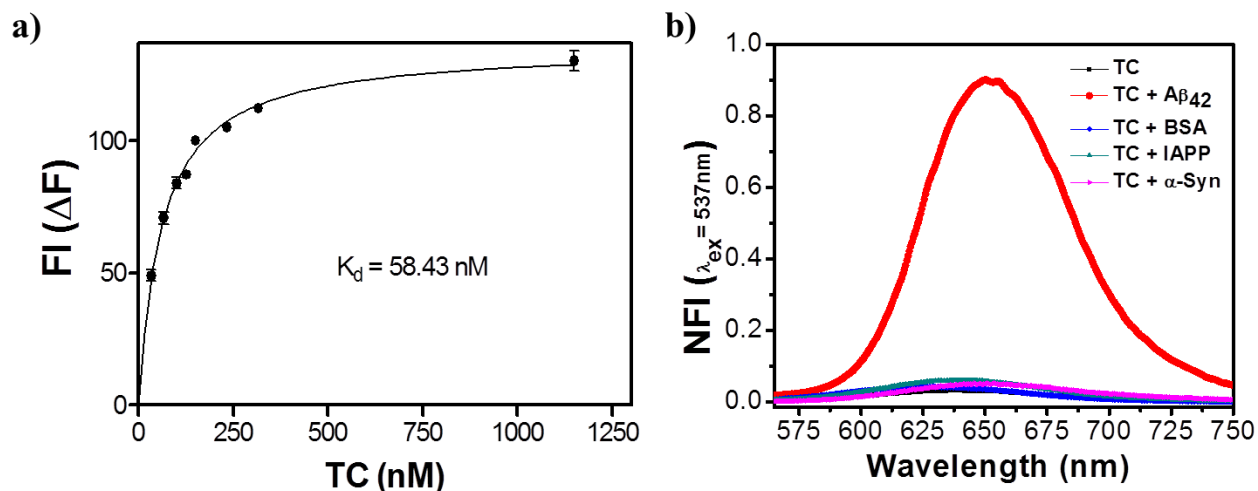


Figure 4. a) Plot of the difference in fluorescence intensity (ΔF) as a function of the concentration of TC in the presence of A β 42 fibrillar aggregates (2 μ M) in solutions (10 mM PBS). b) Normalized fluorescence intensity (NFI) of TC upon interaction with aggregates of A β 42 (5 μ M), α -synuclein (α -Syn) (20 μ M), amylin (IAPP) (20 μ M) and hydrophobic protein bovine serum albumin (BSA).

changes in both absorption and emission spectra of TC corresponding to DNA binding (Figure 5). When this TC bound DNA sample was further treated with A β 42 aggregates (10 μ M, incubate for 15 min), characteristic changes in both absorption and emission spectra were observed which are evidently similar to absorption and emission features corresponding to TC bound A β 42 aggregates (Figure 3b). This competitive binding experiment highlights the fact that in the presence of both A β 42 aggregates and DNA, TC preferably binds to A β 42 aggregates over DNA. In addition, the K_d of A β 42 aggregates bound TC is very low compared to that of the control probes ThT (\sim 0.8 μ M) and Congo red (\sim 1.1 μ M) confirming the superiority of the TC probe in terms of binding affinity towards A β 42 aggregates.

2.4 TC selectivity towards A β fibrillar aggregates

Further to examine the selectivity of TC towards A β 42 aggregates, we performed fluorescence studies in the presence of intracellular protein content bovine serum albumin (BSA) and fibrillar aggregates of α -synuclein (α -Syn) and islet amyloid polypeptide (IAPP, amylin) implicated in

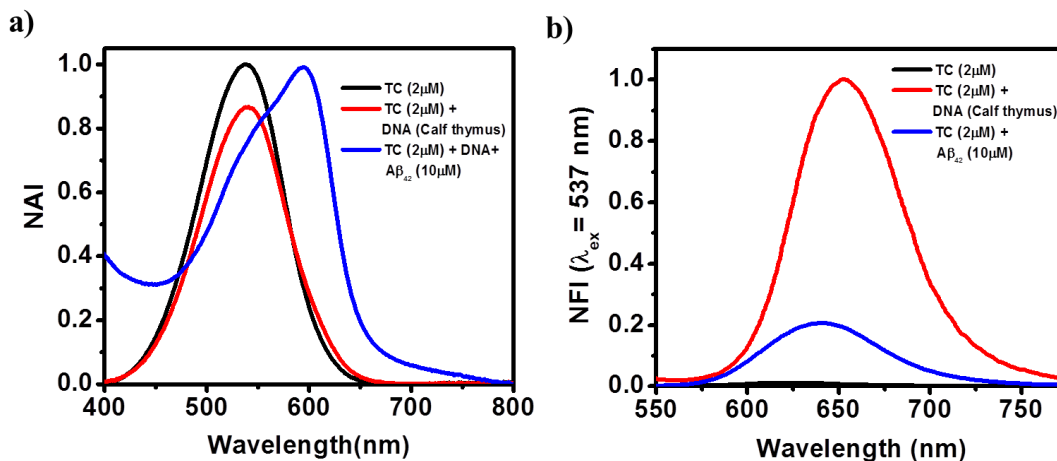


Figure 5. Competitive binding assay. a) Absorption spectra of probe **TC**, **TC** bound with DNA (Calf thymus) and the addition of A β 42 (10 μ M) aggregates to the same sample, showing a red shift with a new band at 595 nm, normalized absorbance intensities (NAI). b) Emission spectra of probe **TC**, **TC** when treated with DNA (Calf thymus) and the addition of A β 42 (10 μ M) aggregates to the same sample, shows better enhancement in fluorescence when compared to **TC** bound to DNA, normalized fluorescence intensities (NFI).

Parkinsons disease and type II diabetes, respectively. Incubation of **TC** with BSA, α -Syn aggregates and IAPP aggregates (20 μ M) did not lead to significant fluorescence enhancements confirming the preferential selectivity of the probe towards A β 42 aggregates over other proteins and peptide aggregates (Figure 4b).

2.5 Binding site determination and FRET studies of **TC** bound to A β fibrillar aggregates

To gain further insight into the binding affinity of the **TC** probe, a displacement assay was performed against ThT-bound A β 42 aggregates. The well-separated emission spectra of ThT (green region) and **TC** (red region) made it possible to observe fluorescence changes corresponding to individual probes during the displacement experiments. Remarkably, a gradual addition of **TC** to the ThT/A β 42 aggregate complex (ThT: 5 μ M and A β 42:10 μ M) resulted in a steady decay in fluorescence at 483 nm ($\lambda_{\text{ex}}= 450$ nm) and a corresponding enhancement in the emission intensity at 654 nm ($\lambda_{\text{ex}}= 537$ nm). This clearly suggested an effective displacement of ThT by **TC** owing to the formation of a much stronger **TC**/A β 42 aggregate complex (Figure 7a).

An interesting observation was made during the titration studies where spectral features corresponding to emission of **TC** (at 654 nm) were observed upon excitation of the sample (**TC/ThT/A β 42 aggregates**) at 450 nm (ThT excitation wavelength). Addition of **TC** (33 nM to 10.233 μ M) to the ThT/A β 42 aggregates complex showed a gradual decrease in the fluorescence emission at 483 nm (ThT) as expected. However, upon 450 nm (ThT) excitation, fluorescence was also observed at 654 nm (**TC**) with a slight red shift. The fluorescence intensity of this unprecedented emission band (**TC**) decreased slowly with further increase in the concentration of added **TC** and finally reached a constant value (Figure 6a & 7b). These changes in the emission characteristics, particularly the fluorescence emission of **TC** upon excitation corresponding to ThT is attributed to fluorescence resonance energy transfer (FRET) between the A β 42 aggregates bound to ThT and **TC**. Evidently, the emission spectrum of ThT significantly overlaps with the absorption spectrum of **TC** making them a suitable donor-acceptor pair on the aggregate surface (Figure 6).²³ At the beginning of the titration, **TC** binds to the ThT/A β 42 aggregate complex by partially displacing ThT, leading to FRET between bound ThT (donor)

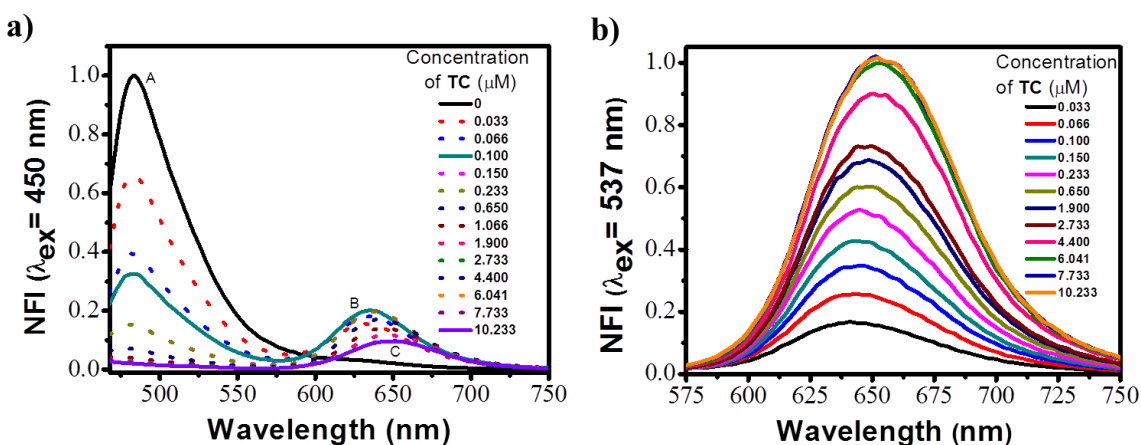


Figure 6. FRET and displacement assay. a) Normalized fluorescence intensities (NFI) of ThT and **TC** (λ_{ex} at 450 nm; fluorescence at 483 nm and ~654 nm) upon titration of a ThT/ A β 42 aggregate complex (ThT, 5 μ M/A β 42 aggregates, 10 μ M) with **TC**. b) Normalized fluorescence intensities (NFI) of **TC** (λ_{ex} at 537 nm; fluorescence measured at ~654 nm) upon titration of a ThT/ A β 42 aggregate complex with **TC**.

and **TC** (acceptor) (Figure 4b). For concentrations of **TC** > 150 nM, displacement of ThT by **TC** resulted in a decreased FRET-fluorescence of **TC** (Figure 7b). However, the FRET-based fluorescence at 654 nm was not quenched completely due to persistent residual ThT-**TC** pairs on an A β 42 aggregate (Figure 6b). The quenching of fluorescence intensity of ThT (at 483 nm) to its basal level indicates that **TC** binds to similar primary binding pockets of A β 42 aggregates occupied by ThT. On the other hand, excitation at 537 nm (**TC**) showed a gradual increase in fluorescence independent of ThT displacement, confirming the presence of multiple binding sites for **TC** on A β 42 fibrillar aggregates. The displacement of ThT was almost instantaneous and did not require any incubation time. The addition of **TC** (1 μ M) to the ThT (10 μ M)/ A β 42 (50 μ M) complex led to a complete change in emission colour of the sample, from green to bright pinkish red, as seen under UV-light illumination ($\lambda_{\text{ex}} = 365$ nm). The addition of excess ThT (50 μ M) did not displace **TC** from its complex with A β 42 aggregates owing to the high binding constant. The A β 42 aggregates stained with **TC** retained red fluorescence even after 50 days of ageing, thus, further indicating the high binding affinity and non-dissociative nature of **TC** upon binding to A β 42 aggregates (Figure 8).

In order to get a microscopic picture of the **TC** to fibril binding, we carried out a molecular docking study. In agreement with experimental indications, our study shows that there are multiple binding sites (such as entry cleft and surface) in the fibril accessible for binding of **TC** (Figure 2c). However, the most favourable binding site was identified in the entry section formed by Leu17, Val18, Phe19, Gly38, Val39 and Val40. The binding affinity calculated by AutoDock is the highest in this site (about -8.5 kcal/mol), whereas, on other sites, it is in the range of -6.0 ~ -8.0 kcal/Mol. A flexible molecular model for **TC** during the docking yields a binding affinity equivalent to -9.86 kcal/mol which corresponds to K_d 55.5 nM (which is in good agreement with

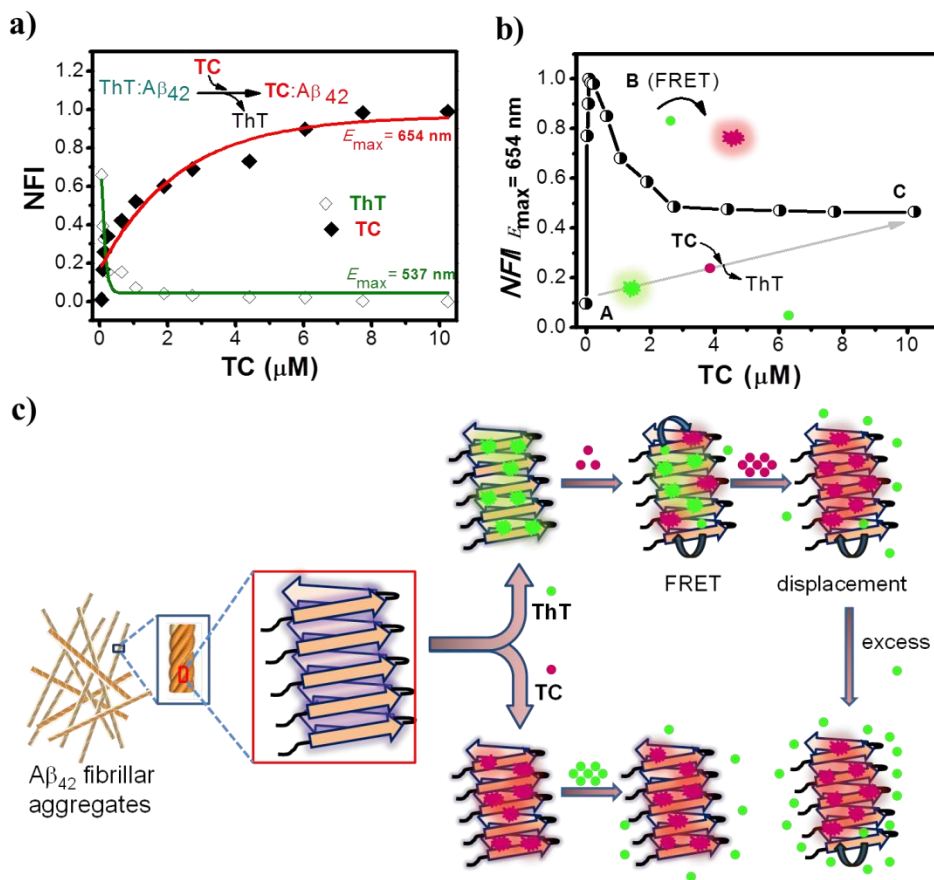


Figure 7. Displacement assay. a) Titration of **TC** to ThT/Aβ42 fibrillar aggregate complex (ThT, 5 μM/Aβ42 fibrils, 10 μM) in 10 mM PBS buffer solution. High-affinity **TC** effectively displaces ThT from the ThT/Aβ42 fibrillar aggregate complex, as monitored by the decrease in fluorescence emission at 483 nm (◇ green trace, $\lambda_{ex} = 450$ nm) and a corresponding increase in fluorescence emission at 654 nm (◆ red trace, $\lambda_{ex} = 537$ nm). b) In displacement assay (a) emission of **TC** monitored at 654 nm (E_{max}) upon excitation at 450 nm (λ_{ex} of ThT). Region A: ThT/Aβ42 fibrillar aggregate complex. Region B: **TC**/ThT/Aβ42 fibrillar aggregate complex, at low concentration **TC** coexists with ThT leading FRET between them. Region C: **TC** displaces ThT, with residual ThT (possibly in the inner cleft of the Aβ42 fibril) which leads to residual FRET. c) Proposed model for the **TC** displacement of ThT and FRET between them on the Aβ42 fibrils. NFI: Normalized fluorescence intensity.

experimental data). As **TC** is positively charged, it is unfavourable to bind in the inner sites which are fully buried, and the partially buried entry site is more favourable. Figure 2c shows that **TC** is clamped in the entry site mainly through hydrophobic interaction with Leu17 and Val39 through π - π stacking interaction with the phenyl ring of Phe19. Water molecules can also enter this site to solvate the positive charge of **TC**. It is relevant to note that all the amino acids from

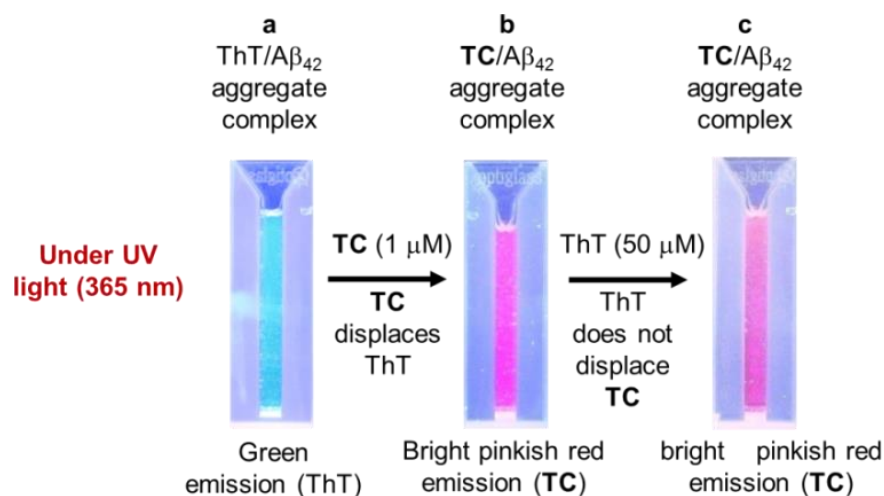


Figure 8. Photographs of ThT (10 μM)/ Aβ₄₂ (50 μM) aggregates complex, after adding TC (ThT displacement) b) and further addition of excess ThT (c) respectively, illuminated under UV light (365 nm).

this binding pocket is hydrophobic and hence we believe that the red shift in the spectra is due to the change from hydrophilic to hydrophobic like micro-environment around the probe. Further, the bulky nature of the diethyl amino group makes it impossible for the TC probe to become buried inside the binding site, rather it is partly exposed to the solvent environment (Figure 9). Figures 9a and 9b show all possible binding sites available for TC and ThT in the fibril. The TC binds to the entry cleft, inner core and surface binding sites while ThT binds only to the entry cleft and the surface binding sites which have to be attributed to the larger van der Waals surface associated with the latter molecule. Due to the larger binding affinity of TC towards the amyloid peptide, it can replace the ThTs in the entry cleft and other surface binding sites. However, ThT in the core sites cannot be displaced by TC and these, therefore, contribute to the population of residual ThT-TC pairs on Aβ₄₂ aggregate contributing to the significant FRET intensity as discussed above. Additionally, we performed docking studies of TC with α-synuclein (PDB code: 4R0U) and IAPP (PDB code: 2KIB) fibrils. It is found that TC can only be docked to the surface or the flanks of these two fibrils. It cannot be docked into the core sites (in particular to

entry cleft site) as in the case of the A β 42 fibril. The docking scores (empirical binding free energies) of TC with α -synuclein and IAPP are in the range between -5.0~-7.0 kcal/mol, which is much lower (magnitude) than that with the A β 42 fibril in the entry site (-8.5 kcal/mol). This result suggests that TC binds much more favourably with A β 42 fibril than with α -synuclein and IAPP (Figure 10).

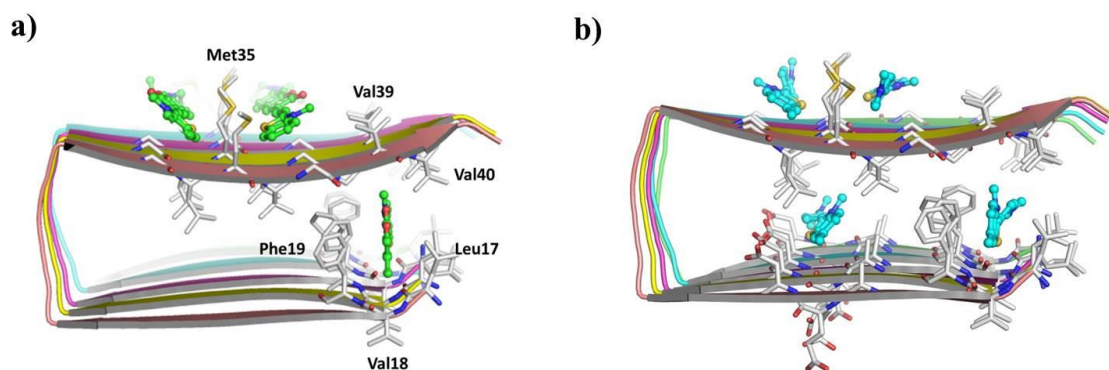


Figure 9. Docking results of a) TC and b) ThT with A β 42 fibril (all binding sites are shown). The fibril is shown in cartoon mode, the binding site residues in stick mode and TC or ThT in stick and ball mode.

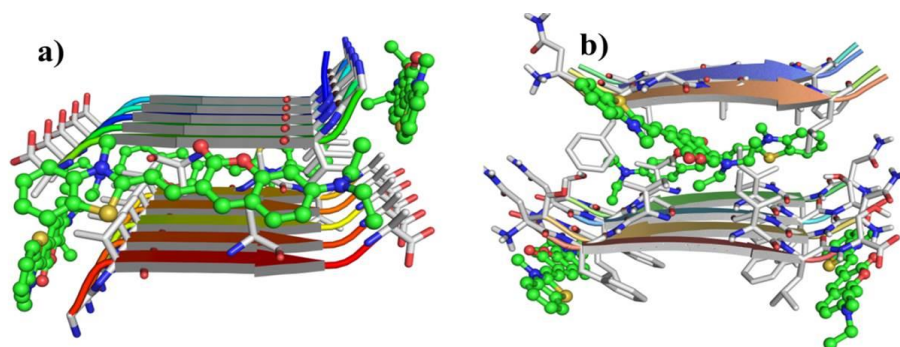


Figure 10. Docking mode of TC with α -synuclein (A) and IAPP (B) fibril. TC is shown in ball and stick model, the protein in cartoon mode and the residues in contact with TC are in stick mode.

2.6 Conclusion

We demonstrated that the hemicyanine-based benzothiazole-coumarin (TC) probe binds to A β 42 aggregates with nanomolar affinity ($K_a = 1.72 \times 10^7 \text{ M}^{-1}$). The probe showed switch-on red fluorescence with a large Stokes shift ($\sim 117 \text{ nm}$) upon binding to A β 42 aggregates along with a

typical colorimetric response which can be attributed to a change in the dielectric nature of micro-environment around **TC** from hydrophilic-like to hydrophobic-like. The **TC** probe also showed specificity as it did not interact with other abnormal protein aggregates of α -Syn and IAPP. Owing to its high binding affinity, the **TC** probe displaced the ThT probe bound to A β 42 aggregates, conversely increasing concentrations of ThT could not displace **TC** bound to A β 42 aggregates. The binding site in the A β 42 fibril for **TC** has been revealed from molecular docking studies. We propose that optimization of **TC** as a lead probe for A β 42 aggregates may afford novel, useful optical-based diagnostic probe for Alzheimer's disease.

Chapter 2B

**A β plaque-selective NIR fluorescence probe to differentiate Alzheimer's
disease from tauopathies**

Protein misfolding and aggregation initiate several neurodegenerative diseases. For instance, misfolding and accretion of A β , α -Syn, tau, IAPP, polyglutamine and superoxide dismutase are considered as causative factors for Alzheimer's, tauopathies, diabetes Huntington's, Parkinson's and amyotrophic lateral sclerosis diseases, respectively.^{2,24,25} AD is the most common and dominant form of dementia, which affects millions of people around the world.¹ Misfolded A β peptide (predominantly A β 42) and hyperphosphorylated tau protein undergo aggregation to form insoluble A β plaques and NFTs, respectively, in the brain, which are the hallmarks of AD.²⁴⁻²⁶ However, tau and NFTs are independently considered as causative factors in many other neurological disorders and tauopathies that include progressive supranuclear palsy, and frontotemporal dementia among others.²⁷ Therefore, selective detection of A β plaques over NFTs and other similar protein aggregates is critical for detecting, monitoring and distinguishing the AD from tau-related neurological disorders and mixed dementia.³ Currently, AD diagnosis is mostly based on the assessment of the cognitive state of the patients, which means the disease is already in an advanced stage, and the brain irreversibly degenerates.^{28,29} The protein aggregates implicated in various diseases mostly share a common β -sheet structure, which makes it difficult to develop selective probes for specific bio-structures.³⁰ Many of the reported probes bind to different protein aggregates without specificity and are not suitable for selectively detecting and diagnosing an individual disease. There is an immense need to develop toxic aggregate-specific imaging agents or tracers, which offers realistic avenues for developing diagnostics to understand the disease progression and study the effect of therapeutic agents on a specific disease condition. In recent times, PET, SPECT and MRI-based techniques have been developed for detecting and imaging A β plaques in the brain.³¹ While PET imaging is a valuable tool to image protein aggregates, it is expensive and hazardous to human health due to the use of radio-labelled

nuclei.⁵ Consequently, much attention has been focused on the development of NIR fluorescence probes owing to their easy synthesis, non-invasive nature, low cost, long shelf-life, minimal interference from autofluorescence and greater penetration depth to extract information from deep inside the specimen; these attributes make them ideal candidates as diagnostic, and imaging agents for toxic A β aggregates.^{6,9,14,32-39} Herein, we report a low molecular weight (>600 Da) coumarin-quinoline (**CQ**) conjugate-based NIR fluorescence probe for selective detection of A β fibrillar aggregates, and its preferential staining of A β plaques in the human brain tissue over NFTs (Figure 11).

2.7 Photophysical and molecular docking studies of CQ with A β fibrillar aggregates

The photophysical properties of **CQ** (2 μ M) were investigated in PBS buffer (10 mM, pH = 7.4) (Figure 11e). The absorption spectrum showed a broad absorption band with absorption maxima (λ_{ex}) at 516 nm. Upon excitation at 516 nm, **CQ** exhibited a feeble fluorescence band with emission maxima (λ_{em}) at 664 nm. In the presence of A β fibrillar aggregates (10 μ M), **CQ** exhibited a red shift of 5 nm in the absorption maxima (521 nm) and a blue shift of 10 nm in the emission maxima (654 nm). Remarkably, **CQ** (2 μ M) exhibited 100-fold fluorescence enhancement in the presence of A β fibrillar aggregates (10 μ M). The quantum yield of **CQ** in PBS buffer (10 mM, pH = 7.4) was 0.08, which increased to 0.36 upon binding to A β 42 fibrillar aggregates. The observed fluorescence enhancement of **CQ** can be attributed to the restricted torsional motion of the probe upon binding to A β fibrillar aggregates that limit molecular relaxation, enhances molecular planarity and decreases nonradiative decay rate, resulting in **CQ** fluorescence enhancement.⁴⁰ To validate the role of restricted molecular motion on the fluorescence enhancement of probe **CQ**, we recorded the fluorescence spectra of **CQ** (5 μ M, 10 mM PBS) as a function of increased glycerol percentage in the sample solution (Figure 12). A

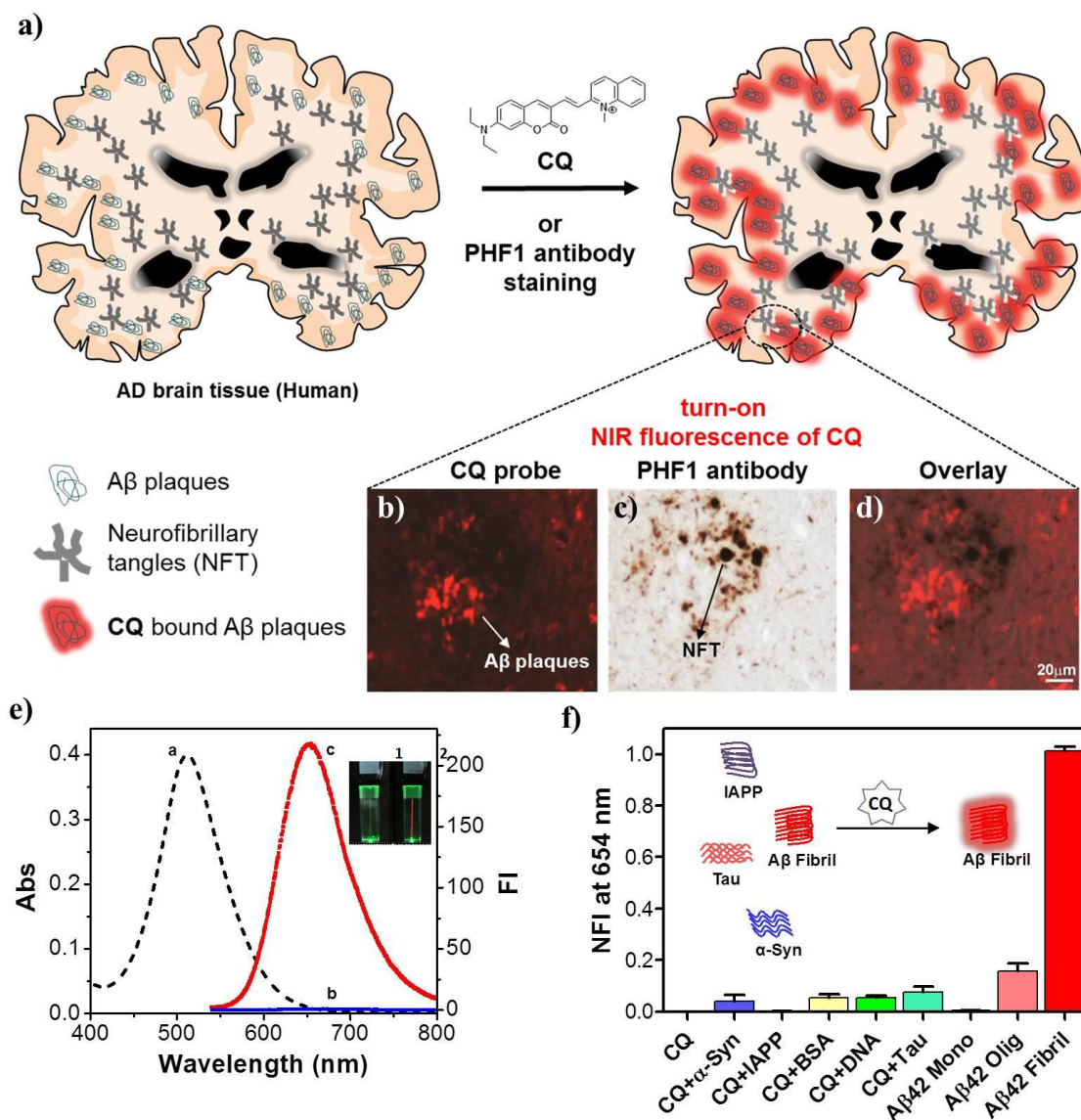


Figure 11. a) Molecular structure of coumarin-quinoline (CQ) and selective staining of Aβ plaques in human brain tissue. CQ stains Aβ plaques in the AD brain tissue while NFTs of tau corresponding to tau pathology were not detected (b), the neuritic component in the same plaque is only stained with the PHF1 antibody (c). The merged image shows there is no colocalization of PHF1 and CQ compound (d). e) Absorption (a) and emission ($\lambda_{ex}=521$ nm) spectra of CQ (2 μM) in the absence (b) and presence (c) of Aβ42 fibrillar aggregates (10 μM) ($\lambda_{em}=654$ nm). Inset: Photographs of cuvettes containing solutions of CQ (2 μM) (1) and CQ (2 μM) + Aβ42 fibrillar aggregates (20 μM) (2), respectively upon illuminating with laser pointer emitting green light, which showed a red beam in a cuvette containing CQ + Aβ42 aggregates. f) Normalized fluorescence intensity (NFI) of CQ upon interaction with α-Syn aggregates (50 μM), IAPP aggregates (50 μM), HSA (50 μM), calf thymus DNA (50 μM), tau aggregates (50 μM), Aβ42 monomer (50 μM), Aβ42 oligomers (50 μM) and Aβ42 aggregates (10 μM). Inset: Selective turn-on fluorescence of CQ upon binding to Aβ42 fibrillar aggregates. Abs = absorbance, FI = fluorescence intensity.

the linear increment in the fluorescence of **CQ** was observed with increase in glycerol percentage, which suggests that increase in viscosity of the solution has restricted molecular motion of **CQ**.¹⁸ Thus, we postulate that restricted molecular motion and attaining molecular planarity together account for the observed enhanced fluorescence of **CQ** in the presence of A β fibrillar aggregates. A significant red shift in absorption spectra has been reported in the case of ThT and Congo red, upon binding to protein aggregates, due to fibril-induced molecular planarization of the probe and subsequent increase in hyperconjugation.²¹ However, **CQ** only exhibited a small red shift (5 nm), which suggests that A β 42 fibrillar environment does not affect its ground state geometry significantly. The time-dependent density functional/molecular mechanics (TD-DFT/MM) study incorporating polarizable electrostatic embedding scheme reproduce the observed red shift for **CQ** bound to A β 42 fibril.

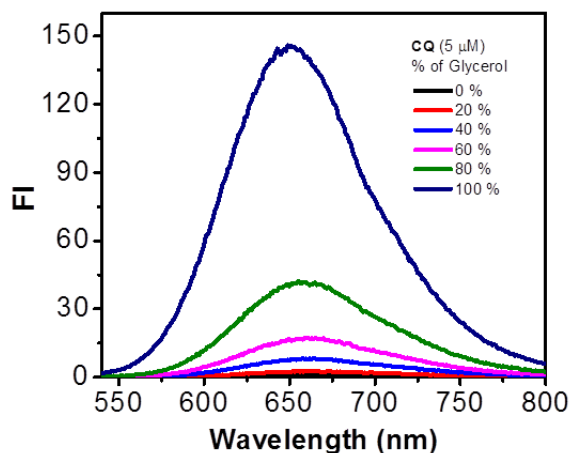


Figure 12. Fluorescence intensity (FI) of **CQ** (5 μ M, 10 mM PBS, $\lambda_{\text{ex}}= 521$ nm) with increasing percentage of glycerol (20%, 40%, 60%, 80% & 100%).

2.8 CQ selectivity towards A β fibrillar aggregates

Next, we studied the emission behaviour of **CQ** with polymorphic forms of the A β peptide (monomer, oligomers and fibrillar aggregates) (Figure 11f). Maximum fluorescence enhancement was observed with A β fibrillar aggregates, followed by oligomers and monomeric

forms. Further, we investigated the selective fluorescence enhancement of **CQ** with macromolecules and protein aggregates implicated in other neurodegenerative diseases (Figure 11f). In the presence of human serum albumin (HSA, 50 μM), **CQ** showed a red shift of ~ 34 nm in emission ($\lambda_{\text{ex}} = 521$ nm); however, fluorescence enhancement was not observed, as seen in the case of **CQ** with $\text{A}\beta$ fibrillar aggregates. Similarly, **CQ** showed minimal fluorescence enhancement in the presence of calf thymus DNA (50 μM) (Figure 11f). α -Syn and IAPP are responsible for Parkinson's disease and type-2 diabetes, respectively, and form fibrillar aggregates similar to $\text{A}\beta$. The preformed fibrillar aggregates of α -Syn (50 μM) and IAPP (50 μM) did not enhance the fluorescence of **CQ** (2 μM), which confirms the selectivity of the probe towards $\text{A}\beta$ fibrillar aggregates. Molecular dynamics and molecular docking studies, followed by free energy calculations using Molecular Mechanics or Generalized Born Surface Area (MM/GBSA), were performed on **CQ** at various binding sites of $\text{A}\beta$, IAPP and α -Syn protofibrils (Figure 13). The binding affinity exhibited by **CQ** at various binding sites of $\text{A}\beta$ fibrillar aggregates was several orders higher compared to that of IAPP and α -Syn fibrillar aggregates, which explained the observed selective binding of **CQ** to $\text{A}\beta$ fibrillar aggregates. Neurofibrillary tangles (NFTs) comprised mainly of tau protein coexist with $\text{A}\beta$ plaques in the brain and play a crucial role in

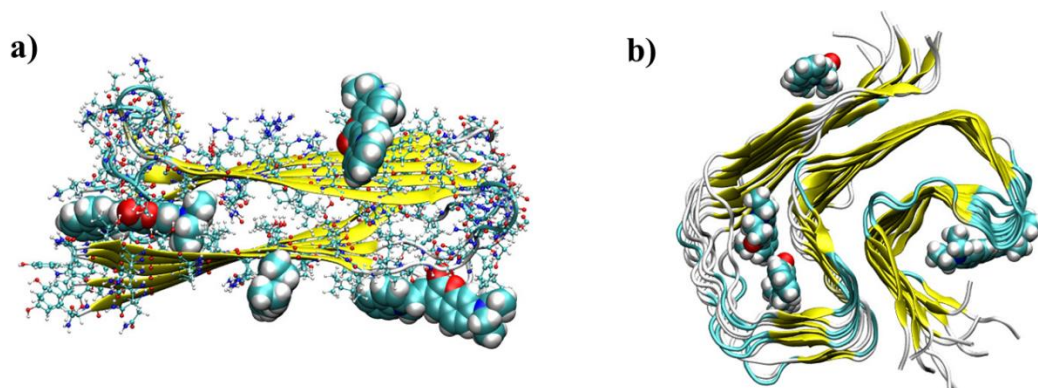


Figure 13. Various binding sites for **CQ** probe in protofibrils of amylin and α -synuclein.

in the toxicity observed in AD; however, tau aggregates are independently involved in several other neurodegenerative disorders.²⁷ Therefore, selective detection of A β plaques over NFTs in AD is critical for diagnosis of AD in the case of mixed dementia. Remarkably, **CQ** (2 μ M) treated with Tau fibrillar aggregates (50 μ M) showed minimal fluorescence enhancement, which suggests that the probe selectively detects and differentiates fibrillar aggregates of A β from tau. Subsequently, we performed competition binding affinity experiments where fluorescence of **CQ** (2 μ M) was recorded in the presence of A β 42 (10 μ M) aggregates containing α -Syn fibrillar aggregates (20 μ M), IAPP fibrillar aggregates (20 μ M), DNA (20 μ M) or HSA (20 μ M). In all the cases, the observed fluorescence enhancement of **CQ** was comparable to that of the probe treated with A β fibrillar aggregates alone. This reveals that probe **CQ** selectively binds and detects A β fibrillar aggregates in the presence of other protein aggregates or macromolecules.

2.9 Calculation of binding parameters, binding site determination and FRET studies of CQ bound to A β fibrillar aggregates

Binding saturation assay was performed to extract the binding affinity of **CQ** towards A β fibrillar aggregates. In this assay, emission spectra were recorded upon addition of increasing concentration of **CQ** (0.052, 0.078, 0.102, 0.210, 0.5, 1 and 5 μ M) to a fixed concentration of A β fibrillar aggregates (10 μ M). The fluorescence intensity at 654 nm was plotted as a function of **CQ** concentration and the data were fitted using single binding site equation to obtain the dissociation constant (K_d). The K_d value determined thus was found to be 86 ± 6.3 nM (binding constant K_a , 12.14 ± 0.43 μ M), which is much lower than the K_d of ThT (~ 0.8 μ M) and Congo red (~ 1.1 μ M) for A β aggregates. Molecular docking study revealed the free energy of binding for **CQ**-A β 42 fibril complex as -12.2 kcal/mol, which translates into nanomolar binding affinity (1.2 nM) of the probe; this is in agreement with the experimentally extracted value of K_d . To

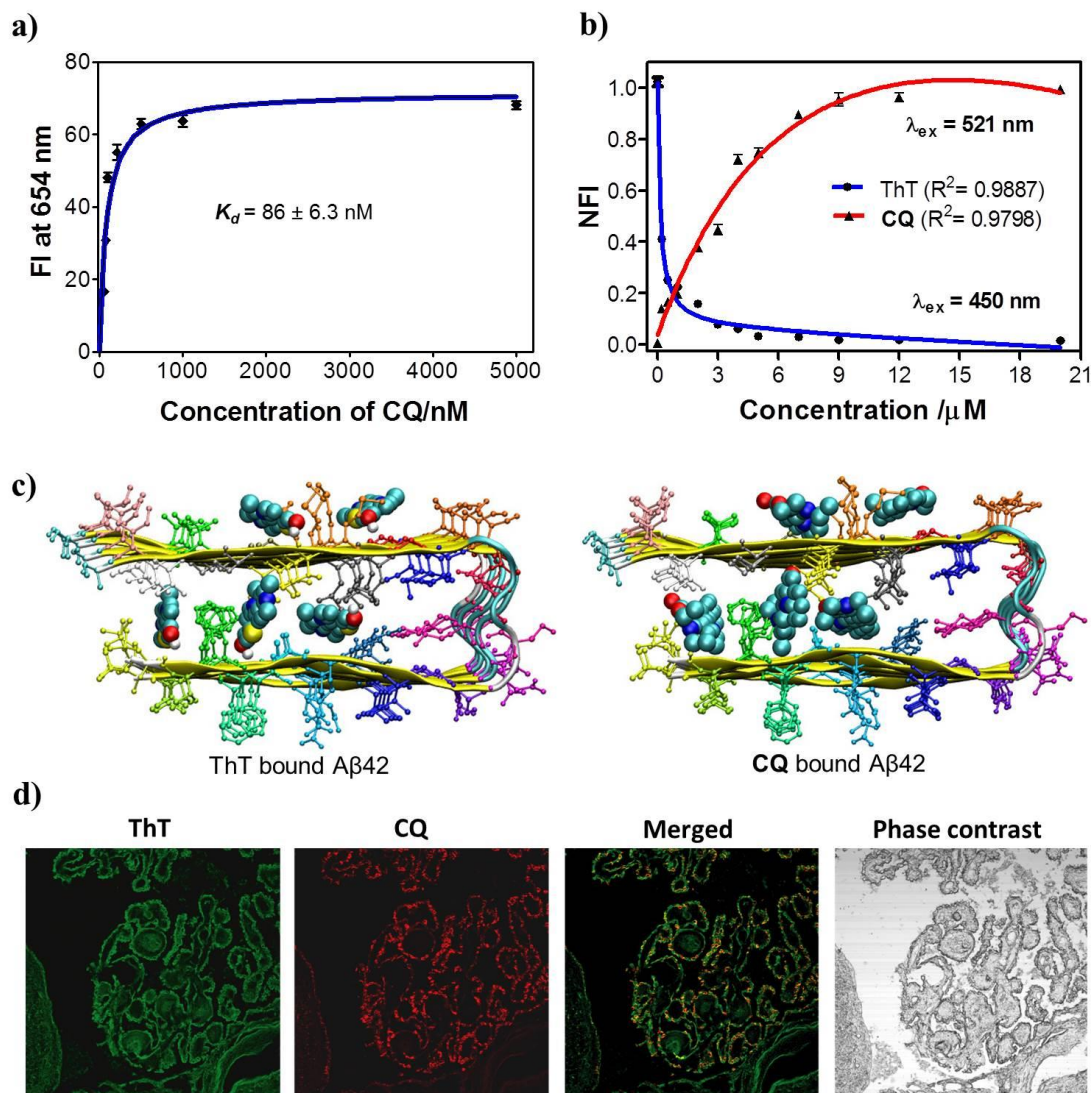


Figure 14. a) Plot of the fluorescence intensity (FI) as a function of the concentration of **CQ** (0.052, 0.078, 0.102, 0.210, 0.5, 1 and 5 mM) in the presence of A β 42 fibrillar aggregate (10 μ M) in PBS (10 mM, pH = 7.4). b) Change in fluorescence of ThT (λ_{ex} at 450 nm; fluorescence measured at 483 nm) and **CQ** (λ_{ex} at 521 nm; fluorescence measured at ~654 nm) upon titrating **CQ** to ThT/A β 42 fibrillar aggregate complex (ThT, 10 μ M/A β 42 fibrils, 20 μ M). c) Binding sites available for ThT and **CQ** within A β 42 fibril (12 mer assembly). d) **CQ** stains multiple amyloid plaque structures with specificity. Dual staining of human brain cross-sections using **CQ** and ThT (100 nM **CQ**: 1.57 mM ThT). While the ThT appears to stain many different amyloid aggregates, the **CQ** produces lower background fluorescence and shows extreme selectivity for amyloid angiopathy. This is evident by the ring-shaped structures localized at the outer wall of the tissue. Each experiment was repeated three times ($n = 3$) and error bars represent the standard deviation (SD) of the fluorescence measurement. NFI = Normalized fluorescence intensity.

gain further insights into the binding sites and affinity of the probe, displacement assay was carried out by titrating **CQ** against ThT (10 μ M) bound A β 42 fibrillar aggregates (20 μ M).

Remarkably, gradual addition of **CQ** (0.02 μM – 20 μM) to the ThT/A β 42 fibrillar aggregate complex resulted in steady decay in fluorescence of ThT at 483 nm ($\lambda_{\text{ex}}= 450$ nm) and enhancement in the emission intensity of **CQ** at 654 nm ($\lambda_{\text{ex}}= 521$ nm). The decrease in emission at 483 nm and a corresponding increase in emission at 654 nm suggest an effective displacement of ThT by **CQ**, driven by the formation of high-affinity **CQ**/A β 42 aggregate complex (Figure 14b and 15). An interesting observation was made during this titration study, where the emission at 654 nm corresponding to **CQ** was observed when the sample (**CQ**/ThT/A β fibrillar aggregates) was excited at 450 nm (ThT excitation maxima). These changes in fluorescence intensity of **CQ** upon ThT excitation can be attributed to FRET between the A β 42 fibrillar aggregates bound to ThT and **CQ**.⁴¹ Initially, during titration, **CQ** bound to the ThT/A β 42 fibrillar complex by forming a FRET pair with ThT bound to A β 42 fibrils (Figure 15). Further increase in concentrations of **CQ** (> 0.2 μM) displaced the ThT bound to A β 42 fibrils, which resulted in decreased FRET-fluorescence of **CQ** (Figure 15). However, FRET-based fluorescence at 654 nm was totally quenched at >15 μM concentration owing to complete displacement of ThT bound to A β 42 fibrillar aggregates. The complete quenching of similar binding pockets as ThT on A β 42 fibrillar aggregates, which was further confirmed by fluorescence intensity of ThT (at 483 nm) clearly indicated that **CQ** had molecular docking studies (Figure 14C). On the other hand, excitation of **CQ** (521 nm) showed a gradual increase in fluorescence intensity even after complete displacement of ThT, which suggests the presence of multiple binding sites for **CQ** on A β 42 fibrillar aggregates (Figure 14C). The molecular docking studies carried out for **CQ** and ThT on A β 42 fibrils showed that these probes have 4 different binding sites within the fibril, namely (i) entry cleft site (ii) core-1 site (iii) core-2 site (iv) surface site (Figure 14C). The data on ThT probe were in agreement with earlier reports, which

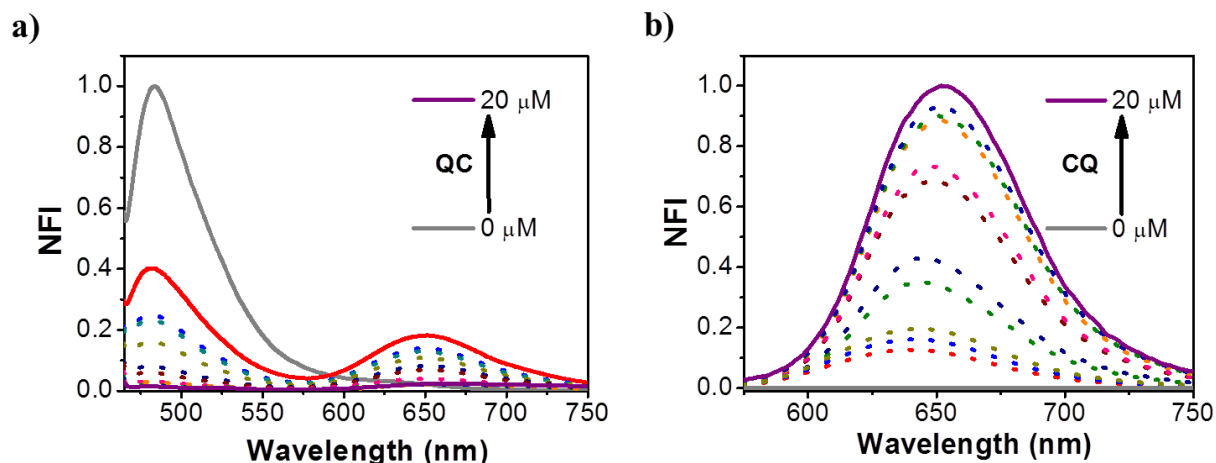


Figure 15. FRET and displacement assay. A) Fluorescence intensities of ThT and CQ (λ_{ex} at 450 nm; fluorescence at 485 nm and ~654 nm) upon titration of a ThT/Aβ42 fibrillar aggregates complex (ThT, 10 mM/Aβ42 fibrillar aggregates, 20 mM) with CQ. B) Fluorescence intensities of CQ (λ_{ex} at 521 nm; fluorescence measured at ~654 nm) upon titration of a ThT/Aβ42 fibrillar aggregates complex with CQ.

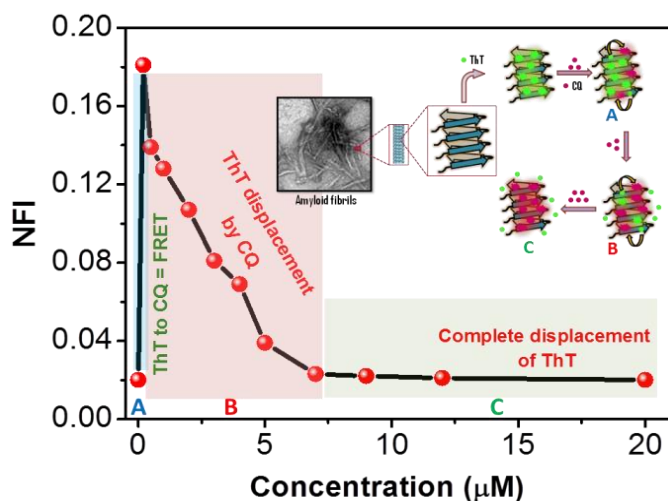


Figure 16. FRET and displacement assay. The fluorescence intensity of CQ (λ_{ex} at 450 nm; fluorescence measured at ~654 nm) upon titration of a ThT/Aβ42 fibrillar aggregates complex with CQ. Inset: Proposed model for the FRET and displacement studies of CQ with ThT/Aβ42 fibrillar aggregates complex.

have also suggested multiple binding complex formation. The calculated/determined binding sites.¹⁵ The entry cleft is the site that is associated with the most stable Aβ42 fibril:CQ affinity value for ThT was found to be much lower compared to that of CQ for Aβ42 fibril. The empirical docking free energy score included van der Waals, electrostatic, hydrogen bonding and

solvation contributions to binding free energy. The electrostatic interaction between the A β 42 fibril:CQ complex was observed to be negligible, suggesting that the van der Waals interactions are the driving force for complex formation. However, molecular docking assumed a rigid target structure and the final free energy was obtained for a single configuration of A β 42 fibril:CQ complexes. In order to gain detailed insights, we analyzed the binding free energy results of A β 42 fibril:CQ complexes obtained from MM/GBSA approaches; this also accounted for sampling effect. In particular, the free energy from this approach included van der Waals, electrostatic, polar, and nonpolar solvation contributions along with entropic contributions obtained using normal mode analysis. Although the electrostatic contributions are used to be dominant compared to van der Waals, they are nullified by the polar solvation free energy. Therefore, van der Waals contribution became the driving force for the formation of stable A β 42 fibril:CQ complexes. Interestingly, depending on the spatial location of the probe on A β 42 fibril, the van der Waals contribution varied and this, in turn, affected the overall binding free energy of CQ. The binding free energy for CQ at all four sites of A β 42 fibril was relatively higher compared to the reported values of ThT, and this clearly established the fact that CQ efficiently displaced bound ThT from A β 42 fibril; this observation was in agreement with experimental FRET data.

2.10 Determination of stability and BBB permeability of CQ

Next, we evaluated log P values for probe CQ using the flask shake method and found this to be 2.4, which suggests that CQ possesses the desirable lipophilicity to cross the blood brain barrier (BBB). In vitro stability studies indicated that CQ is stable in human blood serum (HBS), as more than 97% of the probe was found intact after 60 min incubation HBS at 37 °C (Figure 17). Cytotoxicity of probe CQ was studied in PC12 cells at varying concentrations. Probe CQ was

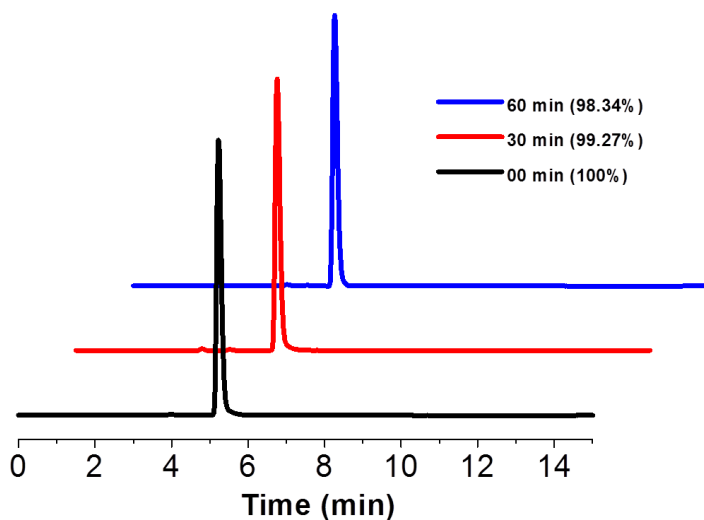


Figure 17. *In vitro* stability assay of CQ

through absorption and mass spectrometry. The brain lysate showed the presence of CQ probe, which underscored the BBB crossing ability of CQ.⁴²

2.11 Selective detection of A β plaques in human brain tissue

The specificity and sensitivity of CQ towards A β plaques were evaluated using thioflavin and immunohistochemistry in AD patient brain tissues. ThT was used as positive control for the detection of amyloid plaques. The concentration of CQ required for visualization of A β plaques was 15,700-fold less than that of ThT [CQ (100 nM): ThT (1.57 mM)]. Notably, the CQ stain responded to destaining better than ThT, which resulted in a significant decrease in background fluorescence (Figure 14d). Furthermore, the CQ stain was found to be more selective for A β plaques while ThT resulted in increased background staining. This superior fluorescence staining by CQ with high signal-to-noise ratio is likely due to its high selectivity and sensitivity towards A β plaques. We further analysed the specificity of CQ using age-matched controls, where the ThT analogue thioflavin S (ThS) was used as a control to stain A β plaques [Figure 18a (ThS, 1.57 mM) & 8b (CQ, 100 nM)]. In the AD brain tissues, although ThS stained A β plaques, it also co-stained many other regions [Figure 18c (ThS, 1.57 mM) & 18d (CQ, 100 nM)]. In

nontoxic until 10 μ M, which is much higher than the working concentrations (2 μ M) used in our experiments. Subsequently, we studied the BBB permeability of CQ in mice. The probe CQ was injected intraperitoneally, and the mice were sacrificed after 1 h. The brain was homogenized and analysed

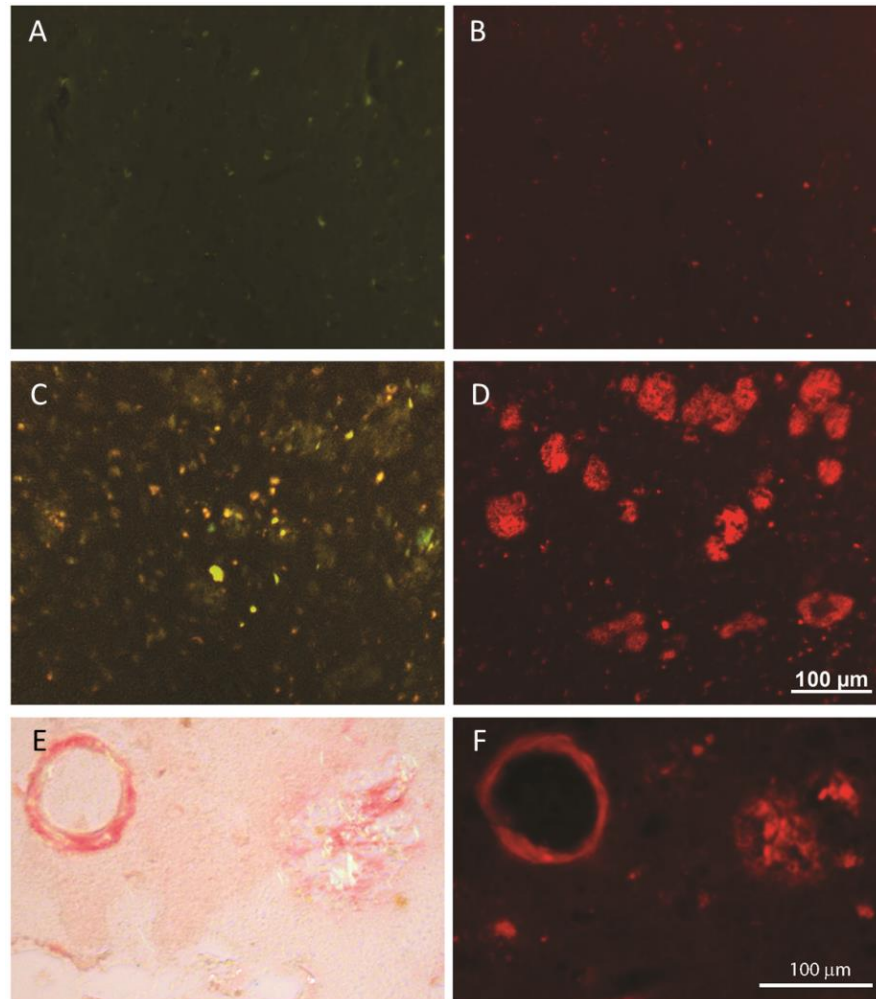


Figure 18. In an aged control individual, the staining with ThS (1.57 mM) (A) and CQ (100 nM) (B) shows very little staining (fluorescence) signal. In AD brain tissue, ThS stains A β plaques yet many other fluorescent structures are apparent (C). However, CQ labels the A β plaques with greater specificity in the adjacent section from the same case (D). CQ (F) labels the same A β plaques and congophilic angiopathy as Congo Red (E)

contrast, CQ stained specifically the A β plaques with high signal-to-noise ratio. Furthermore, CQ stained the same A β plaques and congophilic angiopathy as Congo Red [Figure 18e (congo red), 18f (CQ, 100 nM)]. The CQ stain appeared to be selective for amyloid angiogenesis, which is evident by the green background fluorescence in the dual staining of tissue sections and independent staining of identical cross-sections (Figure 18). To further investigate the selectivity of CQ, we co-stained AD brain specimens with PHF1 antibody, which labels NFTs. As shown in

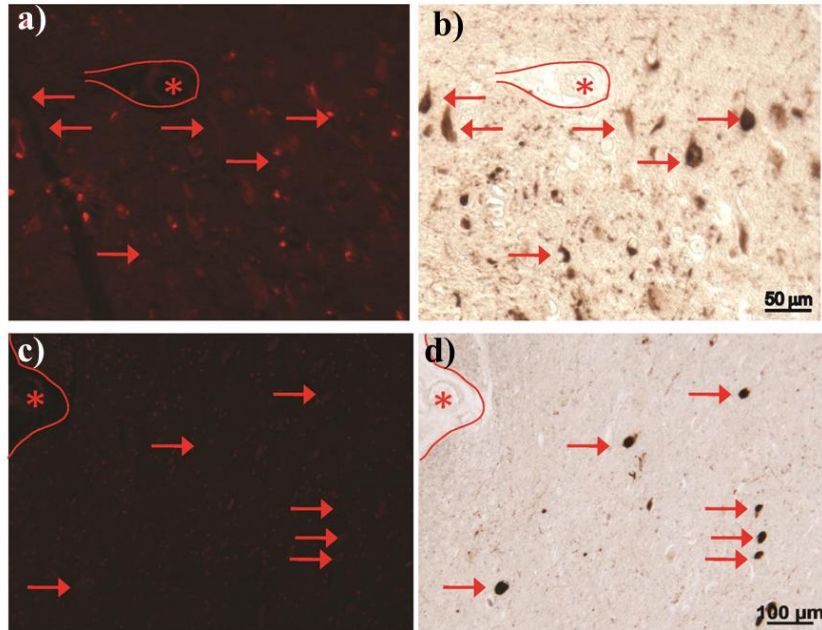


Figure 19. CQ (100 nM) clearly stains A β plaques in the AD brain tissue while NFTs of tau corresponding to Tau pathology were not detected. In a field with many neurofibrillary tangles stained by PHF1, the serial section stained with CQ compound does not reveal the NFTs (a and c). Some NFTs may be seen at near background level, but do not fluoresce at nearly the same intensity as A β plaques. Further, in specific tauopathy, progressive supranuclear palsy (PSP) samples, the tau-positive PSP tangles in the brainstem are not detected by CQ (a-d). *marking landmark vessels

Figure 11b, CQ labelled A β plaque, while PHF1 antibody stained NFTs (Figure 11c). The merged image confirmed the specificity of CQ, as no overlapping staining was observed (Figure 11d). We also analysed another tissue section that was rich in NFTs, as visualised with the PHF1 antibody (Figure 14B); however, the serial adjacent section when stained with CQ (100 nM) revealed no such aggregates (Figure 19a). Finally, we investigated CQ specificity in supranuclear palsy (PSP), which is a known tauopathy. Similar to the results obtained with AD tissue specimens, CQ revealed no staining, whereas PHF1 antibody readily detected the tau-positive PSP pathology in the brainstem (Figure 19c and 19d). Together, these results confirmed that CQ is highly specific for A β plaques, unlike ThT or ThS, which stain both A β plaques and NFTs.

2.12 Conclusion

We have developed a coumarin-quinoline (**CQ**) conjugate-based turn-on NIR fluorescence probe for selective detection of A β 42 aggregates involved in AD pathology. Probe **CQ** was found to exhibit high serum stability and binding affinity (86 nM), and fluorescence enhancement (100-fold) when bound to A β 42 fibrillar aggregates with enhanced quantum yield (0.36). **CQ** particularly bound to A β 42 aggregates and exhibited fluorescence selectively over other biomacromolecules (HSA and DNA) and toxic protein aggregates of tau, α -Syn and IAPP, all of which possess a β -sheet structure similar to A β 42 aggregates. The differential fluorescence staining ability of **CQ**, i.e., distinguishing A β 42 aggregates from tau aggregates is crucial for the clinical diagnosis of AD from tauopathies. Molecular dynamics and free energy calculations of **CQ** with various protein aggregates showed high binding affinity of **CQ** towards A β 42 aggregates, which is key to its selective nature. Probe **CQ** bound to A β 42 aggregates through multiple binding sites, which was determined by molecular docking and FRET studies. We further demonstrated the high specificity of **CQ** for A β plaques in the AD brain tissue, unlike commonly used ThT or ThS, which stain both A β plaques and NFTs. All these remarkable characteristics suggest that **CQ** probe is a promising candidate for developing specific in vitro and in vivo methods for clinical diagnosis. Currently, work is in progress in our laboratory to develop **CQ**-based fluorescence and PET methods for possible early diagnosis of AD.

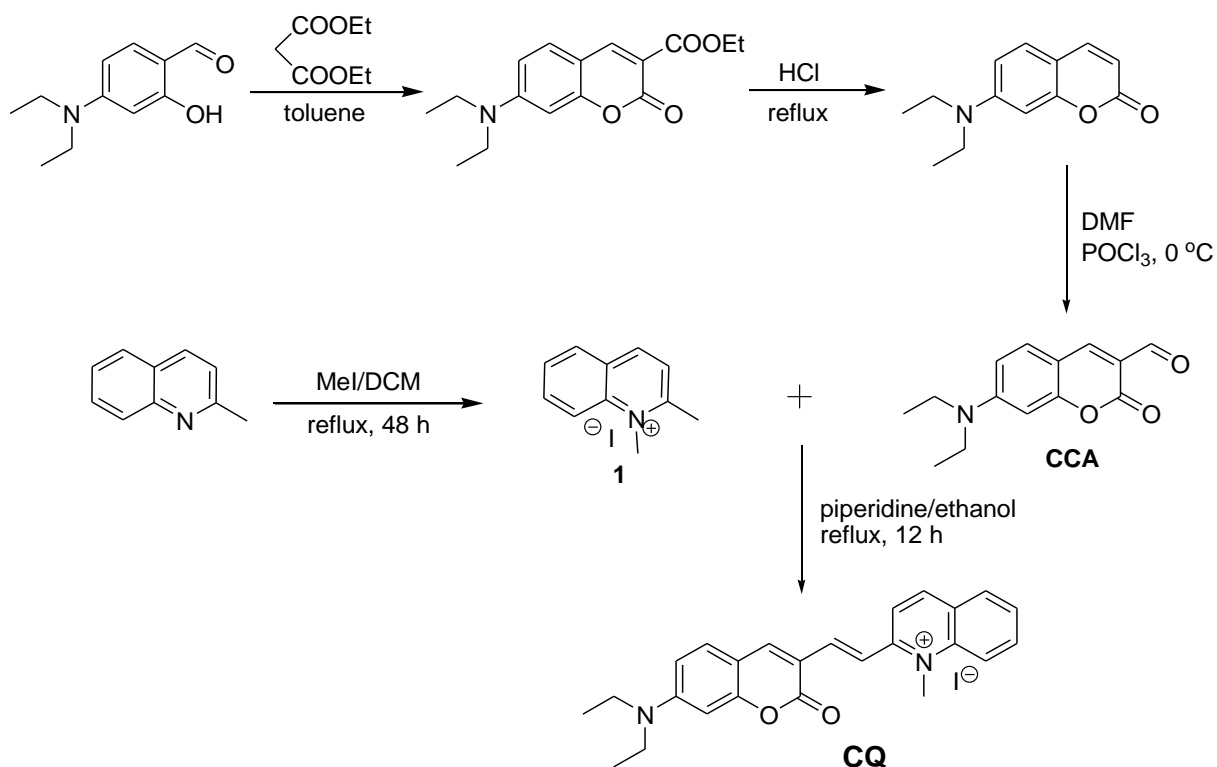
2.13 Experimental section

All reagents and solvents were obtained from Sigma-Aldrich and used without further purification. All air and moisture sensitive reactions were carried out under an argon atmosphere. Absorption spectra were recorded with Perkin Elmer Model Lambda 900 spectrophotometer. Fluorescence spectral measurements were performed by using the Perkin Elmer Model LS 55

fluorescence spectrophotometer. Incubation for fibril formation was performed in the Eppendorf Inova42 incubator.

2.13.1 Synthesis of probes. Probes **TC** and **TP** were synthesized following the literature procedure recently reported from our group.⁴³

Synthesis of 1,2-dimethylquinolin-1-ium iodide (1) and 7-(diethylamino)-2-oxo-2H-chromene-3-carbaldehyde (CCA)



Scheme 1. Synthesis of probe **CQ**

2-Methylquinoline (1 mL, 7 mmol) and iodomethane (2 mL, 28 mmol) were stirred under a nitrogen atmosphere in DCM (10 mL) at 55 °C for 48 h. The completion of the reaction was monitored by TLC. After completion of the reaction, the solvent was evaporated under vacuum. The yellow-coloured crude product was obtained, which was used in subsequent reaction without any further purification. 7-(Diethylamino)-2-oxo-2H-chromene-3-carbaldehyde (**CCA**) was

synthesized by following the reported procedure from our group (Scheme) (Maity et al., 2010).

Synthesis of 2-(2-(7-(diethylamino)-2-oxo-2H-chromen-3-yl)vinyl)-1-methylquinolin-1-ium iodide (CQ)

To a stirred solution of compound **1** (40 mg, 0.14 mmol) in ethanol (2 mL), piperidine (5 μ L) was added. After 10 min., 7-(diethylamino)-2-oxo-2H-chromene-3-carbaldehyde (CCA) (20 mg, 0.08 mmol) in DCM (2 mL) was added to above reaction mixture. The reaction mixture was stirred at reflux condition under a nitrogen atmosphere for 3 h. After completion of the reaction, the solvent was evaporated, and the crude product was purified using column chromatography on silica gel using chloroform: methanol (95:5) solvent system to obtain **CQ** in good yields (70%).

^1H NMR (*DMSO* d_6 , 400 MHz) δ 8.98-8.96 (d, J = 8 Hz, 1H), 8.50-8.30 (m, 3H), 8.176-8.172 (d, J = 1.6 Hz, 1H), 8.15-8.13 (m, 3H), 8.13 (s, 1H), 8.10-7.91 (m, 1H), 7.89-7.58 (m, 1H), 6.86-6.65 (m, 1H), 6.64 (s, 1H), 4.46 (s, 3H), 1.18-1.49 (m, 6H); ^{13}C NMR (*DMSO* d_6 , 100 MHz) δ 159.7, 156.7, 156.2, 152.6, 147.1, 143.4, 142.7, 139., 134.7, 131.3, 130, 127.4, 120.5, 119, 117.6, 113, 110.4, 108.5, 96.3, 44.4, 12.3; HRMS (ESI-MS): found 385.1916, calcd. for $\text{C}_{25}\text{H}_{25}\text{IN}_2\text{O}_2$ $[\text{M}-\text{I}]^+$ m/z = 385.1911.

2.13.2 Preparation of A β 42 oligomers and fibrillar aggregates. A β 42 peptide (0.25 mg) (Merck, calbiochem) was dissolved in hexafluoro-2-propanol (HFIP, 0.2 mL) and incubated at room temperature for 1 h. HFIP was then removed by a flow of nitrogen and further dried under vacuum. HFIP-treated A β 42 was then dissolved in DMSO to a final concentration of 1 mM and diluted to 200 μ M with 10 mM PBS (pH 7.4). The solution was incubated at 37 $^\circ\text{C}$ for 48 h with gentle and constant shaking. The formation of A β 42 fibrils was confirmed by Thioflavin T (ThT) assay. For the oligomer preparation, A β 42 was dissolved in DMSO to a final concentration of 1 mM and diluted to 100 μ M in PBS buffer (10 mM, pH 7.4). The solution was incubated at 37 $^\circ\text{C}$

for 1 h, after which the sample was incubated for 24 h at 4 °C for 1 h. The obtained sample was centrifuged, and the supernatant with oligomers was used for further experiments.^{44,45}

2.13.3 Preparation of amylin (IAPP) fibrillar aggregates and α -Synuclein fibrils.⁴⁶ Amylin peptide (0.1 mg) (Merck, calbiochem) sample of was dissolved in 100 μ L of acetonitrile to disrupt any pre-existing aggregates, and taken up in 200 μ L of 10 mM PBS buffer (pH 7.4). The final concentration of acetonitrile in the fibrillization buffer was 10% (v/v). The solution was sonicated continuously for 1 min to break up any potential aggregates. To form fibrils, the sample was incubated at 37 °C without agitation in an Eppendorf tube for 120 h (5 days). α -Synuclein peptide (0.5 mg) (Sigma-Aldrich) was dissolved in hexafluoro-2-propanol (HFIP, 0.2 mL) and incubated at room temperature for 1 h. HFIP was then removed by a flow of nitrogen and further dried by vacuum. Then α -Synuclein peptide is dissolved TBS buffer to a concentration of 200 μ M. Then the solution is incubated at 37 °C for 3-5 days with the constant shaking of 150 rpm.

2.13.4 Preparation of Tau fibrillar aggregates. tau protein was dissolved in PBS buffer (10 mM, pH 7.4) to a concentration of 100 μ M. Then the tau protein is diluted into aggregation buffer [PBS, dithiothreitol (1 mM)] to the desired concentration (10 μ M) and incubated for 3 h at 37 °C. Then the aggregation is initiated by the addition of heparin (50 μ M) to the sample and incubated for 72 h at 37 °C to obtain fibrillar aggregates.

2.13.5 Determination of the binding constant of TC and CQ for A β 42 aggregates. Increasing concentration of probe **TC** or **CQ** was titrated against a fixed concentration of A β 42 aggregates and fluorescence intensity at 639 nm was recorded ($\lambda_{\text{ex}} = 537$ nm). The K_d binding curve was generated by GraphPad Prism 5.0 (GraphPad Software, Inc., La Jolla, CA, USA) by using below equation, where X is concentration of probe **TC** or **CQ** and Y changes in fluorescence intensity

$$Y = B_{\max} * X / (K_d + X)$$

B_{\max} is the maximum specific binding has the same units as Y.

K_d is the equilibrium binding constant.

2.13.6 Quantum yields determination. Emission spectra of **TC** or **CQ** with and without A β 42 fibrillar aggregates were recorded. Cresyl violet perchlorate in ethanol ($\phi = 0.54$) was used as the standard for the fluorescence quantum yield calculation using the absorption of the test sample. The emission spectra area was obtained from 550-800 nm. Dilute solutions (10^{-6} M) were used to minimize reabsorption effects. Fluorescence measurement was made three times for each dye and averaged. Quantum yields were determined using the following equation

$$\phi_{\text{CQ}} = \phi_{\text{stand}} (F_{\text{CQ}}/F_{\text{stand}}) \times (A_{\text{stand}}/A_{\text{CQ}}) \times (n_{\text{CQ}}^2/n_{\text{stand}}^2)$$

ϕ = Quantum yield, F = Area under fluorescence spectra, A = Absorbance, n = Refractive index

2.13.7 Molecular Docking. Molecular docking was performed using AutoDock 4.2, and the AutoDock-Tools software was used to set up the necessary inputs for the docking program.²⁵ The structure of fibril consisting of 5 A β 42 peptides (PDB code 2BEG²⁶) was taken from the Protein Data Bank and was used as the protein model for docking in this study. The geometry of **TC** or **CQ** in the gas phase was optimized at the level of B3LYP/6-31+G* using the Gaussian09 software. A grid box centred on the protein was defined with a dimension of 90x70x60 Å using a 0.375 Å grid step, which is large enough to encompass the whole protein and leave enough space for docking ligand on the surface. The Lamarckian Genetic Algorithm was used for legend conformation, search and was run for 100 times, which would generate 100 possible protein-ligand complexes. All other parameters were left as default. The resulting ligand conformers were clustered by the root mean square deviation (RMSD). The structure reported in reference and structure with reference number 2n0a reported in protein data bank were used for IAPP and

for α -Syn, respectively. The detailed procedure involved the molecular docking, molecular dynamics followed by free energy calculations using MM-GBSA approach. Various binding sites for IAPP and α -Syn targets are shown in figure 9 (chapter 2a) and figure 10 (chapter 2b). Both fibril structures are proved to have surface and core binding sites for **CQ** probe similar to A β 42 fibril. The binding affinities of **CQ** probe in different binding sites of these fibrils are displayed in Table S2 and S3. As can be seen, the binding affinities of **CQ** towards IAPP and α -Syn in all sites are much order smaller when compared to the A β 42 fibril, which explains why **CQ** probe binds strongly with the last target.

2.13.8 BBB permeability. BBB permeability of the probe **CQ** was assessed by injecting **CQ** (250 μ L of 1 mg/mL of **CQ** dissolved in PBS buffer) intraperitoneally into 6 weeks old BALB C mice (4 mice). As control PBS solution (2 mice) was injected into the mice. After one hour the mice were sacrificed, and the mice brains were carefully extracted from the skull. Each mice brain was thoroughly washed with PBS and transferred into 3 mL of RIPA buffer. The brain was mechanically homogenized for 10 min, and the solution was transferred to falcon tubes followed by centrifugation at 4000 rpm at 4 $^{\circ}$ C. The supernatants of each sample were passed through 0.2 micron filter, and absorption of the brain lysate was measured at 516 nm (absorption maxima of **CQ**) to determine the BBB permeability of **CQ** into the brain.

2.13.9 Brain tissue staining. For staining human AD samples a 1 mM **CQ** stock and a 0.5% (g/mL)/1.57 mM ThT solution was prepared in water. The **CQ** stain working concentration was 100 nM in PBS (calcium free) whereas; ThT was filtered and used without any further dilution. Slides were de-paraffinized and rehydrated by soaking as follows: 10 min xylene I, 10 min xylene II, 10 min 100% ethanol, 5 min 100% ethanol, 5 min 95% ethanol, 3 min 75% ethanol, 3 min 50% ethanol, 3 min 30% ethanol, 3 min 0.85% NaCl, 3 min PBS. Either 100 nM **CQ** stain

or 0.5% (g/mL) ThT were added dropwise and incubated for 2-3 min at room temperature. Slides were then flushed with PBS and immediately submerged in PBS for 10 min. The PBS solution was changed every 2 min. The slides were then washed sequentially in 30% ethanol (1-2 min), 50% ethanol (1-2 min), 30% ethanol (1-2 min) and submerged in water for 10 min. For the final wash, slides were washed in 0.5x PBS for 20 min with stirring. Tissues were visualized using a Nikon TE2000 inverted confocal microscope (Nikon, Tokyo, Japan) with a Radiance 2100MP Rainbow Laser (Bio-Rad Laboratories).

2.14 References

1. Prince, M.; Bryce, R.; Albanese, E.; Wimo, A.; Ribeiro, W.; Ferri, C. P., The global prevalence of dementia: A systematic review and metaanalysis. *Alzheimer's & Dementia* **2013**, *9*, 63-75.
2. Rajasekhar, K.; Chakrabarti, M.; Govindaraju, T., Function and toxicity of amyloid beta and recent therapeutic interventions targeting amyloid beta in Alzheimer's disease. *Chem. Commun.* **2015**, *51*, 13434-13450.
3. DeToma, A. S.; Salamekh, S.; Ramamoorthy, A.; Lim, M. H., Misfolded proteins in Alzheimer's disease and type II diabetes. *Chem. Soc. Rev.* **2012**, *41*, 608-621.
4. Henriksen, G.; Yousefi, B. H.; Drzezga, A.; Wester, H. J., Development and evaluation of compounds for imaging of β -amyloid plaque by means of positron emission tomography. *Eur. J. of Nucl. Med. Mol. Imaging* **2008**, *35*, 75-81.
5. Zhu, L.; Ploessl, K.; Kung, H. F., PET/SPECT imaging agents for neurodegenerative diseases. *Chem. Soc. Rev.* **2014**, *43*, 6683-6691.
6. Staderini, M.; Martin, M. A.; Bolognesi, M. L.; Menendez, J. C., Imaging of β -amyloid plaques by near infrared fluorescent tracers: a new frontier for chemical neuroscience. *Chem. Soc. Rev.* **2015**, *44*, 1807-1819.
7. Wolfe, L. S.; Calabrese, M. F.; Nath, A.; Blaho, D. V.; Miranker, A. D.; Xiong, Y., Protein-induced photophysical changes to the amyloid indicator dye thioflavin T. *Proc. Natl. Acad. Sci.* **2010**, *107*, 16863-16868.
8. Robbins, K. J.; Liu, G.; Selmani, V.; Lazo, N. D., Conformational analysis of thioflavin T bound to the surface of amyloid fibrils. *Langmuir* **2012**, *28*, 16490-16495.

9. Hintersteiner, M.; Enz, A.; Frey, P.; Jatón, A.-L.; Kinzy, W.; Kneuer, R.; Neumann, U.; Rudin, M.; Staufenbiel, M.; Stoeckli, M.; Wiederhold, K.-H.; Gremlich, H.-U., In vivo detection of amyloid- β deposits by near-infrared imaging using an oxazine-derivative probe. *Nat. Biotech.* **2005**, *23*, 577-583.
10. Ono, M.; Watanabe, H.; Kimura, H.; Saji, H., BODIPY-based molecular probe for imaging of cerebral β -amyloid plaques. *ACS Chem. Neurosci.* **2012**, *3*, 319-324.
11. Liu, K.; Guo, T. L.; Chojnacki, J.; Lee, H.-G.; Wang, X.; Siedlak, S. L.; Rao, W.; Zhu, X.; Zhang, S., bivalent ligand containing curcumin and cholesterol as a fluorescence probe for A β plaques in Alzheimer's disease. *ACS Chem. Neurosci.* **2012**, *3*, 141-146.
12. Muthuraj, B.; Layek, S.; Balaji, S. N.; Trivedi, V.; Iyer, P. K., Multiple function fluorescein probe performs metal chelation, disaggregation, and modulation of aggregated A β and A β -Cu complex. *ACS Chem. Neurosci.* **2015**, *6*, 1880-1891.
13. Cohen, S. I. A.; Linse, S.; Luheshi, L. M.; Hellstrand, E.; White, D. A.; Rajah, L.; Otzen, D. E.; Vendruscolo, M.; Dobson, C. M.; Knowles, T. P. J., Proliferation of amyloid- β 42 aggregates occurs through a secondary nucleation mechanism. *Proc. Natl. Acad. Sci.* **2013**, *110*, 9758-9763.
14. Cao, K.; Farahi, M.; Dakanali, M.; Chang, W. M.; Sigurdson, C. J.; Theodorakis, E. A.; Yang, J., Aminonaphthalene 2-cyanoacrylate (ANCA) probes fluorescently discriminate between amyloid- β and prion plaques in brain. *J. Am. Chem. Soc.* **2012**, *134*, 17338-17341.
15. Kuang, G.; Murugan, N. A.; Tu, Y.; Nordberg, A.; Ågren, H., Investigation of the binding profiles of AZD2184 and thioflavin T with amyloid- β (1-42) fibril by molecular docking and molecular dynamics methods. *J. Phys. Chem. B* **2015**, *119*, 11560-11567.
16. Groenning, M., Binding mode of Thioflavin T and other molecular probes in the context of amyloid fibrils-current status. *J. Chem. Biol.* **2010**, *3*, 1-18.
17. Pajouhesh, H.; Lenz, G. R., Medicinal chemical properties of successful central nervous system drugs. *NeuroRx* **2005**, *2*, 541-553.
18. Yan, J.-W.; Ye, W.-J.; Chen, S.-B.; Wu, W.-B.; Hou, J.-Q.; Ou, T.-M.; Tan, J.-H.; Li, D.; Gu, L.-Q.; Huang, Z.-S., Development of a Universal Colorimetric Indicator for G-quadruplex structures by the fusion of thiazole orange and isaindigotone skeleton. *Anal. Chem.* **2012**, *84*, 6288-6292.
19. Sulatskaya, A. I.; Kuznetsova, I. M.; Turoverov, K. K., Interaction of thioflavin T with amyloid fibrils: Fluorescence quantum yield of bound dye. *J. Phys. Chem. B* **2012**, *116*, 2538-2544.
20. Olsen, J. M.; Aidas, K.; Kongsted, J., Excited states in solution through polarizable embedding. *J. Chem. Theory Comput.* **2010**, *6*, 3721-3734.
21. Murugan, N. A.; Olsen, J. M. H.; Kongsted, J.; Rinkevicius, Z.; Aidas, K.; Ågren, H., Amyloid fibril-induced structural and spectral modifications in the thioflavin-T optical probe. *J. Phys. Chem. Lett.* **2013**, *4*, 70-77.

22. Grabowski, Z. R.; Rotkiewicz, K.; Rettig, W., Structural changes accompanying intramolecular electron transfer: Focus on twisted intramolecular charge-transfer states and structures. *Chem. Rev.* **2003**, *103*, 3899-4032.
23. Cook, N. P.; Ozbil, M.; Katsampes, C.; Prabhakar, R.; Martí, A. A., Unraveling the photoluminescence response of light-switching ruthenium(II) complexes bound to amyloid- β . *J. Am. Chem. Soc.* **2013**, *135*, 10810-10816.
24. Knowles, T. P. J.; Vendruscolo, M.; Dobson, C. M., The amyloid state and its association with protein misfolding diseases. *Nat. Rev. Mol. Cell Biol.* **2014**, *15*, 384-396.
25. Soto, C., Unfolding the role of protein misfolding in neurodegenerative diseases. *Nat. Rev. Neurosci.* **2003**, *4*, 49-60.
26. Hamley, I. W., The amyloid beta peptide: A chemist's perspective. role in Alzheimer's and fibrillization. *Chem. Rev.* **2012**, *112*, 5147-5192.
27. Wang, Y.; Mandelkow, E., Tau in physiology and pathology. *Nat. Rev. Neurosci.* **2016**, *17*, 22-35.
28. McKhann, G.; Drachman, D.; Folstein, M.; Katzman, R.; Price, D.; Stadlan, E. M., Clinical diagnosis of Alzheimer's disease: Report of the NINCDS • ADRDA Work Group* under the auspices of department of health and human services task force on Alzheimer's disease. *Neurology* **1984**, *34*, 939.
29. Spires-Jones, Tara L.; Hyman, Bradley T., The Intersection of amyloid beta and tau at synapses in Alzheimer's disease. *Neuron* **2014**, *82*, 756-771.
30. Ross, C. A.; Poirier, M. A., What is the role of protein aggregation in neurodegeneration? *Nat. Rev. Mol. Cell Biol.* **2005**, *6*, 891-898.
31. Adlard, P. A.; Tran, B. A.; Finkelstein, D. I.; Desmond, P. M.; Johnston, L. A.; Bush, A. I.; Egan, G. F., A review of β -amyloid neuroimaging in Alzheimer's disease. *Front. Neurosci.* **2014**, *8*, 327-.
32. Li, Y.; Xu, D.; Ho, S.-L.; Li, H.-W.; Yang, R.; Wong, M. S., A theranostic agent for in vivo near-infrared imaging of β -amyloid species and inhibition of β -amyloid aggregation. *Biomaterials* **2016**, *94*, 84-92.
33. Ren, W.; Xu, M.; Liang, S. H.; Xiang, H.; Tang, L.; Zhang, M.; Ding, D.; Li, X.; Zhang, H.; Hu, Y., Discovery of a novel fluorescent probe for the sensitive detection of β -amyloid deposits. *Biosens. Bioelectron.* **2016**, *75*, 136-141.
34. Kim, D.; Moon, H.; Baik, S. H.; Singha, S.; Jun, Y. W.; Wang, T.; Kim, K. H.; Park, B. S.; Jung, J.; Mook-Jung, I.; Ahn, K. H., Two-photon absorbing dyes with minimal autofluorescence in tissue imaging: application to in vivo imaging of amyloid- β plaques with a negligible background signal. *J. Am. Chem. Soc.* **2015**, *137*, 6781-6789.

35. Cui, M.; Ono, M.; Watanabe, H.; Kimura, H.; Liu, B.; Saji, H., Smart near-infrared fluorescence probes with donor-acceptor structure for in vivo detection of β -amyloid deposits. *J. Am. Chem. Soc.* **2014**, *136*, 3388-3394.
36. Lv, G.; Sun, A.; Wei, P.; Zhang, N.; Lan, H.; Yi, T., A spiropyran-based fluorescent probe for the specific detection of β -amyloid peptide oligomers in Alzheimer's disease. *Chem. Commun.* **2016**, *52*, 8865-8868.
37. Hatai, J.; Motiei, L.; Margulies, D., Analyzing amyloid beta aggregates with a combinatorial fluorescent molecular sensor. *J. Am. Chem. Soc.* **2017**, *139*, 2136-2139.
38. Gao, M.; Yu, F.; Lv, C.; Choo, J.; Chen, L., Fluorescent chemical probes for accurate tumor diagnosis and targeting therapy. *Chem. Soc. Rev.* **2017**, *46*, 2237-2271.
39. Xie, J.-Y.; Li, C.-Y.; Li, Y.-F.; Fei, J.; Xu, F.; Ou-Yang, J.; Liu, J., Near-infrared fluorescent probe with high quantum yield and its application in the selective detection of glutathione in living cells and tissues. *Anal. Chem.* **2016**, *88*, 9746-9752.
40. Yu, W.-T.; Wu, T.-W.; Huang, C.-L.; Chen, I. C.; Tan, K.-T., Protein sensing in living cells by molecular rotor-based fluorescence-switchable chemical probes. *Chem. Sci.* **2016**, *7*, 301-307.
41. Jares-Erijman, E. A.; Jovin, T. M., FRET imaging. *Nat. Biotech.* **2003**, *21*, 1387-1395.
42. Dickstein, D. L.; Biron, K. E.; Ujiie, M.; Pfeifer, C. G.; Jeffries, A. R.; Jefferies, W. A., A β peptide immunization restores blood-brain barrier integrity in Alzheimer disease. *FASEB J.* **2006**, *20*, 426-433.
43. Rajasekhar, K.; Narayanaswamy, N.; Murugan, N. A.; Kuang, G.; Ågren, H.; Govindaraju, T., A high affinity red fluorescence and colorimetric probe for amyloid β aggregates. *Sci. Rep.* **2016**, *6*, 23668.
44. Walsh, D. M.; Lomakin, A.; Benedek, G. B.; Condron, M. M.; Teplow, D. B., Amyloid β -protein fibrillogenesis: Detection of a protofibrillar intermediate. *J. Biol. Chem.* **1997**, *272*, 22364-22372.
45. Stine, W. B.; Jungbauer, L.; Yu, C.; LaDu, M. J., Preparing Synthetic A β in different aggregation States. In *Alzheimer's disease and frontotemporal dementia: Methods and protocols*, Roberson, E. D., Ed. Humana Press: Totowa, NJ, 2011; pp 13-32.
46. Konarkowska, B.; Aitken, J. F.; Kistler, J.; Zhang, S.; Cooper, G. J. S., The aggregation potential of human amylin determines its cytotoxicity towards islet β -cells. *FEBS J.* **2006**, *273*, 3614-3624.

Chapter 3

Peptidomimetics as A β modulators

Chapter 3A

**A Rationally Designed Peptidomimetic Modulators of A β Toxicity in
Alzheimer's Disease**

Over the past two decades, tremendous efforts have been devoted to understanding the pathogenesis of AD.¹ Although the detailed mechanism of neurodegeneration encountered in AD is not entirely understood yet, several reports indicate that the fibrillar aggregation of β -amyloid (A β) 36–42 peptides and, in particular, highly toxic A β 42 play a key role in the pathogenesis of AD.^{2–4} The A β 36–42 peptides are derived from a transmembrane protein called amyloid precursor protein (APP). Amyloidogenic pathway for processing of APP by enzymes β - and γ -secretases lead to the release of A β 36–42 peptides and their deposition in the brain as plaques.⁵ Hence, the development of molecular agents that are capable of inhibiting the A β fibril formation or dissolution of the preformed toxic A β fibrillar aggregates are key concepts for AD treatment.^{6,7} In this chapter we present effective inhibition of A β 42 aggregation using hybrid peptide-peptoid modulators based on the core sequences of A β peptide (KLVFF). The hybrid peptide-peptoids modulators were designed to act on multiple phases of A β 42 aggregation by introducing a non-amino acid moiety with multiple hydrogen bond donor-acceptor sites, at the N-terminal to target A β 42 β -sheet formation. The introduction of peptoid monomers (sarcosine) at alternative positions of the recognition motif (KLVFF) prevents the oligomerization of A β 42 monomers upon its binding through the face of amino acids. Furthermore, the hybrid peptide-peptoid modulators were anticipated to confer proteolysis resistance to the derived peptidomimetics, thus increasing their biostability and bioavailability (the parent peptide KLVFF contains natural amino acids and is not resistant to endoproteases). Thioflavin T (ThT) binding, assayed by fluorescence spectroscopy, was used to probe A β 42 fibril formation and effect of peptidomimetic inhibitors on their growth. Circular dichroism (CD) was used to study the effect of inhibitors on the secondary structure of A β 42 aggregates. The morphological analysis of A β 42 in the absence and presence of peptidomimetic inhibitors was investigated using transmission electron microscopy (TEM). The structural integrity and stability of inhibitory peptides and

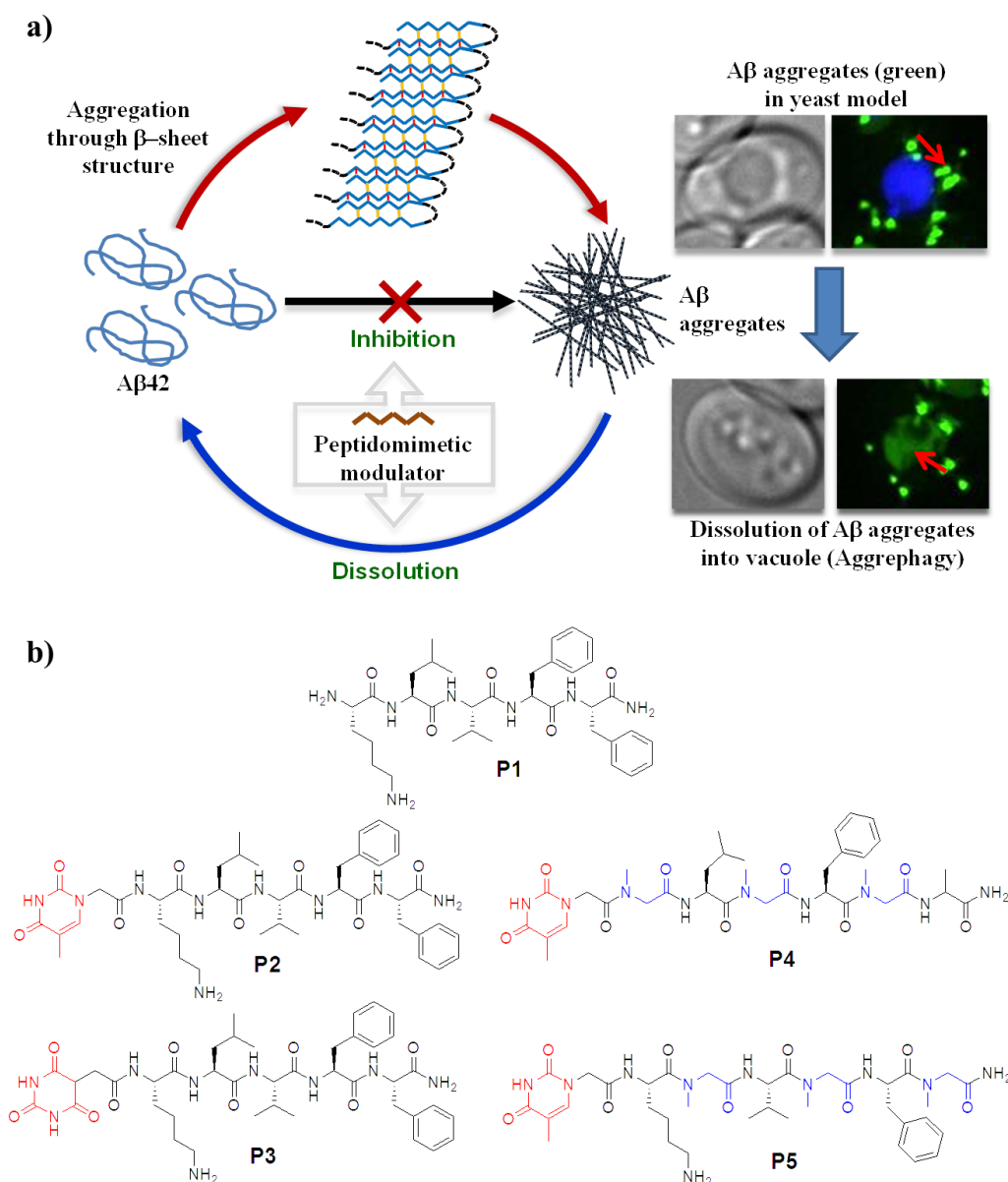


Figure 1. a) Inhibition and dissolution of A β 42 aggregates, and their evaluation in a yeast model for Alzheimer's disease. b) Structures of peptide and peptidomimetic inhibitors.

peptidomimetics were analyzed in the presence of proteases. Further, inhibitory activity was studied in the yeast (*Saccharomyces cerevisiae*) model, which expresses A β 42, to assess the ability of peptidomimetics as therapeutic agents and to understand their mechanism of action in reducing A β 42 toxicity. Thus, we report on the study of structural fine-tuning and inhibitory activities of peptidomimetics towards preventing the formation of A β 42 aggregates and dissolving the preformed toxic aggregates (Figure 1).

3.1 Design strategy for peptidomimetics

The principle of the design was to rationally introduce a minimum number of simple chemical modifications into a small recognition peptide sequence extracted from A β 42, which is considered crucial for β -sheet conformation and fibrillogenesis. These peptidomimetics bind and stabilize the amyloidogenic conformational population of A β 42 and inhibit its aggregation into toxic amyloid aggregates. The chemical modifications are aimed at interfering with hydrogen bonding found in the β -sheet conformations of A β 42. Inhibition of β -sheet formation in A β 42 affects its self-assembly to fibrillar aggregates. We considered KLVFF (A β 16-20) as the recognition sequence, which has been reported in the literature to interact with A β 42 and its aggregates.⁸ Although KLVFF (**P1**) has the ability to interfere with fibrillization, the extent of inhibition is very marginal due to higher stabilization of A β 42 β -sheet conformations than the A β 42/KLVFF complex.⁹ To enhance the stabilization of A β 42/KLVFF complex we introduced small organic moieties with multiple hydrogen bond donors and acceptors at the N-terminal of KLVFF (Figure 1). This specially chosen organic moiety could participate in hydrogen bonding to form much stronger A β 42/inhibitor complex. We selected two organic moieties, thymine and barbiturate, as N-terminal pendent functionalities to obtain peptides **P2** and **P3**, respectively as shown in Figure 1. These organic moieties contain multiple hydrogen bond donor and acceptor centers, which are capable of forming additional hydrogen bonds with β -sheet forming A β 42 monomer or A β 42 aggregates. Subsequently, we performed inhibition studies and concluded that the extent of inhibition was moderate, and moreover, the blood serum or protease stability of **P2** and **P3** was not encouraging. The next level of modification was then considered on **P2** as it displayed better inhibition activity over **P3**. Meredith *et al.* used N-substituted amino acids at alternate positions of KLVFFAE, where α -substituents of Leu, Phe

and Ala were attached to amide nitrogen atom. These modifications were presumed to help retain the recognition ability and inhibition of A β 40 fibrillogenesis or dissolution of A β 40 fibrils. In this case, the inhibitor was anticipated to work by blocking the hydrogen bonding interactions. However, the involvement of other noncovalent interactions from the α -substituents either in the inhibitor or A β 40 were not considered in the design. It should be noted that the fibrillogenesis of A β 40/42 is guided by both hydrogen bonding and other noncovalent interactions.¹⁰ Thus, we intend to target the key role of hydrogen bonding in A β 42 aggregation as well as minimizing other noncovalent interactions among A β 42 and modulators, in our design strategy. Keeping this mind, we introduced sarcosine (Sr) in alternate positions of **P2** to obtain **P4** (Thymine-Sr-Leu-Sr-Phe-Sr-Ala) and **P5** (Thymine-Lys-Sr-Val-Sr-Phe-Sr) (Figure 1). We hypothesized that the peptidomimetics **P4** and **P5** would interact with A β 42 through the face containing natural amino acids (blocking hydrogen bonding) while minimizing other noncovalent interactions to prevent the fibrillogenesis of A β 42.¹¹

3.2 Studying inhibition and dissolution efficiency by thioflavin assay and CD measurements

ThT assay has been widely used to monitor the transformation of A β 42 monomers to fibrillar aggregates. We employed ThT assay to evaluate the ability of our peptidomimetic candidates to either prevent fibril assembly (inhibition) or to breakdown preformed fibrils of A β 42 (dissolution). For the inhibition assay all the peptidomimetics (**P2**, **P3**, **P4** and **P5**) along with control peptide **P1** were added at 0 h of the experiment, whereas for the aggregates reversal (dissolution) assay they were added to A β 42 fibrillar aggregates grown for 2 days. Once they had been incubated together, A β 42/inhibitors were analyzed using ThT by measuring the fluorescence changes. First, we performed concentration-dependent experiments where

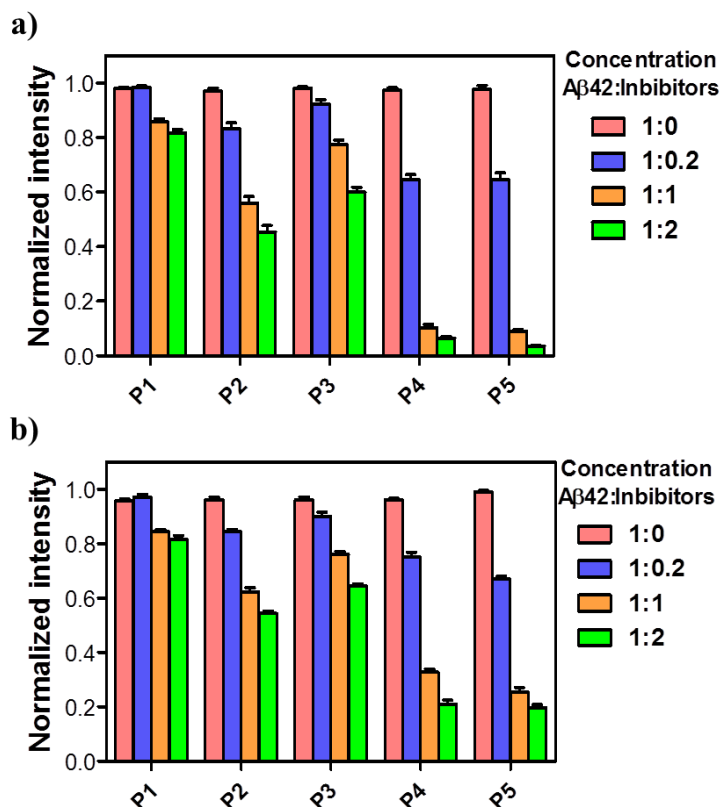


Figure 2. Inhibition and reversal data of Aβ42 aggregates studied by ThT assay. The data in (a) and (b) show the effects of different stoichiometries of **P1**, **P2**, **P3**, **P4** and **P5** on the aggregation of 20 μM Aβ42 (on day 4 for the inhibition assay and day 6 for the reversal assay). Molar ratios (Aβ42:peptide) of 1:0, 1:0.2, 1:1 and 1:2 were used for each peptide. Values are the normalized maximal fluorescence intensity at 485 nm compared to that of the control (Aβ42 with no inhibitor). **P4** and **P5** showed most prominent effect in both the experiments compared to other three peptides (**P1-P3**). Each experiment was repeated three times (n = 3). Error bars represent the standard deviation (SD) of the fluorescence measurement.

different ratios of **P1**, **P2**, **P3**, **P4** and **P5** were incubated with fixed concentrations of Aβ42 (20 μM) and its aggregates to study their effect on both inhibition and reversal assay, respectively. Experiments were performed at stoichiometric ratios (Aβ42/inhibitor) of 1:0.2, 1:1, and 1:2 with the fixed concentration of Aβ42 of 20 μM. Inhibition experiments demonstrated that **P4** and **P5** were able to prevent Aβ42 aggregation as indicated by a reduction in the fluorescence intensity of ThT up to 95% in case of 1:2 stoichiometric ratio after four days of incubation at 37 °C (Figure 2). Conversely, **P1**, **P2** and **P3** showed low to moderate inhibition efficiencies of 20%, 55% and 40%, respectively for 1:2 stoichiometry. Similar trends were observed in the case of fibril reversal assay with dissolution efficiencies

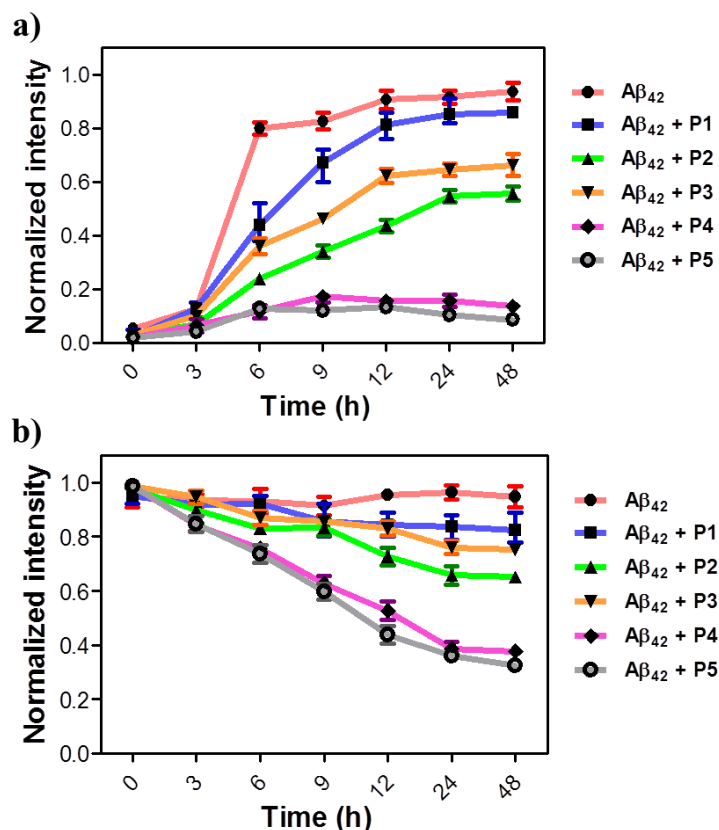


Figure 3. Kinetics of **P1-P5** on inhibition and reversal of Aβ₄₂ fibril using ThT assay. A 20 μM of Aβ₄₂ monomers (a) or their aggregates (b) were incubated with inhibitors (**P1**, **P2**, **P3**, **P4** and **P5**) at 37 °C in 1:2 stoichiometry and their influence on fibrillization or dissolution is quantified by measuring ThT fluorescence intensity, which is represented as normalized fluorescence intensity at 485 nm for a given time point. Each experiment was repeated three times (n = 3). Error bars represent the standard deviation (SD) of the fluorescence measurement.

of 20% (**P1**), 45% (**P2**), 34% (**P3**), 80% (**P4**) and 80% (**P5**), for 1:2 stoichiometric ratios (Figure 2). Thus, **P4** and **P5** were found to be promising as they displayed a pronounced effect on both inhibition and reversal assay. However, the efficiencies of **P4** and **P5** were only marginally better in inhibition assay compared to reversal assay with a difference of about 15%. Increasing the molar ratio of peptides (> 2 fold) did not lead to improvements in inhibition or reversal assay and, therefore, we performed all our further experiments with 1:2 stoichiometry of Aβ₄₂:inhibitor (20μM:40μM). Next, we performed time-dependent assays to monitor the effect of inhibitors on the growth kinetics of Aβ₄₂ monomers to fibrillar aggregates and dissolution of toxic aggregates. A sigmoid growth curve was obtained for the Aβ₄₂ fibrillization, which has been well-reported in the literature.³ The **P1** showed a slight

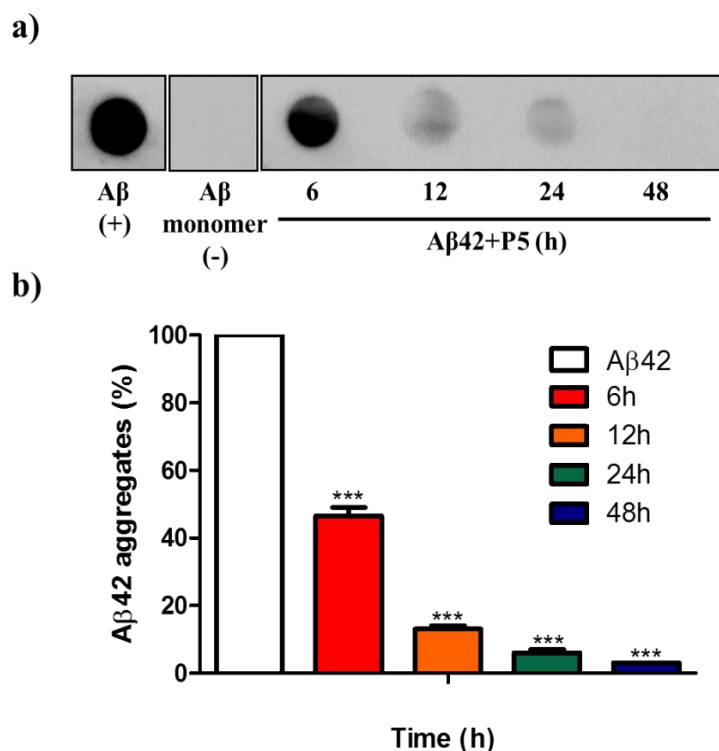


Figure 4. Dot blot analysis indicates that **P5** dissolves Aβ42 aggregates. (a) Aβ42 (20 μM) aggregates were incubated with **P5** at 37 °C in 1:2 stoichiometry and their influence on dissolution is studied at different time points (6 h, 12 h, 24 h and 48 h) by blotting sample on PVDF membrane and treating it with primary Anti-beta-amyloid 1-42 antibody (1:3000) specific for fibrillar aggregates, followed by anti-mouse secondary antibody (1:10000, conjugated with HRP) treatment and final treating with ECL reagent to measure chemiluminescence and to quantify the dissolution of Aβ42 aggregates. (b) The plot of percentage of Aβ42 fibrillar aggregates present at different time point, when compared to control the exact amount of aggregates can be quantified at different time points (6 h has ~9 mM concentration of Aβ42 aggregates). Triplicate values for the control were plotted, and a difference of 3 standard deviations (SD) units between the test and control was considered as significant. $P < 0.05$, ***.

variation in the growth curve, indicating least effect on the Aβ42 aggregation, whereas **P2** and **P3** showed decreased growth phase to < 60%, signifying moderate inhibition efficiency. **P4** and **P5** were most competent among all the candidates with an inhibition efficiency of > 90% as shown in Figure 3. During the growth phase, Aβ42:**P4/P5** complex showed a slight enhancement in fluorescence (9 h), which decreased at further time points indicating that Aβ42 aggregates formed at a faster rate during the growth phase, but at further time points inhibitors managed to dissolve the aggregates and showed a decrease in fluorescence. In time-dependent reversal assays, a similar order of efficiency was observed where **P1/Aβ42**

complex showed a slight decrement in fluorescence and **P2** and **P3** were moderately active in dissolving the A β 42 aggregates with efficiencies of 35% and 25%, respectively. **P4** and **P5** again exhibited best dissolution efficiencies of 68% and 75% on the A β 42 aggregates. To further validate the inhibition efficiency of our most efficient inhibitor **P5**, we performed dot blot analysis in a time-dependent manner using the specific antibody for A β 42 aggregates.¹⁰ A β 42 (20 μ M) aggregates were incubated with **P5** in 1:2 stoichiometry and their influence on the dissolution is quantified at different time points (6, 12, 24 and 48 h) by measuring chemiluminescence intensity (Figure 4). The dot blot analysis data clearly supported our ThT dissolution assay of A β 42 aggregates with **P5** as shown in Figure 4.

To further validate our results, we performed CD studies. A β 42 aggregates are predominantly made of β -sheet assembly, which can be assessed by CD measurements. Hence, a decrease in β -sheet content and corresponding characteristic CD signal intensity directly correlate with the inhibition efficiencies of inhibitors. In this assay, we monitored the intensity of negative CD band centred at 218 nm, characteristic of a β -sheet structure and a decrease in its intensity was correlated with a reduction in the toxic A β 42 aggregates (Figure 5). In these CD measurements, samples similar to ThT fluorescence assays were used to allow for direct comparison between the two experiments. In the case of inhibition assay, A β 42 monomers were incubated with inhibitor candidates for 4 days at 37 °C and then CD measurements were performed to evaluate the inhibition efficiency. The A β 42/**P1** mixture showed a slight decrease in β -sheet content (deduced by a decrease in the negative band at 218 nm). A β 42/**P2** showed a slight blue shift and > 50% reduction in CD intensity (a decrease in intensity at 218 nm compared to the A β 42 control, **P1**) as compared to untreated A β 42 while **P3** showed only ~30% decrease in β -sheet content. Supporting our results inhibition (corresponding to a decrease in CD band intensity at 218 nm) of the formation of

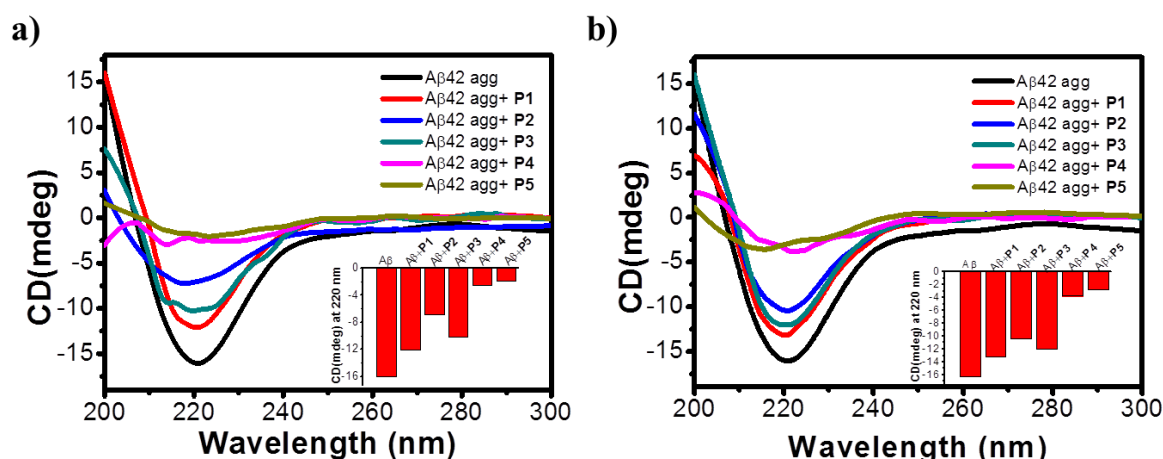


Figure 5. Studying Inhibition and reversal assay of A β 42 aggregates by CD measurements. The data in (a) and (b) show the effects of **P1**, **P2**, **P3**, **P4** and **P5** (40 μ M) on the aggregation of 20 μ M A β 42 (on day 4 for the inhibition assay and day 6 for the reversal assay). Insets in a and b show the intensity of the negative signal at 218 nm (represents β -sheet content) observed in corresponding experiments. **P4** and **P5** effectively decreased the β -sheet content corresponding to A β 42 aggregates compared to **P1-P3**.

A β 42 aggregates (Figure 5). In the reversal assay, A β 42 aggregates were, incubated with the inhibitor candidates for six days at 37 $^{\circ}$ C and then, CD measurements were, performed. CD data were in excellent agreement with the dissolution efficiency obtained in reversal assay experiments monitored by the ThT assay (Figure 2). **P2** and **P3** showed moderate dissolution efficiencies of 40% and 25%, respectively towards the A β 42 aggregates. **P4** and **P5** showed appreciable dissolution efficiencies of > 75% (Figure 5). Overall, inhibition and dissolution efficiencies obtained in the ThT fluorescence assay and CD measurements were in good agreement.

To prove that the above results were purely due to changes in A β 42 and had not been altered by the self-aggregation of inhibitory peptides, we performed a time-dependent assay over a period of 10 days where all the inhibitor candidates (**P1- P5**) were incubated at 37 $^{\circ}$ C, and their effect on the fluorescence of ThT was monitored. Fluorescence enhancement shown by an inhibitor (**P1- P5**) alone was almost negligible, which was further confirmed by CD measurement, even on the tenth day of incubation modulator peptides did not adopt any

secondary conformations.¹⁰

3.3 TEM Analysis

To further consolidate our conclusions drawn from the ThT assay and CD measurements, we performed TEM to analyze the effect of **P4** and **P5** on the process of fibrillization and preformed toxic aggregates of A β 42 (Figure 6). All the experiments were, performed with 20 μ M of A β 42 in PBS buffer (10mM, pH 7.4). For inhibition experiments, A β 42 monomers were, incubated with **P4** or **P5** for 6 days at 37 °C while for reversal experiments preformed A β 42 aggregates were incubated with **P4** or **P5** for 12 days at 37 °C. A β 42, when incubated in PBS buffer at 37 °C for two days, showed the presence of long fibrillar aggregates (Figure 6). **P1** was used as a negative control as it did not show any significant changes in the inhibition or dissolution experiments as monitored in the ThT assay and CD measurements. **P1** incubated with A β 42 showed the presence of fibrillar aggregates in both inhibition and reversal experiments as shown in Figures 6b and 6e, respectively. In contrast, **P4** showed a complete absence of fibrils in the inhibition experiment confirming the prevention of fibrillar growth of A β 42 (Figure 6c). In the case of reversal experiment, there were no signs of fibrils in **P4** (Figure 6f). Similarly, **P5** showed the absence of fibrillar aggregates in inhibition (Figure 6d) and reversal (Figure 6g) experiments. Further, the observed globular structure of **P4** treated A β 42 fibrillar aggregates as shown in Figure 6f could be misunderstood as toxic oligomeric species. To investigate this, we performed a dot blot analysis where A β 42 (20 μ M) aggregates were incubated with **P4** and **P5** in 1:2 (A β 42: inhibitor) stoichiometry for 12 days at 37 °C and then treated with A11 antibody (which specifically binds to toxic A β 42 oligomeric species) followed by treatment with secondary antibody and chemiluminescence intensity was measured. The positive control, A β 42 oligomers showed a signal, whereas A β 42+ **P4** and A β 42+ **P5** did not show any signal indicating absence of toxic oligomeric

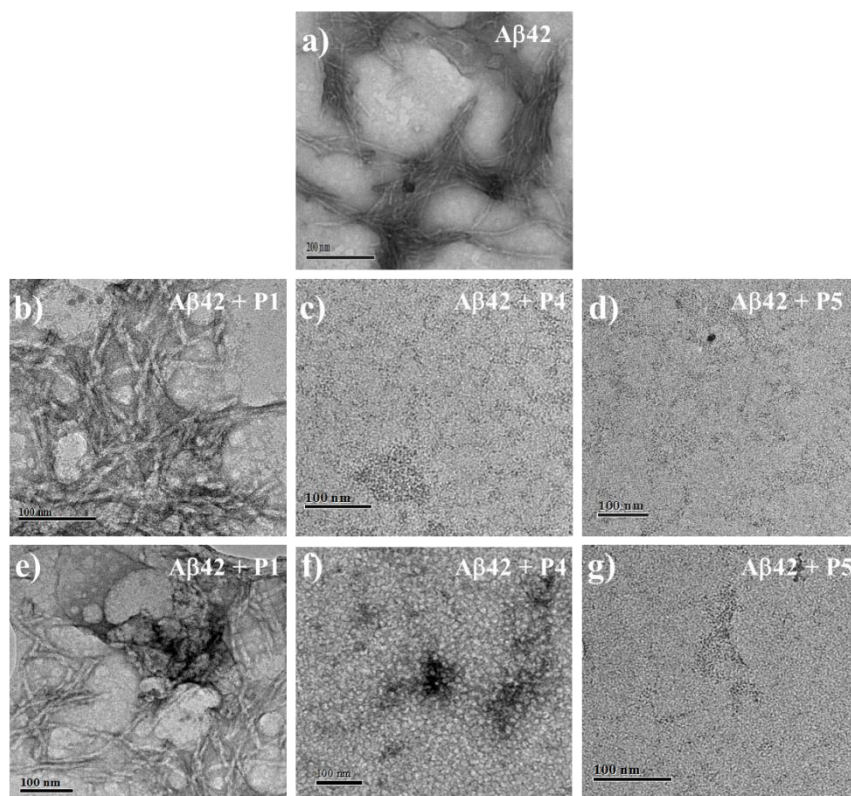


Figure 6. Electron microscopy examination to study the effect of **P1**, **P4** and **P5** on A β 42 fibrillization and dissolution of aggregates. **P1**, **P4** and **P5** were incubated with 20 μ M of A β 42 monomers or their aggregates at 37 $^{\circ}$ C in 1:2 (A β 42:inhibitor) stoichiometry and analyzed on day 6 for the inhibition assay and day 12 for the reversal assay experiments. Inhibition assay: A β 42 a, A β 42 + **P1** b, A β 42 + **P4** c, and A β 42 + **P5** d. Reversal assay: A β 42 + **P1** e, A β 42 + **P4** f, and A β 42 + **P5** g. **P1** showed the least effect on the morphology of A β 42 fibrils, whereas **P4** and **P5** showed prevention of A β 42 fibrils formation in inhibition assay and dissolution of A β 42 aggregates in reversal assay. Scale bar: 100 nm.

species. To further verify the findings, toxicity assay was performed where yeast cells (*saccharomyces cerevisiae*) were incubated with A β 42 oligomers (50 μ M) and A β 42 (50 μ M) aggregates which were treated with **P4** in 1:2 (A β 42:**P4**) stoichiometry, at 37 $^{\circ}$ C and their effect on the growth curve was monitored. A β 42 oligomers showed high toxicity, whereas A β 42+**P4** sample showed the least effect on the growth curve of yeast cells. Therefore, the dot blot analysis and toxicity assay confirm that globular structures seen in Figure 6f are not toxic A β 42 oligomeric species.¹² Therefore, TEM data confirmed that **P4** and **P5** were involved in the inhibition and dissolution of toxic aggregates, which is in agreement with the conclusions drawn from other experiments.

3.4 Blood plasma and proteolytic stability for peptidomimetics

The impact of N-terminal modification (**P2** and **P3**) and Sr (*N*-methylglycine) substitution (**P4** and **P5**) in **P1** were investigated for their proteolytic stability towards blood plasma proteases. The assay involved the incubation of peptides (50 μ M) with blood serum at 37 °C for a period of 24 h and assessing the amount of intact peptides at different time points (0, 3, 6, 12 and 24 h) using RP-HPLC. **P1** exhibited the greatest susceptibility towards the serum proteases with a serum half-life of \sim 3 h, and 80% of the **P1** was degraded at 24 h (Figure 7). In contrast to that, **P2** and **P3** with modified N-terminal of the **P1** (thymine and barbiturate,

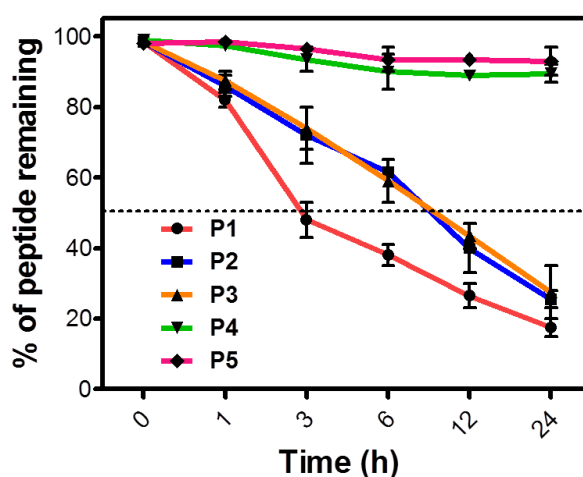


Figure 7. Serum stability of inhibitor candidates. **P1**, **P2**, **P3**, **P4** and **P5** (50 mM) were incubated in human blood serum (HBS) and were analyzed for a duration of 24 h to determine the percentage of intact inhibitor. **P1**, **P2** and **P3** degraded with time, whereas **P4** and **P5** showed high stability towards the serum proteases. Each experiment was repeated three times ($n = 3$).

respectively) showed a better protease stability towards blood plasma. Both **P2** and **P3** followed almost a similar path of degradation with time, where they showed a half-life of \sim 10 h. This was 3 times higher compared to **P1** indicating that the N-terminal modification with a non-amino acid moiety had enhanced the blood protease stability by interfering with the degradation ability of proteases. At 24 h, both **P2** and **P3** were degraded to 70%, which was comparable to **P1** suggesting that stability of both **P2** and **P3** decreased with time. Remarkably, **P4** and **P5** were very stable towards blood plasma proteases in comparison to the other peptides (**P1**, **P2** and **P3**). After 24 h, more than 90% of **P4** and **P5** were intact with

P5 exhibiting relatively higher stability than **P4** (Figure 7). Proteolytic enzymes generally recognize the specific amide bond between the natural amino acids and cleave them. In the case of **P1**, **P2** and **P3** all the amino acids were natural (except N-terminal modifications in **P2** and **P3**, which showed marginally higher stability) and could be easily recognized by proteases; these peptides thus, degraded with time. On the other hand, **P4** and **P5** with an unnatural amino acid (Sr: *N*-methylglycine) in alternate positions were not recognized by the blood plasma proteases, resulting in their high blood plasma protease stability.

To further validate these results, we performed a stability assay for **P1-P5** (50 μ M) in the presence of proteolytic enzymes trypsin and pepsin. Enzymes trypsin and pepsin are well-known to cleave the C-terminal of lysine and amide bond involving aromatic amino acids, respectively. Peptides were incubated with both the enzymes at 37 °C for 24 h, and the amount of the residual intact peptide was monitored in each case at different time points (0, 3, 6, 12 and 24 h) using RP-HPLC. **P1**, **P2** and **P3** were less stable, of which **P1** degradation was fastest followed by **P2** and **P3**. However, **P4** and **P5** were highly stable under similar conditions, and > 90% of the peptidomimetics was intact after 24 h of incubation in the presence of both the enzymes suggesting their poor recognition by the two proteases. Overall, the stability assays with blood plasma and proteolytic enzymes led to similar conclusions and confirmed the stability, order **P5**>**P4**>>**P3**≈**P2**>**P1**.

3.5 Designed peptidomimetics nullify A β toxicity in an autophagy-dependent manner

All the peptides and their analogues (**P1-P5**) were screened for their ability to ameliorate the toxicity caused by A β 42 in a *Saccharomyces cerevisiae* model. N-terminal of A β 42 was tagged with GFP (WT GFP β A) while the WT GFP strain was used as a control. To study the non-toxic nature of inhibitor candidates and their influence on culture growth curves of WT GFP were analyzed. In **P1-P5** (300 μ M) treated cells, the growth curves were similar to that of the untreated sample. No significant growth lag or drop in absorbance (A_{600}) was observed

in the presence of peptides. On the other hand, the growth curve of WT GFP β A exhibited a severe lag with the culture not entering the exponential phase due apparently to A β toxicity³⁶. The apparent growth lag displayed by WT GFP β A strain compared to WT GFP was used for screening the inhibitors (Figure 7). Among five inhibitors, growth curves of WT GFP β A strain in the presence of peptides **P1**, **P2** and **P3** appeared similar to that of untreated cells. However, the cells treated with peptides **P4** and **P5** displayed a growth pattern similar to that of WT GFP. Hence, it is inferred that peptides **P4** and **P5**, but not the others, successfully rescued the growth lag in WT GFP β A strain. Upon **P4** and **P5** treatments, various growth parameters like growth rate and doubling time in WT GFP β A strain showed significant time rescue comparable to that of WT GFP where the growth rate was increased whereas doubling was reduced evidently.

Next, we probed if the inhibitors were able to clear the A β aggregates (tagged with GFP) *in vivo*. For this, we performed a microscopy assay wherein the GFP β A appear as punctate dots when present as aggregates while its clearance in the vacuole is marked by the presence of free GFP. GFP β A-expressing cells, when either untreated or treated with peptide **P1**, displayed characteristic punctate formation inside the cells and no free GFP was present in the vacuole (Figure 7c). The free GFP was observed in vacuoles in culture treated with **P4** and **P5**, but was absent in **P1** (control) and untreated cells (Figure 7c) of WT GFP β A strain. Pertaining to **P4** and **P5**, diffused GFP signal in the vacuole colocalized with the vacuolar lumen staining dye CMAC-Blue, suggesting that incubating cells with these peptides resulted in GFP β A aggregates being degraded in the vacuole to release free GFP.

Autophagy has been shown to play a key role in degrading the β -amyloid oligomers or fibrils.¹³ Degradation of protein aggregates by selective autophagy mechanism is defined as aggrephagy.¹⁴ In a cellular context; the disaggregated fibrils are captured and released into the vacuole for degradation through autophagy. To investigate whether the appearance of free

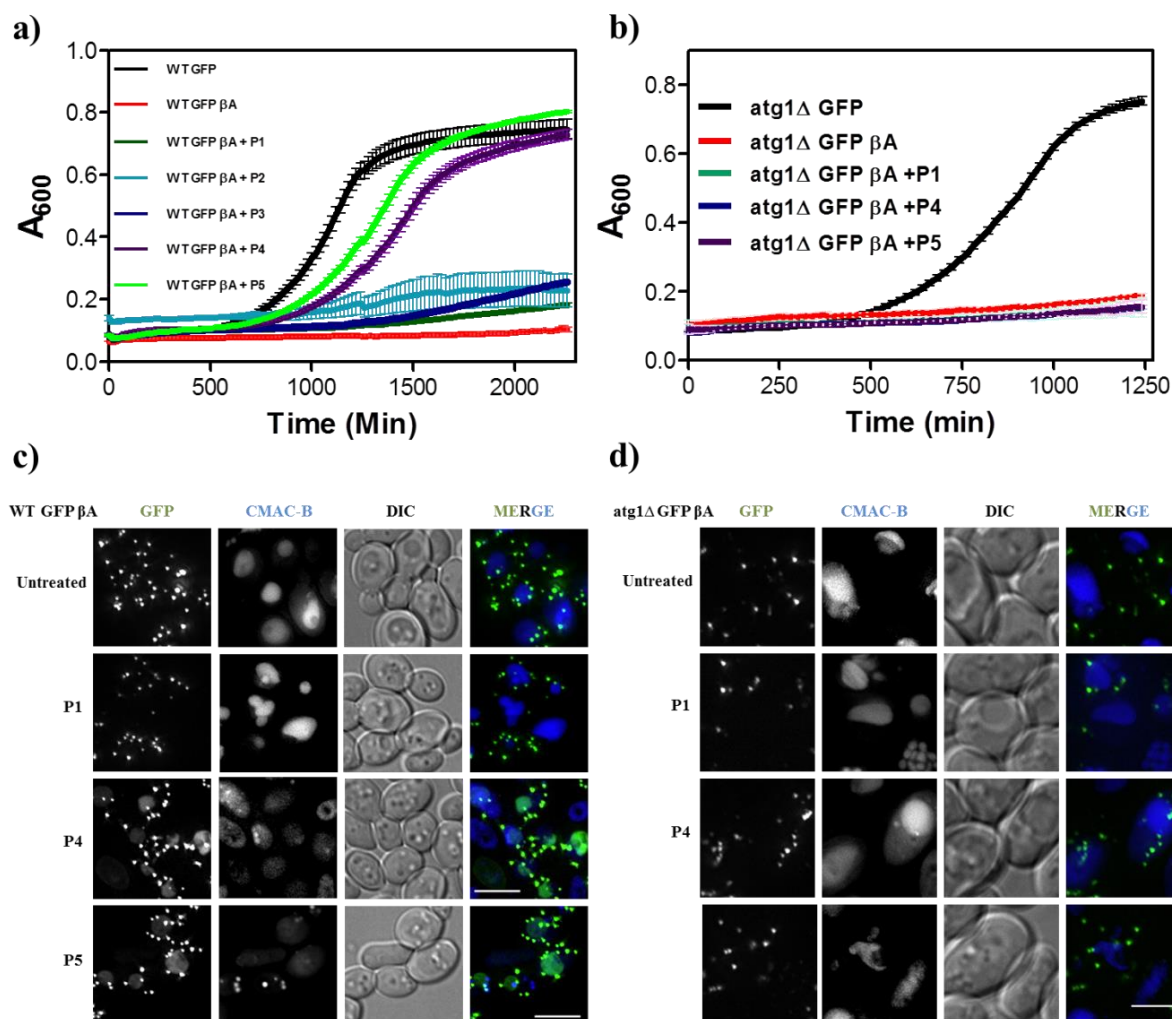


Figure 7. Screening of inhibitors in a yeast model of A β toxicity. a) All inhibitor candidates were screened in WT GFP β A strain at the concentration of 300 μ M. b) Investigation of **P1**, **P4** and **P5** in the *atg1* Δ GFP β A strain by monitoring growth curves at peptide concentrations of 300 μ M. Each experiment was repeated three times ($n = 3$). Error bars represent the standard deviation (SD) of the measurement. Degradation of GFP A β in monitored by fluorescence microscope. c) WT GFP β A and (d) *atg1* β A strains were treated with **P1** (control), **P4** and **P5** and vacuoles stained with CMAC-Blue Scale bars: 7.5 μ m (a) and 5 μ m (b). The concentration of **P1/P4/P5**: 300 μ M.

GFP in the vacuoles of cells treated with **P4** and **P5** was due to autophagy; we repeated the growth rescue experiment in cells defective in autophagy (Δ *atg1* mutant). Although **P4** and **P5** were able to rescue the growth lag in WT GFP β A strain, they failed to do so in *atg1* Δ GFP β A strain (Figure 7b). In addition, vacuolar free GFP was not seen in *atg1* Δ GFP β A strain treated with **P4** and **P5** (Figure 7d) similar to untreated and **P1** treated cells. The peptides neither reduced the A β toxicity nor degraded GFP β A in the autophagy mutant. This

clearly indicated that autophagy was responsible for clearing the A β aggregates, by **P4/P5** treatments in WT GFP β A cells.

3.6 Conclusion

In conclusion, we rationally designed recognition unit based peptidomimetic inhibitors, which target hydrogen bonding and other noncovalent interactions necessary for A β to form toxic aggregates in Alzheimer's disease progression. ThT fluorescence assay and CD data confirmed that peptides with N-terminal thymine-modification (**P2**) and peptidomimetics containing N-terminal thymine and sarcosine (*N*-methylglycine) in alternate positions of KLVFFA (**P4** and **P5**) exhibited both inhibition and dissolution ability towards A β 42 aggregates with the latter two being considerably more efficient. TEM analysis demonstrated that **P4/P5** treated A β 42 monomers or its aggregates showed no signs of fibrillar aggregates compared aggregates found in control study, which further strengthens our hypothesis that **P4** and **P5** are involved in inhibition and dissolution of A β 42 aggregates. Furthermore, peptidomimetics **P4** and **P5** showed high stability towards blood serum and proteolytic enzymes like trypsin and pepsin compared to **P1-P3**. Therapeutic contenders **P4** and **P5** were tested in a *Saccharomyces cerevisiae* model of A β 42, where they could rescue the yeast cells from A β 42 toxicity by clearing them through the autophagy pathway. Although down-regulation of autophagy is implicated in Alzheimer's disease, for the first time we validated the role of active autophagy in clearance of toxic A β aggregates using peptidomimetics. These results on rationally designing peptidomimetic inhibitors for tackling A β 42 toxicity in Alzheimer's disease will strongly impact the identification of novel drug candidates for this hitherto incurable disease.

3.7 Experimental section

3.7.1 Synthesis of peptide and its mimetics, purification, and analysis. The control peptide

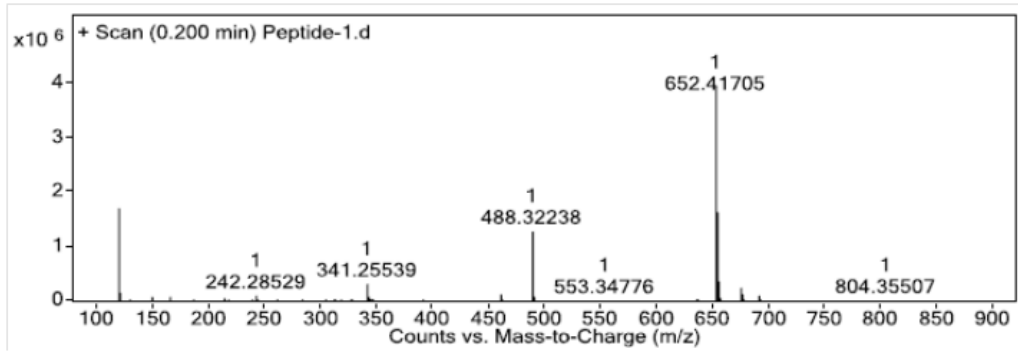
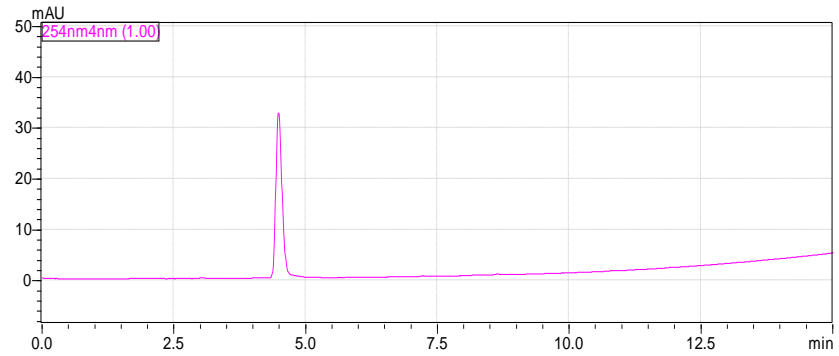
P1 (KLVFF), N-terminal modified peptides **P2** (Thymine-Lys-Leu-Val-Phe-Phe) and **P3** (Barbiturate-Lys-Leu-Val-Phe-Phe), and the N-methyl glycine (sarcosine: Sr) substituted peptidomimetics **P4** (Thymine-Sr-Leu-Sr-Phe-Sr-Ala), and **P5** (Thymine-Lys-Sr-Val-Sr-Phe-Sr) were synthesized following standard 9-fluorenylmethoxycarbonyl (Fmoc) chemistry on an automated peptide synthesizer Syro II from MultiSynTech. Rink amide resin (Novabiochem) was used as a solid support in the synthesis with an amide at the C-terminal. Fmoc-protected sarcosine (Sr) was prepared using standard protection procedure and directly used for the synthesis of **P4** and **P5** using the peptide synthesizer. Amino acids were coupled using HBTU as the activating reagent, DIPEA as the base and DMF as a solvent; for deprotection of Fmoc 40% piperidine in DMF was used. **P1**, **P2** and **P3** were synthesized with a coupling time of 1 h per amino acid, whereas for **P4** and **P5** coupling time was increased to 2 h to obtain higher coupling yields. All the peptides and peptidomimetics were purified using a reverse-phase (RP) preparative HPLC on the C18 column at 40 °C. Product purity was greater than 99% as ascertained by analytical HPLC. The molecular masses of the peptides and their mimetics were verified with HRMS (Q-TOF) analysis.

HPLC and HRMS traces for P1, P2, P3, P4 and P5

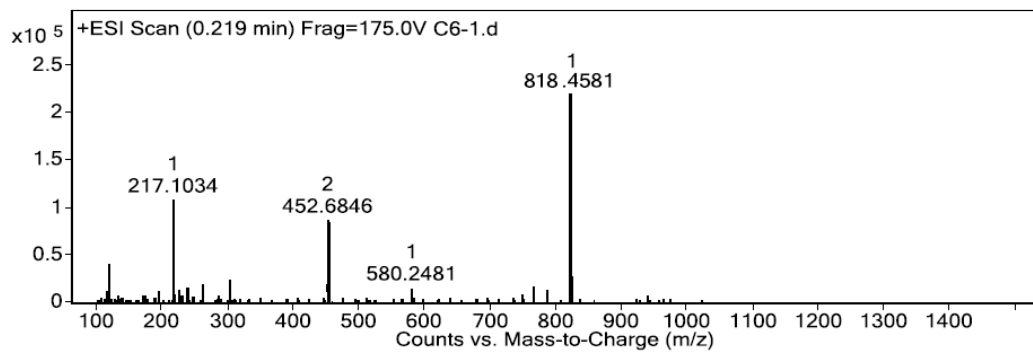
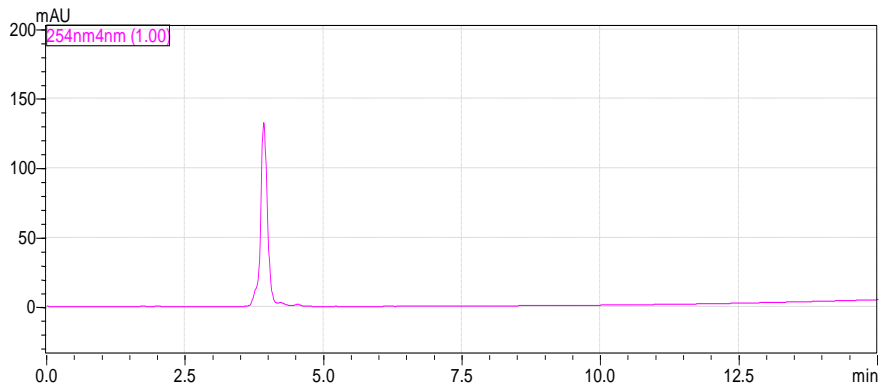
Name	Sequence	Actual mass	Obtained mass [M+H] ⁺
P1	Lys-Leu-Val-Phe-Phe	652.4186	652.4170
P2	Thymine - Lys-Leu-Val-Phe-Phe	818.4565	818.4581
P3	Barbiturate - Lys-Leu-Val-Phe-Phe	820.4357	820.4373
P4	Thymine-Sr -Leu-Sr-Phe-Sr-Ala	728.3731	728.3716
P5	Thymine-Lys-Sr-Val-Sr-Phe-Sr	771.4153	771.4146

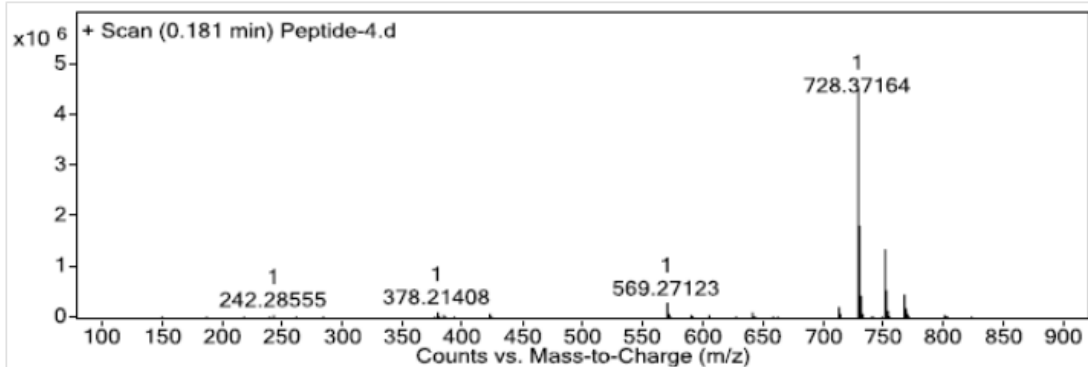
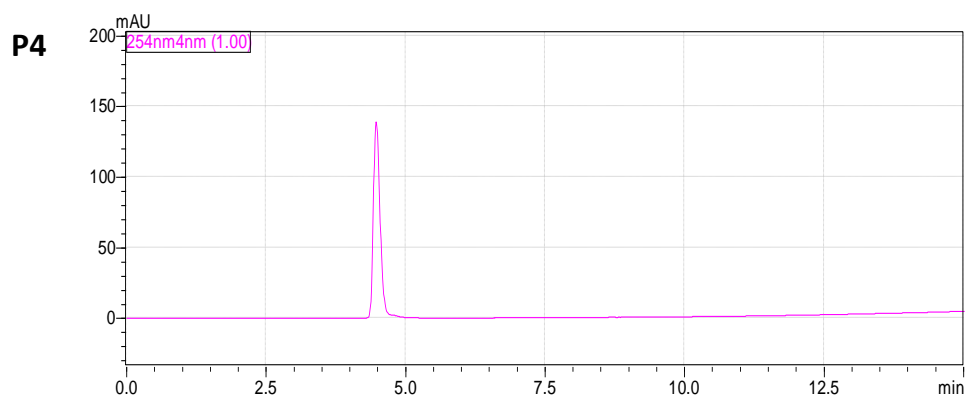
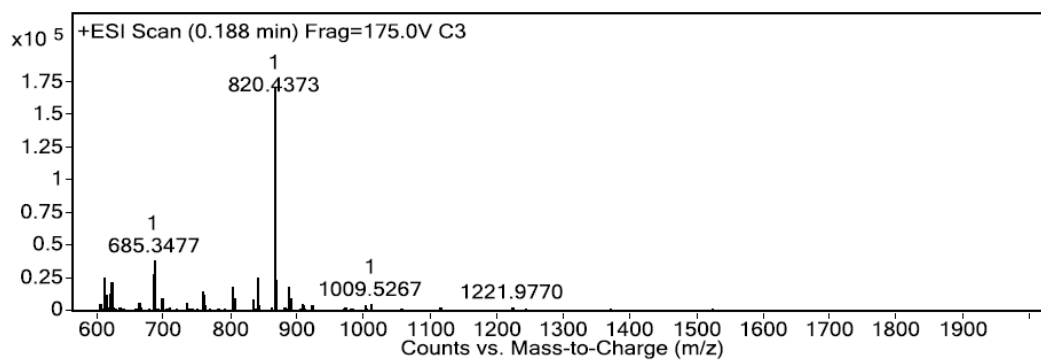
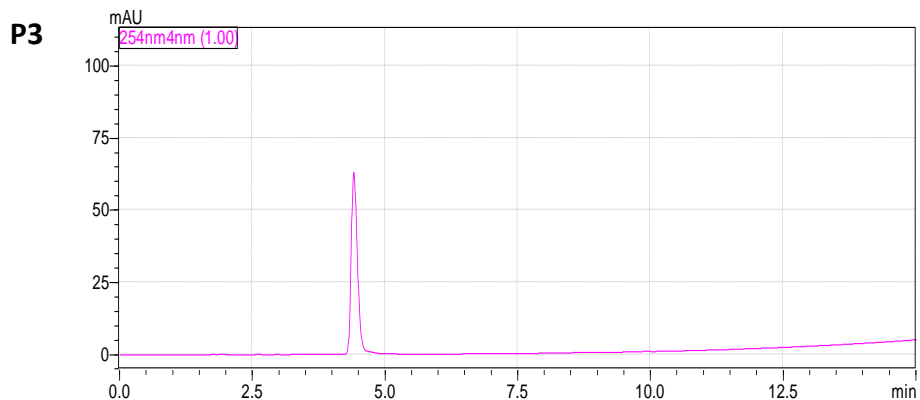
Sr = Sarcosine (N-methylglycine).

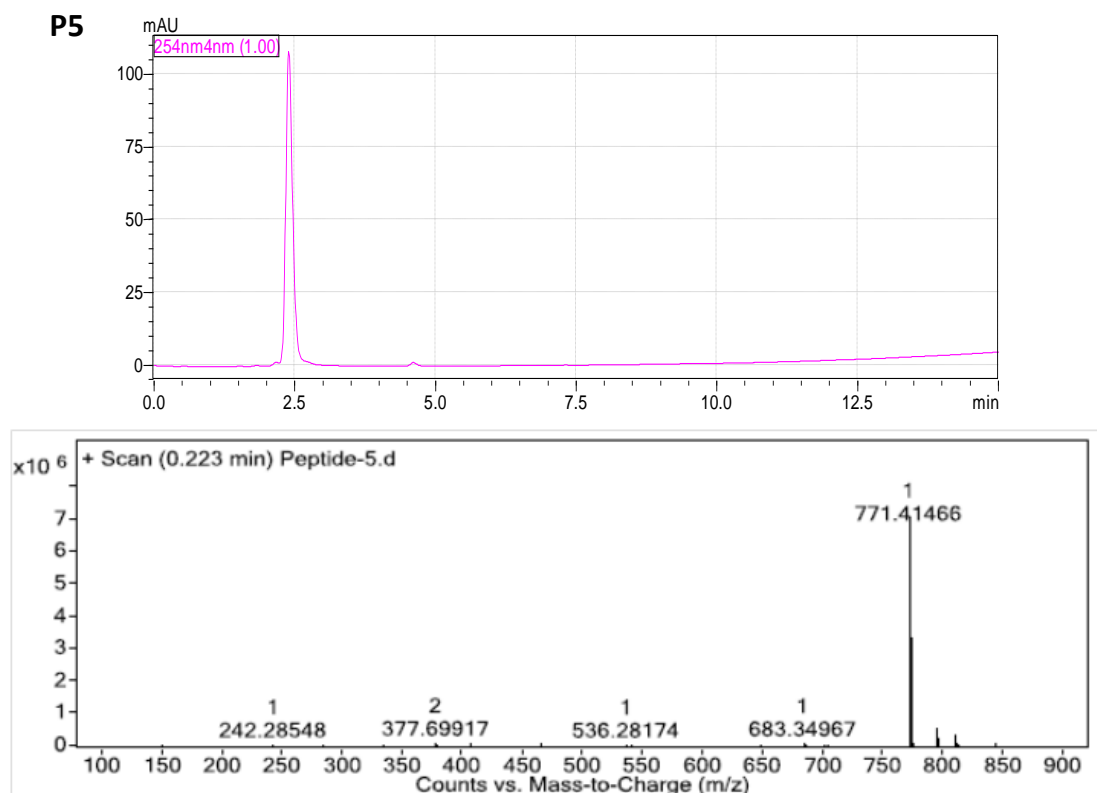
P1



P2







3.7.2 Preparation of A β 42 fibrillar aggregates and oligomers. A β 42 peptide (0.25 mg) (Merck, calbiochem) was dissolved in hexafluoro-2-propanol (HFIP, 0.2 mL) and incubated at room temperature for 1 h. HFIP was then removed by a flow of nitrogen and further dried under vacuum. HFIP-treated A β 42 was then dissolved in DMSO to a final concentration of 1 mM and diluted to 200 μ M with 10 mM PBS (pH 7.4). The solution was incubated at 37 $^{\circ}$ C for 48 h with gentle and constant shaking. The formation of A β 42 fibrils was confirmed by Thioflavin T (ThT) assay. For the oligomer preparation, A β 42 was dissolved in DMSO to a final concentration of 1 mM and diluted to 100 μ M in PBS buffer (10 mM, pH 7.4). The solution was incubated at 37 $^{\circ}$ C for 1 h, after which the sample was incubated for 24 h at 4 $^{\circ}$ C for 1 h. The obtained sample was centrifuged, and the supernatant with oligomers was used for further experiments.

3.7.3 Fluorescence spectroscopy. Fluorescence spectral measurements were carried out using Perkin Elmer Model LS 55 fluorescence spectrophotometer. Maximum fluorescence of ThT was observed with the excitation and emission wavelengths set at 450 and 483 nm, respectively. A ThT concentration of 5-10 μM was used for amyloid fibrillization and dissolution assay based on the A β 42 fibrillar concentration.

3.7.4 Circular dichroism. The circular dichroic (CD) spectra were recorded using a Jasco J-815 spectrometer under a nitrogen atmosphere. Peptides were dissolved in 10 mM PBS buffer at pH 7.4 at concentrations of 20 μM . A 10 mm path length was used for the measurements. Four to five scans were acquired from 200 to 300 nm.

3.7.5 Fibrillogenesis and fibril dissolution assays. Prior to the experiment, **P1, P2, P3, P4** and **P5** were dissolved in HFIP and were evaporated under a stream of dry nitrogen. The dried samples were re-suspended in 10 mM PBS buffer at pH 7.4. An aliquot of A β 42 peptide was then added to the solution with or without one of the inhibitor **P1, P2, P3, P4** and **P5**. The mixtures were vortexed for approximately 30 s and then incubated at 37 °C for 2-3 days without shaking. The final concentration of A β 42 in the mixture was 20 μM . For a dissolution experiment, A β 42 was incubated alone for 2 days to allow fibrils to form. An aliquot of the formed fibrils in 10 mM PBS buffer was then added to the inhibitor peptidomimetics. The amount of fibrils remaining intact was assayed using that fluorescence, CD measurements and transmission electron microscopy as described below.

3.7.6 Transmission electron microscopy (TEM). An aliquot of appropriately formed samples of A β 42 aggregates, A β 42-inhibitor and A β 42 aggregate-inhibitor (5 μL) were adsorbed onto 200-mesh carbon and formavar-coated grids for 2 min and washed for 1 min with distilled water. The samples were negatively stained with 2% uranyl acetate for 5 min and washed for 1 min with distilled water⁴⁴. The samples were air-dried overnight and viewed with a JEOL, JEM 3010 instrument operating at 300 kV.

3.7.7 Dot blot analysis. PVDF membranes (Sigma Aldrich) were activated by incubating them in methanol solution for 5 min followed by washing with 10 mM PBS buffer (3X). Samples were spotted on the membranes (in triplicate), and non-specific sites were blocked by soaking in 5% BSA in PBS buffer and skim milk (0.5-1 hour, RT). Then membranes were incubated with either primary antibody A11 (1:3000) for oligomer or Anti-beta-amyloid 1-42 antibody (Merck millipore) for A β 42 fibrillar aggregates at 4 °C for overnight and then washed with PBS buffer (3 x 5 min). These membranes were further incubated with the anti-mouse secondary antibody (1:10000) conjugated with horseradish peroxidase (HRP) for 30 min at RT. These membranes were washed with PBS buffer (3 x 5 min), incubated with enhanced chemiluminescence (ECL) reagent for 1 min and recorded the chemiluminescence in SYNGENE G-box. The signals from the unknown samples were compared to that of standard and concentration was estimated.¹⁰

3.7.8 Serum stability assay. Human blood serum (HBS) was used to determine serum stability of the inhibitors. The HBS was centrifuged to remove the lipid component, and the supernatant was incubated at 37 °C. 50 Mm of each inhibitor (**P1**, **P2**, **P3**, **P4** and **P5**) was incubated in HBS, and then 40 μ L triplicate aliquots were removed at 0, 1, 3, 6, 10, 16, and 24 h. Each serum sample was quenched with 40 μ L of 6 M urea and incubated at 4 °C for 10 min. Then, each serum sample was quenched with 40 μ L of trichloroacetic acid (20%) and incubated for another 10 min at 4 °C to precipitate the serum proteins. The samples were centrifuged for 10 min, and 200 μ L of the supernatant was analyzed on RP-HPLC using a linear gradient of solvent B (0.3 mL/min flow rate). The control samples containing equivalent amounts of inhibitors in PBS buffer were subjected to the same treatment procedure. The percentage recovery of inhibitors was detected by integration at 254 nm.¹⁵

3.7.9 Protease stability assay. Preliminary stability assays were performed using the enzymes pepsin and trypsin. For all assays, peptides were incubated with the enzyme at 37 °C

for 24 h. All digestion assay data were analyzed by RP-HPLC. Trypsin and pepsin stocks were prepared in 100 mM ammonium bicarbonate (NH_4HCO_3) buffer (pH 8) and 100 mM formic acid buffer (pH 2), respectively. All the peptides/peptidomimetics (**P1**, **P2**, **P3**, **P4** and **P5**) were incubated with trypsin and pepsin enzymes in 100 mM NH_4HCO_3 buffer (pH 8) and formic acid buffer (pH 2), respectively, at 37 °C. The trypsin reactions were halted with 0.05% formic acid, and the pepsin reactions were halted with 100 mM NH_4HCO_3 . Then the samples were analyzed by RP-HPLC using a linear gradient of solvent B (0.3 mL/min flow rate); similar data points were collected at various time points between 0 and 24 h (1 h, 3 h, 6 h, 12 h and 24 h) during incubation and analyzed in triplicates. The percentages of recovered peptide/peptidomimetics were detected by integration at 254 nm.¹⁶

3.7.10 Yeast media, plasmids and media used. Wild type (BY4741; Mat α ; his3 Δ 1; leu2 Δ 0; met15 Δ 0; ura3 Δ 0) and autophagy mutant (*atg1* Δ ;BY4741; Mat α ; his3 Δ 1; leu2 Δ 0; met15 Δ 0; ura3 Δ 0; *atg1*: KanMX4) strains of yeast were employed. Plasmids pRS 416 GFP, pRS 416 β A were gifted by Ian Macreadie (CSIRO, Australia).¹⁷ The plasmid pRS 306 Gal β A was generated by sticky end ligation of vector pRS 306 Gal (Spe I/ Xho I) and insert GFP- β A (Spe I/ Xho I) obtained from the plasmid under pRS 416 vector backbone. These plasmids were used to generate sSNS1, sSNS50 and sSNS51 strains expressing GFP only, GFP-tagged β -amyloid ($\text{A}\beta$) protein in wild-type and autophagy mutant, respectively. These strains expressed genomically integrated GFP tagged $\text{A}\beta$ or GFP only under an inducible galactose promoter. SD-Ura (Synthetic Dextrose without uracil) media and galactose (2%) were used for protein induction.

3.7.11 Yeast culturing and growth assay. Strains were inoculated into SD-Ura growth medium and incubated overnight (250 rpm, 30 °C). The secondary culture was inoculated (absorbance = A_{600} around 0.2 OD) from the primary inoculum and incubated as above till A_{600} reached 0.8 OD. High throughput growth curve analysis (using Varioskan Flash,

Thermo Scientific) in the presence and absence of peptides (300 μ M) was performed by automatically recording A_{600} every 20 min in a 384-well plate.

3.7.12 β -Amyloid degradation assay. The cells were inoculated in SD-Ura medium under appropriate conditions (250 rpm, 30 °C). The secondary culture was inoculated from this primary inoculum and incubated till A_{600} reached 0.8. Then, cells were washed twice with sterile water. Subsequently, the $A\beta$ proteins were induced in yeast cells by incubating them in 2% galactose. During the induction, these cells were incubated in the presence or absence of peptidomimetics (300 μ M). After 12 h, 7-amino-4-chloromethylcoumarin-Blue (CMAC-Blue) was added and incubated further for 2 h after which cultures were imaged on a fluorescent widefield microscope (DV Elite, Deltavision).

Chapter 3B

**Synthesis of hybrid cyclic peptoids and identification of autophagy
enhancer**

Peptides are emerging as promising therapeutic agents in recent years due to their inexpensive synthesis, efficacy, specificity, and low toxicity. However, high susceptibility to proteolysis, flexibility, short half-life, denaturation, and poor target delivery and bioavailability make peptides practically less viable candidates for therapeutics. The deficiencies of linear peptides can be addressed by macrocyclization and crosslinking which provide proper conformational stability.¹⁸⁻²⁰ Although cyclic peptides offer relative stability and cell penetration efficiency, they also suffer from low *in vivo* stability and bioavailability. To address the inherent drawbacks of natural peptides, promising peptidomimetics have been developed.²¹ In particular peptoids, oligomers of *N*-substituted glycine with distinct unnatural structure possesses numerous advantages. Peptoids have long half-lives due to proteolytic resistance and good cell permeability resulting in greater bioavailability.²²⁻²⁴ However, major limitations of peptoids are their conformation flexibility and lack of secondary interactions which can reduce the selectivity and sensitivity. Yet again, the macrocyclization of peptoids has been pursued to restrict conformational flexibility.²⁵ Application of cyclic peptoids is limited by the synthetic procedures and lack of secondary amide in the backbone. The most challenging aspect of cyclic peptidomimetics synthesis is the ring-closure event.^{26,27} The yields obtained in cyclization of longer oligomers are very moderate while the cyclization of short oligomers suffers from poor yields. Increase in ring size of cyclic peptidomimetic reduces bioactivity due to enhanced flexibility. This reiterates the importance of small/medium size cyclic peptoids.

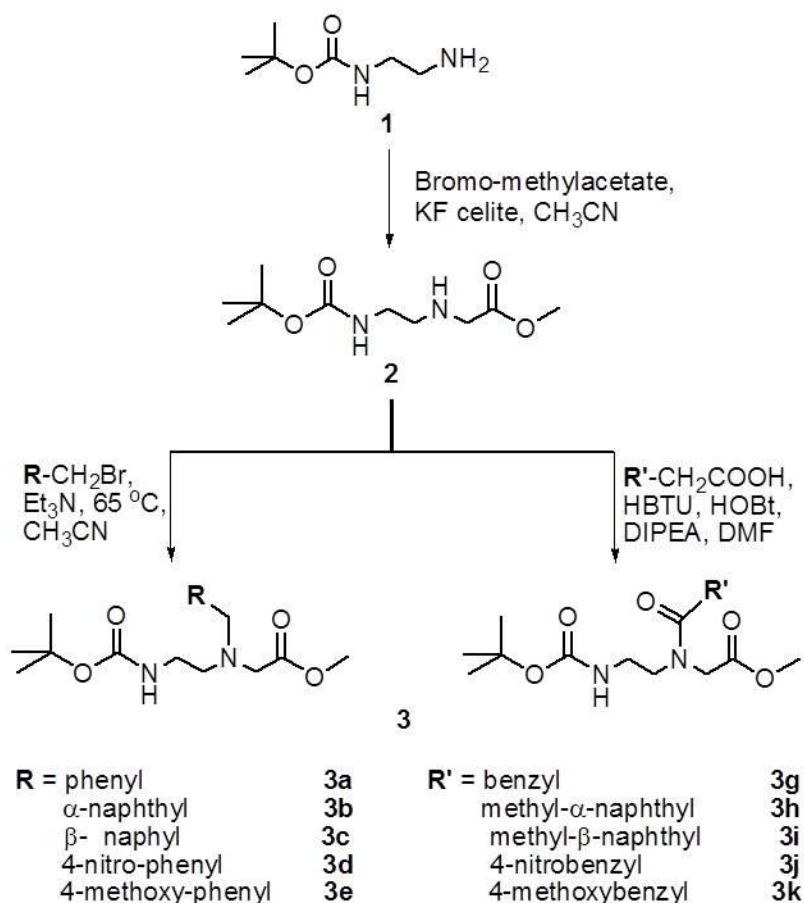
The linear and cyclic peptidomimics are studied for antimicrobial activity, DNA interaction and autophagy modulation.²⁸⁻³⁰ Autophagy is a key mechanism for long-lived protein degradation and organelle turnover and serves as a critical adaptive response that recycles energy and nutrients during starvation or stress. Small molecules have been utilized as probes to understand mechanisms as well as the relationship between autophagy and the

disease.³¹

In this chapter we have shown coupling reagent-free differential cyclization of *N*-(2-aminoethyl)glycine (*aeg*) hybrid peptoid monomer into six and twelve member cyclic peptoids. In literature, *aeg* has been extensively used as a backbone unit for the synthesis of peptide nucleic acids (PNAs).³² Our choice of *aeg* monomer stemmed from the fact that among other advantages, small and medium-size hybrid cyclic peptoids are formed with secondary amide bonds and stable conformation. Further, we employed a simple design strategy wherein ^α*N*-alkyl substituents keep the flexibility intact, while ^α*N*-acyl substituent introduces rigidity and restricted bond rotation in the *aeg* backbone. Thus, by introducing differential conformational features, *aeg* backbone is expected to display differential reactivity for cyclization. To the best of our knowledge, this is the first report wherein *aeg* monomer has been used for direct synthesis of six and twelve member hybrid cyclic peptoids under coupling reagent-free conditions. This cyclic peptoid library was screened to identify modulators of autophagy process.

3.8 Design and synthesis

The *aeg* backbone was synthesized from mono ^t*Boc*-protected ethylene diamine **1** (Scheme 1). The amine **1** was subjected to controlled mono-^α*N*-alkylation by treating with bromomethyl acetate using KF celite to obtain ^t*Boc*-protected *aeg* methyl ester **2**. Then, the second ^α*N*-alkylation of amine **2** was performed with bromomethyl derivatives using triethylamine as base to obtain excellent yields of methyl esters of ^t*Boc*-protected ^α*N*-alkyl-*aeg* monomers **3a-e** (Scheme 1). The amine **2** was coupled to acetic acid derivatives to yield methyl esters of ^t*Boc*-protected ^α*N*-acyl-*aeg* monomers **3g-k**. The ^t*Boc*-protected ^α*N*-benzyl-*aeg* methyl ester monomer (**3a**) was subjected to *in situ* ^t*Boc*-deprotection and subsequent cyclization at 110 °C in *sec*-butanol containing 1% acetic acid (Table 1).³³ The monomer **3a** undergoes intramolecular cyclization to form sixmembered cyclic product (**4a**). Interestingly,



Scheme 1. Synthesis of *tBoc*-protected $^{\alpha}\text{N}$ -alkyl (**3a-e**) and $^{\alpha}\text{N}$ -acyl (**3g-k**) modified *aeg* methyl ester monomers.

under similar conditions $^{\alpha}\text{N}$ -(2'-phenylacetyl)-*aeg* methyl ester (**3g**) gave very good yield of twelve member hybrid cyclic peptoid **4g** through intermolecular cyclization (Table 2). To ascertain generality of this differential cyclization, we have tested variable functionalities for $^{\alpha}\text{N}$ -alkyl and $^{\alpha}\text{N}$ -acyl-substituents (Table 1 and 2). All the monomers were, subjected to *in situ* *tBoc*-deprotection and subsequent cyclization. The peptoid monomers with α - and β -naphthalene functionalities ($^{\alpha}\text{N}$ -alkyl: **3b**, **3c** and $^{\alpha}\text{N}$ -acyl: **3h**, **3i** respectively) were chosen to demonstrate if ring cyclization is independent of type of aromatic moiety and position of attachment. Monomers having electron withdrawing (4-nitrophenyl, **3d** and **3j**) and donating (4-methoxyphenyl, **3e** and **3k**) groups were selected to study the influence of the electronic effects on cyclization. Interestingly, the propensity of differential cyclization was found to be general, as the $^{\alpha}\text{N}$ -alkyl- and $^{\alpha}\text{N}$ -acyl-substituted *aeg* monomers formed the six and twelve

Table 1. Intramolecular cyclization of α N-alkyl-*aeg* monomers to form six membered cyclic products

Reactant	Product	Yield (%) ^[a]
 3a	 4a	73
 3b	 4b	69
 3c	 4c	71
 3d	 4d	79
 3e	 4e	80
 3f	 4f	43

^[a]Yields reported are of purified products

member products (**4b-e** and **4h-k**) respectively. The monomer **3f** with the ethyl linker in α N-alkyl-substituent also gave six member product **4f** (Table 1). This further confirmed our assumption that the flexibility of α N-alkyl-*aeg* favors intramolecular cyclization. In contrast,

Table 2. Intermolecular cyclization of α -N-acyl-aeg monomers 12 membered cyclic product

1. TFA (50 %), DCM
2. sec. butanol, 110 °C

Reactant	Product	Yield (%) ^[a]
		72
		68
		76
		82
		68
		78
		72

^[a]Yields reported are of purified products

carbonyl group of $^{\alpha}N$ -acyl-substituent of *aeg* not only restricted its free-rotation but also rigidified the molecular conformation favoring intermolecular cyclization to form twelve member products. To extend the scope of this methodology, we synthesized adenine and thymine functionalized twelve member products **4l** and **4m** (Table 2).

3.9 Characterization of cyclic hybrid peptoid

NMR and high resolution mass spectroscopy (HRMS) product analysis confirmed the $^{\alpha}N$ -alkyl and $^{\alpha}N$ -acyl enforced differential cyclization of *aeg* methyl ester monomers. The 1H NMR spectra (in *DMSO-d*₆) of monomer units (eg., **3d** and **3j**) showed singlets at 1.5 and 3.7 ppm corresponds to *t*Boc and methyl ester (-OCH₃) groups respectively. In addition to the expected disappearance of proton peak for *t*Boc group in the respective spectra of products (**4d** and **4j**), peaks for free-amine (-NH₂) and -OCH₃ were absent, indicating the possible cyclization of monomers (Figure 8a). The 1H NMR spectrum of product from **3d** showed four peaks (2', 3', 5' and 7') in the region 2.4 – 4.0 ppm, a broad peak at 7.85 ppm and two doublets at 7.51-7.49 and 8.18-8.15 ppm correspond to four -CH₂, amide proton (H_a) and four aromatic protons respectively, confirmed six membered cyclo-*aeg* structure for product **4d** (HRMS mass = 236.1055, [M+H]⁺). The spectrum of product from **3j** (Figure 8a) showed completely different splitting pattern including two amide peaks at 8.05 and 8.12 ppm for H_b and H_c respectively, indicating the possible product as either a trimer or a cyclic dimer. The trimer was ruled out by HRMS analysis (549.1664, [M+Na]⁺), confirming the twelve membered cyclic dimer (*aeg-aeg*) product **4j**. Surprisingly, seven peaks in the region 3.0- 4.3 ppm (2, 3, 5, 9, 11, 14 and 20) corresponding to protons of eight -CH₂ groups revealed that **4j** exists as nonsymmetrical cyclic homodimer. The nonsymmetrical structure of **4j** was further established by ^{13}C NMR and ^{13}C DEPT-135 (distortionless enhancement by polarization transfer) studies.

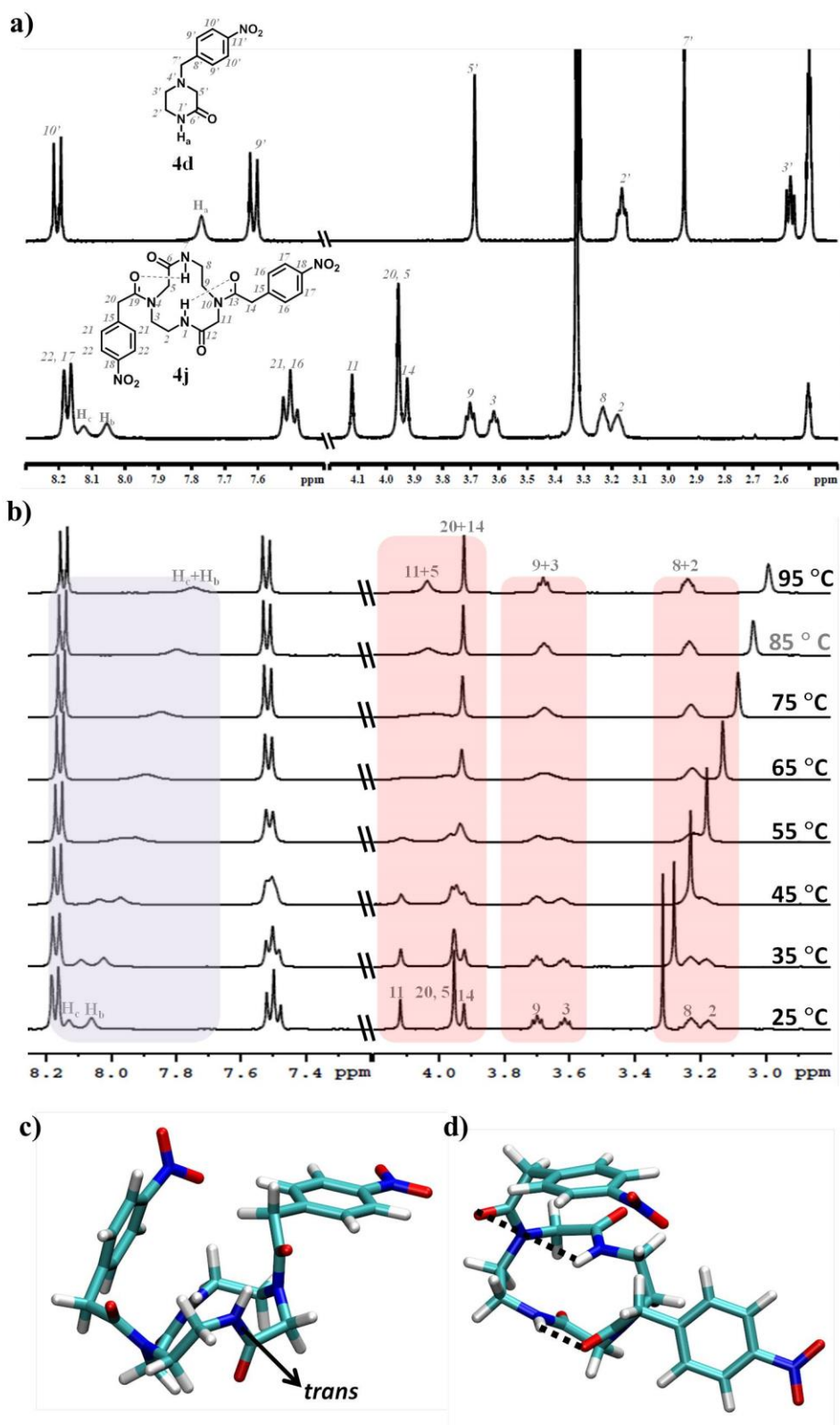


Figure 8. NMR studies and energy minimized structure of **4j**. (a) Comparative ^1H NMR spectra of cyclic products **4d** and **4j** ($\text{DMSO}-d_6$). (b) Variable temperature ^1H NMR spectra of **4j** (in $\text{DMSO}-d_6$). Energy minimized model structure (c) and (d) of **4j** showing *trans* amides and intramolecular hydrogen bonds (••••) respectively.

3.10 Hydrogen bonding interaction in cyclic hybrid peptoids

Next, we investigated the hydrogen bonding patterns in representative examples **4d** and **4j** by temperature and concentration dependent studies.³⁴ ^1H NMR study revealed the presence of intermolecular hydrogen bonding interactions in **4d** (Figure 9). For **4j**, ^1H NMR spectra showed an upfield shift of 0.33 and 0.39 ppm respectively for the amide protons H_b and H_c with increasing temperature from 25 °C to 95 °C confirming the presence of strong hydrogen bonding interactions (Figure 8b). The nature of hydrogen bonding in **4j** was validated by the

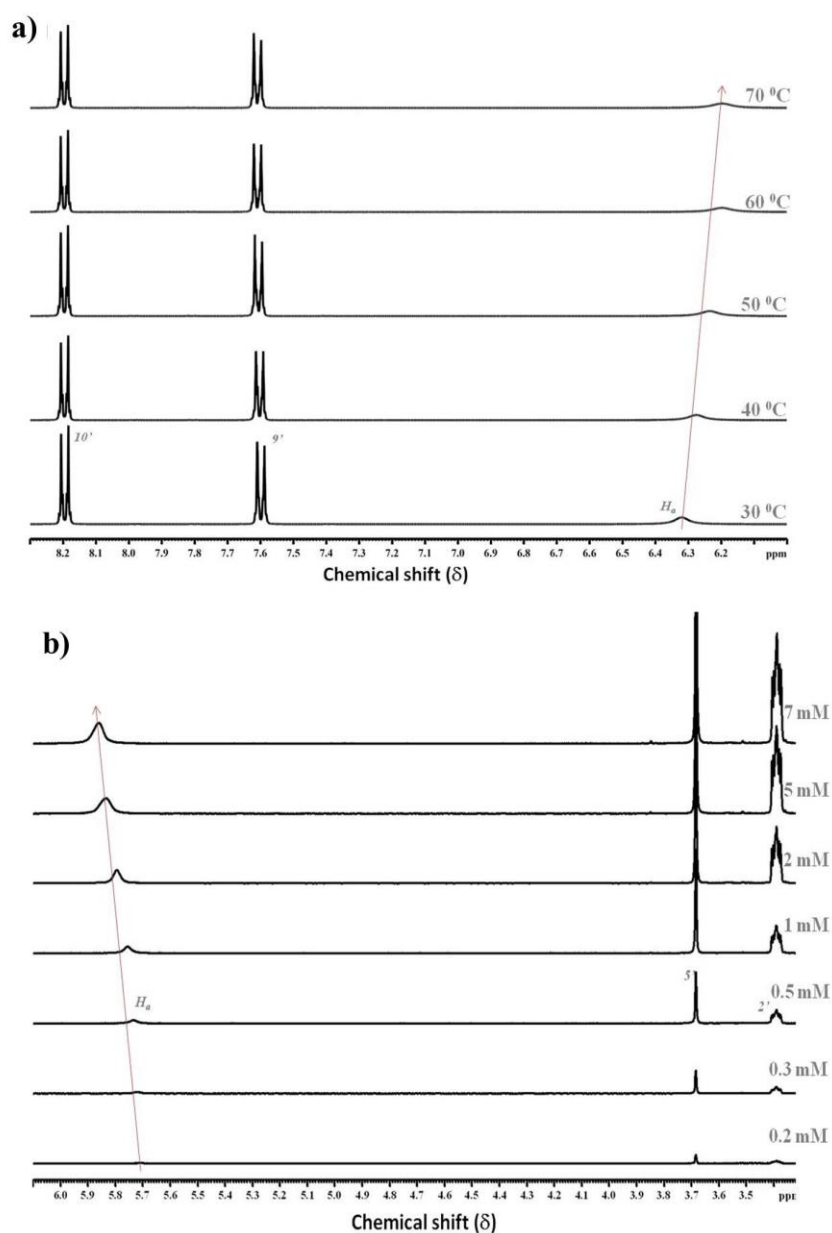


Figure 9. (a) Temperature and (b) concentration-dependent ^1H NMR spectra of **4d** in CD_3CN .

concentration-dependent NMR study. ^1H NMR spectra with decrease in concentration (dilution) of **4j** (3.8, 1.9, 0.95, 0.47 and 0.23 mM) did not show change in the peak position of H_a and H_c which is possible only in case of intramolecular hydrogen bonding interactions. Such intramolecular hydrogen bonding can guide the structural conformation of cyclic peptidomimetics similar that observed in cyclic peptides.³⁵ Temperature coefficient ($\Delta\delta/\Delta T$) values of H_b and H_c were found to be -4.46 and -5.7 ppb respectively.³⁶ Therefore, the strength of hydrogen bonding is moderate and amide protons are less shielded from the $\text{DMSO-}d_6$. ^1H NMR spectra of **4j** in CD_3CN with increase in the temperature showed upfield shift of H_b and H_c (0.146 and 0.09 ppm, Figure 10) with temperature coefficient values -2.3 and -3.62 ppb respectively. The higher values of temperature coefficient suggest stronger hydrogen bonding and shielding of amide protons from solvent (CD_3CN). Interestingly, the difference in upfield shifts of H_b and H_c and their corresponding temperature coefficient values suggest two hydrogen bonds with different bond length, an evidence for nonsymmetrical conformation of **4j**. Further, two set of proton peaks of **4j** merge at higher temperature ($> 65\text{ }^\circ\text{C}$) to form one set, demonstrating the transformation of non-symmetrical to symmetrical conformation (Figure 8b).³⁷ The ^1H - ^{13}C HSQC spectra obtained was remarkably well dispersed, indicative of a non-repetitive folded conformation. The energy minimized structure showed *trans* conformation for amides, concluding that the molecule exists in a low energy stable state (Figure 8c). The model structure also revealed two intramolecular hydrogen bonding between secondary amide protons and $^\alpha\text{N}$ -carbonyls (H_b & $\text{C}^{13}=\text{O}$ and H_c & $\text{C}^{19}=\text{O}$) (Figure 1d). The two intramolecular hydrogen bonds in **4j** exhibit different bond lengths (1.96 Å and 2.01 Å for H_b and H_c respectively) supporting the inference deduced from ^1H NMR spectroscopy. The observed differential cyclization can be understood from the structural aspects of *aeg* monomers. The flexible $^\alpha\text{N}$ -alkyl-*aeg* methyl esters follow the Baldwin rules of intramolecular cyclization. The terminal amine attacks the

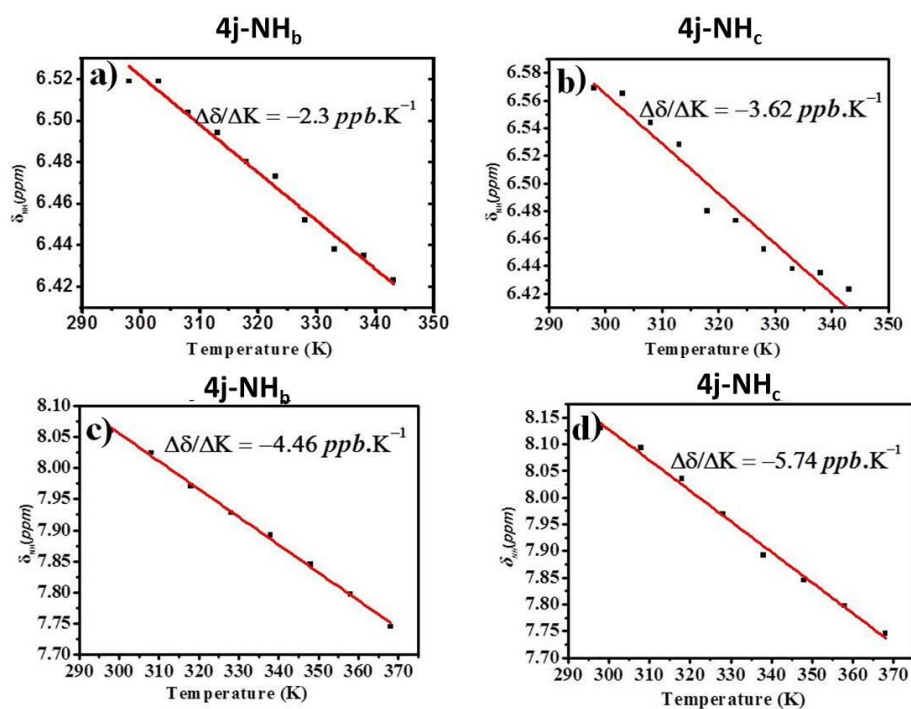


Figure 10. Temperature coefficient values of **4j**. (a) and (b) Determination of temperature coefficient values of amide protons NH_b and NH_c in CD_3CN . (c) and (d) Determination of temperature coefficient values of amide protons NH_b and NH_c in $DMSO-d_6$.

electrophilic methyl ester carbonyl without any hindrance to form six membered products (**4a-e**). While in α -*N*-acyl-*aeg* methyl esters, conformational rigidity prevents the intramolecular reaction. Alternatively, intermolecular nucleophilic attack of free-amine of one monomer onto methyl ester carbonyl of another monomer is energetically favored to form twelve membered products (**4g-m**).

3.11 Cyclic hybrid peptoids as autophagy enhancer

The cyclic peptoids being amphipathic in nature, they are known extensively to act as peptidomimetics.^{38, 39} We therefore envisaged them to be permeable to biological cell membranes. We wanted to test if these peptoids are bioactive against cellular phenomenon such as cell viability and whether they would affect specific cellular process such as autophagy. Cyclic peptoids (**4a-m**) were tested for their ability to affect autophagy, a biological process involved in the turnover of proteins and organelles. The degradation of a

cargo marker indicative of selective autophagy was followed over time in the yeast *Pichia pastoris* (Figure 11a). Interestingly, **4a** increased the rate of degradation of the protein marker through autophagy significantly in a dose dependent manner (Figure 11b). Furthermore, the growth characteristics suggest **4a** is not toxic to yeast cells (Figure 11c-e). Microscopy studies in *S. cerevisiae* showed a faster rate of peroxisome (GFP labeled) degradation through autophagy in presence of **4a** (50 μM) as observed by the appearance of diffused GFP in the

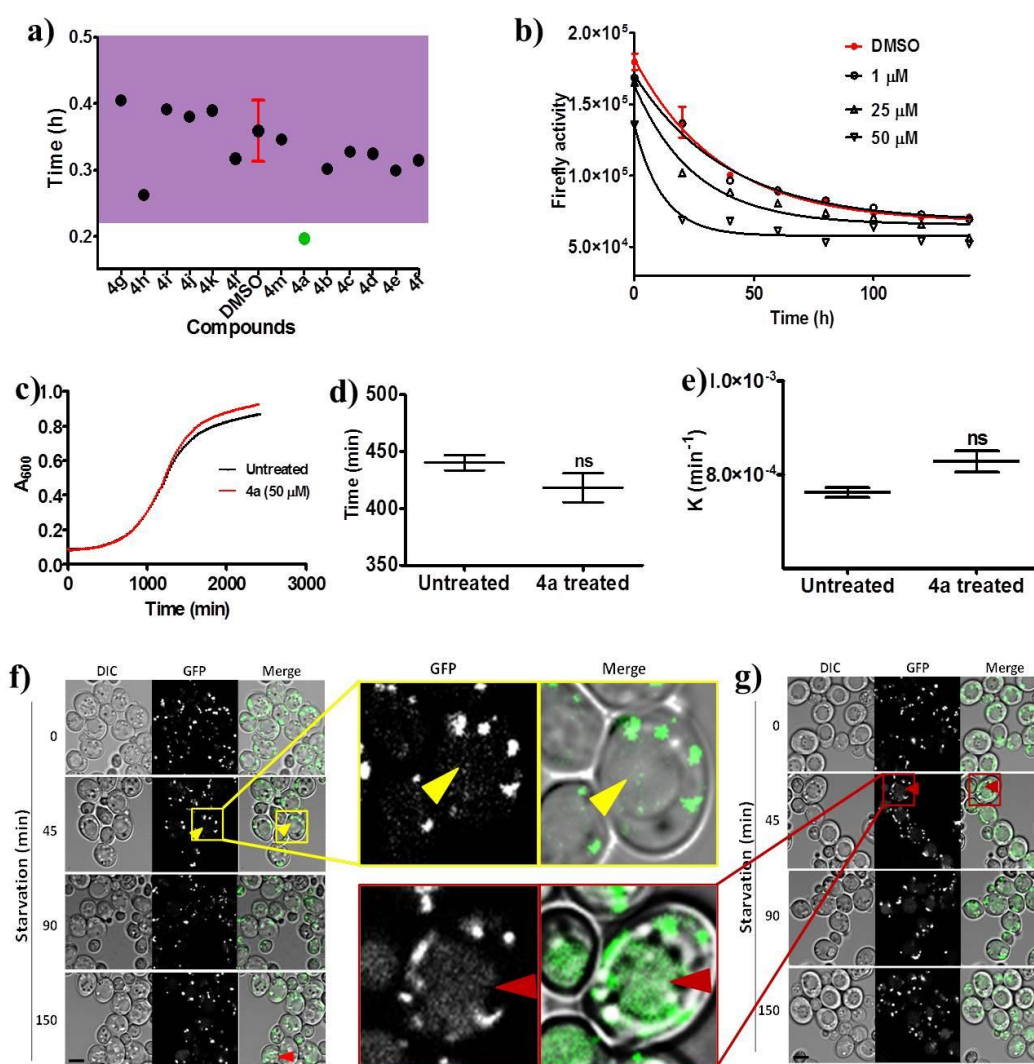


Figure 11. Autophagy studies in yeast. (a) time taken for 50% decrease in cargo activity for the control (DMSO) and **4a-m** at 50 μM , purple area denotes 3 SD (Standard Deviation) units. (b) Dose-response of **4a** (1, 25 and 50 μM) with time. Growth analysis of *S. cerevisiae* in presence and absence of **4a** was carried out (c) growth curve, (d) growth rate, (e) doubling time was plotted using GraphPad Prism. Microscopy images showing degradation of peroxisomes (peroxisomal protein Pot1 fused to GFP) in the vacuole (red arrowheads) in untreated (f) and **4a** treated (g) cells. Scale bar: 4 μm . DIC: differential interference contrast, GFP: green fluorescent protein.

vacuole (arrowheads) over time (Figure 11f and 11g). Strikingly, in presence of **4a**, GFP appeared inside the vacuoles (Figure 11g, inset) at much earlier time points as compared to the untreated cells (Figure 11f, inset). Upregulation of autophagy using small molecules such as **4a** is a promising approach towards elimination of intracellular pathogens and neurodegenerative protein aggregates.³¹

In summary, an elegant methodology for the synthesis of hybrid cyclic peptoids is developed. The conformational flexibility and rigidity of α -*N*-alkyl and α -*N*-acyl-substituted *N*-(2-aminoethyl)glycine backbone enforce intra- and intermolecular cyclization respectively to form six and twelve membered products. Unlike classical peptoids, our hybrid cyclic peptoids exhibit stable conformation and contains secondary amides may useful for providing secondary interactions. Screening of cyclic peptoids library gave an effective rate enhancer (**4a**) of autophagy. We are now working towards SAR on **4a** as well as expanding our synthetic methodology to access diverse hybrid cyclic peptoid library for numerous biological applications.

3.12 Experimental methods

3.12.1 General methods. All chemicals and analytical grade reagents were obtained from Sigma-Aldrich and used as purchased without any further purification unless otherwise mentioned. TLC analyses were performed over aluminum plates coated with Merck silica gel 60 F₂₅₄ and visualization under UV light (254 and 365 nm). ¹H NMR, ¹³C NMR, ¹³C DEPT-135, HSQC and HMBC were performed using Bruker AV-400 spectrometer with chemical shifts reported in parts per million (in CDCl₃ or CD₃CN or DMSO *d*₆, with tetramethylsilane as internal standard). Mass spectra were obtained from Agilent 6538 UHD HRMS/Q-TOF high resolution spectrometer.

3.12.2 Synthesis of *N*-tert-butyloxycarbonyl-1,2-ethylenediamine (1). To a solution of ethylenediamine (50 mL, 750 mmol) in chloroform (300 mL), di-tert-butylidicarbonate (8.6 mL,

37.5 mmol) dissolved in chloroform (250 mL) was added dropwise using pressure equaliser at 0 °C. Reaction was monitored by thin layer chromatography and on completion of the reaction, reaction mixture was filtered. The filtrate was concentrated, extracted with the organic layer, dried over anhydrous sodium sulfate and concentrated in vacuo to obtain colourless viscous liquid **1** in good yield (90 %). ¹H NMR (CDCl₃, 400 MHz) δ 4.86 (s, 1H), 3.16-3.17 (m, 2H), 2.77-2.80 (m, 2H), 1.44 (s, 9H), 1.39 (s, 2H); ¹³C NMR (CDCl₃, 100 MHz) δ 155.2, 78.25, 42.4, 40.8, 27.4.

3.12.3 Synthesis of *N*-(2-(*N*-Tert-butyloxycarbonyl)aminoethyl)glycine methyl ester (2**).** To a solution of *tert*-butyl *N*-(2-aminoethyl)carbamate (**1**) (3 g, 18.72 mmol) in acetonitrile (25 mL), KF-celite (10 g, 131.04 mmols) was added and allowed to be stirred for 15 min. Bromomethyl acetate (1.42 mL, 14.97 mmol) dissolved in acetonitrile (20 mL) was added dropwise for 15 min. using pressure equaliser and then the reaction mixture was allowed to be stirred for 7 h. The reaction was monitored by thin layer chromatography, and on completion, the reaction mixture was filtered, the filtrate was concentrated. The crude product was purified by column chromatography on silica gel using 0.3% methanol in chloroform as an eluent to afford brown liquid product **2** in good yield (83 %); ¹H NMR (CDCl₃, 400 MHz) δ 4.98 (s, 1H), 3.72 (s, 3H), 3.41(s, 2H), 3.189-3.230 (m, 2H), 2.72-2.75 (t, 2H, *J* = 5.6 Hz), 1.60 (s, 1H), 1.44 (s, 9H); ¹³C NMR (CDCl₃, 100 MHz) δ 172.9, 156.0, 51.8, 50.3, 48.7, 40.1, 28.4.

3.12.4 General synthetic procedure for *N*-alkyl-*N*-(2-aminoethyl)glycine monomers

To a solution of **2** (1.1 mmol) in acetonitrile (15 mL) was added TEA (2 mmol) at room temperature under argon atmosphere and stirred for 15 min. Then bromomethyl derivative was added and the reaction mixture was refluxed (81 °C) for 6 – 8 h. The reaction was monitored by thin layer chromatography, on completion of the reaction solvent is dried, and the crude product was purified by silica gel column chromatography.

***N*-(2-Boc-aminoethyl)-*N*-(benz-1-ylmethyl)glycine (**3a**).** Eluted with 5% ethyl acetate in

hexane and obtained as colourless liquid; yield (68%); ^1H NMR (CDCl_3 , 400 MHz) δ 7.31 (s, 5H), 5.15 (s, 1H), 3.78 (s, 2H), 3.69 (s, 3H), 3.32 (s, 2H), 3.19 (d, $J = 4.4$ Hz, 2H), 2.76-2.81 (t, $J = 6$ Hz, 2H), 1.45 (s, 9H); ^{13}C NMR (CDCl_3 , 100 MHz) δ 169.6, 160.8, 156.0, 135.7, 129.7, 129.3, 127.7, 79.5, 51.6, 47.6, 38.2, 37.3, 28.5; LCMS mass calcd: 322.1 $[\text{M}+\text{H}]^+$ found: 322.4.

***N*-(2-Boc-aminoethyl)-*N*-(naphth-1-ylmethyl)glycine (3b).** Eluted with 0.1% methanol in chloroform and obtained as liquid; yield (60%); ^1H NMR (CDCl_3 , 400 MHz) δ 7.74-7.81 (m, 3H), 7.43-7.50 (m, 3H), 7.40 (s, 1H), 5.02 (s, 1H), 3.81 (s, 2H), 3.27 (s, 2H), 3.12 (s, 2H), 2.71-2.76 (t, $J = 6.2$, 2H), 1.43 (s, 1H); ^{13}C NMR (CDCl_3 , 100 MHz) δ 169.5, 162.4, 160.0, 140.1, 137.3 135.7, 129.1, 129.3, 129.7, 127.7, 126.8, 79.9, 52.6, 44.6, 36.2, 35.3, 28.5; LCMS mass calcd: 372.2 $[\text{M}+\text{H}]^+$ found: 372.4.

***N*-(2-Boc-aminoethyl)-*N*-(naphth-1-ylmethyl)glycine (3c).** Eluted with 6% ethyl acetate in hexane and obtained as light brown semi solid; yield (61%); ^1H NMR (CDCl_3 , 400 MHz) δ 7.71-7.83 (m, 3H), 7.50 (s, 1H), 7.43-7.50 (m, 3H), 5.17 (s, 1H), 3.93 (s, 2H), 3.37 (s, 2H), 3.32 (s, 2H), 2.80-2.82 (t, $J = 5.3$, 2H), 1.43 (s, 1H); ^{13}C NMR (CDCl_3 , 400 MHz) δ 169.5, 162.4, 160.0, 140.1, 137.3 135.7, 129.1, 129.3, 129.7, 127.7, 126.8, 79.9, 52.6, 44.6, 36.2, 35.3, 28.5; LCMS mass calcd: 372.2 $[\text{M}+\text{H}]^+$ found: 372.4.

***N*-(2-Boc-aminoethyl)-*N*-((4-nitrobenz)-1-ylmethyl)glycine (3d).** Eluted with 0.1% methanol in chloroform and obtained as brownish liquid; yield (78%); ^1H NMR (CDCl_3 , 400 MHz) δ 7.21-7.24 (m, 2H), 6.84-6.69 (m, 2H), 5.26 (s, 1H), 4.32 (s, 2H), 3.66 (s, 2H), 3.45 (s, 3H), 3.34-3.36 (t, 2H, $J = 3.6$ Hz), 3.21 (s, 2H), 1.45 (s, 9H); ^{13}C NMR (CDCl_3 , 100 MHz) δ 168.4, 161.4, 132.5, 128.9, 126.6, 124.8, 79.8, 53.1, 44.5, 36.4, 36.5, 28.8; LCMS mass calcd: 368.1 $[\text{M}+\text{H}]^+$ found: 368.5.

***N*-(2-Boc-aminoethyl)-*N*-((4-methoxybenz)-1-ylmethyl)glycine (3e).** Eluted with 0.07% methanol in chloroform and obtained as a white solid; yield (76%); ^1H NMR (CDCl_3 , 100

MHz) δ 7.23-7.27 (m, 2H), 6.67-6.70 (m, 2H), 6.02 (s, 1H), 4.31 (s, 2H), 3.66 (s, 2H), 3.45 (s, 3H), 3.34-3.39 (t, 2H, $J = 4.3$ Hz), 3.33 (s, 3H), 3.21 (s, 2H), 1.45 (s, 9H); ^{13}C NMR (CDCl_3 , 100 MHz) 169.6, 161.4, 136.3, 128.8, 126.3, 123.2, 79.8, 53.1, 44.3, 38.3, 36.4, 36.5, 28.2; LCMS mass calcd: 353.2 $[\text{M}+\text{H}]^+$ found: 353.3.

***N*-(2-Boc-aminoethyl)-*N*-(benz-1-ylethyl)glycine (3f)**. Eluted in chloroform and obtained as colourless liquid; yield 43%; ^1H NMR (CDCl_3 , 400 MHz) δ 7.34-7.40 (m, 5H), 5.13 (s, 1H), 3.76 (s, 2H), 3.69 (s, 3H), 3.32 (s, 2H), 3.24-3.28 (t, 2H, $J = 6.3$ Hz) 3.19 (d, $J = 4.4$ Hz, 2H), 2.76-2.81 (t, 2H, $J = 6$ Hz), 1.45 (s, 9H); ^{13}C NMR (CDCl_3 , 100 MHz) δ 169.6, 160.8, 156.0, 135.7, 129.7, 129.3, 127.7, 79.5, 51.6, 47.6, 38.2, 37.3, 28.5; LCMS mass calcd: 337.2 $[\text{M}+\text{H}]^+$ found: 337.8.

3.12.5 General synthetic procedure for *N*-acyl-*N*-(2-aminoethyl)glycine monomers

To a solution of acetic acid derivative (1 mmol) in DMF was added HBTU (1.2 mmol) followed by HOBT (1.2 mmols) at 0 °C under argon atmosphere. The reaction mixture was stirred till a clear solution was obtained and then added **2** (1.1 mmol). Using a syringe DIPEA (3 mmol) was slowly added in portions to the reaction mixture and the reaction was stirred for 5–6 h at room temperature. The reaction was monitored by thin layer chromatography, on completion of the reaction the reaction mixture was poured into water. The organic layer was separated, dried (Na_2SO_4) and evacuated. The crude product was purified by silica gel column chromatography.

***N*-(2-Boc-aminoethyl)-*N*-(benz-1-ylacyl)glycine (3g)**. Eluted with 15% ethyl acetate in hexane and obtained as a white solid; yield (89%); ^1H NMR (CDCl_3 , 400 MHz) δ 7.20-7.33 (m, 5H), 5.38 (s, 1H), 4.00 (s, 2H), 3.76 (s, 2H), 3.75 (s, 3H), 3.49 (t, $J = 5.6$ Hz, 2H), 3.21 (q, $J = 5.6$ Hz, 2H), 1.45 (s, 9H); ^{13}C NMR (CDCl_3 , 100 MHz) δ 169.6, 161.4, 156.0, 133.5, 128.6, 126.5, 125.8, 79.5, 51.1, 47.3, 37.4, 36.3, 27.2; LCMS mass calcd: 351.3 $[\text{M}+\text{H}]^+$ found: 351.4.

***N*-(2-Boc-aminoethyl)-*N*-(naphth-1-ylacyl)glycine (3h).** Eluted with 0.4% methanol in chloroform and obtained as colourless liquid; yield (83%); ^1H NMR (*DMSO* d_6 , 400 MHz) δ 7.81-7.90 (m, 4H) 7.75 (s, 1H), 7.45-7.52 (m, 2H), 7.38 (dd, $J = 1.48$ Hz, $J = 8.4$ Hz, 1H), 7.00 (t, $J = 5.7$ Hz, 1H), 4.06 (s, 2H), 3.91 (s, 2H), 3.63 (s, 3H), 3.44 (t, $J = 6$ Hz), 3.14 (q, $J = 6$ Hz, 2H), 1.39 (s, 9H); ^{13}C NMR (*DMSO* d_6 , 100 MHz) δ 168.4, 161.9, 156.2, 132.1, 135.6, 128.9, 127.9, 126.5, 125.8, 124.2, 78.5, 52.1, 43.3, 37.2, 36.9, 28.8; LCMS mass calcd: 401.2 $[\text{M}+\text{H}]^+$ found: 401.6.

***N*-(2-Boc-aminoethyl)-*N*-(naphth-2-ylacyl)glycine (3i).** Eluted with 15% ethyl acetate in hexane and obtained as white semi-solid; yield (75%); ^1H NMR (*DMSO* d_6 , 400 MHz) δ 7.85-7.93 (m, 4H) 7.73 (s, 1H), 7.46-7.51 (m, 2H), 7.36-7.39 (d, 1H, $J = 1.5$), 6.89-7.11 (t, $J = 5.3$ Hz, 1H), 4.06 (s, 2H), 3.91 (s, 2H), 3.63 (s, 3H), 3.42-3.56 (t, $J = 6.1$ Hz), 3.23-3.33 (q, $J = 6$ Hz, 2H), 1.39 (s, 9H); ^{13}C NMR (*DMSO* d_6 , 100 MHz) δ 169.6, 161.4, 156.0, 133.5, 132.6, 128.6, 126.9, 126.5, 125.8, 125.0, 79.5, 51.1, 47.3, 38.2, 36.3, 28.3; LCMS mass calcd: 401.2 $[\text{M}+\text{H}]^+$ found: 401.3.

***N*-(2-Boc-aminoethyl)-*N*-((4-nitrobenz)-1-yl acyl)glycine (3j).** Eluted with 0.2% methanol in chloroform and obtained as a brown solid; yield (68%); ^1H NMR (*CDCl* $_3$, 400 MHz) δ 7.20-7.23 (m, 2H), 6.89-6.49 (m, 2H), 5.26 (s, 1H), 4.32 (s, 2H), 3.66 (s, 2H), 3.45 (s, 3H), 3.34-3.39 (t, 2H, $J = 4.3$ Hz), 3.21 (s, 2H), 1.43 (s, 9H); ^{13}C NMR (*CDCl* $_3$, 100 MHz) δ 168.6, 160.4, 156.2, 132.5, 128.9, 126.6, 124.8, 79.8, 53.1, 44.3, 36.4, 36.5, 28.2; LCMS mass calcd: 395.1 $[\text{M}+\text{H}]^+$ found: 396.4.

***N*-(2-Boc-aminoethyl)-*N*-((4-methoxybenz)-1-yl acyl)glycine (3k).** Eluted with 0.05% methanol in chloroform and obtained as a white solid; yield (70%); ^1H NMR (*CDCl* $_3$, 400 MHz) δ 7.23-7.27 (m, 2H), 6.67-6.70 (m, 2H), 6.02 (s, 1H), 4.31 (s, 2H), 3.66 (s, 2H), 3.45 (s, 3H), 3.34-3.39 (t, 2H, $J = 4.3$ Hz), 3.33 (s, 3H), 3.21 (s, 2H), 1.45 (s, 9H); ^{13}C NMR

($CDCl_3$, 100 MHz) δ 169.6, 161.4, 154.2, 136.3, 128.8, 126.3, 123.2, 79.8, 53.1, 44.3, 38.3, 36.4, 36.5, 28.2; LCMS mass calcd: 381.2 [M+H]⁺ found: 381.3.

2-(N-(2-(Tert-butoxycarbonyl) ethyl)-2-chloroacetamido) acetate (3k-1). To a solution of **2** (3 g, 12.9 mmol) in acetonitrile (100 ml), KF-celite (7.224 g, 90 mmol) was added and stirred for 10 min. Chloroacetyl chloride (1.43 mL, 18.1 mmol) was added slowly using syringe for 10 minutes, reaction was allowed to stir for 7 hours. Reaction was monitored by thin layer chromatography and on completion reaction mixture was filtered, filtrate was concentrated. The crude product was purified using column chromatography on silica gel using $CHCl_3$ as an eluent to afford a colourless liquid product in good yield (85%); ¹H NMR (400 MHz, $CDCl_3$) δ 5.40 (s, 1H), 4.14 (s, 2H), 4.04 (s, 2H), 3.76 (s, 3H), 3.52-3.55 (t, J = 5.9 Hz, 2H), 3.26-3.30 (q, J = 6 Hz, 2H), 1.44 (s, 9H); ¹³C NMR ($CDCl_3$, 100 MHz) 169.4, 161.4, 156.0, 79.5, 51.1, 47.3, 37.4, 36.3, 27.3; LCMS mass calcd: 309.7 [M+H]⁺ found: 309.4.

N-(2-Boc-aminoethyl)-N-(adenin-9-ylacyl)glycine (3l). To a solution of Adenine (3g, 8.11mmol) in DMF (25 ml), NaH (0.2 g, 8.11 mmol) was added and allowed to stir the reaction mixture for 1 h. Then **3f-1** (3.02 g, 9.73 mmol) in DMF (5ml) was added to the above reaction mixture slowly. The reaction mixture was allowed to stir overnight. Reaction mixture was filtered and was extracted with water and chloroform. Dried over Na_2SO_4 and evacuated. The crude product was purified using column chromatography on silica gel using $CHCl_3$: MeOH (97.3:2.7) as an eluent to afford a white solid product in good yield (72%); ¹H NMR (400 MHz, $CDCl_3$) δ 8.34 (s, 1H), 7.91 (s, 1H), 5.71 (s, 1H), 5.58 (s, 2H), 5.10 (s, 2H), 4.07 (s, 2H), 3.75 (s, 3H), 3.65 (t, J = 5.8 Hz, 2H), 3.40 (q, J = 5.8 Hz, 2H), 1.41 (s, 9H); ¹³C NMR ($CDCl_3$, 100 MHz) 169.1, 160.0, 156.2, 154.4, 149.5, 143.7, 132.5, 128.9, 126.6, 124.8, 123.1, 79.8, 53.1, 44.8, 44.3, 36.4, 36.5, 28.2; LCMS mass found: 408.6 [M+H]⁺ calcd: 408.2.

***N*-(2-Boc-aminoethyl)-*N*-(thymine-1-ylacetyl)glycine (3m).** Eluted with 1.4% methanol in chloroform and obtained as a white powder; yield (73%); ^1H NMR (CDCl_3 , 400 MHz) δ 8.16 (s, 1H), 6.96 (s, 1H), 5.49 (s, 1H), 4.57 (s, 2H), 4.05 (s, 2H), 3.76 (s, 3H), 3.53 (t, $J = 5.8$ Hz, 2H), 3.34 (q, $J = 5.9$ Hz, 2H), 1.92 (d, $J = 1.04$ Hz, 3H), 1.45 (s, 9H); ^{13}C NMR (CDCl_3 , 100 MHz) δ 170.8, 170.4, 167.6, 167.2, 164.4, 155.8, 151.0, 142.0, 108.2, 78.1, 78.0, 49.2; LCMS mass calcd: 399.4 $[\text{M}+\text{H}]^+$ found: 399.2.

3.12.6 General synthetic procedure for cyclization. To a solution of *N*-alkyl-*N*-(2-aminoethyl)glycine or *N*-acyl-*N*-(2-aminoethyl)glycine monomers (200 mg) was added TFA, DCM (v/v 1:1) (5 mL) and a few drops of triisopropylsilane (TIPS) at 0 °C. Reaction mixture was stirred for 1 h, solvent is dried and the product obtained is dissolved in *sec*-butanol (10 mL), reflux the reaction mixture at 110 °C, under argon atmosphere for 10–12 h. Reaction was monitored by thin layer chromatography, on completion of reaction solvent is dried and the crude product was purified by silica gel column chromatography.

4-Benzylpiperazin-2-one (4a). Eluted with 0.3% methanol in chloroform and obtained as white powder; yield 73%; M.P 163 °C- 165 °C; ^1H NMR (CDCl_3 , 400 MHz) δ 7.24-7.32 (m, 5H), 6.67 (s, 1H) 3.57 (s, 2H), 3.32-3.35 (m, 2H), 3.15(s, 1H), 2.62-3.64 (t, 2H, $J = 5.6$ Hz); ^{13}C NMR (CDCl_3 , 100 MHz) δ 169.7, 136.9, 129.0, 128.4, 127.5, 61.8, 56.9, 48.5, 41.4; DEPT-135 (CDCl_3 , 100 MHz) δ 129.0, 128.4, 127.5, 61.8, 56.9, 48.5, 41.4; HRMS mass calculated for $\text{C}_{11}\text{H}_{14}\text{N}_2\text{O}_1$, 191.1179 $[\text{M}+\text{H}]^+$. found: 191.1167; Elemental analysis. found: C, 68.92; H, 7.32; N, 15.65.calcd: C, 69.45; H, 7.42; N, 14.73.

4-(Naphthalen-1-ylmethyl)piperazin-2-one (4b). Eluted with 0.1% methanol in chloroform and obtained as white powder; yield 69%; M.P 172 °C- 175 °C; ^1H NMR (CDCl_3 , 400 MHz) δ 7.87-7.90 (m, 3H), 7.81 (s, 1H), 7.73 (s, 1H), 7.46-7.52 (m, 3H), 3.16 (m, 2H), 2.95 (s, 2H), 2.57-2.60 (t, 2H, $J = 5.6$); ^{13}C NMR (CDCl_3 , 100 MHz) δ 167.6, 135.1, 132.8, 132.3, 127.7, 127.5, 127.4, 127.1, 127.12, 126.0, 125.7, 60.8, 56.7, 48.4, 40.35; DEPT-135 (CDCl_3 ,

100 MHz) δ 127.7, 127.5, 127.4, 127.1, 127.12, 126.0, 125.7, 60.8, 56.7, 48.4, 40.35; HRMS mass calculated for $C_{15}H_{16}N_2O_1$, 241.1335 $[M+H]^+$. found: 241.1319; Elemental analysis. found: C, 74.81; H, 6.11; N, 11.32. calcd: C, 74.97; H, 6.71; N, 11.66.

4-(Naphthalen-2-ylmethyl)piperazin-2-one (4c). Eluted with 0.12% methanol in chloroform and obtained as white crystalline powder; yield (69%); M.P 171 °C- 173 °C; 1H NMR ($CDCl_3$, 400 MHz) δ 7.82-7.88 (m, 3H), 7.76 (m, 2H), 7.46-7.52 (m, 3H), 3.23 (m, 2H), 2.91 (s, 2H), 2.57-2.60 (t, 2H, $J = 5.6$); ^{13}C NMR ($CDCl_3$, 100 MHz) δ 167.6, 133.2, 132.4, 131.3, 127.7, 127.5, 127.4, 127.1, 127.12, 126.0, 125.7, 60.8, 56.7, 48.4, 40.35; DEPT-135 ($CDCl_3$, 100 MHz) δ 127.7, 127.5, 127.4, 127.1, 127.12, 126.0, 125.7, 60.8, 56.7, 48.4, 40.35; HRMS mass calculated for $C_{15}H_{16}N_2O_1$, 241.1335 $[M+H]^+$. Found: 241.1326; Elemental analysis. Found: C, 72.97; H, 6.22; N, 11.18. Calcd: C, 74.97; H, 6.71; N, 11.66.

4-(4-Nitrobenzyl)piperazin-2-one (4d). Precipitated by diethyl ether and isolated as light brown powder; yield 71%; M.P 178 °C- 180 °C; 1H NMR ($CDCl_3$, 400 MHz) δ 8.16-8.19 (d, 2H, $J = 8.4$ Hz), 7.50-7.52 (d, 2H, $J = 8.8$ Hz), 6.83 (s, 1H), 3.66 (s, 2H), 3.34-3.37 (m, 2H), 3.15 (s, 1h), 2.64-2.66 (t, 2H, $J = 5.6$ Hz); ^{13}C NMR ($CDCl_3$, 100 MHz) δ 169.2, 147.4, 144.9, 129.4, 123.7, 60.9, 56.9, 48.7, 41.2; DEPT-135 ($CDCl_3$, 100 MHz) δ 129.4, 123.7, 60.9, 56.9, 48.7, 41.2; HRMS calculated for $C_{11}H_{13}N_3O_3$, 236.1035 $[M+H]^+$. found: 236.1055; Elemental analysis. found: C, 56.11; H, 5.32; N, 17.68. Calcd: C, 56.16; H, 5.57; N, 17.86.

4-(4-Methoxybenzyl)piperazin-2-one (4e). Eluted with 0.08% methanol in chloroform and obtained as white crystalline powder; yield (69%); M.P 156 °C- 159 °C; 1H NMR ($CDCl_3$, 400 MHz) δ 8.14-8.19 (d, 2H, $J = 7.4$ Hz), 7.50-7.52 (d, 2H, $J = 8.8$ Hz), 6.83 (s, 1H), 3.23 (m, 2H), 2.91 (s, 2H), 2.57-2.60 (t, 2H, $J = 5.68$); ^{13}C NMR ($CDCl_3$, 100 MHz) δ 167.2, 145.5, 144.3, 129.4, 123.7, 60.8, 56.7, 48.4, 40.35; DEPT-135 ($CDCl_3$, 100 MHz) δ 129.4, 123.7, 60.8, 56.7, 48.4, 40.35; HRMS mass calculated for $C_{12}H_{16}N_2O_2$, 221.1285 $[M+H]^+$.

Found: 221.1251; Elemental analysis. found: C, 65.59; H, 7.63; N, 11.11. calcd: C, 65.43; H, 7.32; N, 11.32.

4-Phenethylpiperazin-2-one (4f). Eluted in chloroform and obtained as brown powder; yield 43%; M.P 155 °C- 159 °C; ^1H NMR (CDCl_3 , 400 MHz) δ 7.27-7.31 (m, 2H), 7.18-7.22 (m, 3H), 6.59 (s, 1H), 3.36-3.39 (m, 2H), 3.22 (s, 2H), 2.79-2.83 (m, 2H), 2.67-2.73 (m, 2H); ^{13}C NMR (CDCl_3 , 100 MHz) δ 169.5, 139.58, 128.6, 128.4, 126.2, 56.8, 49.1, 41.2, 33.4, 29.6; DEPT-135 (CDCl_3 , 100 MHz) δ 128.6, 128.4, 126.2, 56.8, 49.1, 41.2, 33.4, 29.6; HRMS mass calculated for $\text{C}_{12}\text{H}_{16}\text{N}_2\text{O}_1$, 205.1335 $[\text{M}+\text{H}]^+$. found: 205.1336; Elemental analysis found: C, 71.56; H, 8.01; N, 13.56. calcd: C, 71.36; H, 7.90; N, 13.71.

4,10-(*N,N'*)-Bis(benz-1-ylacetyl) cyclo(aeg-aeg) (4g). Eluted with 0.8% methanol in chloroform and obtained as white powder; yield 72%; M.P 189 °C- 196 °C; ^1H NMR ($\text{DMSO } d_6$, 400 MHz) δ 7.44-7.56 (m, 10H), 7.25 (s, 1H), 4.46 (s, 2H), 4.31 (s, 2H), 4.01-4.04 (t, 2H, $J = 5.2$ Hz), 3.98 (s, 2H), 3.94 (s, 2H), 3.81-3.84 (t, 2H, $J = 5.2$), 3.50 (b, 2H), 3.35 (b, 2H); ^{13}C NMR ($\text{DMSO } d_6$, 100 MHz) δ 169.7, 168.1, 166.8, 134.2, 133.8, 128.9, 128.7, 128.5, 127.15, 49.15, 46.0, 42.7, 41.2, 40.8, 40.6, 38.5, 29.6; DEPT-135 ($\text{DMSO } d_6$, 100 MHz) δ 128.9, 128.7, 128.5, 127.15, 49.15, 46.0, 42.7, 41.2, 40.8, 40.6, 38.5, 29.6; HRMS mass calculated for $\text{C}_{20}\text{H}_{24}\text{N}_8\text{O}_8$, 459.2003 $[\text{M}+\text{Na}]^+$. found: 459.1945; Elemental analysis. found: C, 66.23; H, 6.45; N, 12.17. calcd: C, 66.19; H, 6.25; N, 12.32.

4,10-(*N,N'*)-Bis(naphth-1-ylacetyl) cyclo(aeg-aeg) (4h). Precipitated using diethyl ether to obtain white crystalline powder; M.P 180 °C- 184 °C; ^1H NMR ($\text{DMSO } d_6$, 400 MHz) δ 8.14 (s, 1H), 8.07 (s, 1H), 7.91-7.96 (m, 4H), 7.81-7.83 (d, $J =$, 2H), 7.49-7.52 (m, 3H), 7.42-7.46 (m, 2H), 7.30-7.35 (m, 2H), 4.18-4.22 (m, 6H), 3.97 (s, 2H), 3.75-3.77 (t, 2H, $J = 4.3$ Hz), 3.64-3.62 (t, $J =$, 2H), 3.25 (b, 2H), 3.20 (b, 2H); ($\text{DMSO } d_6$, 100 MHz) δ 169.7, 169.4, 166.6, , 133.5, 132.4, 131.7, 131.3, 128.7, 128.6, 127.6, 127.5, 127.4, 127.0, 126.7, 126.5, 126.4, 126.3, 126.0, 125.9, 49.2, 46.1, 42.7, 41.4, 41.6, 41.0, 40.69, 38.6; DEPT-135 (DMSO

d_6 , 100 MHz) δ 128.7, 128.6, 127.6, 127.5, 127.4, 127.0, 126.7, 126.5, 126.4, 126.3, 126.0, 125.9, 49.2, 46.1, 42.7, 41.4, 41.6, 41.0, 40.69, 38.6; HRMS mass calculated for $C_{32}H_{32}N_4O_4$, 559.2316 $[M+Na]^+$. found: 559.2277; Elemental analysis. found: C, 71.83; H, 5.91; N, 10.68. calcd: C, 71.62; H, 6.01; N, 10.44.

4,10-(*N,N'*)-Bis(naphth-2-ylacyl) cyclo(aeg-aeg) (4i). Eluted with 0.5% methanol in chloroform and obtained as white crystalline powder; yield 68%; M.P 183 °C- 187 °C; 1H NMR (*DMSO d*₆, 400 MHz) δ 7.77-7.48 (m, 3H), 7.68 (s, 1H), 7.45-7.48(m, 2H), 7.36-7.38 (d, 1H, $J = 8.3$ Hz), 6.74 (s, 1H), 6.63 (s, 1H) 4.28 (s, 2H), 4.14 (s, 2H), 3.93 (s, 2h), 3.88 (s, 2H), 3.81-3.84 (t, 2H, $J = 4.9$), 3.62-3.65 (t, 2H, $J = 5.3$), 3.35 (b, 2H), 3.11 (b, 2H); ^{13}C NMR (*DMSO d*₆, 100 MHz) δ 169.7, 169.4, 166.6, , 133.5, 132.4, 131.7, 131.3, 128.7, 128.6, 127.6, 127.5, 127.4, 127.0, 126.7, 126.5, 126.4, 126.3, 126.0, 125.9, 49.2, 46.1, 42.7, 41.4, 41.6, 41.0, 40.69, 38.6; DEPT-135 (*DMSO d*₆, 100 MHz) δ 128.7, 128.6, 127.6, 127.5, 127.4, 127.0, 126.7, 126.5, 126.4, 126.3, 126.0, 125.9, 49.2, 46.1, 42.7, 41.4, 41.6, 41.0, 40.69, 38.6; HRMS mass calculated for $C_{32}H_{32}N_4O_4$, 559.2316 $[M+Na]^+$. found: 559.2307; Elemental analysis. found: C, 71.94; H, 6.02; N, 10.34. calcd: C, 71.62; H, 6.01; N, 10.44.

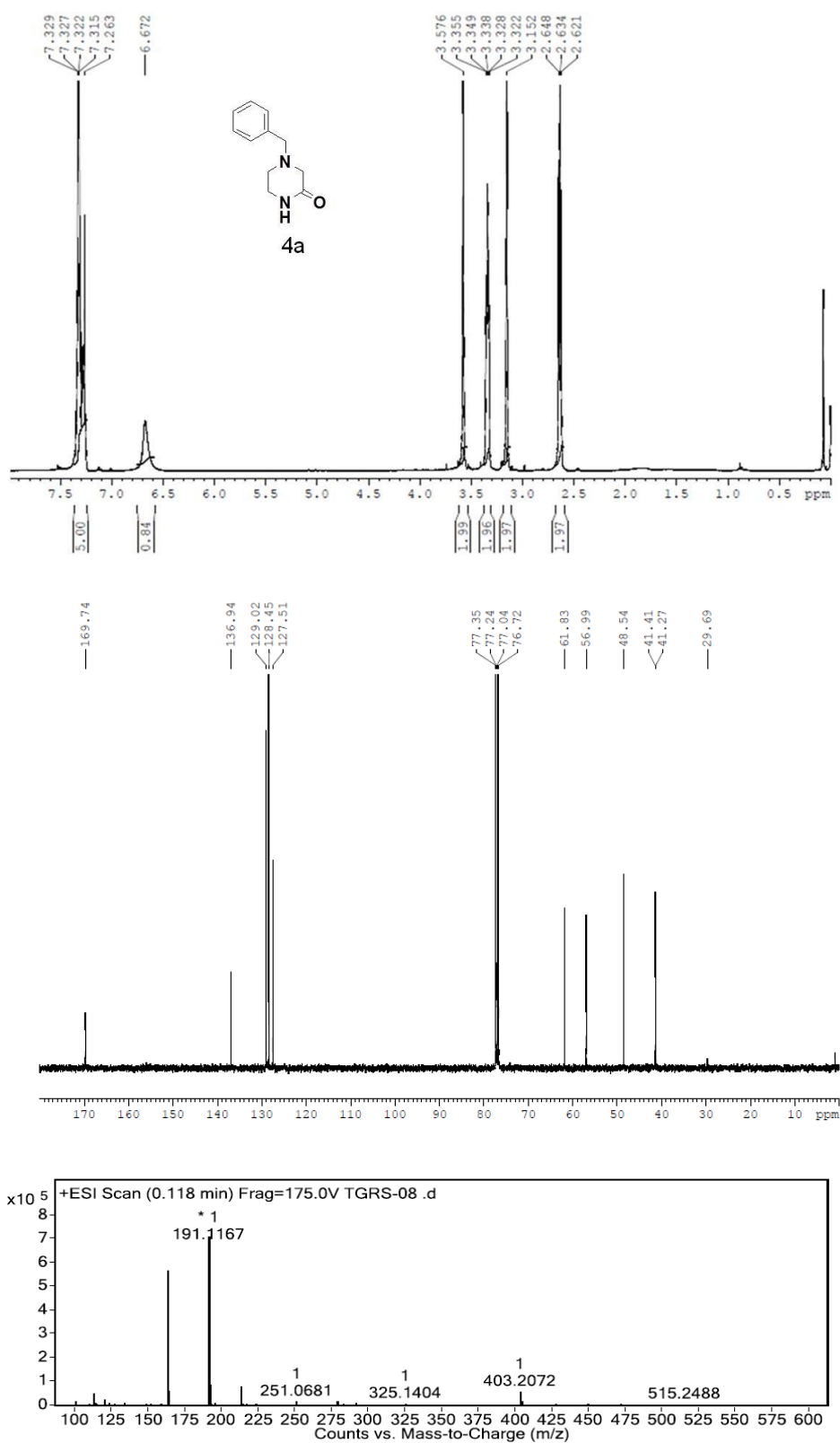
4,10-(*N,N'*)-Bis((4-methoxybenz)-1-yl acyl) cyclo(aeg-aeg) (4j). Eluted with 1.2% methanol in chloroform and obtained as white crystalline powder; yield 68%; M.P 184 °C- 179 °C; 1H NMR (*DMSO d*₆, 100 MHz) δ 7.14-7.16 (s, 4H, $J = 8.4$ Hz), 6.84-6.87 (s, 4H, $J = 8.8$ Hz), 6.63 (s, 1H), 6.50 (s, 1H), 4.25 (s, 2H), 4.10 (s, 2H), 3.70 (s, 4H), 3.66 (s, 2H), 3.61-3.63 (t, 2H, $J = 4.8$ Hz), 3.36 (b, 2H), 3.16 (b, 2H); ^{13}C NMR (*DMSO d*₆, 100 MHz) δ 169.0, 157.7, 128.7, 128.5, 124.7, 54.2, 48.1, 45.1, 41.6, 40.1, 39.7, 39.3, 39, 37.5; HRMS mass calculated for $C_{26}H_{32}N_4O_6$, 519.2214 $[M+Na]^+$. found: 519.2167; Elemental analysis. found: C, 62.64; H, 6.50; N, 10.96. calcd: C, 62.89; H, 6.50; N, 11.28.

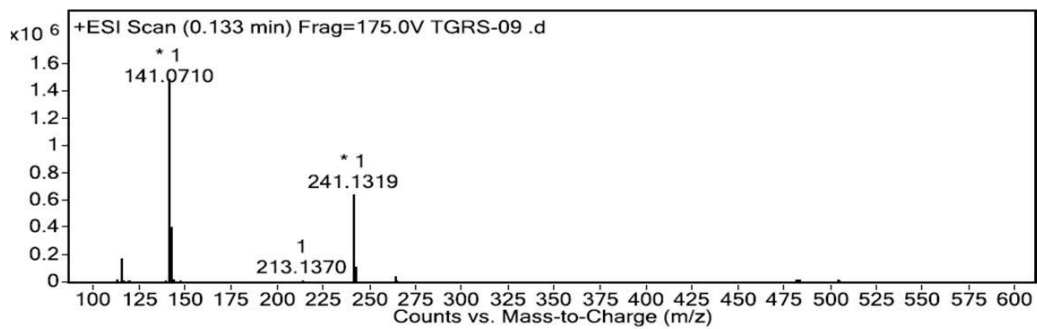
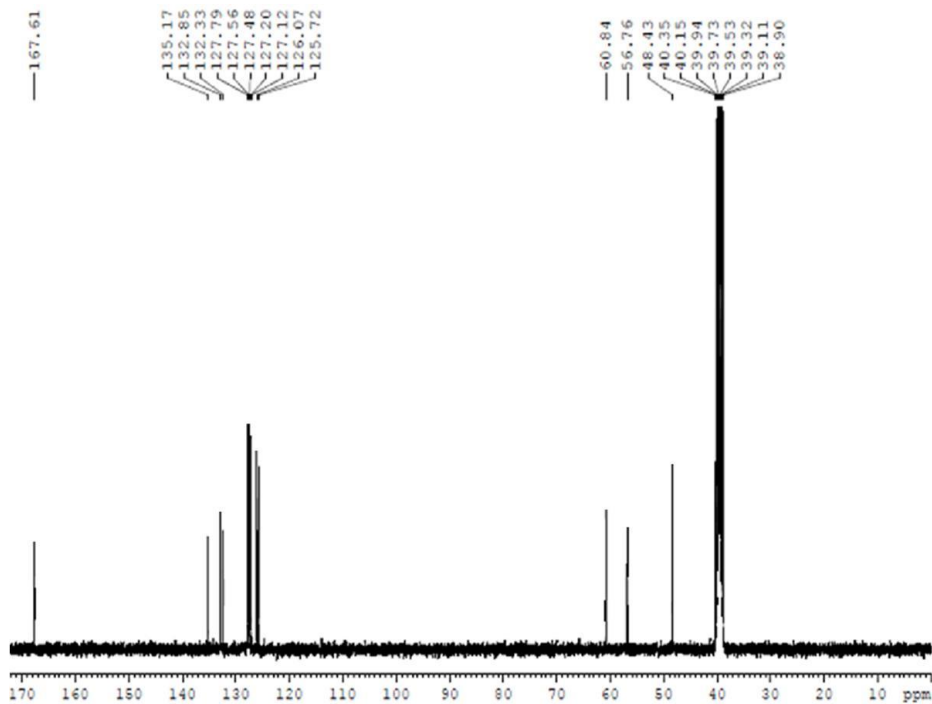
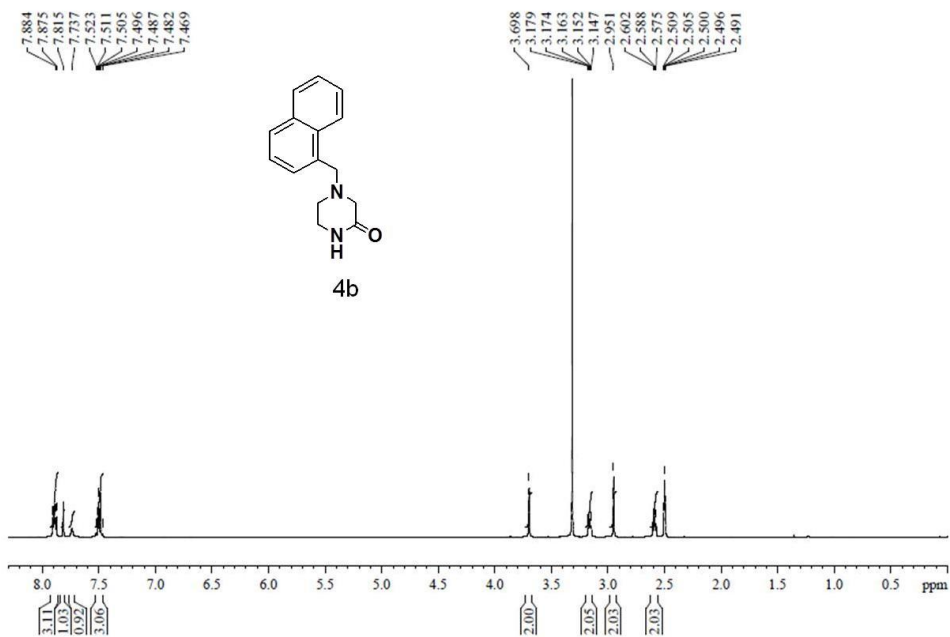
4,10-(*N,N'*)-Bis((4-nitrobenz)-1-yl acyl) cyclo(aeg-aeg) (4k). Precipitated by diethyl ether and isolated as light brown powder; yield 82%; M.P 195 °C- 200 °C; 1H NMR (*DMSO d*₆,

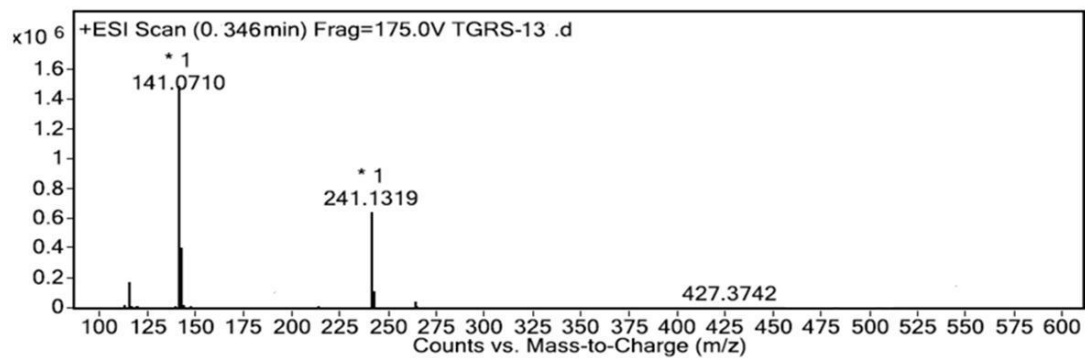
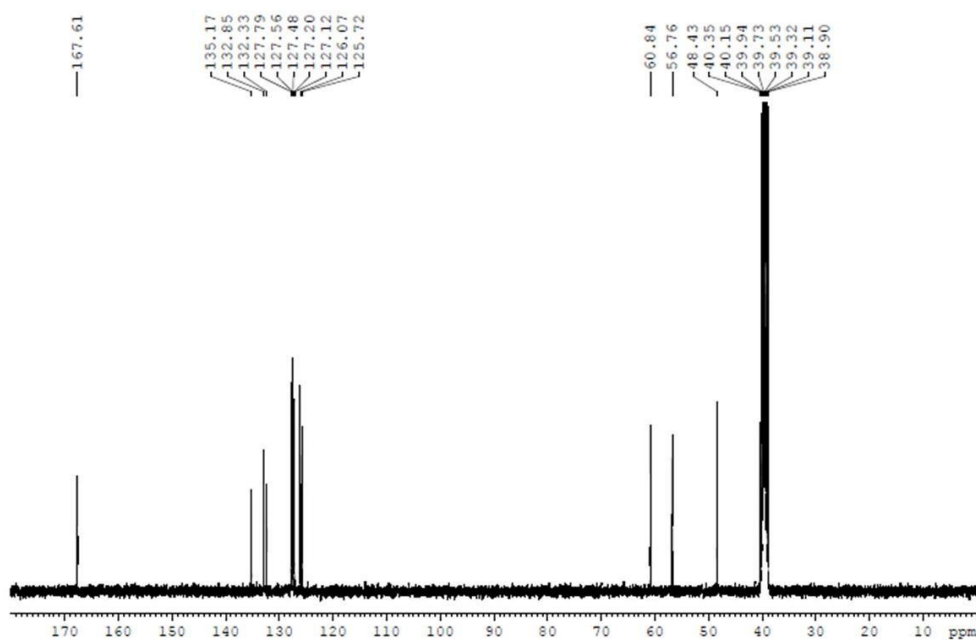
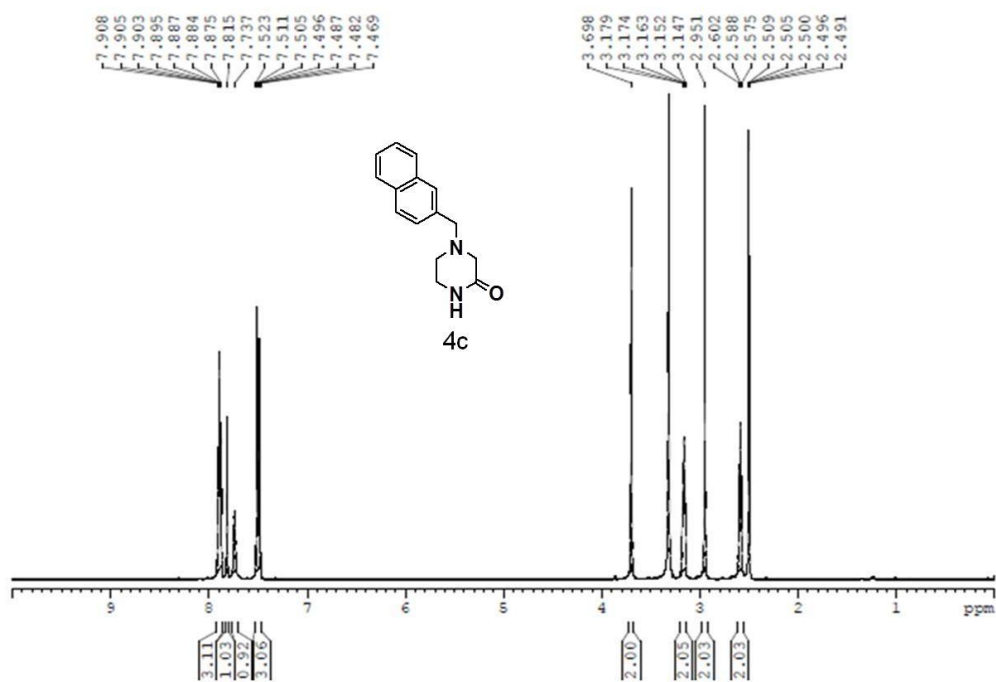
400 MHz) δ 8.184-8.186 (d, 4H, $J = 0.8$ Hz), 8.16 (s, 1H), 8.07 (s, 1H), 7.47-7.52 (m, 4H), 4.11 (s, 2H), 3.95 (s, 4H), 3.92 (s, 2H), 3.68-3.71 (t, 2H, $J = 5.6$ Hz), 3.6-3.62 (t, 2H, $J = 5.6$ Hz), 3.21 (b, 2H), 3.18 (b, 2H); ^{13}C NMR (*DMSO* d_6 , 100 MHz) δ 168.2, 168.1, 166.4, 165.7, 146.2, 143.9, 130.9, 130.8, 123.16, 123.12, 48.3, 45.7, 42.1, 40.1, 40.0, 38.8, 38.3; DEPT-135 (*DMSO* d_6 , 100 MHz) δ 130.9, 130.8, 123.16, 123.12, 48.3, 45.7, 42.1, 40.0, 39.47, 38.8, 38.3; HRMS mass calculated for $\text{C}_{24}\text{H}_{26}\text{N}_6\text{O}_8$, 549.1710 $[\text{M}+\text{Na}]^+$. found: 549.1664; Elemental analysis. found: C, 54.35; H, 4.68; N, 15.83. calcd: C, 54.75; H, 4.98; N, 15.96.

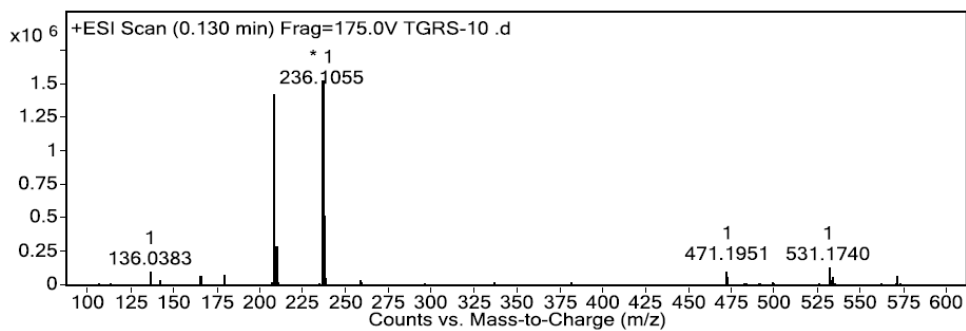
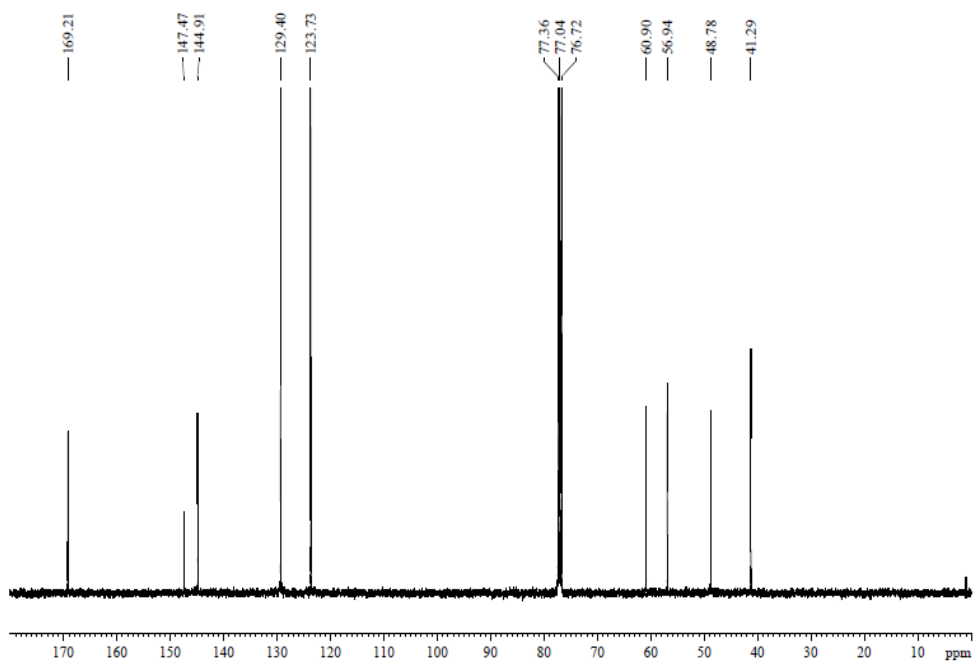
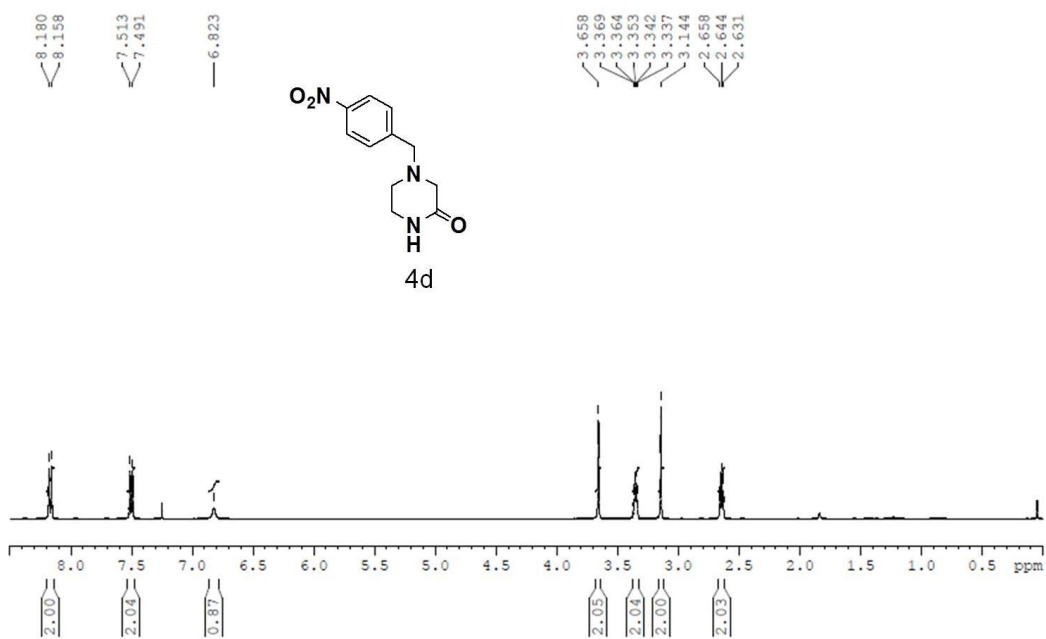
4,10-(*N,N'*)-Bis(adenin-9-ylacyl) cyclo(*aeg-aeg*) (4l). Isolated as white powder; yield 78%; ^1H NMR (*DMSO* d_6 , 400 MHz) δ 8.81 (b, 4H), 8.34 (s, 2H), 8.32 (s, 2H), 8.27 (s, 2H), 8.22 (s, 2H), 5.34-5.38 (d, $J =$, 4H), 4.27 (s, 2H), 4.01 (s, 2H), 3.81-3.84 (t, $J =$, 2H), 3.66-3.68 (t, $J =$, 2H), 3.42 (b, 2H), 3.26 (b, 2H); ^{13}C NMR (*DMSO* d_6 , 100 MHz) δ 166.0, 165.3, 164.6, 164.5, 158.8, 158.5, 151.6, 149.1, 146.8, 144.1, 117.7, 114.7, 47.3, 45.8, 44.7, 44.6, 41.2, 40.1; DEPT-135 (*DMSO* d_6 , 100 MHz) δ 146.7, 146.6, 144.1, 47.2, 45.8, 44.7, 44.6, 41.2, 39.8, 39.7, 39.3; HRMS mass calculated for $\text{C}_{22}\text{H}_{26}\text{N}_{14}\text{O}_4$, 573.2159 $[\text{M}+\text{Na}]^+$. found: 573.2110; Elemental analysis. found: C, 47.07; H, 4.73; N, 34.52. calcd: C, 47.20; H, 4.76; N, 35.01.

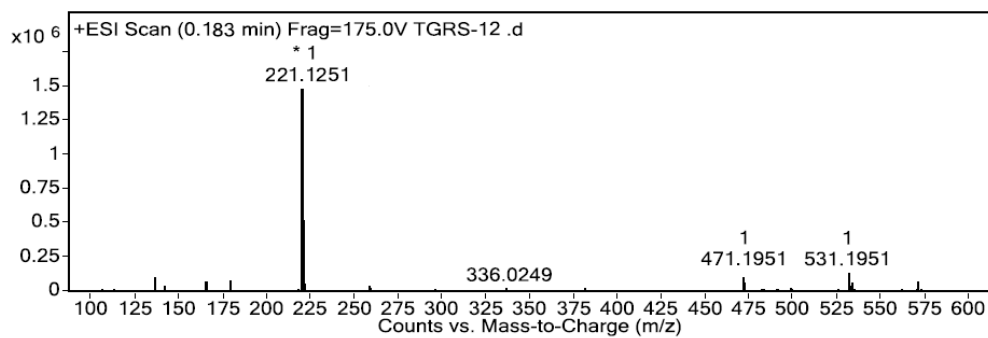
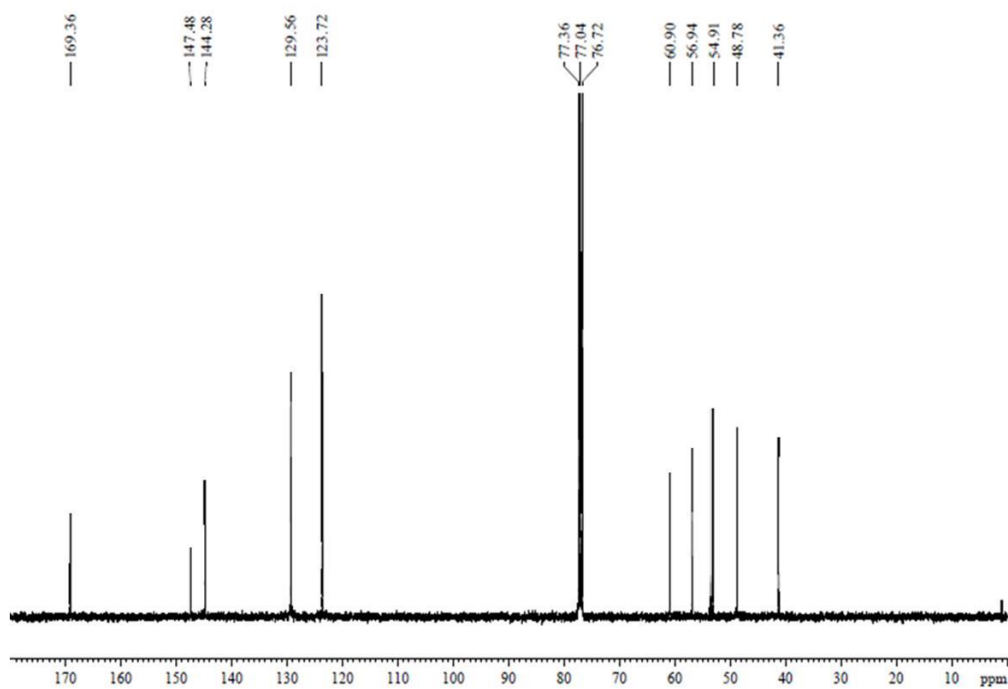
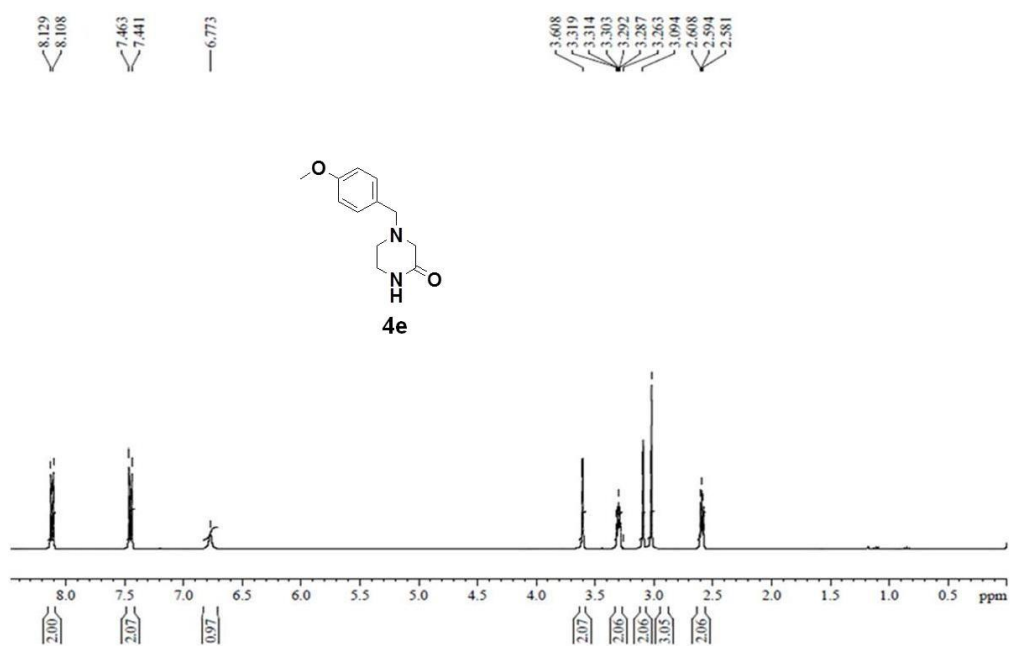
4,10-(*N,N'*)-Bis(thymin-1-ylacyl) cyclo(*aeg-aeg*) (4m). Isolated as white powder; yield 72%; ^1H NMR (*DMSO* d_6 , 400 MHz) δ 11.27 (s, 1H), 11.26 (s, 1H), 8.15 (s, 1H), 8.09 (s, 1H), 7.36 (s, 1H), 7.32 (s, 1H), 4.61 (s, 2H), 4.58 (s, 2H), 4.07 (s, 2H), 3.93 (s, 2H), 3.63-3.66 (t, 2H, $J = 5.2$), 3.58-3.60 (t, 2H, $J = 4.8$), 3.29 (b, 2H), 3.18 (b, 2H), 1.74 (s, 6H); ^{13}C NMR (*DMSO* d_6 , 100 MHz) δ 166.1, 165.5, 165.4, 164.3, 151.0, 142.1, 142.0, 108.0, 48.1, 47.9, 47.1, 45.7, 41.0, 11.8; DEPT (*DMSO* d_6 , 100 MHz) δ 142.1, 142.0, 48.1, 47.9, 47.1, 45.7, 41.0, 39.8, 39.7, 39.5, 11.8; HRMS mass calculated for $\text{C}_{20}\text{H}_{24}\text{N}_8\text{O}_8$, 555.1878 $[\text{M}+\text{Na}]^+$. found: 555.1891; Elemental analysis. found: C, 66.23; H, 5.15; N, 13.02. calcd: C, 66.19; H, 6.25; N, 12.87.

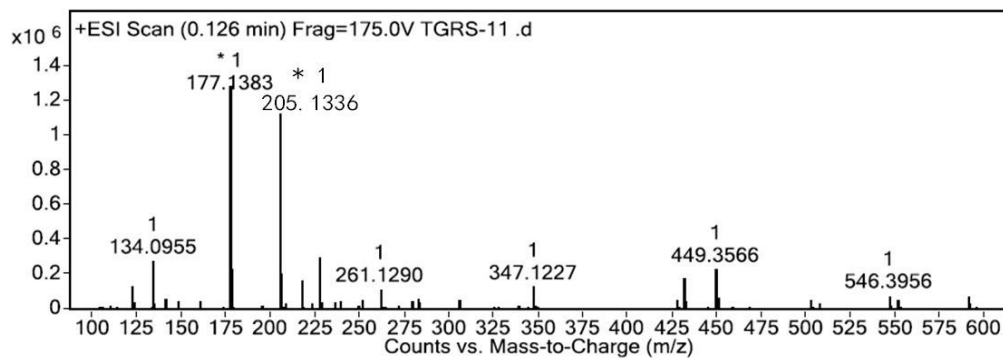
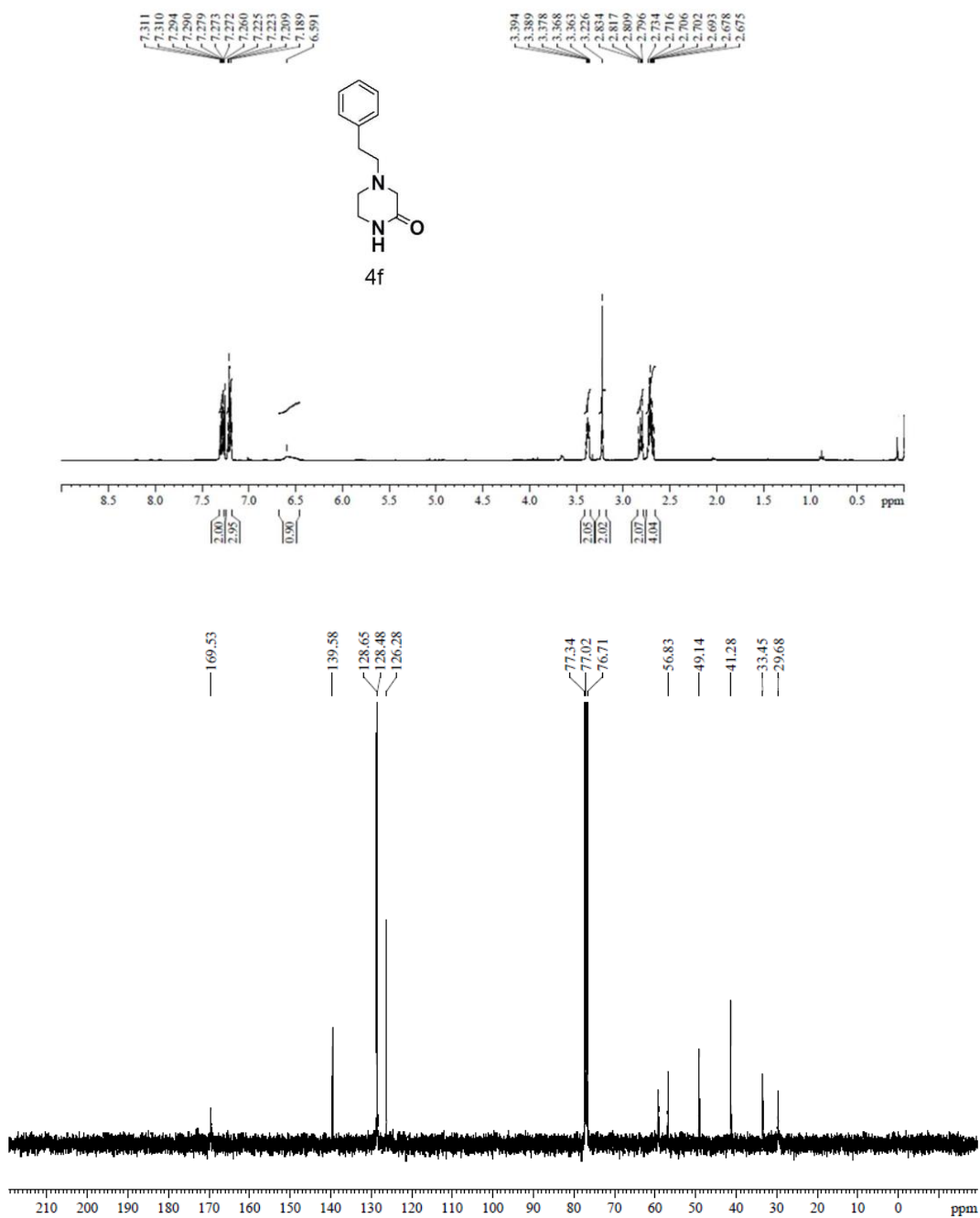
3.12.8 ^1H and ^{13}C NMR and Mass (HRMS) spectra.

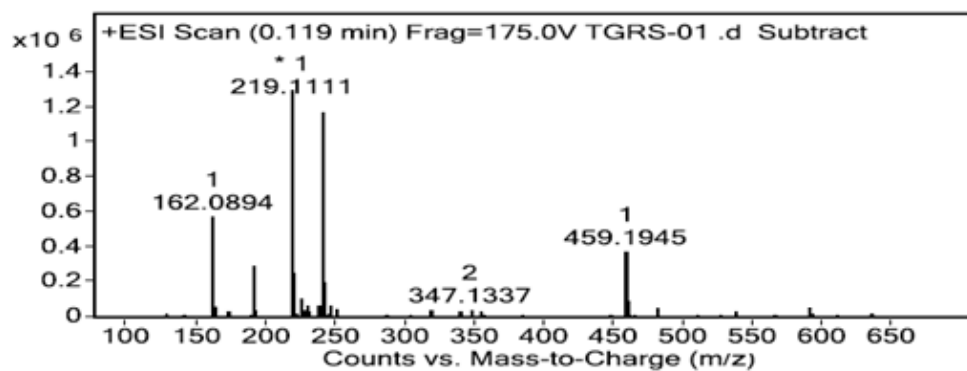
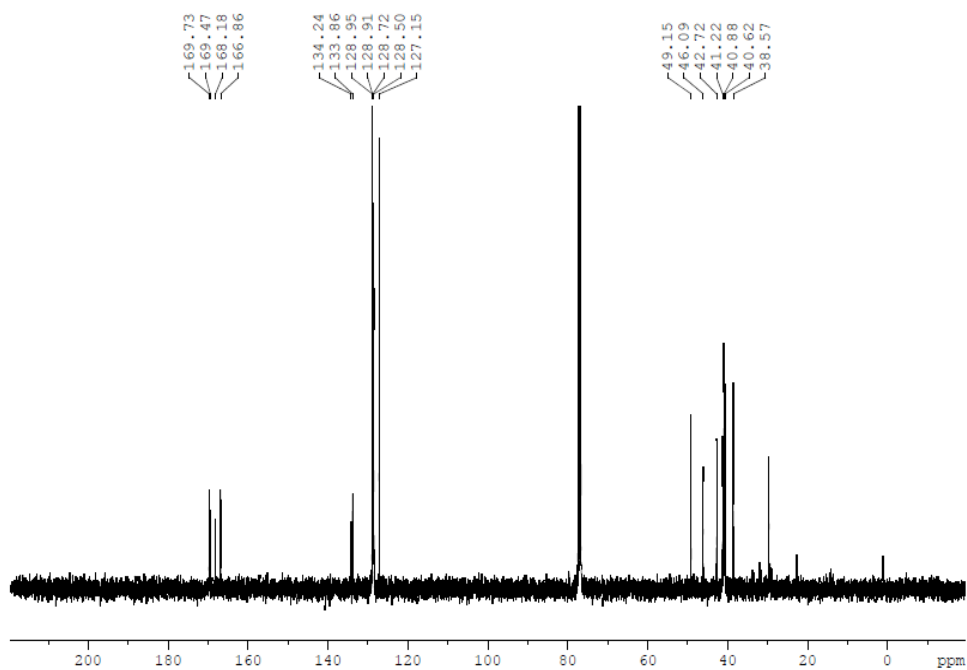
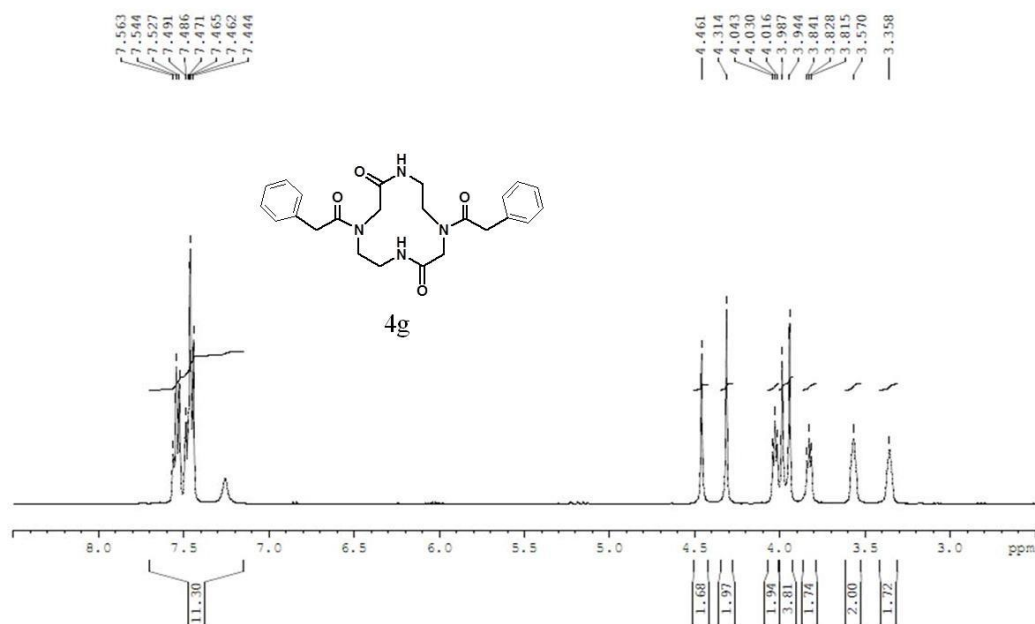


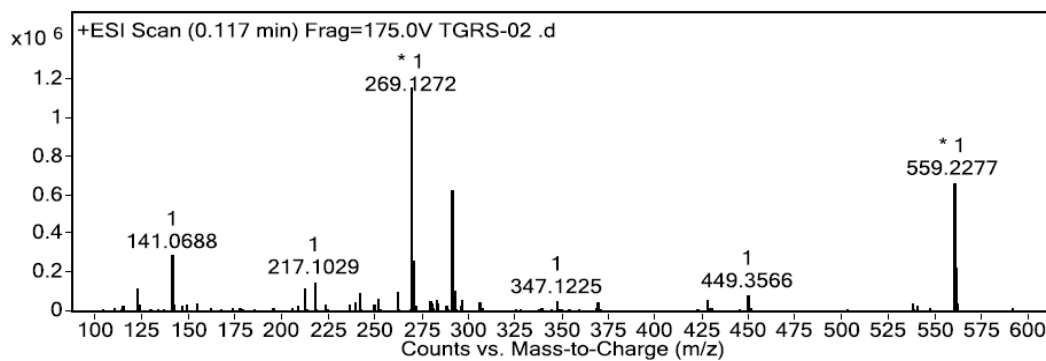
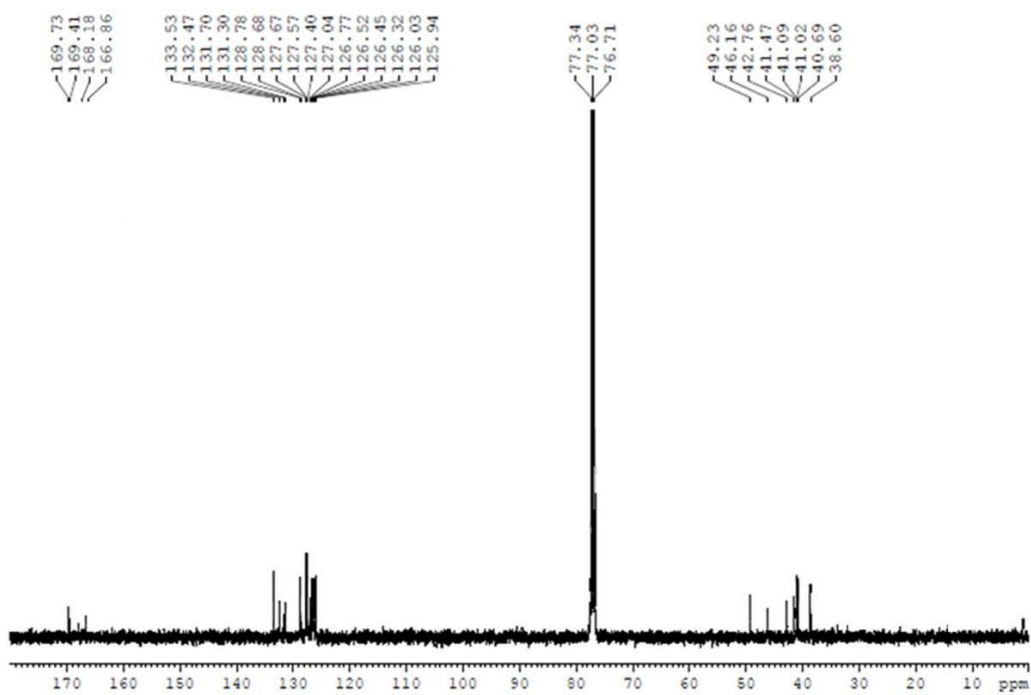
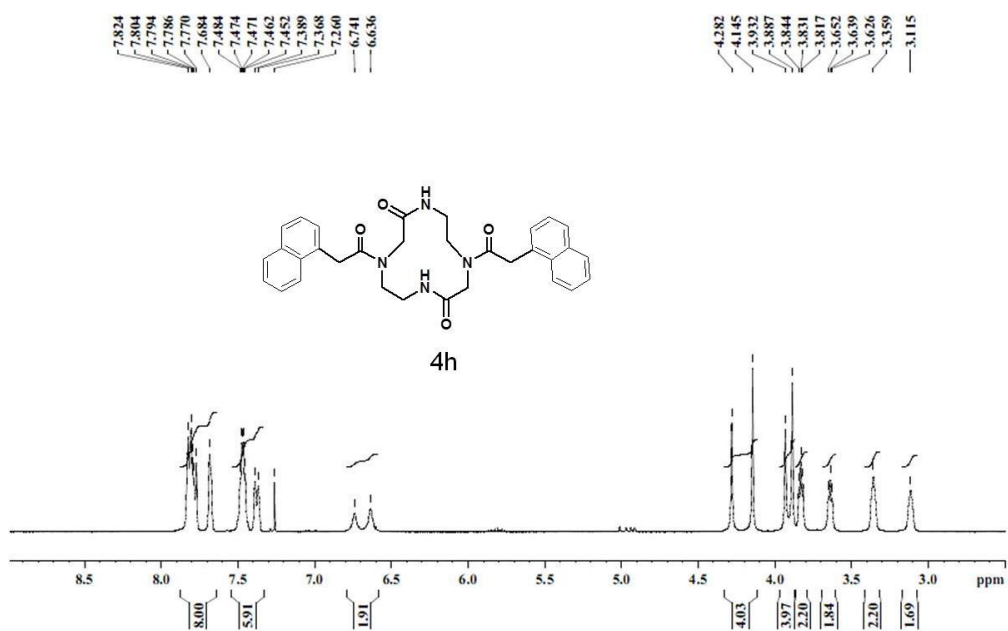


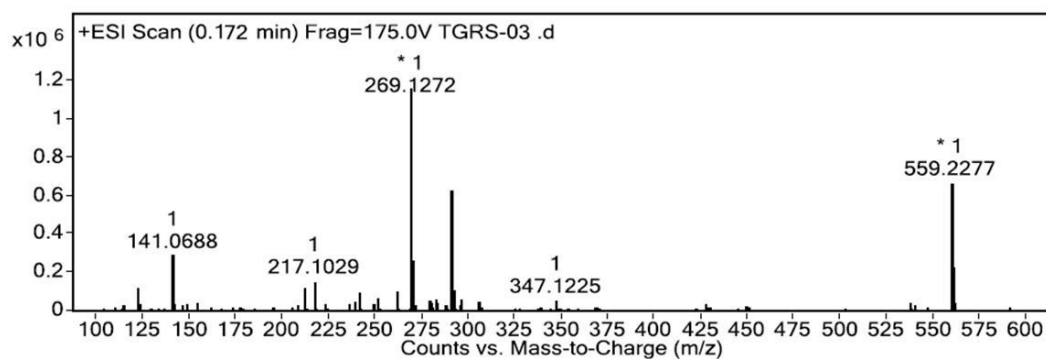
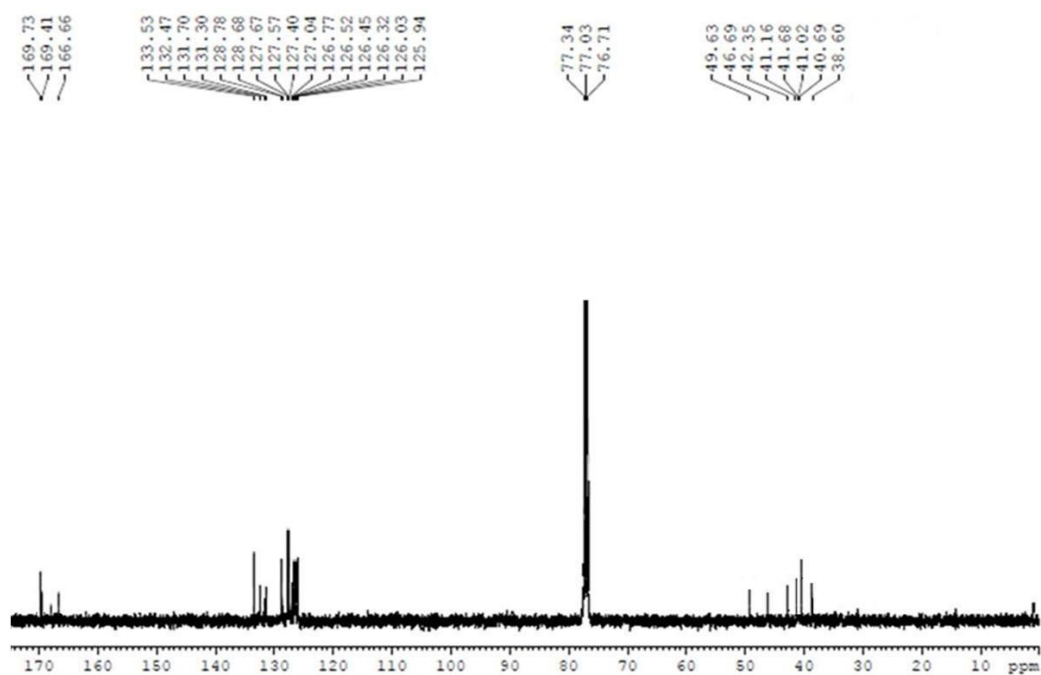
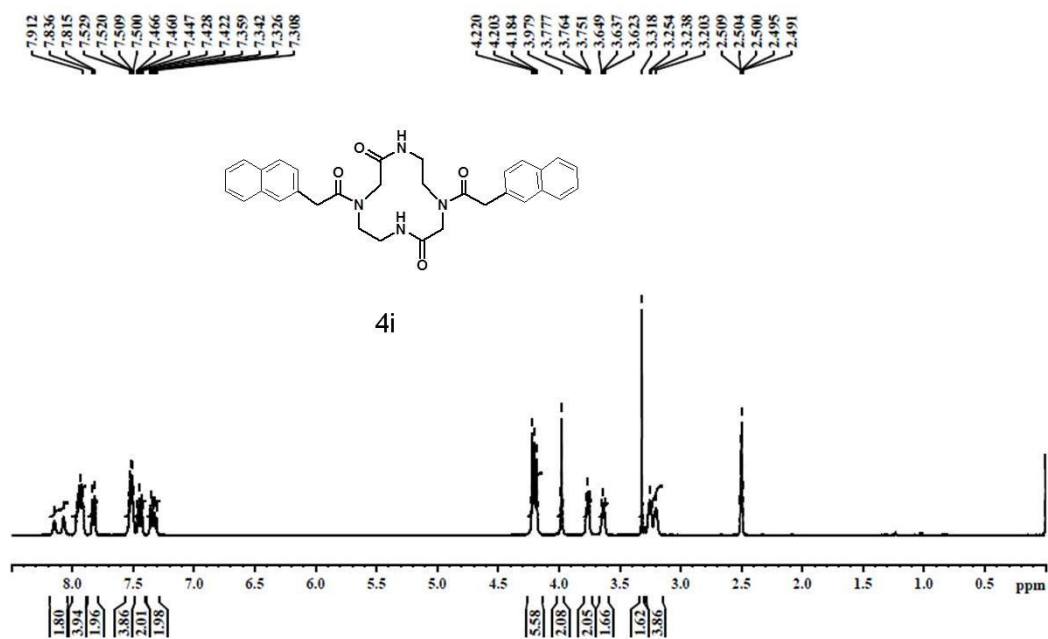


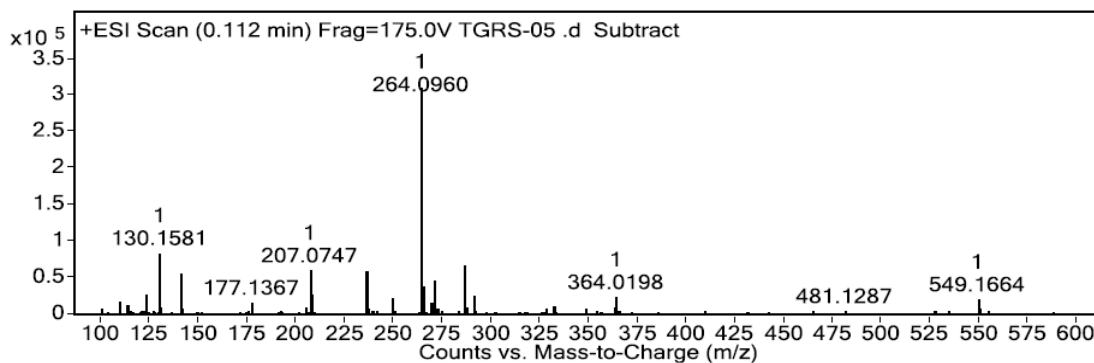
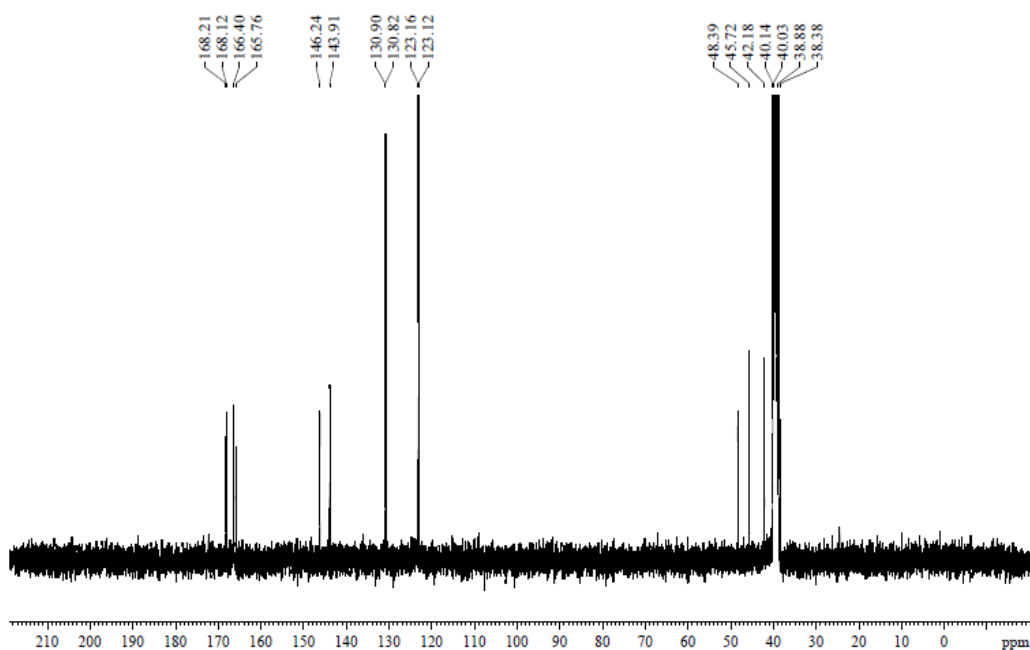
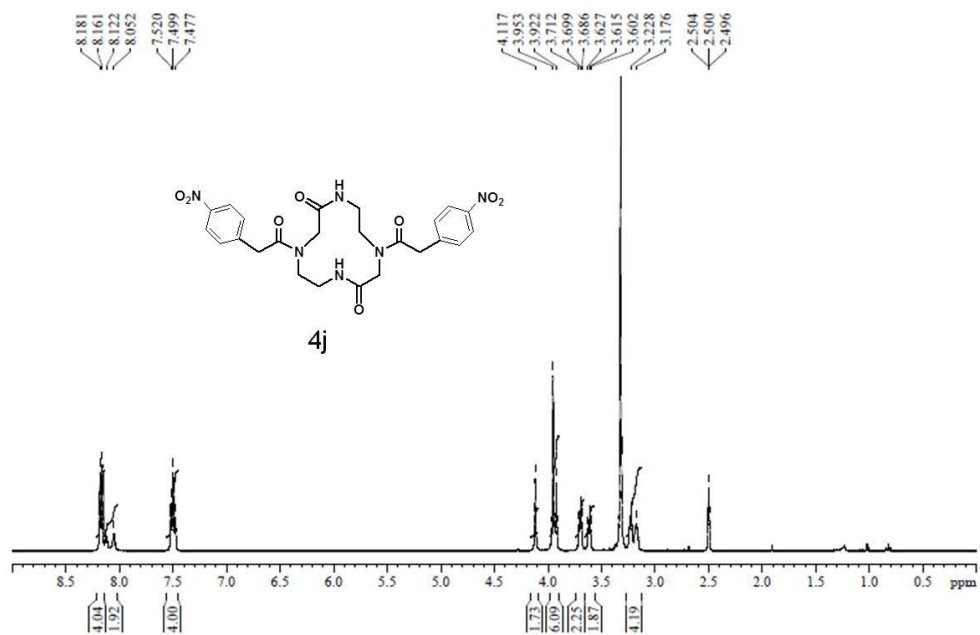


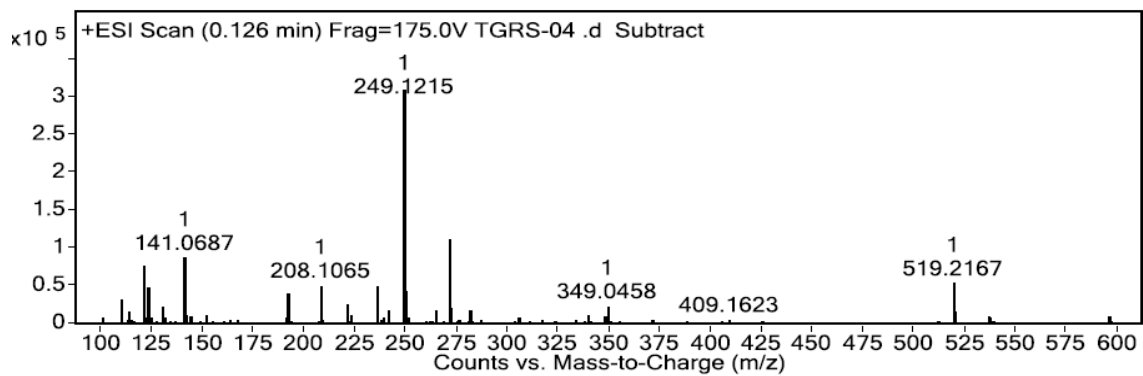
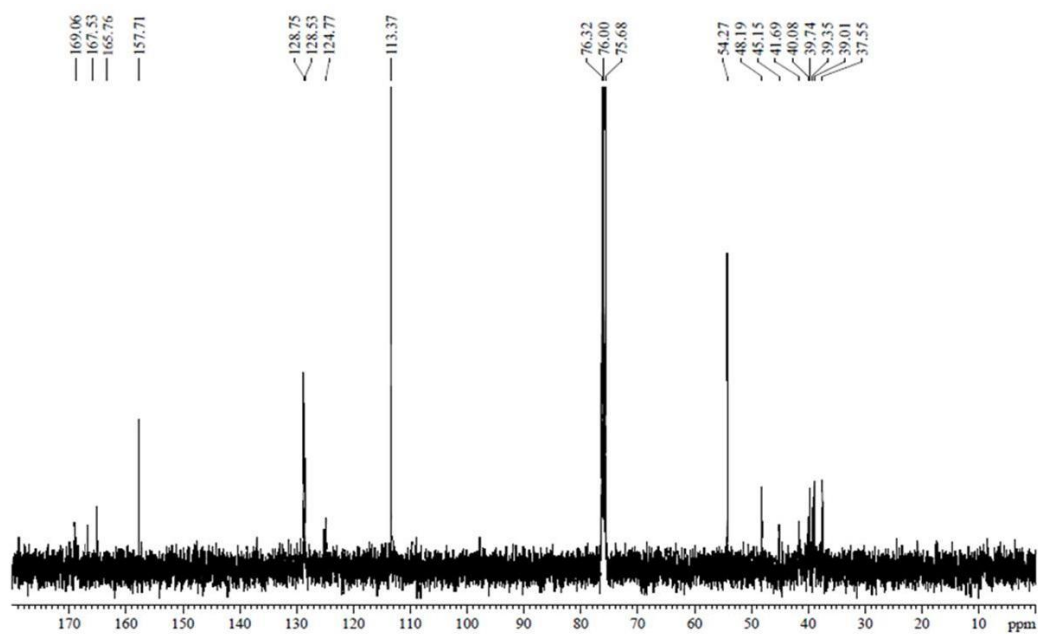
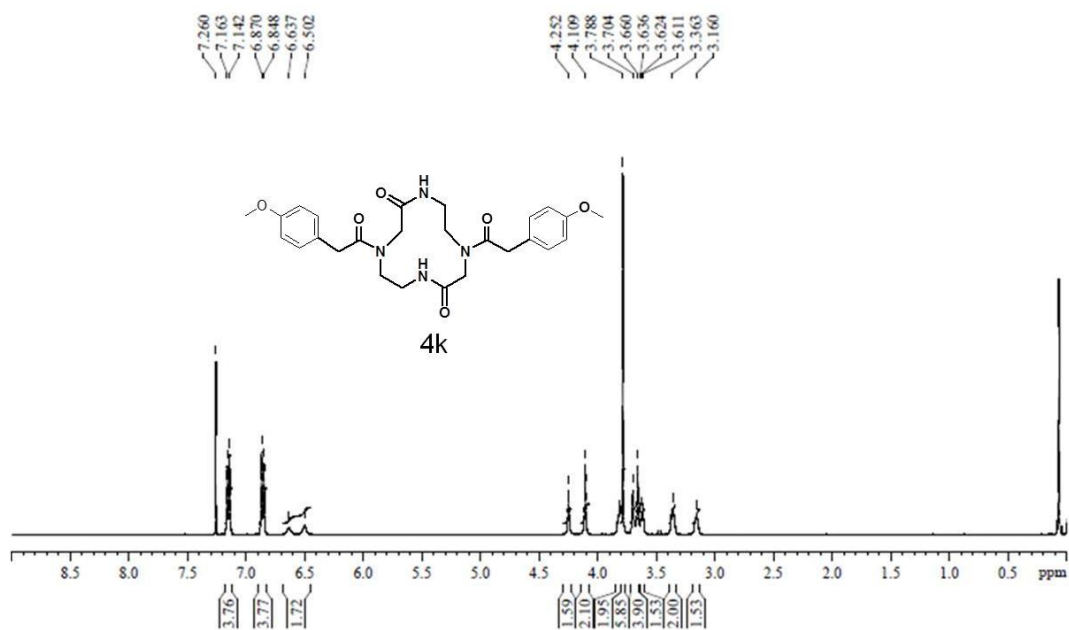


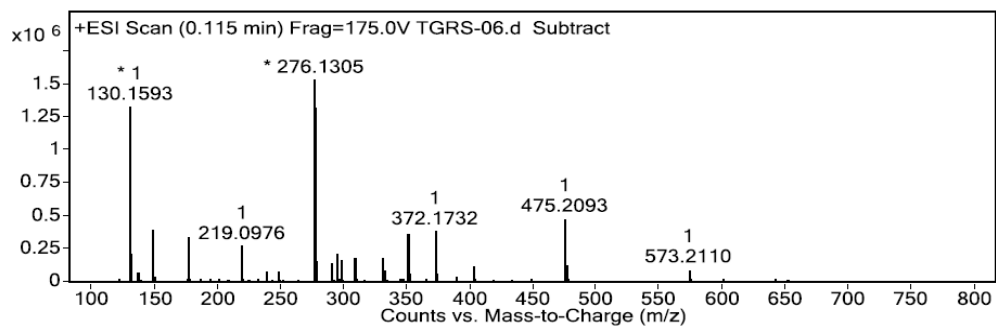
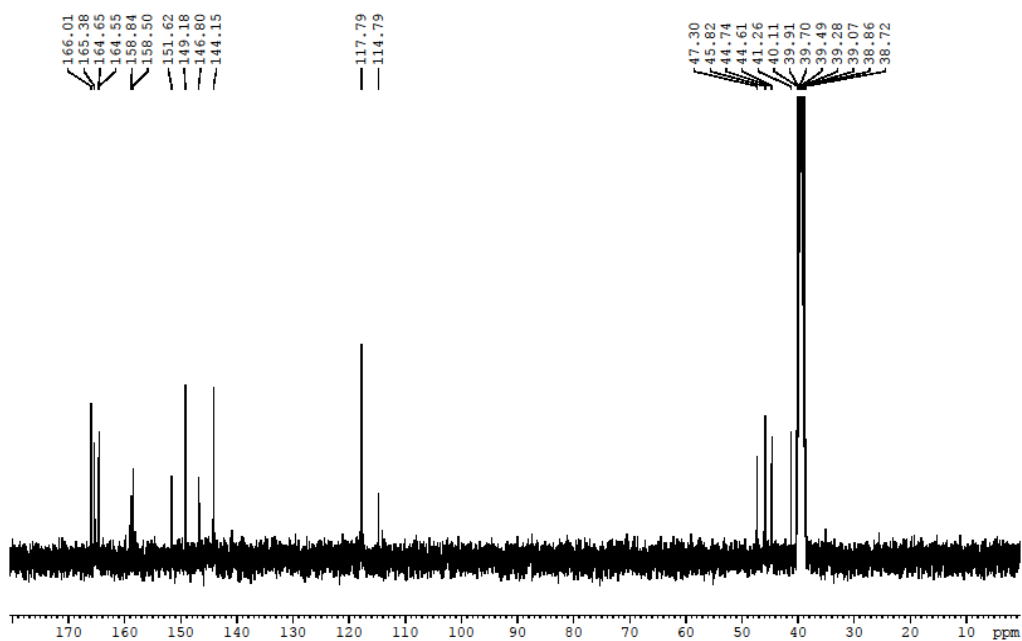
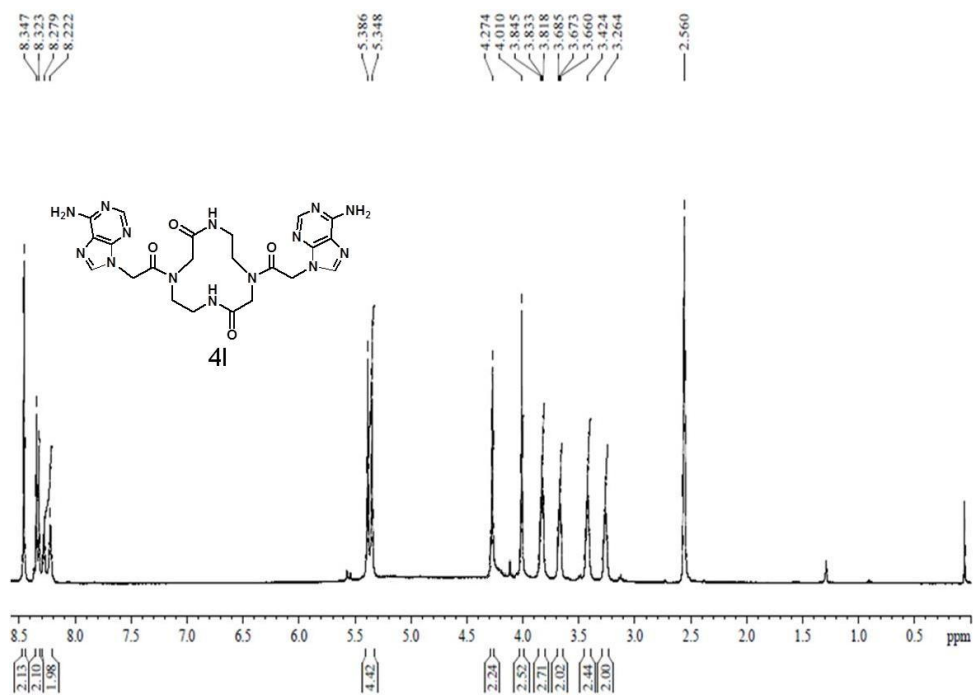












Chapter 3C

Natural tripeptide-based inhibitor of multifaceted A β toxicity

AD is the most complicated among all the neurodegenerative diseases, and several hypotheses (based on A β aggregates, A β oligomer, tau, metal ion, and oxidative stress) have been proposed as plausible mechanisms behind the pathogenesis.^{2, 40, 41} A β aggregation is polymorphic in nature and predominantly leads to the formation of oligomers and fibrillar aggregates.^{5, 42-44} A β in the oligomeric state is less stable and more toxic compared to the fibrillar aggregate state and therefore, developing inhibitors targeting both the polymorphic forms of A β is necessary for the successful therapeutic intervention of A β toxicity in AD.^{45, 46} On the other hand, high concentrations of biometals (Fe, Cu, and Zn) have been found to be associated with A β in amyloid plaques of the AD patient's brain.⁴⁸ A β -metal ion complexation influences the aggregation pathway of A β and is shown to stabilize the toxic oligomeric state *in vitro*.³ Moreover, A β bound to redox-active metal ions (Cu²⁺ and Fe³⁺) produces ROS such as hydroxyl radicals, superoxide and H₂O₂ through Fenton-type reaction, which subsequently induces oxidative stress and eventually leads to neuronal death.⁴⁹⁻⁵¹ Overall, the multifaceted toxicity induced by A β oligomers and aggregates, with or without metal inclusion, leads to neuronal cell death. Hence, a multifaceted approach to developing effective therapeutic agents for the treatment of AD is crucial. In this context, designing multifunctional molecules that inhibit the formation of or dissolve the A β aggregates (oligomers and fibrils), disrupt the A β -metal ion complex by metal sequestration and prevent ROS generation, prevent membrane disruption and provide the antioxidant effect, is a promising therapeutic strategy for curing or preventing the progression of AD.⁵²

Several bi-functional peptide molecules with metal chelation and anti-aggregation units have been reported in the literature, which is shown to inhibit the formation of A β aggregation and disrupt the A β -metal ion complex. Li *et al.* have reported cyclen (metal chelator) conjugated to KLVFF (A β 16-20, aggregation inhibitor), wherein the cyclen-KLVFF-Cu²⁺ complex cleaves the A β peptide and prevent its toxic effects.⁵³ Similarly, Faller

et al. have used a fragment of A β peptide (A β 12-20) and showed both metal chelation and inhibition of aggregation.⁵⁴ Short, unnatural peptides had been explored as bi-functional ligands to inhibit A β toxicity.⁵⁵ Recently, Yuan *et al.* have developed a bifunctional A β aggregation inhibitor GGHRYAAFFARR (GR), in which GGH act as a metal chelator for Cu(II) while RYYAAFFARR (RR) inhibit the aggregation.⁵⁶ In living systems, several peptides and proteins interact with metal ions to perform numerous biological functions.⁵⁷ These metal-binding peptides or proteins exhibit selective and high binding affinity towards specific metal ions. In the cellular milieu, redox-active metal ions (Fe and Cu) mostly exist in the complexed form with peptides or proteins.⁵⁸ This chelating property of peptides and proteins has not been fully explored to develop peptide-derived metal chelators. In addition, biological origin, selectivity and high affinity for metal chelation, non-immunogenic nature and biocompatibility of these metallopeptides make them ideal candidates to alleviate metal-induced A β toxicity. In this context, Gly-His-Lys (GHK), a natural tripeptide present in human serum, was chosen to design an effective inhibitor of multifaceted A β toxicity.^{59, 60} Remarkably, high concentrations of GHK (200 μ g/L) present in human adult serum readily form a complex with Cu²⁺ (GHK-Cu²⁺) with high affinity (binding constant $K_a \sim 10^{14}$).⁶¹ A β 42 complexes Cu²⁺ with a K_a of $\sim 10^9$ and hence, a chelating molecule with $K_a > 10^9$ is required to sequester Cu²⁺ from the A β inclusion complex.⁶² In this context, GHK with $K_a \sim 10^{14}$ can easily sequester the metal ion from the A β -Cu²⁺ complex. Moreover, Cu²⁺ bound to GHK exists in the redox-dormant state.⁶³ As a prerequisite and desired property, GHK is incapable of removing Cu²⁺ from biologically-relevant protein complexes ($K_a \sim 10^{15}$ - 10^{17}) and is an ideal candidate for selectively sequestering metal ion from the A β -Cu²⁺ complex. On the other hand, peptides and peptidomimetics based on the recognition sequence in A β have been developed as a class of modulators of its aggregation.⁶⁴⁻⁶⁷ In recent times, although a number of peptides and peptidomimetics have been reported to show moderate to good activity

against A β aggregation *in vitro*, most of them are designed to target a particular aspect of A β toxicity *viz.*, aggregation. These designs lack multi-functionality, which is essential for effectively tackling multifaceted A β toxicity. Here we design a multifunctional inhibitor for multifaceted A β toxicity, by conjugating GHK and a peptidomimetic analogue of the core recognition unit from A β . The hybrid peptoid mimic SrVSRFSr, (where Sr = sarcosine) based on the core recognition unit KLVFFA in A β was selected from our previous work, to obtain

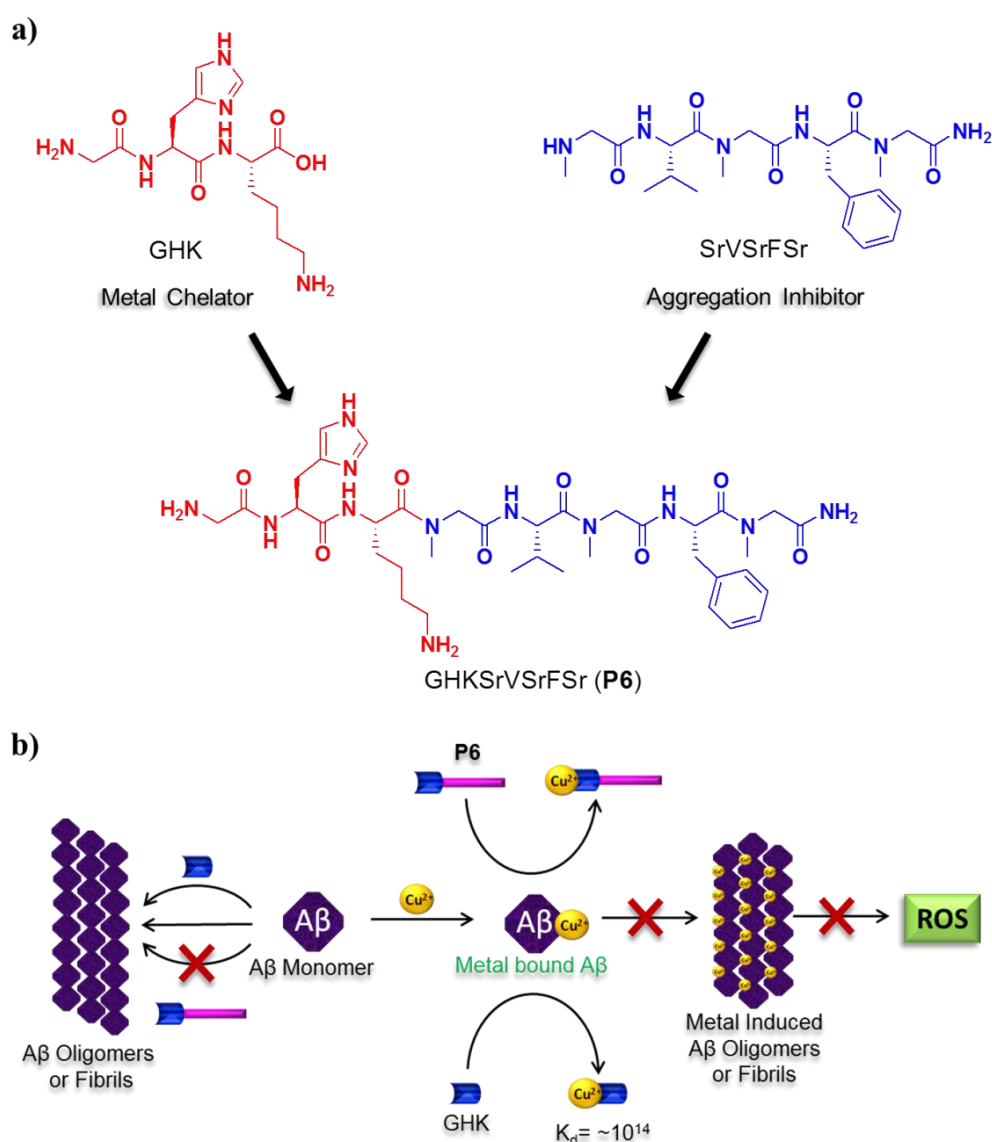


Figure 12. Design of the multifunctional peptidomimetic inhibitor. (A) Molecular structures of the natural tripeptide GHK, A β aggregation inhibitor (Sr-V-Sr-F-Sr, Sr: Sarcosine) and their multifunctional peptidomimetic conjugate **P6**. (B) Mechanism of inhibition of multifaceted A β toxicity by multifunctional **P6**.

multifunctional metal chelating agent.⁶⁸ GHK was conjugated at the N-terminal of SrVSRFSr to obtain the multifunctional peptidomimetic **P6** (Gly-His-Lys-Sr-Val-Sr-Phe-Sr) (Figure 12a).

3.13 Design strategy

Peptides or peptidomimetics reported in the literature generally modulate A β aggregation, which plays an important role in the progression of AD. Apart from aggregation-induced toxicity, there are many other toxic effects caused by the direct or indirect role of A β in AD. Among them, metal-induced A β toxicity is well-documented, where A β binds to metal ions, in particular, Cu²⁺ and generates ROS and related oxidative stress.⁶⁷ Herein, a multifunctional GHK-peptidomimetic conjugate **P6** is reported, which concurrently inhibits A β aggregation and membrane disruption and prevents copper-induced A β toxicity (ROS generation and antioxidant property). The tripeptide GHK functions as a metal chelator in **P6** owing to its higher binding affinity towards Cu²⁺ compared to A β 42. GHK is known to bind Cu²⁺ by coordinating with the N3 nitrogen of the imidazole in histidine, -NH₂ of glycine and the amide nitrogen of the glycine-histidine peptide bond. For this reason, GHK was chosen as the N-terminal moiety to retain its binding affinity towards Cu²⁺ in the **P6** conjugate.⁶⁹ The multifunctional **P6** is expected to inhibit multifaceted toxicity related to A β aggregation and A β -Cu²⁺ inclusion complex. (Figure 12b).

3.14 Inhibition of A β 42 fibrillar aggregates

A β 42, a disordered peptide, folds into an ordered β -sheet structure and further self-assembles to form toxic fibrillar aggregates.⁵ These fibrillar aggregates play a crucial role in initiating the symptoms observed in AD. Inhibiting the formation of fibrillar aggregates is considered as one of the most prominent approaches to developing effective therapeutic agents for AD. To study the effect of **P6** on the aggregation propensity of A β 42, ThT assay and CD measurements were performed. ThT (λ_{ex} = 450 nm, λ_{em} = 485 nm) is a molecular dye that

shows minimal fluorescence in the presence of A β 42 monomers and enhanced fluorescence when bound to fully formed A β 42 aggregates. Therefore, ThT assay was performed to study the effect of **P6** on the fibrillization of A β 42. The A β 42 (10 μ M) was incubated alone and independently with GHK (20 μ M, control: metal chelating peptide), a pentapeptide LPFFD (20 μ M, control: A β aggregation inhibitor), SrVSrFSr (20 μ M) and **P6** (20 μ M) at 37 °C for 48 h, and then ThT was added and fluorescence was measured at 485 nm (Figure 13a). ThT fluorescence of A β 42 with GHK was comparable to that of A β 42 alone, indicating that GHK has a negligible effect on A β 42 aggregation. The positive control LPFFD and SrVSrFSr showed a decrease in ThT fluorescence, corresponding to ~30% and ~35% inhibition of A β 42 aggregation respectively. On the other hand, ~50% of A β 42 aggregation was inhibited by **P6**, which was ~20% higher than the positive controls. Next, the effect of varying concentrations of **P6** (10 - 100 μ M) on the aggregation tendency of fixed concentration of A β 42 (10 μ M) was studied. Increasing concentration of **P6** up to 1:5 (A β 42: **P6**) ratio exhibited improved inhibition efficiency, but beyond this concentration, the inhibition efficiency did not improve (Figure 13b). To assess the effectiveness of the **P6** conjugate, **P6** (20 μ M) and the combination of GHK (20 μ M) and SrVSrFSr (20 μ M) was studied against A β 42 aggregation. Interestingly, **P6** exhibited better inhibition efficacy compared to the physical combination of individual constituents, i.e., GHK and SrVSrFSr, which clearly supports the idea of using their covalent conjugate (**P6**).

Further, the inhibition efficiency of **P6** was evaluated by performing CD measurements. In these measurements, the β -sheet content (A β 42 fibrillar aggregates are rich in β -sheet) was measured by monitoring the characteristic negative CD band observed at 220 nm.⁷⁰ The A β 42 (10 μ M) was incubated alone and independently with GHK (20 μ M), LPFFD (20 μ M), SrVSrFSr (20 μ M) and **P6** (20 μ M) at 37 °C for 48 h, and then CD spectra were recorded (Figure 13c). GHK did not alter CD signal at 220 nm corresponding to β -sheet of the A β 42

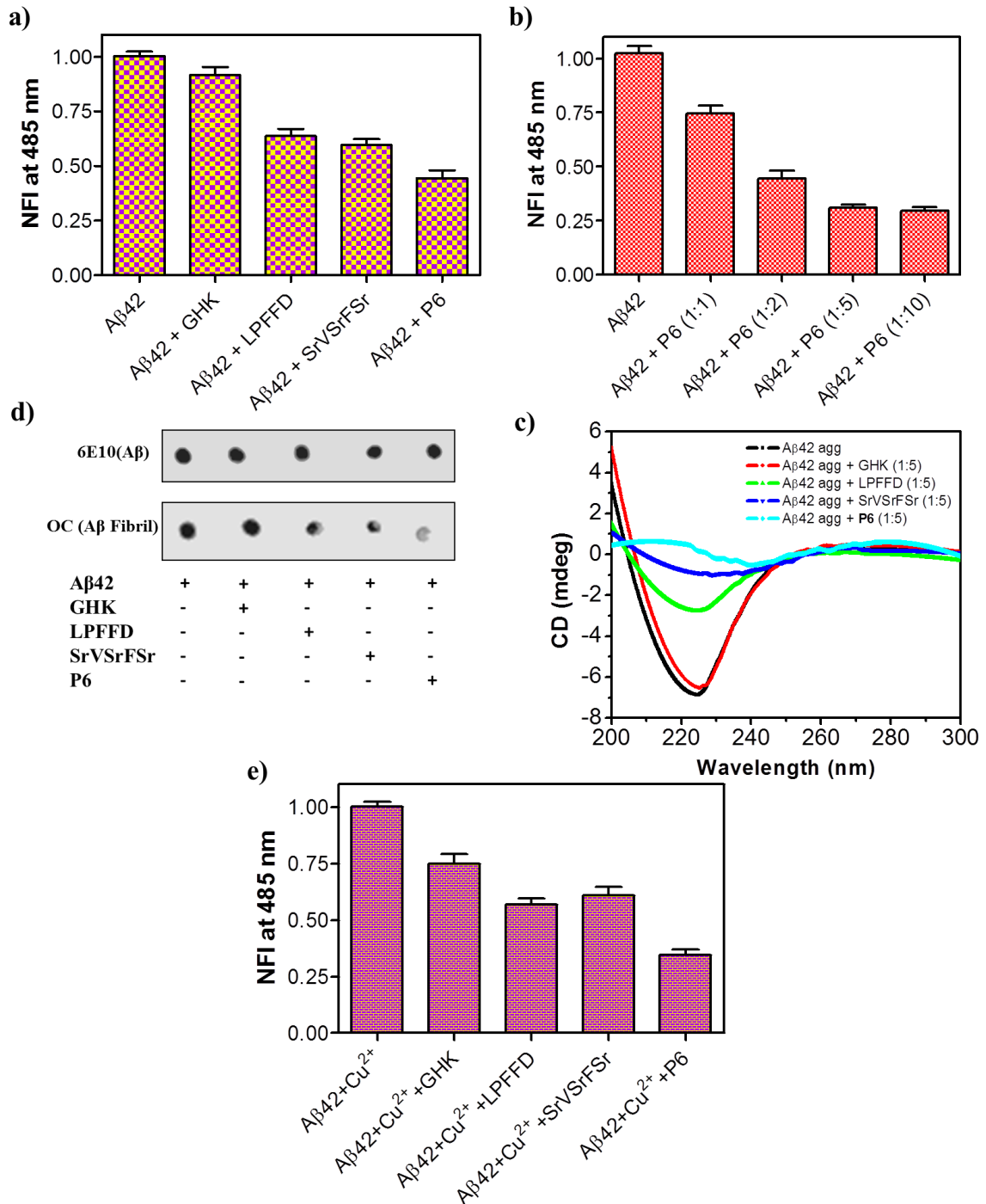


Figure 13. Inhibition of A β 42 aggregates studied by thioflavin (ThT) assay and CD measurements. (A) A β 42 (10 μ M) was incubated alone and independently with peptides GHK, LPFFD, SrVSrFSr and **P6** in 1:2 stoichiometry and their influence on aggregation are quantified by measuring ThT fluorescence intensity, which is represented as normalized fluorescence intensity at 485 nm for a given time point (48 h). (B) The effects of different stoichiometries of **P6** on the aggregation of A β 42 (10 μ M). (C) CD measurements of A β 42 (10 μ M) incubated independently with 20 μ M of the peptide (GHK or LPFFD or SrVSrFSr or **P6**) at 37 $^{\circ}$ C for 48 h. (D) Dot blot analysis of A β 42 (10 μ M) peptide incubated independently with 50 μ M peptide (GHK or LPFFD or SrVSrFSr or **P6**) at 37 $^{\circ}$ C. 6E10 or OC (1:3000) is used as primary antibody followed by secondary antibody (HRP conjugated

anti-mouse antibody (1:10000)). Chemiluminescence was recorded by treating blots with ECL reagent for 2 min. (E) A β 42 (10 μ M) and Cu²⁺ was incubated alone and independently with peptides GHK, LPFFD, SrVSRFSr and **P6** in 1:2 stoichiometry and their influence on aggregation is quantified by measuring ThT fluorescence intensity, which is represented as normalized fluorescence intensity at 485 nm for a given time point (24 h). Each experiment was repeated three times (n = 3) and error bars represent the standard deviation (SD) of the normalized fluorescence intensity (NFI).

fibrillar aggregates. LPFFD modulated the A β 42 aggregation as it showed a 60% decrease in the β -sheet content of A β 42 and SrVSRFSr also prevented A β 42 β -sheet formation by 80%. Remarkably, **P6** completely altered the CD signal at 220 nm, indicating effective prevention of A β 42 aggregation (Figure 13c). Therefore, ThT assay and CD measurements clearly showed that **P6** efficiently inhibited the formation of toxic A β 42 fibrillar aggregates. Further, we analysed the A β 42 fibrillar aggregation inhibition property of **P6** by dot blot analysis. In a set of independent experiments during the preparation of A β 42 fibrillar aggregates in PBS (10 mM, pH = 7.4), A β 42 monomer (10 μ M) was incubated with GHK (50 μ M), LPFFD (50 μ M), SrVSRFSr (50 μ M) or **P6** (50 μ M) independently for 48h at 37 °C. Then the samples were spotted on a nitrocellulose membrane and treated with the OC antibody (which binds and detects A β 42 fibrillar aggregates) or the 6E10 antibody as a control (which binds to all forms of A β species) (Figure 13d). The data revealed that GHK did not prevent the formation of fibrillar aggregates, whereas LPFFD and SrVSRFSr showed ~50% and ~60% inhibition respectively. Remarkably, the **P6**-treated sample showed >80% reduction in the A β 42 fibrillar aggregates, which confirms the effective inhibition activity towards A β 42 fibrillar aggregates. Redox metal such as copper is known to bind A β 42 and mediate its aggregation process and is a major contributor towards the A β toxicity through mechanisms involving ROS generation among other related routes.³ Therefore, we studied the effect of **P6** on Cu²⁺ mediated A β 42 aggregation. The A β 42 (10 μ M) and Cu²⁺ were incubated together and independently with GHK (20 μ M), LPFFD (20 μ M) and **P6** (20 μ M) at 37 °C for 24 h, and then ThT was added, and the fluorescence was measured at 485 nm (Figure 13e). GHK being

the metal chelator exhibited ~20% inhibition of Cu²⁺ mediated Aβ₄₂ aggregation. Whereas, the positive controls LPFFD and SrVSrFSr showed ~40% and ~35% inhibition of Aβ₄₂+Cu²⁺ aggregation, respectively. On the other hand, **P6** showed ~70% inhibition of Aβ₄₂+Cu²⁺ aggregation. The enhancement in the inhibition of copper-mediated Aβ₄₂ aggregation by **P6** demonstrates the multifaceted targeting of Aβ toxicity (Figure 13a).

3.15 Inhibition of Aβ oligomeric aggregates

Oligomers are considered the most toxic form of Aβ among all other polymorphic forms, including fibrillar aggregates.⁴² Recent studies have shown that oligomers induce synaptic dysfunction and cell membrane disruption among other adverse effects, and all these synergistically contribute towards neuronal death in the brain.⁴⁶ Therefore, an effective inhibitor not only prevents the formation of Aβ fibrillar aggregates but also the toxic oligomeric species. Many of the inhibitors of Aβ aggregation reported in the literature are not successful in preventing oligomerization and in some cases they are known to stabilize Aβ in the oligomeric state.⁴⁹ Therefore, studying the effectiveness of the designed molecule against Aβ oligomer formation is crucial for assessing its potential as an inhibitor of Aβ toxicity. Aβ oligomeric species were prepared through standard protocols and were detected using immunohistochemistry (IHC) in dot blot analysis.^{66, 71} In a set of independent experiments during the preparation of Aβ oligomer species in PBS (10 mM, pH = 7.4), Aβ₄₂ (10 μM) was added with GHK (50 μM), LPFFD (50 μM), SrVSrFSr (50 μM) or **P6** (50 μM). The samples were then spotted on a nitrocellulose membrane and treated with the A11 antibody (which binds and detects Aβ oligomeric species) or the 6E10 antibody as a control (which binds to all forms of Aβ species) (Figure 14a). The data revealed that GHK did not prevent the formation of oligomeric species, whereas LPFFD and SrVSrFSr showed ~60% and ~75% inhibition, respectively. Remarkably, the **P6**-treated sample showed >95% reduction in the Aβ oligomeric species. Most of the peptide-based bifunctional inhibitors have not focused on

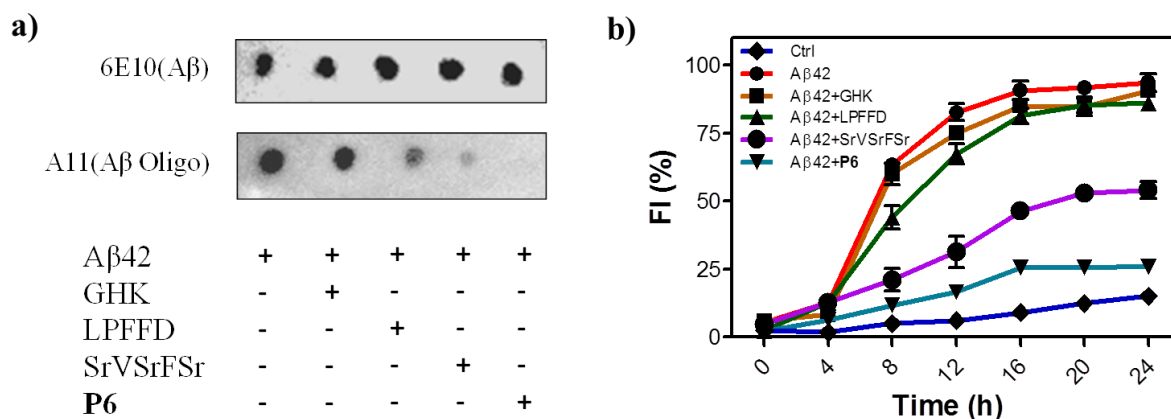


Figure 14. Inhibition of A β oligomeric aggregates. (A) Dot blot analysis of A β 42 (10 μ M) peptide incubated independently with 50 μ M peptide (GHK or LPFFD or SrVSrFSr or **P6**) at 37 $^{\circ}$ C. 6E10, or A11 (1:3000) is used as primary antibody followed by secondary antibody (HRP conjugated anti-mouse antibody (1:10000)). Chemiluminescence was recorded by treating blots with ECL reagent for 2 min. (B) Carboxyfluorescein fluorescence intensity (FI, 516 nm) measured in solutions of A β 42 peptide (10 μ M) with liposome (carboxyfluorescein loaded) in the presence of 50 μ M peptide (GHK or LPFFD or SrVSrFSr or **P6**) monitored for a duration of 24 h, incubated at 37 $^{\circ}$ C. Ctrl = only carboxyfluorescein loaded liposomes, each experiment was repeated three times (n = 3) and error bars represent the standard deviation (SD) of the fluorescence intensity (FI).

inhibition of A β oligomers, whereas **P6** effectively inhibits the formation of soluble and toxic A β oligomeric species are showcasing its advantage over other reported molecules.

Cell membrane disruption is considered as one of the predominant forms of A β -induced toxicity. A β oligomers interact with the lipid membrane and create holes in the cellular membrane, leading to cellular toxicity.⁷² To mimic such a scenario *in vitro*, liposomes loaded with a fluorescence dye (carboxyfluorescein) were used as a model system (membrane mimic). Liposomes were incubated with A β 42 at 37 $^{\circ}$ C, and the fluorescence was monitored at 516 nm (carboxyfluorescein) for 24h.^{73, 74} A β oligomers formed during the aggregation process interacted with and created pores into the liposome membrane. As a consequence, damaged liposomes released the fluorescent dye into the solution, enhancing the fluorescence, which was correlated with the oligomeric species present in the sample. To study this process, the dye-loaded liposome solutions (PBS, 10 mM, pH = 7.4) containing A β 42 monomer (10 μ M) were incubated independently with GHK (50 μ M), LPFFD (50

μM), SrVSrFSr (50 μM) and **P6** (50 μM), and the fluorescence ($\lambda_{\text{em}}= 516 \text{ nm}$) was measured at intervals of 4 h for 24 h (Figure 14b). A β 42+GHK containing liposome solutions exhibited a steep increase in fluorescence with time similar to A β 42 alone, indicating GHK was ineffective in preventing the oligomer formation. LPFFD being an aggregation inhibitor did not prevent the fluorescence enhancement or the liposome leakage caused by A β 42 oligomers. Interestingly, SrVSrFSr showed a significant decrease in the fluorescence intensity compared to LPFFD, which is in agreement with dot blot analysis and reveals that SrVSrFSr has higher oligomer inhibition efficiency over LPFFD. Interestingly, the **P6**-treated sample (liposomes+A β 42+**P6**) showed the least fluorescence enhancement, which confirmed that **P6** interacted with the A β 42 monomer and inhibited the formation of toxic oligomeric species, which in turn prevented the membrane disruption. Overall, these studies confirmed that **P6** is an effective inhibitor of the formation of polymorphic A β oligomers and aggregates.

3.16 Metal ion sequestration from the A β 42-Cu²⁺ complex

A β -bound Cu²⁺ undergoes a continuous cycle of redox process to generate ROS through a Fenton-type reaction.⁷⁵ Therefore, sequestration of Cu²⁺ from the A β species is considered an important strategy to prevent redox process-induced ROS generation to suppress the metal directed A β toxicity. First, we studied the metal sequestration ability of **P6** was studied by performing the mass spectral analysis. The A β 42-Cu²⁺ complex treated with **P6** showed mass peak at 431 (m/2 of **P6**-Cu²⁺) corresponding to the **P6**-Cu²⁺ complex which confirmed by the efficient Cu²⁺ sequestration by **P6** (Figure 15a). To further understand the Cu²⁺ sequestration properties by **P6**, the inherent fluorescence of tyrosine (¹⁰Tyr) residue (excitation: 285 nm and emission: 308 nm) in A β 42 was utilized. Interestingly, ¹⁰Tyr fluorescence quenching at 308 nm by the close proximity of Cu²⁺ bound to A β 42 is a well-studied phenomenon (Figure 15b).⁷⁶ The extraction of metal ion from the A β 42-Cu²⁺ complex by **P6** is expected to restore

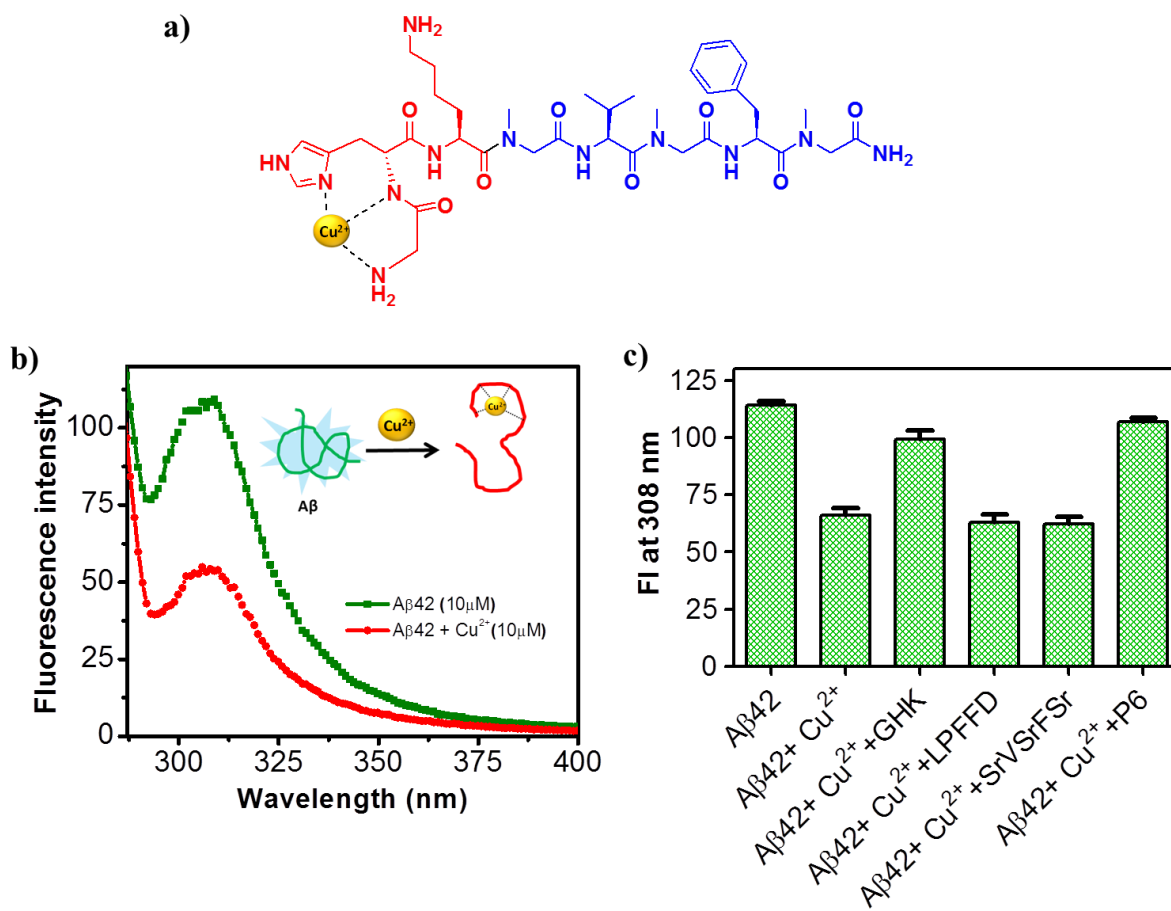


Figure 15. Extraction of Cu^{2+} from $\text{A}\beta_{42}\text{-Cu}^{2+}$ complex. (A) Tyrosine fluorescence of $\text{A}\beta_{42}$ ($10\ \mu\text{M}$) and after addition of $10\ \mu\text{M}$ Cu^{2+} in PBS buffer ($10\ \text{mM}$, $\text{pH}\ 7.4$). (B) Tyr fluorescence intensity (FI) measured for $\text{A}\beta_{42}\text{-Cu}^{2+}$ complex in the presence of $10\ \mu\text{M}$ peptide (GHK or LPFFD or SrVSrFSr or **P6**). The fluorescence intensities were measured at $308\ \text{nm}$ with excitation at $285\ \text{nm}$. Each experiment was repeated three times ($n = 3$), and error bars represent the standard deviation (SD) of the fluorescence measurement.

¹⁰Tyr fluorescence at $308\ \text{nm}$. Consequently, the extent of restoration of fluorescence at $308\ \text{nm}$ is an indicator of the ability of a metal chelator to remove Cu^{2+} from $\text{A}\beta_{42}$. For this study, $\text{A}\beta_{42}$ ($10\ \mu\text{M}$) in PBS ($10\ \text{mM}$, $\text{pH} = 7.4$) was incubated with Cu^{2+} ($10\ \mu\text{M}$) followed by the addition of GHK ($10\ \mu\text{M}$), LPFFD ($10\ \mu\text{M}$), SrVSrFSr ($10\ \mu\text{M}$) or **P6** ($10\ \mu\text{M}$) and then the fluorescence was recorded for all samples at $308\ \text{nm}$. Remarkably, GHK and **P6** restored the ¹⁰Tyr fluorescence by $\sim 88\%$ and $\sim 93\%$, respectively, signifying their ability to sequester Cu^{2+} from the $\text{A}\beta_{42}\text{-Cu}^{2+}$ complex (Figure 15c). As expected, LPFFD and SrVSrFSr showed the negligible copper sequestration ability (Figure 15c). Further increase in the concentration of

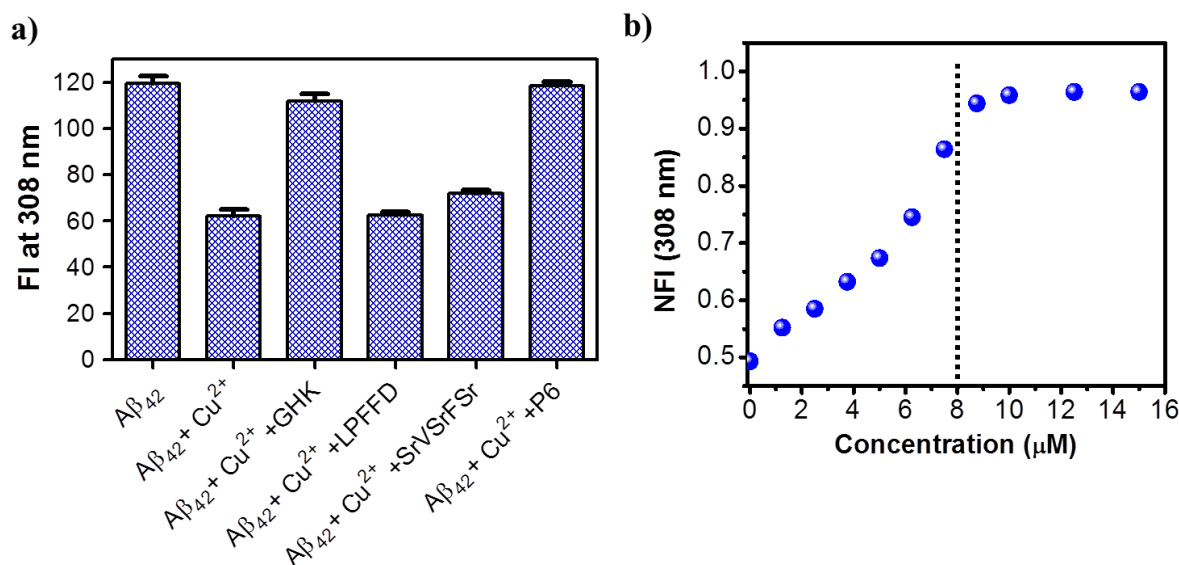


Figure 16. Extraction of metal ion from Aβ₄₂-Cu²⁺ complex. (A) Tyr fluorescence measured for Aβ₄₂-Cu²⁺ (10 μM) in the presence of 20 μM peptide (GHK or LPFFD or **P6**). The fluorescence intensity was measured at 308 nm with excitation at 285 nm. (B) Fluorescence enhancement at 308 nm upon addition of **P6** to Aβ₄₂-Cu²⁺ complex in a concentration-dependent manner. **P6** and Cu²⁺ exhibit 1:1 binding stoichiometry.

P6 to 1:2 (Aβ₄₂-Cu²⁺, GHK or LPFFD or **P6**) resulted in increased Cu²⁺ sequestration efficiency (Figure 16a).

A concentration-dependent experiment was performed to determine the binding stoichiometry by adding increasing concentrations of **P6** (1.25, 2.5, 3.75, 5, 6.25, 7.5, 8.75, 10, 12.5 and 15 μM) to the Aβ₄₂-Cu²⁺ complex (10 μM) (Figure 16b). The ¹⁰Tyr fluorescence increased gradually and saturated for **P6** >10 μM, which corresponds to a 1:1 binding stoichiometry for **P6** and Cu²⁺ complexation. The Aβ₄₂, in the presence of other relevant metal ions like Zn²⁺, Fe³⁺ and Al³⁺, showed negligible changes in the ¹⁰Tyr fluorescence. To ascertain the binding and sequestration selectivity of **P6** towards Cu²⁺ in the presence of other metal ions, Aβ₄₂-Cu²⁺ complex (10 μM) in PBS (10 mM, pH = 7.4) was incubated with Zn²⁺ (10 μM), Fe³⁺ (10 μM), Al³⁺ (10 μM) and Ca²⁺ (10 μM) independently, followed by **P6** addition to all the samples and the monitoring of ¹⁰Tyr fluorescence of Aβ₄₂-Cu²⁺. The ¹⁰Tyr fluorescence was enhanced, which indicated that **P6** specifically bound and

sequestered Cu^{2+} from the $\text{A}\beta\text{42-Cu}^{2+}$ complex even in the presence of other free metal ions in the sample.

3.17 Antioxidant properties of P6

The redox cycle of the metal ion in $\text{A}\beta\text{-Cu}^{2+}$ complex generates ROS through Fenton-type reaction. Therefore, investigating the effective silencing of copper redox cycle in the $\text{A}\beta\text{-Cu}^{2+}$ complex by **P6** is crucial to assessing its antioxidant property and as a potential multifunctional inhibitor of $\text{A}\beta$ toxicity. To evaluate the redox silencing property of **P6** ascorbate assay was performed, wherein Cu^{2+} was treated with a reducing agent (ascorbate) to induce the redox cycle. Under reducing condition, Cu^{2+} is reduced to Cu^+ , which being unstable oxidizes back to Cu^{2+} and generates hydroxyl ions in the process. Hydroxyl radicals are the major form of ROS contributing to the toxicity in AD, and these radicals can be detected *in vitro* by using Coumarin-3-carboxylic acid (3-CCA).⁷⁷ Hydroxyl radicals transform non-fluorescent 3-CCA to a highly fluorescent compound 7-hydroxycoumarin-3-carboxylic acid (7-OH-CCA) ($\lambda_{\text{ex}}= 395$ nm and $\lambda_{\text{em}}= 452$ nm). To PBS (10 mM, pH = 7.4) solutions containing Cu^{2+} (5 μM) and 3-CCA (50 μM), peptide GHK (10 μM), LPFFD (10 μM), SrVSrFSr (10 μM) or **P6** (10 μM) were added independently, and the fluorescence at 452 nm was monitored upon addition of ascorbate (150 μM) for 70 min at regular intervals of 5 min. Interestingly, GHK and **P6**-treated solutions showed negligible fluorescence, indicating that the GHK or **P6**-bound Cu^{2+} (redox-dormant state) was not involved in the redox cycle to generate hydroxyl radicals even under highly reducing conditions (ascorbate). On the other hand, the solution treated with LPFFD and SrVSrFSr showed an increase in fluorescence as a function of time, indicating its minimal interference in the redox cycle of Cu^{2+} or its inability to silence it (Figure 17a). Therefore, GHK and **P6** prevented the generation of hydroxyl radicals by binding and suppressing the redox cycle of Cu^{2+} in state reducing conditions, and the bound metal ion remained in the redox-dormant (Figure 17b).

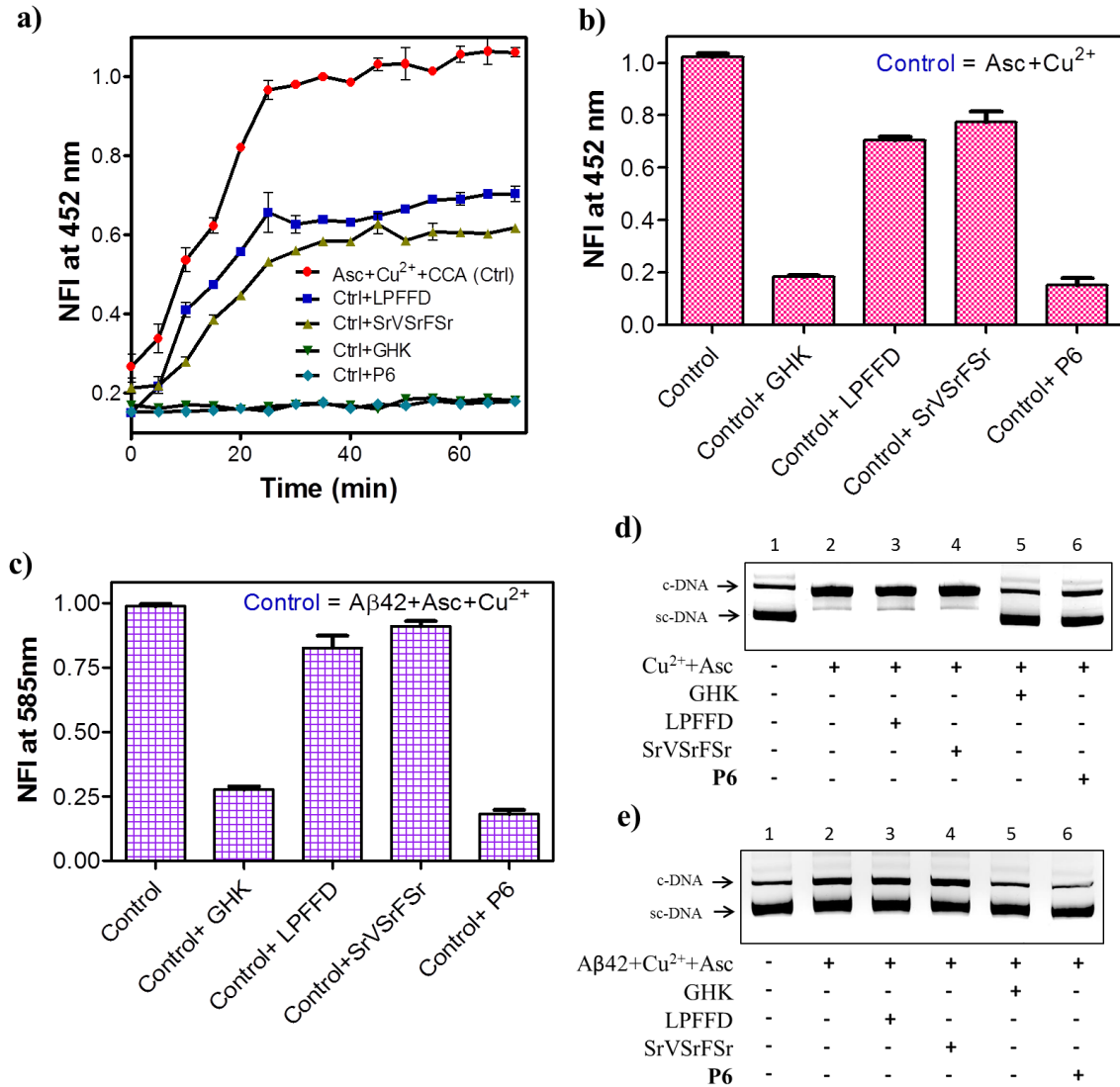


Figure 17. Antioxidant properties of **P6**. a) 7-OH-CCA fluorescence intensity (452 nm) measured in solutions of Cu²⁺ (5 μM) with ascorbate (150 μM) in presence of 10 μM peptide (GHK or LPFFD or **P6**) monitored in time-dependent manner for a duration of 70 min at 37 °C. b) Fluorescence intensity (452 nm) of 7-OH-CCA generated with Cu²⁺ (5 μM) and ascorbate (150 μM) in presence of 10 μM peptide (GHK or LPFFD or **P6**) after 70 min of incubation at 37 °C. c) Resorufin fluorescence intensity (585 nm) measured in solutions of Aβ₄₂ (5.1), Cu²⁺ (5 μM), ascorbate (150 μM) HRP and amplex red (10 μM) in presence of 10 μM peptides (GHK, LPFFD and **P6**) after 60 min of incubation at 37 °C. DNA damage. Agarose gel electrophoresis of plasmid DNA (pBR322, 2 μg/mL or 0.75 μg/mL) treated with (d) peptide (GHK, 10 μM or LPFFD, 10 μM or SrVSrFSr, 10 μM or **P6**, 10 μM) and Cu²⁺ (5 μM) in presence of ascorbate (150 μM) or (e) Aβ₄₂ (1.1 μM), peptide (GHK, 2 μM or LPFFD, 2 μM or **P6**, 2 μM), Cu²⁺ (1 μM) and ascorbate (100 μM) incubated at 37 °C. Super coiled DNA (sc-DNA), circular DNA (c-DNA). Each experiment was repeated three times (n = 3), and error bars represent the standard deviation (SD) of the normalized fluorescence intensity (NFI).

Aβ₄₂-Cu²⁺ generates hydrogen peroxide (H₂O₂) that subsequently disintegrates to hydroxyl radicals; this scenario of H₂O₂ production *in vitro* was studied by the hydrogen peroxide

assay. In this experiment, A β 42-Cu²⁺, under reducing conditions (ascorbate), generated H₂O₂ that was detected using horseradish peroxidase (HRP) and Amplex Red system. HRP uses Amplex Red (non-fluorescent) as an electron donor during the reduction of hydrogen peroxide to water, and in the process, generates the fluorescent resorufin dye ($\lambda_{\text{ex}} = 571 \text{ nm}$; $\lambda_{\text{em}} = 585 \text{ nm}$). Hence, the fluorescence intensity of resorufin is directly correlated to H₂O₂ generation.⁷⁸ To solutions containing A β 42 (5.1 μM), Cu²⁺ (5 μM), HRP and Amplex Red (10 μM) in PBS buffer (10 mM, pH = 7.4), peptide GHK (10 μM), LPFFD (10 μM), SrVSrFSr (10 μM) or **P6** (10 μM) were added. Then the samples were incubated for 10 min followed by the addition of ascorbate (150 μM), and fluorescence was recorded at 585 nm ($\lambda_{\text{ex}} = 571 \text{ nm}$) after 1 h, for all the samples. **P6** and GHK exhibited ~82% and ~72% decrease in the H₂O₂ generation, respectively, whereas LPFFD and SrVSrFSr showed negligible effects (Figure 17c). This study confirmed that **P6** efficiently sequestered the metal ion from the A β 42-Cu²⁺ and transformed it into a redox-dormant state, thereby preventing the generation of ROS. In addition, **P6** also inhibited the formation of toxic polymorphic forms (fibrils and oligomers) of A β 42 (Figures 13 and 14) in keeping with the initial design principles of this study, which demonstrates the multifunctional property of **P6**.

3.18 DNA cleavage

The ROS generated by A β -Cu²⁺ triggers neuronal toxicity through pathways that include DNA damage and lipid peroxidation among others. H₂O₂ and hydroxyl radicals generated by A β -Cu²⁺ complex cause DNA damage by either base pair modification or phosphodiester backbone cleavage.⁷⁹ A simple *in vitro* experiment was conducted to demonstrate the ability of **P6** to prevent DNA damage from ROS generated by the A β 42-Cu²⁺ complex. Plasmid DNA (pDNA) was used as a model for cellular DNA to assess ROS-induced damage. DNA was subjected to *in-situ* generated ROS in the absence and presence of **P6**, followed by the analysis of structural stability and integrity of DNA through agarose gel electrophoresis.⁸⁰

pDNA exists predominantly in supercoiled and relaxed forms, as visualized by the distinct bands in agarose gel (Figure 17). First, the study was conducted on pDNA stability towards hydroxyl radicals generated by Cu^{2+} in a reducing environment created by ascorbate. To PBS (10 mM, pH = 7.4) solutions containing Cu^{2+} (5 μM), pDNA (pBR322, 2 $\mu\text{g}/\text{mL}$) and peptide (GHK, 10 μM , LPFFD, 10 μM or SrVSrFSr, 10 μM or **P6**, 10 μM), ascorbate (150 μM) was added and the samples were incubated for 3 min at 37 °C followed by agarose gel electrophoresis (Figure 17d). A fragmented form of pDNA in the gel was observed in the presence of copper under the reducing (ascorbate) condition, by the action of *in situ* generated hydroxyl radicals. The addition of GHK or **P6** to the above samples showed protection of pDNA (as indicated by the intact and stable supercoiled band) in the presence of copper ascorbate system while LPFFD and SrVSrFSr failed to prevent the pDNA damage (as indicated by disappearance of a supercoiled band of pDNA) (Figure 17d). This is a clear indication that both GHK and **P6** bind to Cu^{2+} and prevent the production of hydroxyl radicals, whereas LPFFD and SrVSrFSr is not capable of complexing Cu^{2+} and failed to prevent the pDNA damage. To ascertain the $\text{A}\beta\text{-Cu}^{2+}$ -induced radical generation and DNA toxicity, gel electrophoresis was performed. To a solution containing $\text{A}\beta_{42}$ (1.02 μM), Cu^{2+} (1 μM), pDNA (pBR322, 0.75 $\mu\text{g}/\text{mL}$) and peptide (GHK, 2 μM or LPFFD, 2 μM or SrVSrFSr, 2 μM or **P6**, 2 μM) in PBS buffer (10 mM, pH = 7.4), ascorbate (100 μM) was added and the samples were incubated for 20 min, followed by agarose gel electrophoresis (Figure 17e). In the control sample ($\text{A}\beta_{42}\text{-Cu}^{2+}$), c-DNA band intensified which corresponds to the nicked form of pDNA. As expected, LPFFD and SrVSrFSr failed to prevent the pDNA damage, whereas both GHK and **P6** protected pDNA (c-DNA band comparable to control) from cleavage by sequestering Cu^{2+} from the $\text{A}\beta_{42}\text{-Cu}^{2+}$ complex and preventing the ROS generation (Figure 17e). These results further strengthened the fact that **P6** can sequester Cu^{2+} from $\text{A}\beta_{42}$ by forming a stable redox-dormant complex, thereby inhibit the ROS generation

and indirectly prevent the DNA cleavage.

3.19 Serum stability

Although peptides are considered excellent drug candidates, poor bioavailability and serum stability hinder their effective use as drugs.⁸¹ Therefore, assessing the serum stability of peptides and their peptidomimetics is important in evaluating their bioavailability and possibility of using them as drug candidates. The peptides (GHK, LPFFD, SrVSrFSr and **P6**) were separately incubated in human blood serum at 37 °C for 24 h. The amount of intact peptides were determined at different time points (0, 3, 6, 12 and 24 h) using RP-HPLC (Figure 18). GHK showed the greatest susceptibility towards serum proteases with a serum half-life of 3 h, and 90% of the GHK degraded over a period of 24 h. LPFFD showed a serum half-life of 8.5 h, and 75% of the peptide degraded after 24 h. Whereas, SrVSrFSr showed the least susceptibility towards serum proteases and only 2% of the SrVSrFSr degraded over a period of 24 h owing to the presence of unnatural amino acid (sarcosine) at alternating positions. Remarkably, the peptidomimetic **P6** was found to be stable against serum proteases when compared to natural peptides GHK and LPFFD, and ~85% of the peptide was still intact after 24 h.⁸² The reported peptide-based bifunctional inhibitors consist of natural amino acids which compromise their serum stability, whereas the presence of sarcosine-based peptoid (SrVSrFSr) at the C-terminal in **P6** makes it less susceptible to the serum protease enzymes.

3.20 Cell toxicity

After demonstrating the potential of **P6** as an effective inhibitor of multifaceted A β toxicity (aggregation to form oligomers and fibrillar aggregates, membranes disruption, copper-induced ROS generation, antioxidant property to reduce oxidative stress), a study was conducted to determine the efficiency of **P6** in reducing multifaceted A β toxicity in a cellular context. All the experiments were performed in the low serum media (2% FBS in RPMI) to

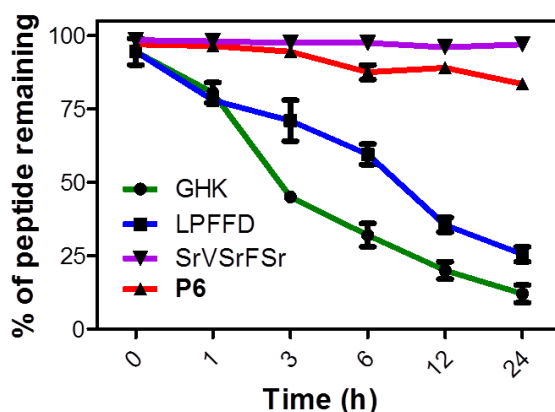


Figure 18. Serum stability of inhibitors. peptides (50 μM) (GHK, LPFFD, SrVSrFSr and **P6**) were incubated in human blood serum (HBS) and analyzed over a duration of 24 h. Each experiment was repeated three times ($n = 3$). Error bars represent the standard deviation (SD) of all the measurement.

minimize the interference of bovine serum albumin (BSA) competing with the probe for copper chelation. However, there may be minimum interference of BSA in our *in cellulo* experiments. The ability of peptides to rescue PC12 cells from toxicity induced from A β 42-

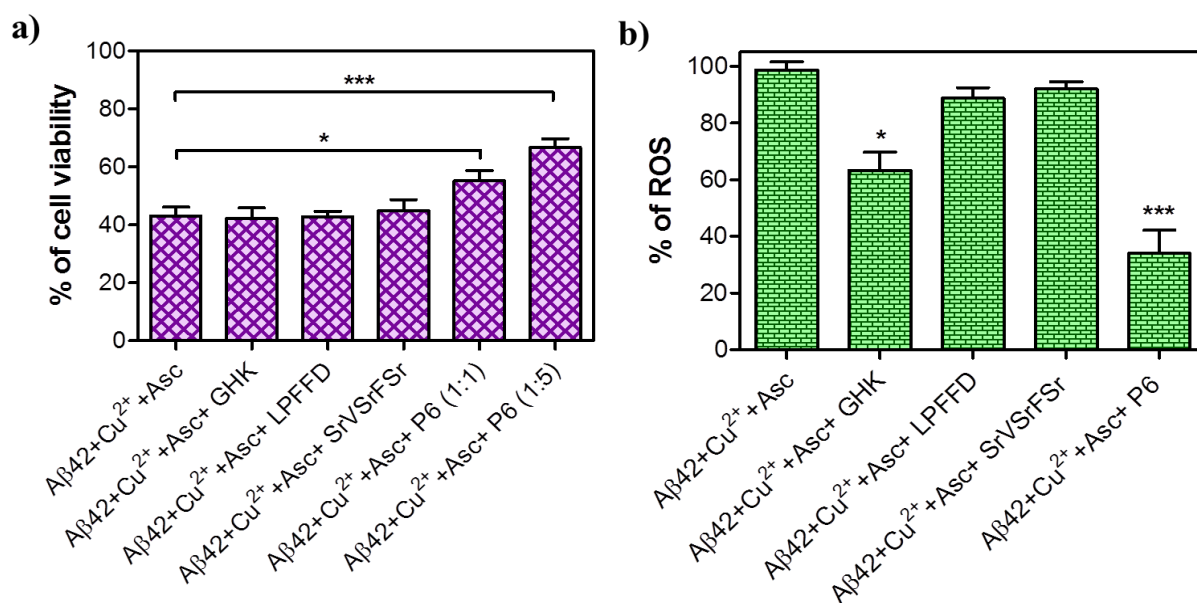


Figure 19. A β toxicity in PC12 cells (A) PC12 cell viability observed after incubation (24 h) with A β 42 (10 μM), Cu²⁺ (10 μM), ascorbate (200 μM), and with peptide GHK (10 μM) or LPFFD (10 μM) or SrVSrFSr (10 μM) or **P6** (10 μM and 50 μM) independently. (B) ROS generation in PC12 cell when incubated with A β 42 (10 μM), Cu²⁺ (10 μM), ascorbate (100 μM), and with peptide (GHK (50 μM) or LPFFD (50 μM) or SrVSrFSr (10 μM) or **P6** (50 μM)) is measured by DCF fluorescence. ROS produced is quantified by measuring DCF fluorescence intensity at 529 nm for a given time point. Each experiment was repeated three times ($n = 3$) and error bars represent the standard deviation (SD).

Cu²⁺ complex was studied through 3-(4,5-dimethylthiazol-2-yl)2,5-diphenyltetrazolium bromide (MTT) assay.⁵¹ Aβ42-Cu²⁺ (10 μM) with ascorbate (200 μM)-treated PC12 cells were incubated independently with GHK (10 μM), LPFFD (10 μM), SrVSrFSr (10 μM) and **P6** (10 μM). Aβ42-Cu²⁺ (10 μM) with ascorbate (200 μM) exhibited 57% reduction in cell viability (43% viable cells) compared with untreated cells showing 100% cell viability (Figure 19a). The PC12 cells treated with GHK (10 μM), LPFFD (10 μM) or SrVSrFSr (10 μM) found to have negligible protection from the toxicity induced by Aβ42-Cu²⁺ complex (Figure 19a). Remarkably, **P6** (10 μM)-treated cells showed significant improvement in the cell viability (55%) from Aβ42-Cu²⁺-induced toxicity. Increase in the concentration of **P6** (50 μM) enhanced cell viability from 43% (**P6** untreated) to 66% (**P6** treated, 50 μM); however, a further increase in the concentration of **P6** (> 50 μM) did not improve the cell viability significantly. The effect of peptides on Aβ42-Cu²⁺-induced ROS generation was studied by DCFDA assay in PC12 cells. DCFDA (2,7-dichlorofluorescein diacetate) is a fluorescent dye that measures hydroxyl, peroxy and other ROS levels within the cell.⁸³ The non-fluorescent DCFDA is oxidized by ROS inside the cells to fluorescent 2, 7-dichlorofluorescein (DCF, λ_{ex}=495 nm, and λ_{em}=529 nm). DCFDA-treated PC12 cells were incubated with Aβ42-Cu²⁺ (10 μM), ascorbate (200 μM) and with peptide GHK (50 μM), or LPFFD (50 μM) or SrVSrFSr (10 μM) or **P6** (50 μM) independently. LPFFD-treated cells had a minimal effect on ROS generation (minimal change in fluorescence at 529 nm) by the Aβ42-Cu²⁺ complex while GHK showed 30% decrease in fluorescence observed in cells owing to its metal chelating ability, compared to 100% fluorescence exhibited by cells treated with Aβ42-Cu²⁺ alone. Remarkably, **P6** exhibited 57% reduction in ROS generated by the Aβ42-Cu²⁺ complex, indicating that **P6** is more efficient in preventing ROS generation than the GHK peptide (Figure 19b). These results are in good agreement with the *in vitro* ascorbate and hydrogen peroxide antioxidant assays, and confirm that **P6** rescued PC12 cells by inhibiting

A β 42-Cu²⁺-induced ROS generation. Overall, the biocompatible, cell-permeable and nontoxic hybrid peptoid **P6** inhibits A β aggregation and prevents metal-induced toxicity, making it a potential inhibitor of multifaceted A β toxicity.

3.21 Conclusion

In conclusion, a multifunctional peptidomimetic **P6** was developed, inspired from the naturally occurring copper-chelating tripeptide GHK and a hybrid peptoid-based inhibitor of A β aggregation to target multifaceted A β toxicity. **P6** efficiently inhibited the formation of toxic A β polymorphic species (oligomers and fibrils). **P6** prevented the formation of toxic oligomeric species, which affect cell membrane integrity. Similar to GHK, **P6** sequestered Cu²⁺ from the A β 42-Cu²⁺ complex and maintained it in a redox-dormant state even in high reducing environments, which effectively prevented the production of ROS like hydroxyl radicals and H₂O₂. The antioxidant property of **P6** was confirmed by both ascorbate and hydrogen peroxide assays, which showed the suppression of ROS generated by Cu²⁺-bound A β 42. Further, the DNA damage induced by the A β 42-Cu²⁺ complex was efficiently alleviated by the sequestration of the metal ion and the inhibition of its redox cycling. The ability of **P6** to inhibit multifaceted A β toxicity *in vitro* was further confirmed in PC12 cells. Cells were rescued from A β 42-Cu²⁺-induced toxicity when treated with **P6**, and consequently, the amount of ROS generated was reduced. Therefore, the properties of inhibiting A β aggregation, preventing membrane disruption, selectively sequestering Cu²⁺ from the A β 42-Cu²⁺ complex, transforming it into a redox-dormant state and displaying antioxidant property together proved the multifunctional nature of **P6**, and its ability to alleviate multifaceted A β toxicity. Moreover, **P6** was found to be nontoxic to cells, and exhibited appreciable serum stability and biocompatibility, making it an ideal peptidomimetic candidate for targeting A β toxicity in AD. Furthermore, there is an enormous scope for have improving the efficiency of **P6** through chemical modifications, and efforts in this direction

been already initiated in our research group.

3.22 Experimental section

3.22.1 Synthesis, purification, and analysis of peptides and peptidomimetics. The GHK, LPFFD and **P6** were synthesized as per standard 9-fluorenylmethoxycarbonyl (Fmoc) chemistry on rink amide resin through solid phase peptide synthesis protocols. HBTU (2-(1H-Benzotriazole-1-yl)-1,1,3,3-tetramethyluronium hexafluorophosphate) was used as the coupling reagent, DIPEA (N,N-Diisopropylethylamine) as the base and DMF (Dimethylformamide) as the solvent. Fmoc deprotection was carried out using 20% piperidine in DMF. For the synthesis of peptide **P6**, the coupling time was increased to 2 h to obtain higher coupling yields, compared to the normal coupling time of 1 h. All the peptides were purified using a reverse-phase (RP) preparative HPLC on the C18 column at 40 °C. Product purity was greater than 98%, as ascertained by analytical HPLC. The mass of the peptides was analyzed using HRMS (Q-TOF).

3.22.2 Synthesis of FITC-P6. To a solution of **P6** (1 mM) in DMF, fluorescein isothiocyanate (1 mM) and DIPEA (1.5 mM) was added and stirred for 24 h at RT. The reaction mixture was then precipitated in diethyl ether and centrifuged. The supernatant was decanted, and the precipitate was dissolved in water, and the product was purified by HPLC.

3.22.3 Preparation of A β 42 oligomers and fibrils. A β 42 peptide (0.25 mg) (Merck, calbiochem) was dissolved in hexafluoro-2-propanol (HFIP, 0.2 mL) and incubated at room temperature for 1 h. HFIP was then removed by a flow of nitrogen and further dried under vacuum. HFIP-treated A β 42 was then dissolved in DMSO to a final concentration of 1 mM and diluted to 200 μ M with 10 mM PBS (pH 7.4). The solution was incubated at 37 °C for 48 h with gentle and constant shaking. The formation of A β 42 fibrils was confirmed by Thioflavin T (ThT) assay. For the oligomer preparation, A β 42 was dissolved in DMSO to a final concentration of 1 mM and diluted to 100 μ M in PBS buffer (10 mM, pH 7.4). The

solution was incubated at 37 °C for 1 h, after which the sample was incubated for 24 h at 4 °C for 1 h. The obtained sample was centrifuged, and the supernatant with oligomers was used for further experiments.⁸⁴

3.22.4 A β inhibition assays. All the peptides (GHK, LPFFD, and **P6**) were dissolved in PBS buffer (10 mM, pH 7.4). Then peptides (GHK, LPFFD, SrVSrFSr or **P6**, 20 μ M) were added individually to a freshly prepared A β 42 (10 μ M) sample in PBS buffer (10 mM, pH 7.4). Following this, the mixtures were vortexed for approximately 30 s and incubated at 37 °C for 1 day without shaking. A number of fibrils remaining intact was assayed using ThT fluorescence and CD measurements as described below. For the copper-mediated A β 42 aggregation inhibition experiment, A β 42 (10 μ M) in HEPES (20 μ M, pH= 6.6, 150 μ M NaCl), peptides (GHK, LPFFD, SrVSrFSr or **P6**, 20 μ M) were added independently and vortexed for approximately 30 s followed by incubation at 37 °C for 24 h without shaking. Then the samples were analysed by ThT assay.

3.22.5 Fluorescence spectroscopy. Fluorescence spectral measurements were carried out using Cary eclipse fluorescence spectrophotometer (Agilent technologies). ThT was added at the end of the experiment, and its fluorescence was recorded with excitation and emission wavelengths set at 450 and 483 nm, respectively. ThT concentration of 5-10 μ M was used for amyloid inhibition assay based on the A β 42 fibrillar concentration.

3.22.6 Circular dichroism. The circular dichroic (CD) spectra were recorded using a Jasco J-815 spectrometer under a nitrogen atmosphere. All peptides were dissolved in PBS buffer (10 mM, pH 7.4) and a 10 mm path length was used for the measurements. Four to five scans were acquired from 200 to 300 nm.

3.22.7 Dot blot analysis. PVDF membranes (Sigma Aldrich) were activated by incubating them in methanol solution for 5 min followed by washing with 10 mM PBS buffer (3X). Samples were spotted on the membranes (in triplicate), and non-specific sites were blocked

by soaking in 5% BSA in PBS buffer and skim milk (0.5-1 hour, RT). Then membranes were incubated with either primary antibody A11 (1:3000) for oligomer or Anti-beta-amyloid 1-42 antibody (Merck millipore) for A β 42 fibrillar aggregates at 4 °C for overnight and then washed with PBS buffer (3 x 5 min). These membranes were further incubated with the anti-mouse secondary antibody (1:10000) conjugated with horseradish peroxidase (HRP) for 30 min at RT. These membranes were washed with PBS buffer (3 x 5 min), incubated with enhanced chemiluminescence (ECL) reagent for 1 min and recorded the chemiluminescence in SYNGENE G-box. The signals from the unknown samples were compared to that of standard and concentration was estimated.⁶⁶

3.22.8 Liposome leakage assay. The liposomes were prepared using DPPC and cholesterol in a 70:30 molar ratio. All the lipids were dissolved (2 mM stock) in chloroform, and the solvent was evaporated to make lipid films under a nitrogen atmosphere. Then the sample was dried overnight in a desiccator to remove solvent traces completely. The lipid film was rehydrated with 500 μ L of carboxyfluorescein solution (100 μ M) in 10 mM PBS buffer and vigorously vortexed for 30 min to emulsify the lipid mixtures. Then the sample was dipped into the liquid nitrogen for instant cooling, and after 5 min, the frozen solution was dipped into a water bath at 60 °C for thawing. The process was repeated five times, and the excess dye was removed by ultracentrifugation. The pellet was rehydrated in PBS buffer and extruded through a 0.45 μ m polycarbonate membrane to obtain the dye-loaded liposomes (range 2 to 0.5 μ m). To a solution of the A β 42 peptide (monomer) and liposomes (10 μ L from 2 mM stock) in PBS buffer (10 mM, pH = 7.4), the peptide (GHK or LPFFD or SrVSrFSr or **P6**) was added in an independent set of experiments. Then the samples were incubated at 37 °C for 24 h. Emission was monitored at 516 nm (λ_{ex} = 485 nm) for every 4 h, which corresponded to the dye release from the liposomes.⁸⁵

3.22.9 Ascorbate assay. To a solution of Cu^{2+} , 3-CCA and the peptide (GHK, or LPFFD or SrVSrFSr or **P6**), in PBS buffer (10 mM, pH = 7.4), high concentrations of the reducing agent ascorbate (150 μM) was added and incubated at 37 °C. To detect the hydroxyl radicals generated, a non-fluorescent dye coumarin-3-carboxylic acid (3-CCA) was used, where $\text{OH}\cdot$ reacted with 3-CCA to form a fluorescent 7-OH-CCA ($\lambda_{\text{ex}}= 395 \text{ nm}$ and $\lambda_{\text{em}}= 452 \text{ nm}$).⁷⁷ The fluorescence intensity at 452 nm was measured with time using the microplate reader of Cary eclipse fluorescence spectrophotometer (Agilent technologies).

3.22.10 Hydrogen peroxide assay. High concentration of the reducing agent ascorbate (150 μM) was added to a solution of $\text{A}\beta_{42}$, Cu^{2+} and peptide (GHK or LPFFD or SrVSrFSr or **P6**) in PBS (10 mM, pH = 7.4), and the sample was incubated at 37 °C. To detect the H_2O_2 generated by the $\text{A}\beta_{42}\text{-Cu}^{2+}$ complex, the samples were incubated with horseradish peroxidase (HRP) and Amplex Red. HRP, in the presence of H_2O_2 , cleaves the Amplex Red to yield the fluorescent resorufin molecule ($\lambda_{\text{ex}}= 571 \text{ nm}$ and $\lambda_{\text{em}}= 585 \text{ nm}$).⁷⁸ The fluorescence intensity at 585 nm was measured using microplate reader of Cary Eclipse fluorescence spectrophotometer (Agilent Technologies).

3.22.11 pDNA analysis by agarose gel electrophoresis. The DNA damage was assessed by agarose gel electrophoresis. pDNA (pBR322) was incubated with either the copper ascorbate system (ascorbate assay) or $\text{A}\beta\text{-Cu}^{2+}$ ascorbate system (hydrogen peroxide assay) in PBS buffer (10 mM, pH = 7.4) with each peptide (GHK, LPFFD, SrVSrFSr and **P6**) for 10 min and 30 min, respectively. Then the samples were loaded on 1 % agarose gel and electrophoresed for 25 min at 190 V at room temperature. Further, the gel was stained with Ethidium Bromide and visualized in UV light (Biorad chemitouch).

3.22.12 Serum stability assay. Human blood serum (HBS) was used to determine serum stability of the inhibitors. The HBS was centrifuged to remove the lipid component, and the supernatant was incubated at 37 °C. 50 Mm of each inhibitor (**P1**, **P2**, **P3**, **P4** and **P5**) was

incubated in HBS, and then 40 μ L triplicate aliquots were removed at 0, 1, 3, 6, 10, 16, and 24 h. Each serum sample was quenched with 40 μ L of 6 M urea and incubated at 4 °C for 10 min. Then, each serum sample was quenched with 40 μ L of trichloroacetic acid (20%) and incubated for another 10 min at 4 °C to precipitate the serum proteins. The samples were centrifuged for 10 min, and 200 μ L of the supernatant was analyzed on RP-HPLC using a linear gradient of solvent B (0.3 mL/min flow rate). The control samples containing equivalent amounts of inhibitors in PBS buffer were subjected to the same treatment procedure. The percentage recovery of inhibitors was detected by integration at 254 nm.⁸¹

3.22.13 Cell viability assay. To assess the effects of **P6** in the absence and presence of $A\beta_{42}\text{-Cu}^{2+}$ on PC12 cells, MTT (3-(4,5-Dimethylthiazol-2-yl)-2,5-Diphenyltetrazolium Bromide) assay was performed. PC12 cells were seeded in a 96-well plate at a density of 12,000 cells/well in RPMI (Roswell Park Memorial Institute) medium (Gibco, Invitrogen) with foetal bovine serum (FBS, 10%), horse serum (HS, 5%) and pen-strep (1 %) at 37 °C in an atmosphere of 5 % CO_2 . Then the media in the plates was replaced with low serum media (RPMI, 2% serum) and exposed for 24 h to freshly prepared $A\beta_{42}\text{-Cu}^{2+}$ (10 μ M) in the presence of each peptide (GHK, LPFFD, SrVSRFSr and **P6**) independently with ascorbate (100 μ M). Then 10 μ L of MTT (5 mg/mL solution in PBS) was added to each well and incubated for 3 h. Subsequently, the media was discarded and 100 μ L of 1:1 (DMSO: methanol) solution was added; the reduced MTT was measured by recording absorption at 570 nm (significance was determined by one way ANOVA from GraphPad prism).²⁶ To assess the cell permeability of **P6**, **FITC-P6** (20 μ M) was incubated with PC12 cells (2% FBS in RPMI) for 2 h, then the cells are washed with RPMI media for three times and visualized under fluorescence microscope (Dmi8, Leica). The **FITC-P6** was found to be cell-permeable and localizes in the cytoplasm.

3.22.14 Measuring intracellular ROS levels. To assess the effects of **P6** on ROS generated

by A β 42-Cu²⁺ in PC12 cells through DCFDA assay, PC12 cells were seeded in a 96-well plate at a density of 12,000 cells/well in RPMI medium (Gibco, Invitrogen) with foetal bovine serum (FBS; 10%), horse serum (HS; 5%) and pen-strep (1 %; Genetix) at 37 °C in an atmosphere of 5 % CO₂. After the cells were grown for 18 h, the media was changed to RPMI, followed by an incubation of 6 h. Then the cells were washed with PBS and incubated with 2,7-dichlorodihydrofluorescein diacetate (DCFDA; Invitrogen) dissolved in RPMI media for 30 min. The cells were washed and incubated with A β peptide (10 μ M), Cu²⁺ (10 μ M) and ascorbate (300 μ M) at 37 °C as control; the control was independently incubated with 50 μ M of each peptide (GHK, LPFFD, SrVSrFSr and **P6**) for 40 min at 37 °C. The cells were washed with PBS, and the fluorescence intensity was measured with excitation and emission wavelengths at 495 nm and 529 nm, respectively (significance was determined by one way ANOVA from GraphPad prism).⁸³

3.23 Reference

1. Selkoe, D. J., Folding proteins in fatal ways. *Nature* **2003**, *426*, 900-904.
2. Rajasekhar, K.; Chakrabarti, M.; Govindaraju, T., Function and toxicity of amyloid beta and recent therapeutic interventions targeting amyloid beta in Alzheimer's disease. *Chem. Commun.* **2015**, *51*, 13434-13450..
3. Savelieff, M. G.; Lee, S.; Liu, Y.; Lim, M. H., Untangling amyloid β , Tau, and metals in Alzheimer's disease. *ACS Chem. Biol.* **2013**, *8*, 856-865.
4. DeToma, A. S.; Salamekh, S.; Ramamoorthy, A.; Lim, M. H., Misfolded proteins in Alzheimer's disease and type II diabetes. *Chem Soc Rev.* **2012**, *41*, 608-621.
5. Rauk, A., The chemistry of Alzheimer's disease. *Chem. Soc. Rev.* **2009**, *38*, 2698-2715.
6. Nie, Q.; Du, X.-g.; Geng, M.-y., Small molecule inhibitors of amyloid β peptide aggregation as a potential therapeutic strategy for Alzheimer's disease. *Acta Pharmacol. Sin* **2011**, *32*, 545-551.
7. Takahashi, T.; Mihara, H., Peptide and Protein Mimetics Inhibiting Amyloid β -Peptide aggregation. *Acc. Chem. Res.* **2008**, *41*, 1309-1318.
8. Serpell, L. C., Alzheimer's amyloid fibrils: Structure and assembly. *Biochim. Biophys. Acta.* **2000**, *1502*, 16-30.

9. Hochdörffer, K.; März-Berberich, J.; Nagel-Steger, L.; Epple, M.; Meyer-Zaika, W.; Horn, A. H. C.; Sticht, H.; Sinha, S.; Bitan, G.; Schrader, T., Rational Design of β -Sheet ligands against A β 42-induced toxicity. *J. Am. Chem. Soc.* **2011**, *133*, 4348-4358.
10. Ghanta, J.; Shen, C.-L.; Kiessling, L. L.; Murphy, R. M., A Strategy for designing inhibitors of β -amyloid toxicity. *J. Biol. Chem.* **1996**, *271*, 29525-29528.
11. Etienne, M. A.; Aucoin, J. P.; Fu, Y.; McCarley, R. L.; Hammer, R. P., Stoichiometric inhibition of amyloid β -Protein Aggregation with Peptides Containing Alternating α,α -disubstituted amino acids. *J. Am. Chem. Soc.* **2006**, *128*, 3522-3523.
12. Hong, H.-S.; Rana, S.; Barrigan, L.; Shi, A.; Zhang, Y.; Zhou, F.; Jin, L.-W.; Hua, D. H., Inhibition of Alzheimer's amyloid toxicity with a tricyclic pyrone molecule in vitro and in vivo. *J. Neurochem.* **2009**, *108*, 1097-1108.
13. Hung, S.-Y.; Huang, W.-P.; Liou, H.-C.; Fu, W.-M., Autophagy protects neuron from A β -induced cytotoxicity. *Autophagy* **2009**, *5*, 502-510.
14. Overbye, A.; Brinchmann, M. F.; Seglen, P. O., Proteomic analysis of membrane-associated proteins from rat liver autophagosomes. *Autophagy* **2007**, *3*, 300-322.
15. Halai, R.; Callaghan, B.; Daly, N. L.; Clark, R. J.; Adams, D. J.; Craik, D. J., Effects of cyclization on stability, structure, and activity of α -conotoxin RgIA at the $\alpha 9\alpha 10$ nicotinic acetylcholine receptor and GABAB receptor. *J. Med. Chem.* **2011**, *54*, 6984-6992.
16. Lovelace, E. S.; Armishaw, C. J.; Colgrave, M. L.; Wahlstrom, M. E.; Alewood, P. F.; Daly, N. L.; Craik, D. J., Cyclic MrIA: A stable and potent cyclic conotoxin with a novel topological fold that targets the norepinephrine transporter. *J. Med. Chem.* **2006**, *49*, 6561-6568.
17. Mumberg, D.; Müller, R.; Funk, M., Yeast vectors for the controlled expression of heterologous proteins in different genetic backgrounds. *Gene* **1995**, *156*, 119-122.
18. White, C. J.; Yudin, A. K., Contemporary strategies for peptide macrocyclization. *Nat. Chem.* **2011**, *3*, 509-524.
19. Fowler, S. A.; Stacy, D. M.; Blackwell, H. E., Design and synthesis of macrocyclic peptomers as mimics of a quorum sensing signal from staphylococcus aureus. *Org. Lett.* **2008**, *10*, 2329-2332.
20. Thakkar, A.; Trinh, T. B.; Pei, D., Global Analysis of peptide cyclization efficiency. *ACS Comb. Sci.* **2013**, *15*, 120-129.
21. Wu, Y.-D.; Gellman, S., Peptidomimetics. *Acc. Chem. Res.* **2008**, *41*, 1231-1232.
22. Fowler, S. A.; Blackwell, H. E., Structure-function relationships in peptoids: Recent advances toward deciphering the structural requirements for biological function. *Org. Biomol. Chem.* **2009**, *7*, 1508-1524.
23. Tan, N. C.; Yu, P.; Kwon, Y.-U.; Kodadek, T., High-throughput evaluation of relative cell permeability between peptoids and peptides. *Bioorg. Med. Chem.* **2008**, *16*, 5853-5861.

24. Nnanabu, E.; Burgess, K., Cyclic semipeptoids: Peptoid–organic hybrid macrocycles. *Org. Lett.* **2006**, *8*, 1259-1262.
25. Ovadia, O.; Linde, Y.; Haskell-Luevano, C.; Dirain, M. L.; Sheynis, T.; Jelinek, R.; Gilon, C.; Hoffman, A., The effect of backbone cyclization on PK/PD properties of bioactive peptide-peptoid hybrids: The melanocortin agonist paradigm. *Bio. Med. Chem.* **2010**, *18*, 580-589.
26. Shin, S. B. Y.; Yoo, B.; Todaro, L. J.; Kirshenbaum, K., Cyclic peptoids. *J. Am. Chem. Soc.* **2007**, *129*, 3218-3225.
27. Roy, O.; Faure, S.; Thery, V.; Didierjean, C.; Taillefumier, C., Cyclic β -peptoids. *Org. Lett.* **2008**, *10*, 921-924.
28. Chongsiriwatana, N. P.; Wetzler, M.; Barron, A. E., Functional synergy between antimicrobial peptoids and peptides against gram-negative bacteria. *Antimicrob Agents Chemother.* **2011**, *55*, 5399-5402.
29. Murphy, J. E.; Uno, T.; Hamer, J. D.; Cohen, F. E.; Dwarki, V.; Zuckermann, R. N., A combinatorial approach to the discovery of efficient cationic peptoid reagents for gene delivery. *Proc. Natl. Acad. Sci.* **1998**, *95*, 1517-1522.
30. Zhang, L.; Yu, J.; Pan, H.; Hu, P.; Hao, Y.; Cai, W.; Zhu, H.; Yu, A. D.; Xie, X.; Ma, D.; Yuan, J., Small molecule regulators of autophagy identified by an image-based high-throughput screen. *Proc. Natl. Acad. Sci.* **2007**, *104*, 19023-19028.
31. Fleming, A.; Noda, T.; Yoshimori, T.; Rubinsztein, D. C., Chemical modulators of autophagy as biological probes and potential therapeutics. *Nat. Chem. Biol.* **2011**, *7*, 9-17.
32. Egholm, M.; Nielsen, P. E.; Buchardt, O.; Berg, R. H., Recognition of guanine and adenine in DNA by cytosine and thymine containing peptide nucleic acids (PNA). *J. Am. Chem. Soc.* **1992**, *114*, 9677-9678.
33. Kaur, N.; Zhou, B.; Breitbeil, F.; Hardy, K.; Kraft, K. S.; Trantcheva, I.; Phanstiel Iv, O., A Delineation of diketopiperazine self-assembly processes: Understanding the molecular events involved in N^c-(Fumaroyl)diketopiperazine of l-Lys (FDKP) interactions. *Mol. Pharmaceutics* **2008**, *5*, 294-315.
34. Cordier, F.; Grzesiek, S., Temperature-dependence of protein hydrogen bond properties as studied by high-resolution NMR. Edited by P. E. Wright. *J. Mol. Biol.* **2002**, *317*, 739-752.
35. White, T. R.; Renzelman, C. M.; Rand, A. C.; Rezai, T.; McEwen, C. M.; Gelev, V. M.; Turner, R. A.; Lington, R. G.; Leung, S. S. F.; Kalgutkar, A. S.; Bauman, J. N.; Zhang, Y.; Liras, S.; Price, D. A.; Mathiowetz, A. M.; Jacobson, M. P.; Lokey, R. S., On-resin N-methylation of cyclic peptides for discovery of orally bioavailable scaffolds. *Nat. Chem. Biol.* **2011**, *7*, 810-817.
36. Cierpicki, T.; Otlewski, J., Amide proton temperature coefficients as hydrogen bond indicators in proteins. *J. Biomol NMR* **2001**, *21*, 249-261.

37. Maulucci, N.; Izzo, I.; Bifulco, G.; Aliberti, A.; De Cola, C.; Comegna, D.; Gaeta, C.; Napolitano, A.; Pizza, C.; Tedesco, C.; Flot, D.; De Riccardis, F., Synthesis, structures, and properties of nine-, twelve-, and eighteen-membered N-benzyloxyethyl cyclic α -peptoids. *Chem. Commun.* **2008**, 3927-3929.
38. De Santis, E.; Hjelmgaard, T.; Faure, S.; Roy, O.; Didierjean, C.; Alexander, B. D.; Siligardi, G.; Hussain, R.; Jávorfí, T.; Edwards, A. A.; Taillefumier, C., Cyclic α,β -peptoid octamers with differing side chain patterns: synthesis and conformational investigation. *Amino Acids* **2011**, *41*, 663-672.
39. Kwon, Y.-U.; Kodadek, T., Quantitative evaluation of the relative cell permeability of peptoids and peptides. *J. Am. Chem. Soc.* **2007**, *129*, 1508-1509.
40. Roychaudhuri, R.; Yang, M.; Hoshi, M. M.; Teplow, D. B., Amyloid β - protein assembly and Alzheimer disease. *J. Biol. Chem.* **2009**, *284*, 4749-4753.
41. Teplow, D. B., On the subject of rigor in the study of amyloid β - protein assembly. *Alzheimers Res Ther.* **2013**, *5*, 39-39.
42. Colletier, J.-P.; Laganowsky, A.; Landau, M.; Zhao, M.; Soriaga, A. B.; Goldschmidt, L.; Flot, D.; Cascio, D.; Sawaya, M. R.; Eisenberg, D., Molecular basis for amyloid- β polymorphism. *Proc. Natl. Acad. Sci. U S A* **2011**, *108*, 16938-16943.
43. Aguzzi, A.; O'Connor, T., Protein aggregation diseases: Pathogenicity and therapeutic perspectives. *Nat. Rev. Drug Discov.* **2010**, *9*, 237-248.
44. Ciechanover, A.; Kwon, Y. T., Degradation of misfolded proteins in neurodegenerative diseases: therapeutic targets and strategies. *Exp. Mol. Med.* **2015**, *47*, e147.
45. Hayden, E. Y.; Teplow, D. B., Amyloid β -protein oligomers and Alzheimer's disease. *Alzheimers Res Ther.* **2013**, *5*, 60.
46. Sakono, M.; Zako, T., Amyloid oligomers: Formation and toxicity of A β oligomers. *FEBS Journal* **2010**, *277*, 1348-1358.
47. Prince, M.; Bryce, R.; Albanese, E.; Wimo, A.; Ribeiro, W.; Ferri, C. P., The global prevalence of dementia: A systematic review and metaanalysis. *Alzheimer's & Dementia* **2013**, *9*, 63-75.
48. Bush, A. I., The metallobiology of Alzheimer's disease. *Trends Neurosci.* **2003**, *26*, 207-214.
49. Zhao, Y.; Zhao, B., Oxidative stress and the pathogenesis of Alzheimer's disease. *Oxid. Med. Cell Longev.* **2013**, *2013*, 10.
50. Cassagnes, L.-E.; Herve, V.; Nepveu, F.; Hureau, C.; Faller, P.; Collin, F., The catalytically active copper-amyloid-beta state: Coordination site responsible for reactive oxygen species production. *Angew. Chem. Int. Ed.* **2013**, *52*, 11110-11113.

51. Reybier, K.; Ayala, S.; Alies, B.; Rodrigues, J. V.; Bustos Rodriguez, S.; La Penna, G.; Collin, F.; Gomes, C. M.; Hureau, C.; Faller, P., Free superoxide is an intermediate in the production of H₂O₂ by copper(I)-A β peptide and O₂. *Angew. Chem. Int. Ed.* **2016**, *55*, 1085-1089.
52. Muthuraj, B.; Layek, S.; Balaji, S. N.; Trivedi, V.; Iyer, P. K., Multiple Function Fluorescein Probe Performs Metal Chelation, Disaggregation, and Modulation of Aggregated A β and A β -Cu Complex. *ACS Chem. Neurosci.* **2015**, *6*, 1880-1891.
53. Wu, W.-h.; Lei, P.; Liu, Q.; Hu, J.; Gunn, A. P.; Chen, M.-s.; Rui, Y.-f.; Su, X.-y.; Xie, Z.-p.; Zhao, Y.-F.; Bush, A. I.; Li, Y.-m., Sequestration of copper from β -amyloid promotes selective lysis by cyclen-hybrid cleavage agents. *J. Biol. Chem.* **2008**, *283*, 31657-31664.
54. Jensen, M.; Canning, A.; Chiha, S.; Bouquerel, P.; Pedersen, J. T.; Ostergaard, J.; Cuvillier, O.; Sasaki, I.; Hureau, C.; Faller, P., inhibition of cu-amyloid- β by using bifunctional peptides with β -sheet breaker and chelator moieties. *Chem. Eur. J.* **2012**, *18*, 4836-4839.
55. Marquez, M.; Blancas-Mejia, L. M.; Campos, A.; Rojas, L.; Castaneda-Hernandez, G.; Quintanar, L., A bifunctional non-natural tetrapeptide modulates amyloid-beta peptide aggregation in the presence of Cu(II). *Metallomics* **2014**, *6*, 2189-2192.
56. Zhang, Q.; Hu, X.; Wang, W.; Yuan, Z., Study of a Bifunctional A β aggregation inhibitor with the abilities of anti-amyloid- β and copper chelation. *Biomacromolecules* **2016**, *17*, 661-668.
57. Yu, F.; Cangelosi, V. M.; Zastrow, M. L.; Tegoni, M.; Plegaria, J. S.; Tebo, A. G.; Mocny, C. S.; Ruckthong, L.; Qayyum, H.; Pecoraro, V. L., Protein design: Toward functional metalloenzymes. *Chem. Rev.* **2014**, *114*, 3495-3578.
58. Arredondo, M.; Nunez, M. T., Iron and copper metabolism. *Mol. Aspects Med.* **2005**, *26*, 313-327.
59. Saha, A.; Mohapatra, S.; Kurkute, P.; Jana, B.; Mondal, P.; Bhunia, D.; Ghosh, S.; Ghosh, S., Interaction of A β peptide with tubulin causes an inhibition of tubulin polymerization and the apoptotic death of cancer cells. *Chem. Commun* **2015**, *51*, 2249-2252.
60. Wang, C.; Yang, A.; Li, X.; Li, D.; Zhang, M.; Du, H.; Li, C.; Guo, Y.; Mao, X.; Dong, M.; Besenbacher, F.; Yang, Y.; Wang, C., Observation of molecular inhibition and binding structures of amyloid peptides. *Nanoscale* **2012**, *4*, 1895-1909.
61. Trapaidze, A.; Hureau, C.; Bal, W.; Winterhalter, M.; Faller, P., Thermodynamic study of Cu²⁺ binding to the DAHK and GHK peptides by isothermal titration calorimetry (ITC) with the weaker competitor glycine. *Biol. Inorg. Chem.* **2012**, *17*, 37-47.
62. Hatcher, L. Q.; Hong, L.; Bush, W. D.; Carducci, T.; Simon, J. D., Quantification of the binding constant of copper(II) to the amyloid-beta peptide. *J. Phys. Chem. B* **2008**, *112*, 8160-8164.
63. Lau, S. J.; Sarkar, B., The interaction of copper(II) and glycyl-l-histidyl-l-lysine, a growth-modulating tripeptide from plasma. *Biochem. J.* **1981**, *199*, 649-656.

64. Funke, S. A.; Willbold, D., Peptides for therapy and diagnosis of Alzheimer's disease. *Curr. Pharm. Des.* **2012**, *18*, 755-767.
65. Soto, C.; Sigurdsson, E. M.; Morelli, L.; Asok Kumar, R.; Castano, E. M.; Frangione, B., β -sheet breaker peptides inhibit fibrillogenesis in a rat brain model of amyloidosis: Implications for Alzheimer's therapy. *Nat. Med.* **1998**, *4*, 822-826.
66. Turner, J. P.; Lutz-Rechtin, T.; Moore, K. A.; Rogers, L.; Bhave, O.; Moss, M. A.; Servoss, S. L., Rationally designed peptoids modulate aggregation of amyloid-beta 40. *ACS Chem. Neurosci.* **2014**, *5*, 552-558.
67. Luo, Y.; Vali, S.; Sun, S.; Chen, X.; Liang, X.; Drozhzhina, T.; Popugaeva, E.; Bezprozvanny, I., A β 42-binding peptoids as amyloid aggregation inhibitors and detection ligands. *ACS Chem. Neurosci.* **2013**, *4*, 952-962.
68. Rajasekhar, K.; Suresh, S. N.; Manjithaya, R.; Govindaraju, T., Rationally designed peptidomimetic modulators of a β toxicity in Alzheimer's disease. *Sci. Rep.* **2015**, *5*.
69. Mayes, J.; Tinker-Mill, C.; Kolosov, O.; Zhang, H.; Tabner, B. J.; Allsop, D., β -amyloid fibrils in Alzheimer disease are not inert when bound to copper ions but can degrade hydrogen peroxide and generate reactive oxygen species. *J. Biol. Chem.* **2014**, *289*, 12052-12062.
70. Marshall, K. E.; Marchante, R.; Xue, W.-F.; Serpell, L. C., The relationship between amyloid structure and cytotoxicity. *Prion* **2014**, *8*, 192-196.
71. Wu, J. W.; Breydo, L.; Isas, J. M.; Lee, J.; Kuznetsov, Y. G.; Langen, R.; Glabe, C., Fibrillar oligomers nucleate the oligomerization of monomeric amyloid β but do not seed fibril formation. *J. Biol. Chem.* **2010**, *285*, 6071-6079.
72. Kotler, S. A.; Walsh, P.; Brender, J. R.; Ramamoorthy, A., Differences between amyloid- β aggregation in solution and on the membrane: Insights towards elucidation of the mechanistic details of Alzheimer's disease. *Chem. Soc. Rev.* **2014**, *43*, 6692-6700.
73. Ambroggio, E. E.; Kim, D. H.; Separovic, F.; Barrow, C. J.; Barnham, K. J.; Bagatolli, L. A.; Fidelio, G. D., Surface Behavior and lipid interaction of alzheimer β -amyloid peptide A β 42: A membrane-disrupting peptide. *Biophysical Journal* **2005**, *88*, 2706-2713.
74. Saha, A.; Mondal, G.; Biswas, A.; Chakraborty, I.; Jana, B.; Ghosh, S., In vitro reconstitution of a cell-like environment using liposomes for amyloid beta peptide aggregation and its propagation. *Chem. Commun* **2013**, *49*, 6119-6121.
75. Gamez, P.; Caballero, A. B., Copper in Alzheimer's disease: Implications in amyloid aggregation and neurotoxicity. *AIP Adv.* **2015**, *5*, 092503.
76. Jiang, D.; Zhang, L.; Grant, G. P. G.; Dudzik, C. G.; Chen, S.; Patel, S.; Hao, Y.; Millhauser, G. L.; Zhou, F., The elevated copper binding strength of amyloid- β aggregates allows the sequestration of copper from albumin: A pathway to accumulation of copper in senile plaques. *Biochemistry* **2013**, *52*, 547-556.
-

77. Guilloreau, L.; Combalbert, S.; Sournia-Saquet, A.; Mazarguil, H.; Faller, P., Redox chemistry of copper–amyloid- β : The generation of hydroxyl radical in the presence of ascorbate is linked to redox-potentials and aggregation state. *ChemBioChem* **2007**, *8*, 1317-1325.
78. Dickens, M. G.; Franz, K. J., A prochelator activated by hydrogen peroxide prevents metal-induced amyloid β aggregation. *ChemBioChem* **2010**, *11*, 59-62.
79. De Bont, R.; van Larebeke, N., Endogenous DNA damage in humans: A review of quantitative data. *Mutagenesis* **2004**, *19*, 169-185.
80. Lopez-Gomollon, S.; Sevilla, E.; Bes, M. T.; Peleato, M. L.; Fillat, M. F., New insights into the role of Fur proteins: FurB (All2473) from *Anabaena* protects DNA and increases cell survival under oxidative stress. *Biochemical Journal* **2009**, *418*, 201-207.
81. Fosgerau, K.; Hoffmann, T., Peptide therapeutics: current status and future directions. *Drug Discovery Today* **2015**, *20*, 122-128.
82. Yu, R.; Seymour, V. A. L.; Berecki, G. z.; Jia, X.; Akcan, M.; Adams, D. J.; Kaas, Q.; Craik, D. J., Less is More: Design of a highly stable disulfide-deleted mutant of analgesic cyclic α -conotoxin Vc1.1. *Sci. Rep.* **2015**, *5*, 13264.
83. Huang, S.-H.; Ke, S.-C.; Lin, T.-H.; Huang, H.-B.; Chen, Y.-C., Effect of C-terminal residues of A β on copper binding affinity, structural conversion and aggregation. *PLoS ONE* **2014**, *9*, e90385.
84. Ryan, D. A.; Narrow, W. C.; Federoff, H. J.; Bowers, W. J., An improved method for generating consistent soluble amyloid-beta oligomer preparations for in vitro neurotoxicity studies. *J. Neurosci. Methods* **2010**, *190*, 171-179.
85. Paul, A.; Nadimpally, K. C.; Mondal, T.; Thalluri, K.; Mandal, B., Inhibition of Alzheimer's amyloid- β peptide aggregation and its disruption by a conformationally restricted α/β hybrid peptide. *Chem. Commun.* **2015**, *51*, 2245-2248.

Chapter 4

Small molecule based amyloid modulators

Chapter 4A

Clioquinol synthetic derivatization to obtain nontoxic and multifunctional modulators for A β toxicity in Alzheimer's disease

A β peptides, in particular highly toxic A β 42 undergo misfolding, and β -sheet and hydrophobic interaction driven aggregation to form polymorphic oligomers, protofibrils and fully grown fibrils.^{1,2} The prominent role played by A β aggregates in AD, make them the prime target to develop therapeutics.³⁻⁵ Metal dyshomeostasis is another critical consequence observed in AD pathology. The coexistence of metal ions such as Cu²⁺, Zn²⁺ and Fe²⁺ with amyloid plaques infers strong interaction of metal ions with A β peptide. Moreover, A β peptide bound redox metals (Cu and Fe) undergo redox cycling to generate reactive oxygen species (ROS), and the resultant oxidative stress cause neuronal death.⁶ Therefore, modulating the metal-dependent and independent A β aggregation, and alleviating ROS related oxidative stress is a promising strategy for developing therapeutic agents.⁷⁻¹³ Clioquinol (Clq) and its derivative PBT2 were the first few compounds developed in that directions, unfortunately both of them have failed at different levels of clinical trials.¹⁴ However, excellent metal chelation and aggregation modulation properties of Clq have constantly attracted the interest of the scientific community. Thus, Clq can as an ideal molecular platform to perform further synthetic modification to derive efficient and nontoxic modulators. Our design strategy was based on suitably modifying Clq molecular platform to obtain HMMs with metal chelating ability, modulating A β aggregation and ROS generation while being non-toxic to normal cells, in contrast to the parent compound (Clq) (Figure 1). Further, we introduced polyphenolic moiety in the molecular design to alleviate oxidative stress related to the accumulation of excessive intracellular and extracellular ROS. The designed Clq-based HMMs were accessed through simple and high yielding synthetic routes. We performed detailed studies of designed HMMs including thioflavin T (ThT) assay, dot blot analysis to ascertain the modulation of A β aggregation by HMMs. The metal chelation and the antioxidant nature of HMMs confirm their effectiveness to modulate the metal-A β aggregation

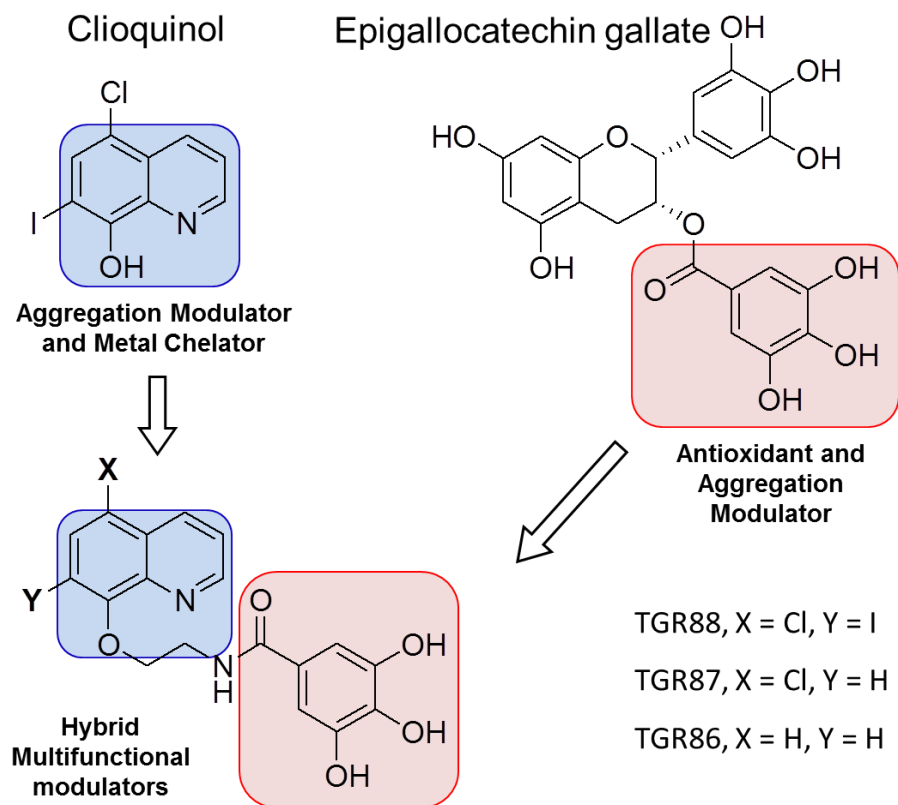
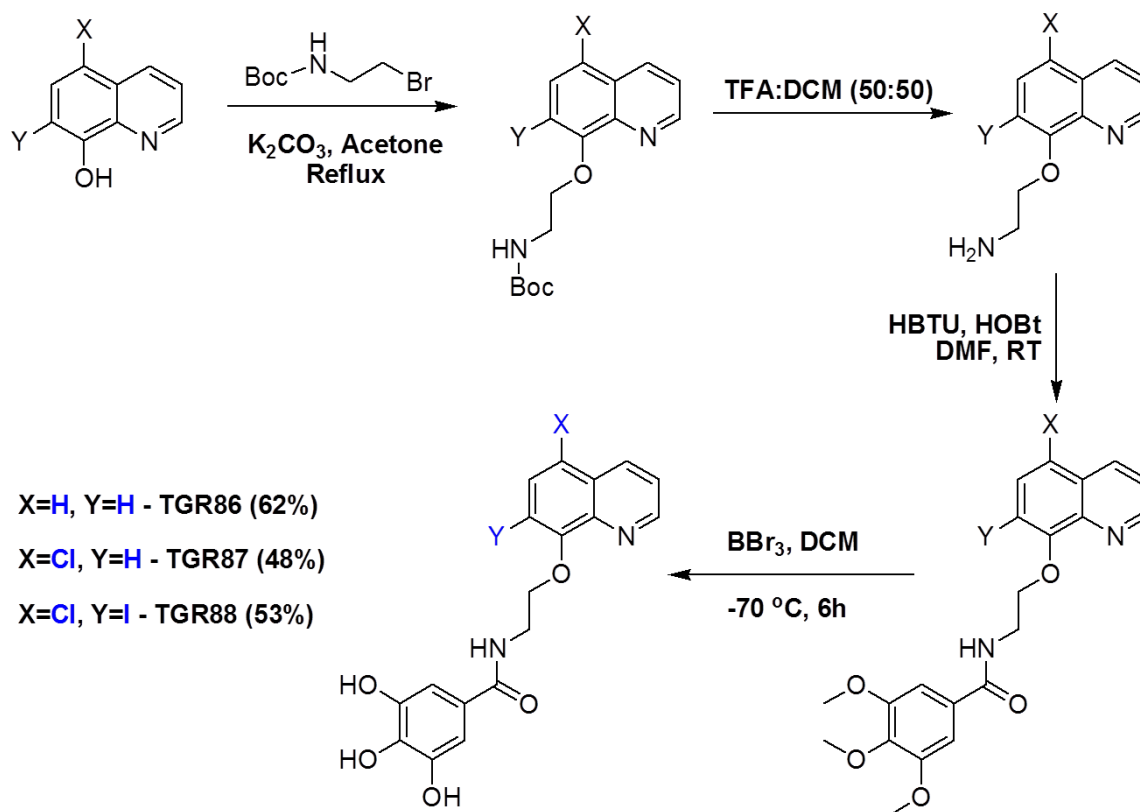


Figure 1. Design of clioquinol (Clq) and epigallocatechin gallate (EGCG) inspired hybrid multifunctional modulators (HMMs).

and ROS generation. Further, *in vitro* activity of HMMs and their ability to prevent A β mediated mitochondrial damage was assessed by cellular assays.

4.1 Design strategy

Clq is an established metal chelator and modulator of metal-induced A β aggregation.¹⁵ The high toxicity of Clq and its analogues as revealed from the clinical studies at various stages hampered their possibility of becoming potential drug candidates.¹⁴ However, Clq molecular platform provides ample opportunity to develop novel modulators of multifaceted A β toxicity, which are non-toxic to cells. The 8-hydroxyquinoline moiety of Clq plays a pivotal role in metal chelation and modulation of metal-A β aggregation. Therefore, any change in this functional moiety could lead to the loss of the metal chelating property. Moreover, 8-hydroxyquinoline has been shown



Scheme 1. Synthetic of HMMs.

to exhibit minimal cytotoxicity towards neuronal cells compared to Clq.¹⁶ This and clinical studies implied that the presence of halogen (iodo- and chloro-) substituents and related impurities (viz., di-iodo derivative) play a crucial role in the observed cytotoxicity of Clq. In this context, we sought to develop Clq-based HMMs of multifaceted A β toxicity, which are non-toxic to normal cells. The designed HMMs were to retain the core 8-hydroxyquinoline moiety with variable halogenated derivatives to understand and reduce the cellular toxicity. The 8-hydroxyquinoline moieties were synthetically conjugate with naturally occurring polyphenolic compounds, which exhibit excellent antioxidant properties (Scheme 1). For instance, epigallocatechin gallate (EGCG), a key component in green tea has been shown to prevent ROS generated by A β aggregates and partially modulate A β aggregation.¹⁷ To introduce

multifunctionality in our molecular design, we conjugated 8-hydroxyquinoline moieties with gallic acid, a key structural component of EGCG to obtain TGR86-88 as shown in Figure 1. We assumed that hybrid conjugates of 8-hydroxyquinoline or Clq derivatives with gallic acid inherit the A β aggregation modulation and metal chelation ability from Clq and antioxidant property from EGCG. These HMMs are expected to inhibit multifaceted A β toxicity induced by both metal-dependent and independent A β aggregates and related mitochondrial damage with improved cellular viability.

4.2 Inhibition of A β aggregation and Cu²⁺ induced A β aggregation

ThT binding assay was performed to evaluate the inhibition of A β 42 aggregation by the HMMs, in comparison with Clq. The A β 42 (10 μ M) was incubated alone and independently with 50 μ M of Clq, TGR86, TGR87 and TGR88 at 37 °C for 48 h in PBS (pH 7.4, 10 mM). ThT (10 μ M) was added to these incubated solutions and fluorescence was monitored at 485 nm (Figure 2a). The HMMs, TGR86, TGR87 and TGR88 exhibited >50% of A β 42 aggregation inhibition compared to control Clq which showed ~20% inhibition. Among the HMMs, TGR86 showed maximum aggregation inhibition efficiency of 90%, followed by TGR87 (79%) and TGR88 (50%). To further validate the observed aggregation inhibition data, we performed dot blot analysis of the samples used in ThT binding assay. We employed A β 42 aggregates specific antibody (OC) to determine the extent of aggregation inhibition (Figure 2b). In agreement with data from ThT binding assay, TGR86 exhibited maximum aggregation inhibition efficiency and the overall inhibition efficiency is in the order TGR86> TGR88>TGR87> Clq. Taking together data from ThT binding assay and dot blot analysis TGR86 was found to be the best A β 42 aggregation inhibitor. Subsequently, we performed a concentration-dependent A β 42 aggregation inhibition study with the lead HMM TGR86 (Figure 2a). The TGR86 exhibited concentration-

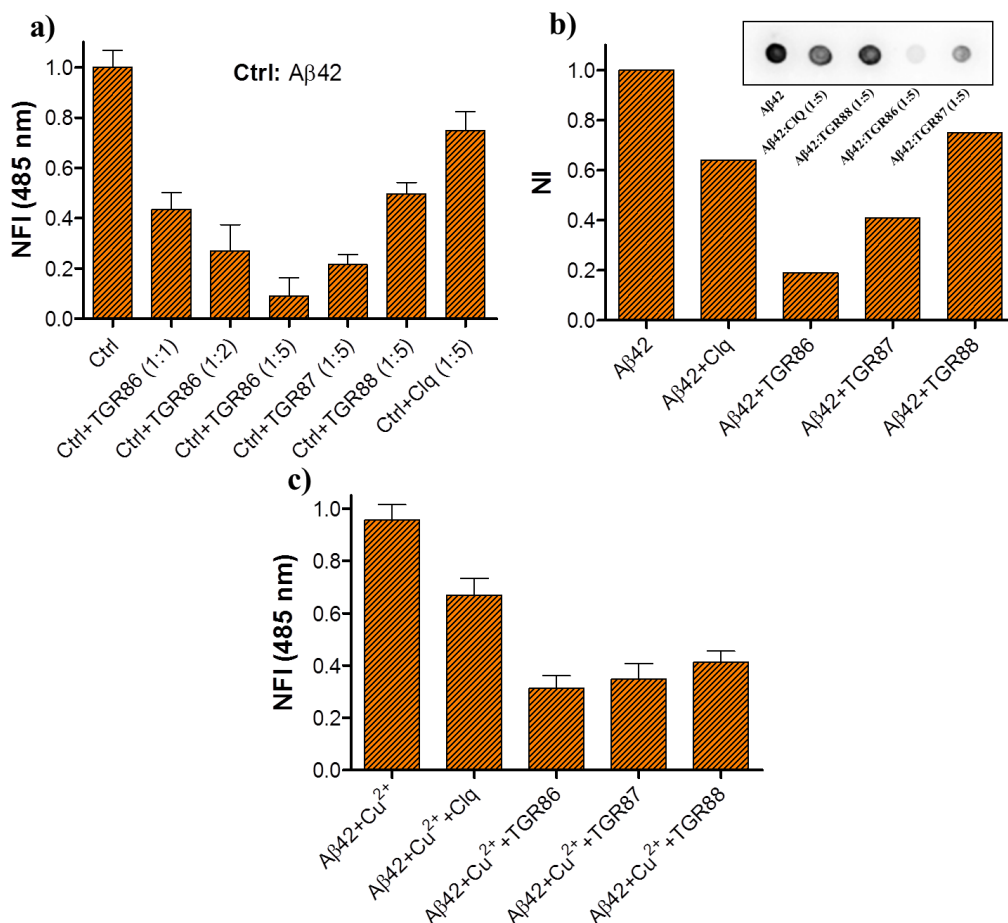


Figure 2. Inhibition of Aβ42 aggregates studied by ThT binding assay and dot blot analysis (a) Aβ42 (10 μM) was incubated alone and independently with Clq, TGR86, TGR87 and TGR88 in 1:5 stoichiometry and aggregation inhibition was quantified through normalized fluorescence intensity (NFI) of ThT at 485 nm. (b) Dot blot analysis of Aβ42 (10 μM) peptide incubated independently with 50 μM Clq, TGR86, TGR87 and TGR88. OC (1:3000) is used as primary antibody followed by secondary antibody (HRP conjugated anti-mouse antibody, 1:10000). Chemiluminescence was recorded by treating blots with ECL reagent for 2 min and the intensity is quantified. (c) Aβ42 (10 μM) and Cu²⁺ was incubated alone and independently with Clq, TGR86, TGR87 and TGR88 in 1:5 stoichiometry and their influence on metal-mediated aggregation were quantified through normalized fluorescence intensity (NFI) of ThT at 485 nm after 24 h. Each experiment was repeated minimum three times (n = 3), and error bars represent the standard deviation (SD) of the NFI.

control Clq that has no appreciable inhibition at the same concentration. However, Clq showed ~20% inhibition efficiency at higher concentrations (50 μM). Further, at 1:2 (Aβ42:TGR86) ratio TGR86 (20 μM) exhibited 55% inhibition of Aβ42 aggregation. Next, the effect of HMMs on metal-induced Aβ aggregation was studied by performing ThT binding assay. The Aβ42 (10 μM)

was incubated with Cu^{2+} (10 μM) in the presence or absence of Clq, TGR86, TGR87 and TGR88 at 37 °C for 24 h in PBS (pH 7.4, 10 mM), and then ThT was added and the fluorescence was measured at 485 nm (Figure 2c). All the HMMs (50 μM) exhibited >60% (TGR86: 70%, TGR87: 66%; TGR88: 60%) aggregation inhibition efficiency, which is 50% higher than the Clq (30% inhibition). This signifies that HMMs exhibit efficient binding to a Cu^{2+} and bring about effective reduction in the Cu^{2+} induced $\text{A}\beta$ aggregation. Thus, designed HMMs, especially TGR86 effectively modulate the metal-dependent and independent $\text{A}\beta$ aggregation effectively.

4.3 Molecular interactions of HMMs with $\text{A}\beta_{42}$ aggregates

Molecular docking studies were carried out to understand the binding site and binding parameters of HMMs on $\text{A}\beta$ aggregates. These studies revealed that Clq and HMMs predominantly bind to $^{20}\text{FAEDVGSNKG}^{29}$ ($\text{A}\beta_{20-29}$), a region involved in both turn and β -sheet structure formation. Moreover, Ser26, Asn27 and Lys28 of $\text{A}\beta_{42}$ were found to be the potential amino acids interacting with HMMs. Remarkably, TGR86 showed a high binding affinity (-7.4 kcal/mol) to $\text{A}\beta_{42}$ compared to Clq (-5.5 Kcal/Mol), and other HMMs with halogen substituents TGR87 (-6.9 Kcal/Mol) and TGR88 (-6.7 Kcal/Mol) (Figure 3). These molecular docking results are in good agreement with the experimental results obtained from ThT binding assay and dot blot analysis. Notably, it is observed that the hydroxyl groups and other oxygen atoms of the TGR86 were potentially involved in the formation of hydrogen bonding with the Ser26, Asn27 and Lys28 of $\text{A}\beta_{42}$ aggregates which resulted in enhanced binding affinity (Figure 3b). Whereas, Clq with one hydroxyl group available for hydrogen bonding interactions showed weak binding towards $\text{A}\beta_{42}$ aggregates. We also observed that binding interaction of TGR86-88 enhanced by the π -alkyl interaction with Lys28 which reflected in their relative high binding affinity towards $\text{A}\beta_{42}$ aggregates compared to Clq.¹⁸ Moreover, Lys28 is apparently involved in the salt bridge

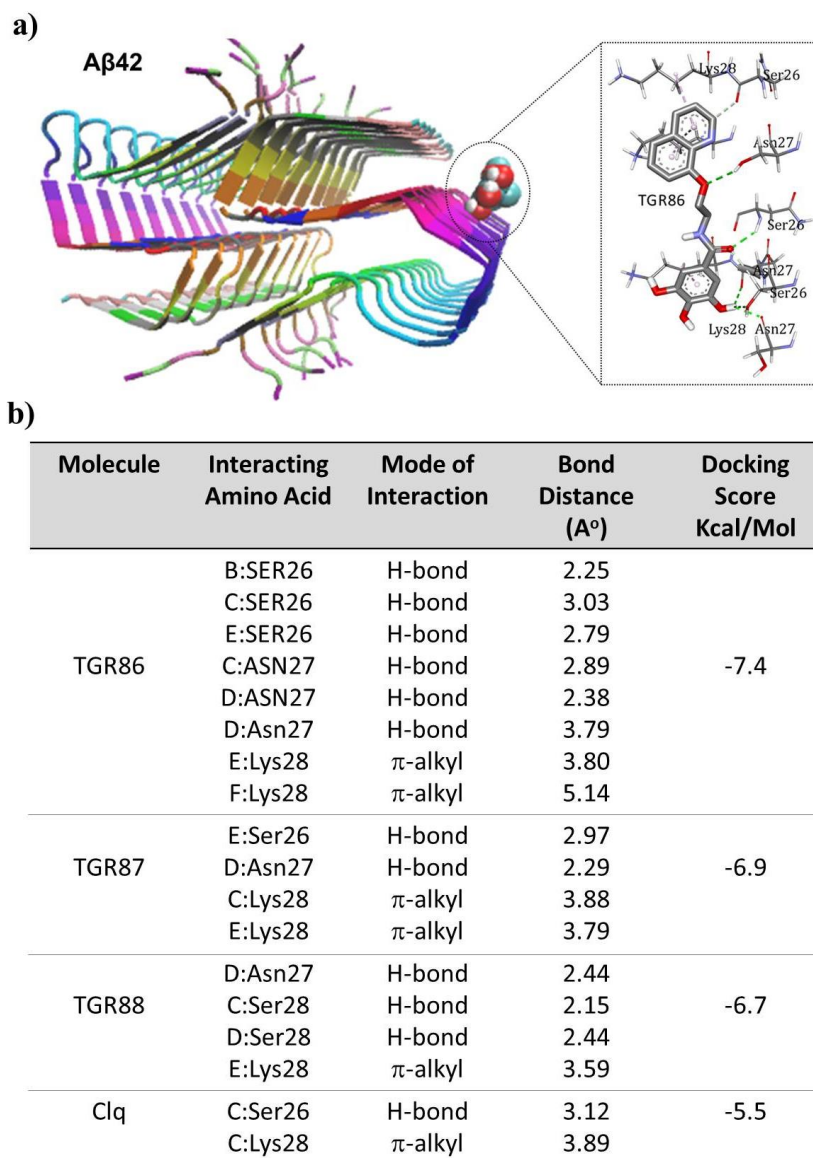


Figure 3. a) Docking mode of TGR86 with A β aggregates. TGR86 is shown in CPK model, the protein in cartoon mode and the residues in contact with TGR86 are in stick mode (PDB ID = 5KK3). b) Summary of molecular interactions between HMMs or Clq and A β 42 aggregates studied through molecular docking. TGR86 showed highest binding affinity towards A β 42 aggregates compared to Clq, TGR87 and TGR88.

formation with Asp23 and hence assist in β -sheet formation in A β aggregation.¹⁹ Therefore, we believe that disruption of this Lys28-Asp23 salt bridge by HMMs through competitive π -alkyl interaction reduces the A β aggregation.²⁰ Overall, our molecular docking studies suggest that strong hydrogen bonding and π -alkyl interaction of HMMs plays a vital role in enhancing the

binding interaction and inhibition of A β aggregation, in comparison to Clq.

4.4 Cu²⁺ chelation and antioxidant properties of HMMs

The ability of HMMs to chelate Cu²⁺ was studied by UV-vis absorption spectroscopy. In our HMMs, the O-alkylation masked the hydroxyl group of the 8-hydroxyquinoline moiety, and hence we embarked on the assessment of their metal-chelating property. All the HMMs (TGR86, TGR87 and TGR88) (20 μ M) in PBS buffer (pH 7.4, 10 mM) showed absorption maxima at 250 nm, and a shoulder peak at 313 nm (Figure 4). Clq bind Cu²⁺ in 2:1 stoichiometric ratio through hydroxyl and pyridine nitrogen to form a metal ligand complex.²¹ To assess the metal chelation and binding ratio of HMMs to Cu²⁺, we performed the concentration-dependent study by titrating Cu²⁺ (0-50 μ M) to a fixed concentration of HMMs (20 μ M) in PBS buffer (Figure 4). The shoulder absorption band of HMMs at 313 nm showed a hyperchromic shift as a function of the increase in the concentration of Cu²⁺ which confirmed metal chelation ability of TGR86-88. The observed hyperchromicity of the absorption band at 313 nm reached saturation for concentrations of Cu²⁺ > 10 μ M which infer that HMMs bind to Cu²⁺ in 2:1 stoichiometric ratio and established that our HMMs (TGR86-88) retain the metal chelating ability similar to Clq.

Redox cycle of copper in A β -Cu²⁺ complex generates ROS through Fenton-type reaction

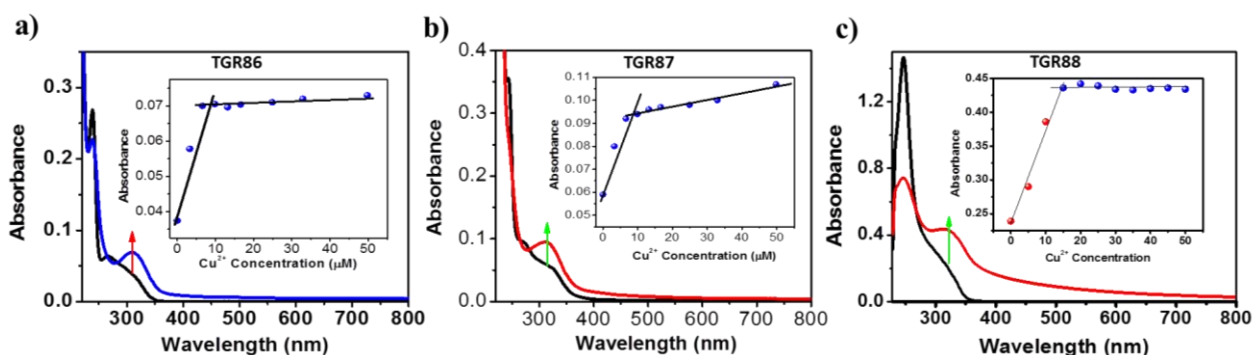


Figure 4. Determining the binding ratio of HMMs (TGR86, TGR87 and TGR88) to towards Cu²⁺. To a given concentration of HMMs (20 μ M) increasing concentration of Cu²⁺ (0-50 μ M) is added, and absorption is recorded.

which has a detrimental effect in AD pathology owing to resultant oxidative stress and oxidation of biomolecules such as DNA, protein and lipids, which cause neuronal death.²² Therefore, preventing the redox cycle (redox silencing) of Cu^{2+} bound to $\text{A}\beta$ ($\text{A}\beta\text{-Cu}^{2+}$ complex) to prevent the generation of excessive ROS using suitably designed antioxidant ligands is one of the crucial steps to tackle multifaceted toxicity in AD.⁹ As discussed, TGR86-88 have been appropriately designed to bind Cu and prevent the redox cycle, ROS generation and overall acts as efficient antioxidants. We performed ascorbate assay to evaluate the ability of TGR86-88 to redox silence copper and alleviate oxidative stress. In this assay, free Cu^{2+} generate hydroxyl ($\cdot\text{OH}$) radicals in the presence of natural reducing agent ascorbate, and the extent of suppression of radical generation in the presence of HMMs is assessed using a radical-responsive fluorescence probe. For instance, $\cdot\text{OH}$ react with non-fluorescent coumarin 3-carboxylic acid (3-CCA) transforming it to a highly fluorescent 7-hydroxycoumarin-3-carboxylic acid (7-OH-CCA) ($\lambda_{\text{ex}}= 395$ nm and $\lambda_{\text{em}}= 452$ nm).²³ In this experiment, Clq or HMMs (10 μM) were independently added to solutions (PBS, 10 mM, pH = 7.4) containing Cu^{2+} (5 μM) and 3-CCA (50 μM), and the fluorescence was monitored at 452 nm upon addition of ascorbate (150 μM) after 60 min of incubation (Figure 5a). TGR86-88 showed ~80% reduction in the $\cdot\text{OH}$ generation similar to control Clq, which confirmed that HMMs retain their metal-chelating property and maintain Cu^{2+} in a redox-silent state. Further, the antioxidant property of HMMs was studied in the presence of $\text{A}\beta\text{-Cu}^{2+}$ ascorbate system. $\text{A}\beta_{16}\text{-Cu}^{2+}$ in the presence of ascorbate generates hydrogen peroxide (H_2O_2) that subsequently converts to $\cdot\text{OH}$. Clq or TGR86-88 (10 μM) were indecently added to PBS buffer (pH = 7.4, 10 mM) containing $\text{A}\beta_{16}$ (5.1 μM), Cu^{2+} (5 μM) and CCA (50 μM). These samples were treated with ascorbate (150 μM), and the fluorescence at 452 nm ($\lambda_{\text{ex}}= 395$ nm) was recorded after 90 min of incubation (Figure 5b). Clq and HMMs showed

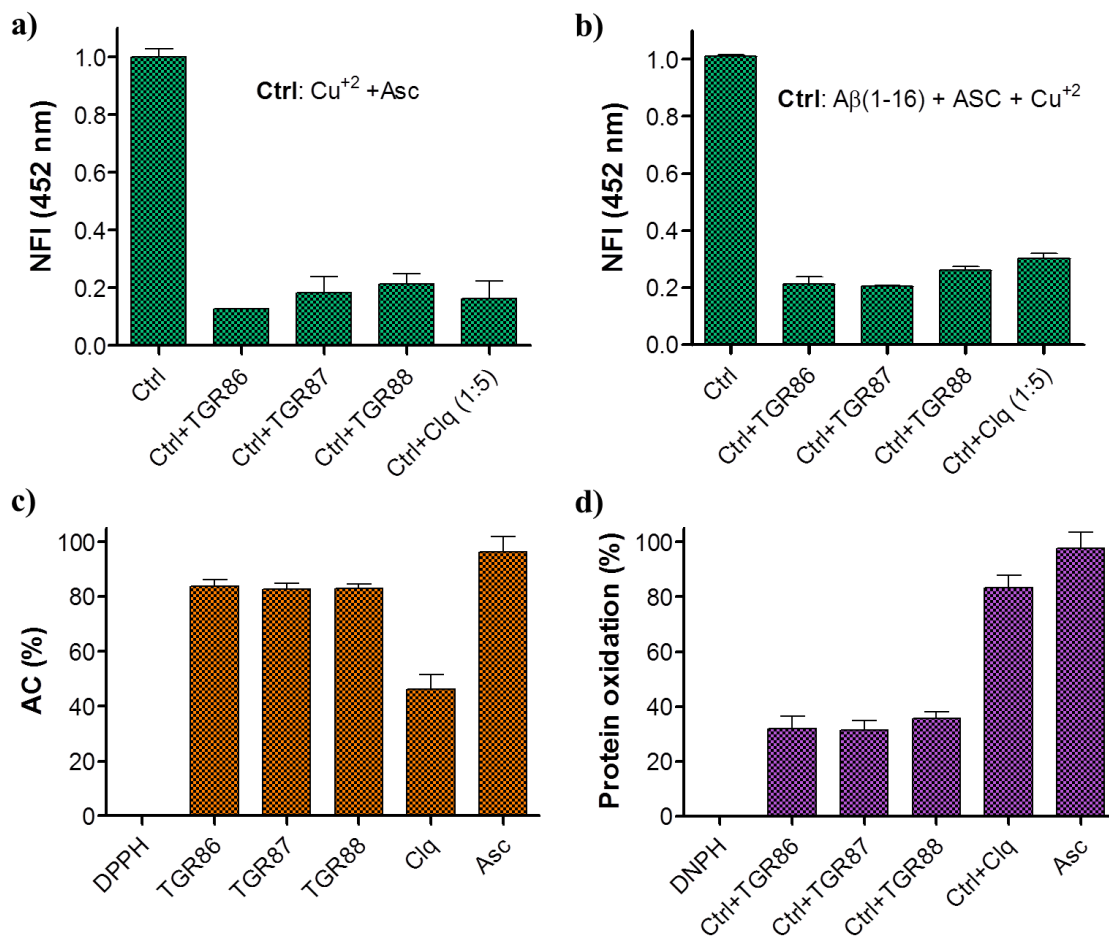


Figure 5. a) The normalized fluorescence intensity (452 nm) of 7-OH-CCA ($\lambda_{\text{ex}} = 392 \text{ nm}$) generated in ascorbate assay, with Cu^{2+} (5 μM), 3-CCA (50 μM) and ascorbate (150 μM) in presence of 10 μM Clq or HMMs (TGR86, TGR87 and TGR88) after 60 min of incubation at 37 $^{\circ}\text{C}$. b) The normalized fluorescence intensity (452 nm) of 7-OH-CCA generated in ascorbate assay, with $\text{A}\beta(1-16)$ (5.1 μM), Cu^{2+} (5 μM) and CCA (50 μM), Clq or HMMs (10 μM) (TGR86, TGR87 and TGR88) after 90 min of incubation at 37 $^{\circ}\text{C}$. c) DPPH radical, scavenging property of the Clq or HMMs (10 μM) was analysed and plotted as their percentage of antioxidant capacity (% of AC). d) BSA (1mg/mL), Cu^{2+} (0.1 mM) and H_2O_2 (2.5 mM), Clq and HMMs (0.1 mM) are added independently, the percentage of the protein or BSA oxidation was analyzed and quantified through DNPH absorption at 370 nm. Each experiment was repeated three times ($n = 3$), and error bars represent the standard deviation (SD) of the NFI.

~75% reduction in the $\cdot\text{OH}$ generation, which infers that HMMs interact with Cu^{2+} bound to $\text{A}\beta(1-16)$ and prevent the redox process responsible ROS production. Thus, results from ascorbate assay confirmed that TGR86-88 efficiently chelate to Cu^{2+} and prevent redox cycling under the reducing environment.

Next, we studied the effect of HMMs on ROS generated through metal-independent pathway through DPPH assay.²⁴ DPPH is an organic compound with stable free radical and predominantly absorb at 517 nm. The presence of scavengers quench the radicals and cause a reduction in the absorption intensity at 517 nm, which is correlated to scavenging or antioxidant property of compounds under study.²⁴ In this assay, DPPH (50 μ M) was added to the solutions of Clq or HMMs (10 μ M) in methanol and absorption was recorded at 517 nm after 30 min of incubation (Figure 5c). The control Clq showed only ~50% of antioxidant capacity (AC), whereas compounds TGR86-88 exhibited AC efficiency of >80% (TGR86: 83%, TGR87: 82%; TGR88: 83%). The enhanced AC is attributed to gallic acid moiety incorporated in our HMMs, and these data validated the multifunctional nature of TGR86-88 compared to Clq. To reiterate further, our HMMs modulate ROS generation in the presence or absence of redox metal linked to A β toxicity, thereby acting as an effective antioxidant compared to control Clq, which can only prevent the metal-mediated ROS.

4.5 Protein Oxidation

The oxidative stress generated in neuronal cells by the A β aggregates in the presence or absence of metals is considered a major causative factor in AD pathology.²² The ROS generated by A β aggregates in the presence of Cu²⁺ cause oxidation of biomacromolecules such as proteins, which further leads to the neuronal death. The ROS (H₂O₂ and \cdot OH radicals) generated by A β -Cu²⁺ complex cause oxidation of both amino acid side chains and protein backbone, which is responsible for protein fragmentation and crosslinking.²⁵ The protein oxidation leads to the formation of protein carbonyls, and the measurement of carbonyls give a reasonable approximation of the extent of oxidation. The protein carbonyls can be measured and quantified using 2,4-dinitrophenylhydrazine (DNPH).²⁶ DNPH reacts with carbonyls in protein backbone to

form hydrazones which can be detected spectroscopically by monitoring the absorption intensity at 370 nm. We performed a simplified version of protein oxidation, where the $\text{Cu}^{2+} + \text{H}_2\text{O}_2$ system was used to generate ROS and BSA employed as a protein target to assess the extent of oxidation. Clq and HMMs (0.1 mM) were independently added to PBS buffer (pH = 7.4, 10 mM) solutions containing BSA (1mg/mL), Cu^{2+} (0.1 mM) and H_2O_2 (2.5 mM) (Figure 5d). The samples were incubated at 37 °C for 24 h in the dark followed by the addition of DNPH (5 mM). Further incubation of the samples for 10 min, absorption was recorded at 370 nm to determine the percentage of protein oxidation. In the presence of control compound Clq, protein oxidation of ~70% was observed, whereas HMMs exhibited a significant reduction in the protein oxidation to <40% (TGR86: 32%, TGR87: 31%; TGR88: 35%). These results clearly suggest that HMMs with a polyphenolic moiety (gallic acid) effectively quench ROS generated and prevent the oxidation of protein (BSA). In contrast, Clq having single hydroxyl group could only partially prevent the protein oxidation.

4.6 Cellular Toxicity

After demonstrating the multifunctional nature of HMMs to inhibit $\text{A}\beta$ toxicity ($\text{A}\beta$ aggregation and metal-induced $\text{A}\beta$ aggregation, ROS generation and oxidative stress, and averting protein oxidation), we studied their efficacy in cellular systems. First, we determined the cellular viability of HMMs by the 3-(4,5-dimethylthiazol-2-yl)2,5-diphenyltetrazolium bromide (MTT) assay in PC12 cells (neuronal cell line). The cells were treated with increasing concentrations of HMMs (5-40 μM) and incubated at 37 °C for 24 h. The Clq (40 μM) showed cell viability of only ~50%, as it has been reported to be neurotoxic and reportedly failed in clinical trials (Figure 6a).¹⁴ On the other hand, TGR88 and TGR87 with halogen and galic acid substituents exhibited improved cell viability of ~60% and ~70%, respectively. Remarkably, TGR86 showed ~90%

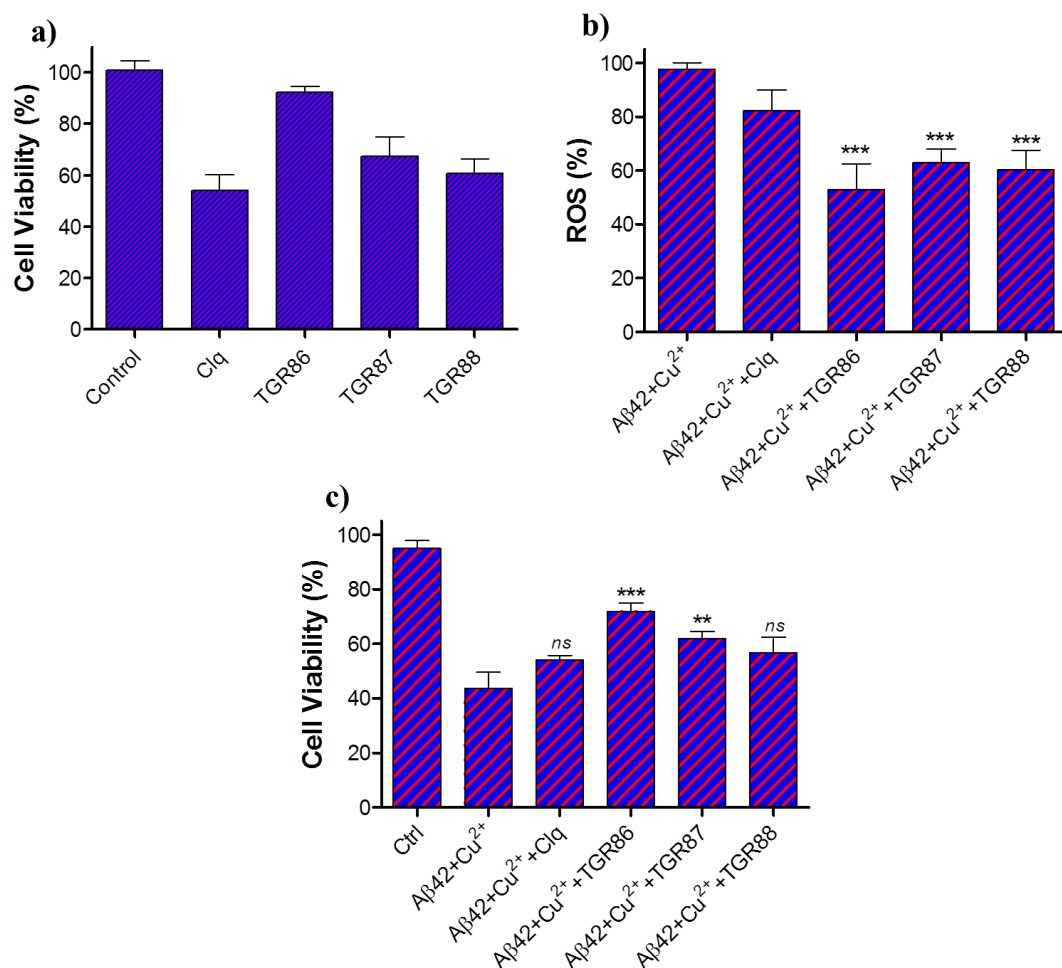


Figure 6. (a) Cell viability of PC12 cells incubated with Clq or HMMs (TGR86, TGR87 and TGR88) (40 μM). (b) ROS generation in the PC12 cell when incubated with Aβ42 (10 μM), Cu²⁺ (10 μM), ascorbate (200 μM), and with Clq (20 μM), TGR86 (20 μM), TGR87 (20 μM) and TGR88 (20 μM) independently. ROS produced is quantified by measuring DCF fluorescence intensity at 529 nm for a given time point. (c) Cell viability (PC12 cells) observed after incubation (24 h) with Aβ42 (10 μM), Cu²⁺ (10 μM), ascorbate (200 μM), and with Clq (20 μM), TGR86 (20 μM), TGR87 (20 μM) and TGR88 (20 μM) independently. Each experiment was repeated three times (n = 3), and error bars represent the standard deviation (SD).

cellular viability, which is in agreement with one of the design strategies viz., removal of halogen substituents to reduce the cytotoxicity of the parent compound Clq. Next, we evaluated the antioxidant property of HMMs in *in cellulo* conditions. The effect of TGR86-88 on Aβ42-Cu²⁺ induced ROS generation was studied by DCFDA (2,7-dichlorofluorescein diacetate) assay in PC12 cells. DCFDA is a non-fluorescent dye used to measure ROS (hydroxyl, peroxy and

other related species) *in cellulo* conditions.²⁷ DCFDA is oxidized by ROS within the cells to a green fluorescent dye 2, 7-dichlorofluorescein (DCF, $\lambda_{\text{ex}}= 495 \text{ nm}$, and $\lambda_{\text{em}}= 529 \text{ nm}$).²⁸ The PC12 cells pretreated with DCFDA were incubated with A β 42-Cu²⁺ complex (10 μM), ascorbate (200 μM) and Clq or HMMs (50 μM) (Figure 6b). PC12 cells treated with Clq showed 82% of ROS generation when compared to cells treated with A β 42-Cu²⁺ complex alone (100%). Interestingly, HMMs treated cells showed significant decrease in ROS generation (TGR86: 53%, TGR87: 60%; TGR88: 63%). This data is in good agreement with the results from ascorbate assay and confirm the efficient antioxidant nature of HMMs *in vitro* and *in cellulo* conditions. Further, we studied the protective nature of HMMs towards PC12 cells from the multifaceted toxicity exhibited by the A β 42-Cu²⁺ complex.⁹ PC12 cells treated with A β 42-Cu²⁺ complex (10 μM) and ascorbate (200 μM) were incubated independently with Clq or HMMs (20 μM) (Figure 6c). A β 42-Cu²⁺ treated cells showed ~50% decrease in viability compared to untreated cells. The compounds Clq and TGR88 were failed to provide any appreciable protection to cells against A β 42-Cu²⁺ toxicity. However, TGR87 treated cells showed relatively enhanced viability (60%) from A β 42-Cu²⁺ toxicity. Remarkably, TGR86 showed significant enhancement in the viability (74%) and provided excellent protection against A β 42-Cu²⁺ toxicity to cells. Therefore, TGR86 is a promising candidate among the three HMMs to modulate the overall multifaceted A β 42 toxicity and retains similar metal chelating property while successfully overcoming the major drawback viz., neurotoxicity of Clq.

4.7 Prevention of Mitochondrial Damage

A β -mediated mitochondrial dysfunctioning in neuronal cells is an important pathway contributing to multifaceted toxicity in AD.²⁹ A β is known to interact with mitochondria and cause impairment of oxidative phosphorylation, trigger alteration in mitochondrial dynamics,

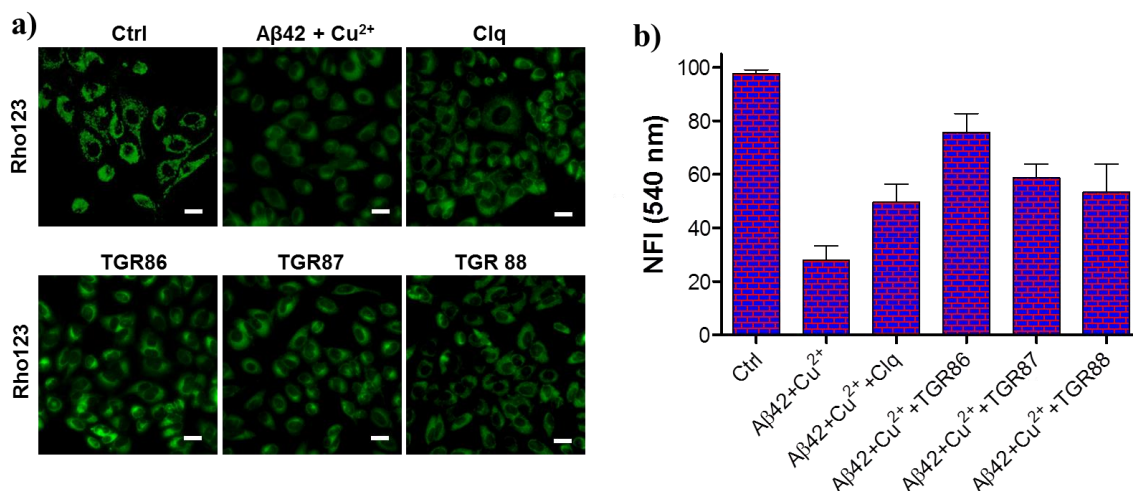


Figure 7. (a) Microscopic images of PC12 cells treated with Rho123, observed after incubation (12 h) with Aβ42 (10 μM), Cu²⁺ (10 μM), ascorbate (200 μM), and with Clq (20 μM), TGR86 (20 μM), TGR87 (20 μM) and TGR88 (20 μM) independently. (b) Quantification of Rho123 fluorescence at 534 nm ($\lambda_{\text{ex}} = 511$ nm) in PC12 cells. Each experiment was repeated three times ($n = 3$), and error bars represent the standard deviation (SD).

disturb ATP synthesis and subsequently leading to neuronal death.³⁰ The preliminary changes observed during mitochondrial damage is the reduction in mitochondrial membrane potential (MMP) and generation of the ROS.³⁰ The changes in MMP can be directly correlated to actual functioning of the mitochondria.³¹ Thus, the effectiveness of HMMs in preventing the mitochondrial damage caused by Aβ-Cu²⁺ complex in PC12 cells was evaluated by measuring the MMP with the help of Rhodamine 123 (Rho123). Rho123 is a green fluorescent dye, a membrane potential dye specifically binds to mitochondrial membrane and show change in emission intensity as a function of membrane potential.³² PC12 cells treated with Aβ42-Cu²⁺ complex (10 μM) with ascorbate (200 μM) were incubated independently with Clq or HMMs (20 μM) for 12 h, followed by the addition of Rho123 (500 nM) and monitoring fluorescence emission at 534 nm ($\lambda_{\text{ex}} = 508$ nm) (Figure 7). The cells treated with Aβ42-Cu²⁺ and ascorbate showed ~65% in the MMP compared to untreated cells (97%). The cells treated with Aβ42-Cu²⁺ and ascorbate were incubated with Clq, TGR87 and TGR88 showed significant improvement in

MMP to 50%, 58% and 53%, respectively. Interestingly, TGR86 showed a recovery in MMP of 75% compared to A β 42-Cu²⁺ treated cells (35%). It is reasonable to propose that TGR86 binds and prevents the interaction of toxic A β 42-Cu²⁺ complex with mitochondrial membrane and thus preventing its dysfunction. We believe that averting the mitochondrial damage could be one of the probable pathways of HMMs (TGR86) to rescue the cells from A β toxicity.

4.8 Conclusion

In summary, we successfully amalgamated the metal chelation and antioxidant properties of Clq and EGCG, respectively into hybrid multifunctional modulators (HMMs) to efficiently target multifaceted A β toxicity of Alzheimer's disease. Among the three HMMs, TGR86 was found to be the most cell viable and promising lead molecule. TGR86 inhibited metal independent and dependent A β aggregation (ThT binding assay and dot blot analysis). Further, TGR86 efficiently prevented ROS generated by Cu²⁺ in reduced condition and from A β 42-Cu²⁺ complex. Remarkably, TGR86 modulate metal-independent ROS generation compared to control Clq which failed under similar condition. Furthermore, the protein damage induced by the H₂O₂ and Cu²⁺ was efficiently protected by TGR86. Among all the designed HMMs, TGR86 exhibited highest cellular viability at elevated concentrations when compared to Clq. *In vitro* inhibition of multifaceted A β toxicity was further verified *in cellulo* conditions. The PC 12 cells were rescued from A β 42-Cu²⁺ induced multifaceted toxicity by TGR86. The protective nature of TGR86 to PC12 from A β toxicity is possibly through its interaction and prevention of A β aggregation, quenching ROS generation and antioxidant effect and averting mitochondrial damage. Overall, the multifunctional properties suggest that TGR86 is a potential candidate and serves as a privileged structure to develop therapeutic agents for treating AD.

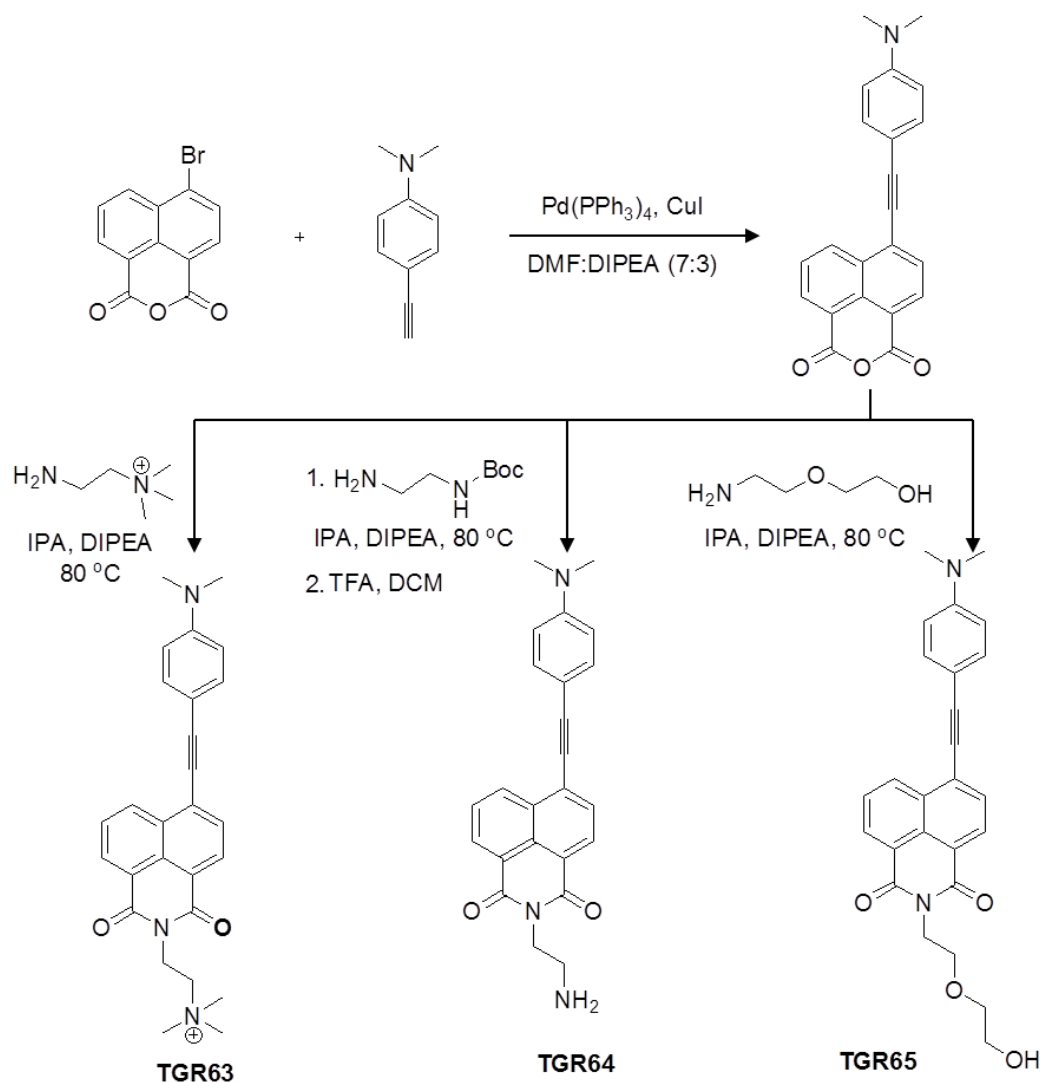
Chapter 4B

**Synthesis of naphthalene monoimide derivatives as effective modulators
of toxicity in Alzheimer's and Parkinson disease**

Neurodegeneration has been shown to have a common mechanism of disease pathogenesis in many neurodegenerative diseases such as AD, Parkinson disease (PD), Huntington disease (HD), amyotrophic lateral sclerosis (ALS) and prion disease.³³ Protein misfolding and aggregation is commonly observed and one of the route causes of neurodegeneration. Under disease conditions protein misfolds and self-aggregate rapidly to form fibrillar aggregates through β -sheet formation further supported by hydrophobic interactions.³⁴ The protein aggregation is at the core of the disease progression and pathogenesis, and therefore targeting protein aggregation is considered a promising strategy to develop therapeutic agents for these neurodegenerative diseases.³⁵ Herein, we present design and synthesis of naphthalene monoanhydride (NMA) derivatives to modulate the aggregation of $A\beta$ and α -Syn implicated in AD and PD, respectively.

4.9 Design strategy

$A\beta$ and α -Syn aggregates predominantly consist of β -sheet structures with hydrophobic pockets.¹ We intend to design small molecule-based modulators with hydrophobic nature for better and stronger interaction with hydrophobic pockets of amyloid fibrils.³⁶ We have used NMA as the core hydrophobic platform to build novel molecules. Surprisingly, NMAs are not being used for developing modulators for amyloid ($A\beta$ and α -Syn) toxicity. The simple molecular structure of NMA provides a huge scope of further synthetic modifications. We conjugated the Bromo-NMA to *N,N*-dimethylaniline at the 8th position through an alkyne linker using sonogashira coupling reaction. *N,N*-Dimethylaniline conjugated to NMA was believed to provide a balanced hydrophobicity to improve the aggregation inhibition property. However, hydrophobic nature of NMA derivatives poses solubility issues during *in cellulo* and *in vivo* experiments. To address this issue, we further modified the NMA derivatives with *N,N,N*-trimethylethylenediamine, ethylenediamine and 2-(2-aminoethoxy) ethanol to obtain the naphthalene monoimide (NMI)



Scheme 2. Synthesis of NMI derivatives.

derivatives TGR63, TGR64 and TGR65, respectively (Scheme 2). Next, we performed various biophysical studies to validate the effect of NMI derivatives on A β and α -Syn aggregation.

4.10 Inhibition of A β 42 fibrillar aggregates

We employed ThT binding assay to evaluate the ability of NMI derivatives (TGR63, TGR64 and TGR65) to either prevent A β 42 fibrillar assembly (inhibition) or to break down the preformed fibrils (dissolution). For the inhibition assay, all the NMI derivatives (TGR63, TGR64 and TGR65) were added independently to A β peptide (10 μ M) at 0 h of the experiment, whereas for

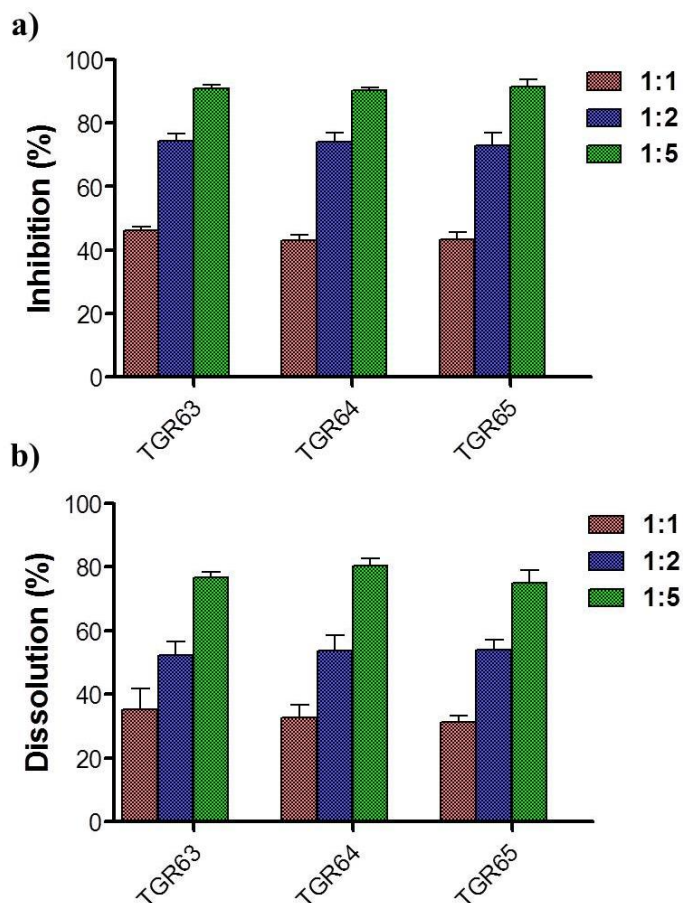


Figure. 8 Inhibition (a) and dissolution (b) of A β 42 aggregates studied by thioflavin (ThT) assay. The data in (a) and (b) show the effects of different stoichiometries of TGR63, TGR64 and TGR65 on the aggregation of 10 μ M A β 42 (day 3 of the inhibition assay and day 6 of the dissolution assay). Molar ratios (A β 42:inhibitor) of 1:1, 1:2 and 1:5 were used for each inhibitor. Values are the normalized to maximal fluorescence intensity at 485 nm compared to that of the control (A β 42 with no inhibitor). Each experiment was repeated three times ($n = 3$). Error bars represent the standard deviation (SD) of the fluorescence measurement.

the aggregates dissolution assay they were added to A β 42 fibrillar aggregates grown for 2 days. Upon incubating for a predetermined period, A β 42/inhibitors samples were analyzed using ThT by measuring the fluorescence change at 485 nm. A β 42 (10 μ M) and its aggregates were used to study the effect of NMI derivatives (TGR63, TGR64 and TGR65) on both inhibition and dissolution assays. Experiments were performed at various stoichiometric ratios (A β 42/inhibitor) of 1:1, 1:2, and 1:5 with a fixed concentration of A β 42 (10 μ M). Inhibition experiments demonstrated that TGR63, TGR64 and TGR65 were able to prevent A β 42 aggregation (Figure

8). TGR63, TGR64 and TGR65 showed concentration-dependent inhibition. At 1:1 ratio all the inhibitors (TGR63, TGR64 and TGR65) showed ~50 % decrease in the formation of A β aggregates. Further, with an increase in the concentration of inhibitors (ratios of 1:2 and 1:5) have effectively decreased the A β aggregation to 75% and 90%, respectively. Similar results were observed in the case of fibril reversal assay with dissolution efficiencies of 80% (TGR63), 75% (TGR64), and 78% (TGR65), for 1:5 stoichiometric ratio (Figure 8). At 1:1 and 1:2 ratios, inhibitors (TGR63, TGR64 and TGR65) have shown dissolution efficiencies of ~35% and ~50%, respectively. Thus, TGR63, TGR64 and TGR65 were found to be promising molecules as they displayed pronounced effect in both inhibition and dissolution assays.

4.11 NMI derivatives rescue of neuronal cells from amyloid toxicity

Next, we studied the efficiency of TGR63, TGR64 and TGR65 in modulating A β aggregates induced cellular toxicity. The ability of TGR63, TGR64 and TGR65 to rescue PC12 cells from A β 42 toxicity was studied through cell viability assay (MTT assay). A β 42 (20 μ M) treated PC12 cells were incubated alone and independently with TGR63, TGR64 and TGR65 (40 μ M) for 24 h

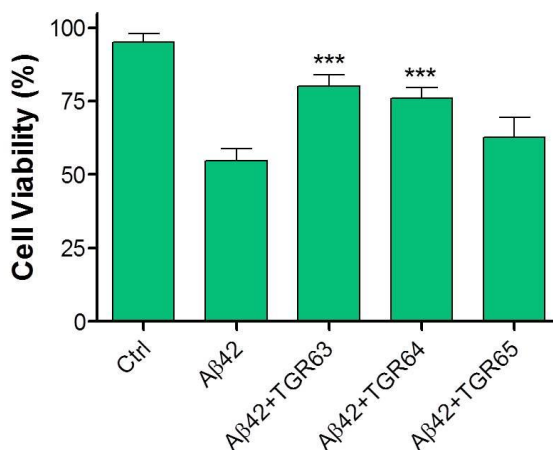


Figure 9. A β toxicity in PC12 cells. Cellular viability observed after incubation (24 h) with A β 42 (20 μ M) with TGR63 (40 μ M) or TGR64 (40 μ M) or TGR65 (40 μ M), independently. Each experiment was repeated three times (n = 3), and error bars represent the standard deviation (SD).

and then cellular viability was assessed (Figure 9). TGR65 exhibited only a slight improvement in cell viability (62%) compared to A β 42 treated cells (54%). Remarkably TGR63 and TGR64 improved cell viability to 80% and 78%, respectively. ThT binding assay in Figure 8 has shown that NMI derivatives (TGR63, TGR64 and TGR65) exhibit similar amyloid aggregation inhibition property and a similar trend in the rescue of PC12 cells from amyloid toxicity as expected. However, TGR63 and TGR64 exhibited enhanced protection, indicating that improved cell viability is not solely driven by aggregation modulation. Therefore, TGR63 and TGR64 would possibly be involved in other cellular mechanisms to exhibit better cellular viability from inhibition of amyloid toxicity.

4.12 Structure-activity relationship

Next, we investigated the structure-activity relationship (SAR) of NMI derivatives towards rescuing PC12 cells from A β toxicity (Figure 10). The lead compounds TGR63 and TGR64 are structurally similar except for the quaternary amine in TGR63, and a primary amine in TGR64. The absence of amine in the TGR65 has shown only a slight improvement in the cell viability from A β toxicity which indicates that ethylenediamine has a significant role in rescuing the cells. TGR63 has shown slightly better cellular rescue from A β toxicity compared to TGR64, which indicate that *N,N,N*-trimethylethylenediamine is an essential structural moiety and we retained this moiety in designing further analogues for structure-activity study. To evaluate the role of 4-ethynyl-*N,N*-dimethylbenzenamine (EMB) moiety present in TGR63 and TGR64, we have synthesized TGR66 with the absence EMD. TGR66 could not rescue cells (54% viability) from A β toxicity which indicated that EMB in TGR63 and TGR64 play a significant role in enhancing the cell viability as observed in case of TGR63 or TGR64 (Figure 11). Further, we synthesized TGR67, structurally similar to TGR63 without EMB group, and TGR68 with *N,N*-

dimethylamine group is directly coupled to 8th position of NMI, without ethynylbenzene linker to structurally understand the role of EMB (Figure 10). In cellular viability assay, TGR67 and TGR68 showed cell viability of 54% and 56%, respectively compared to A β treated cells (54%). Structural changes in EMB has substantially reduced the protective nature of NMI derivatives indicating that EMB is an essential structural moiety in TGR63 for the rescue of cells from A β toxicity. From these studies, TGR63 is found to be the most potent compound, and therefore all further studies were performed using TGR63.

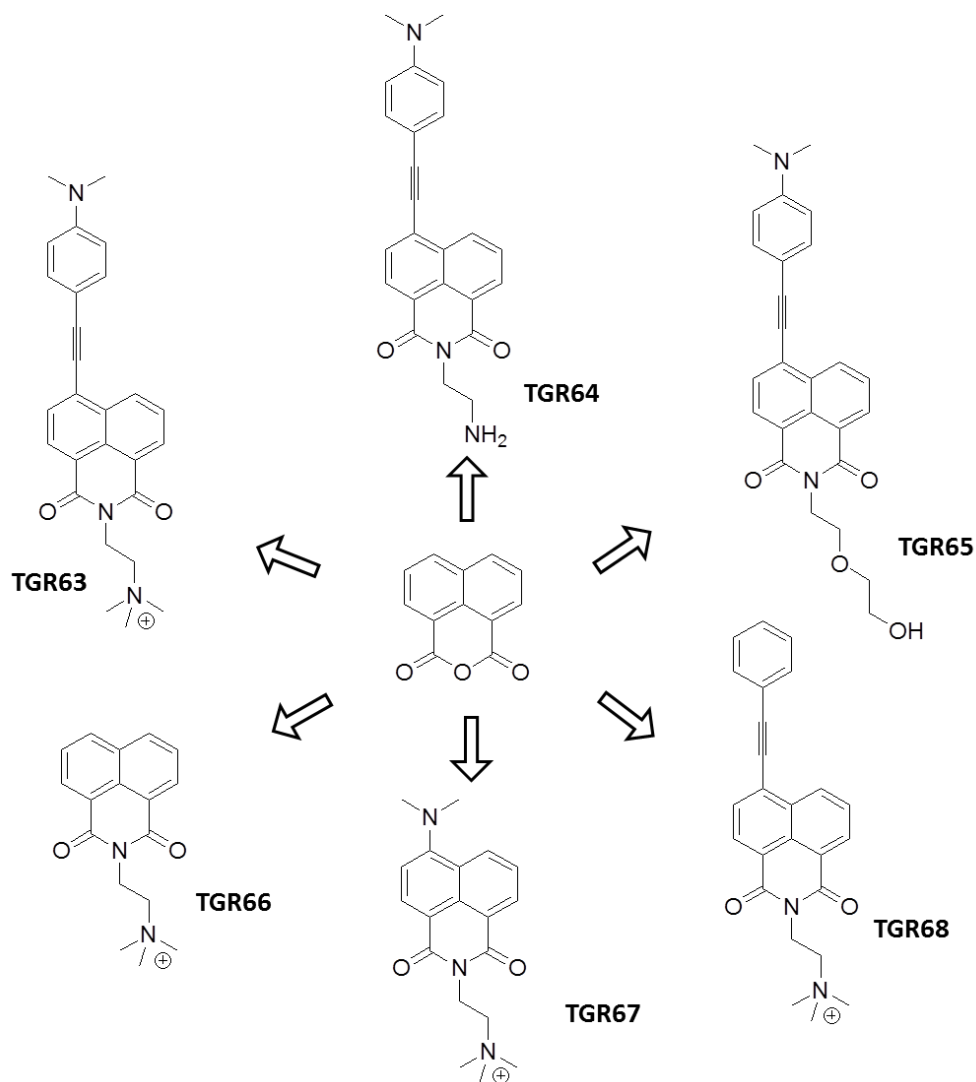


Figure 10. NMI derivatives synthesized for SAR.

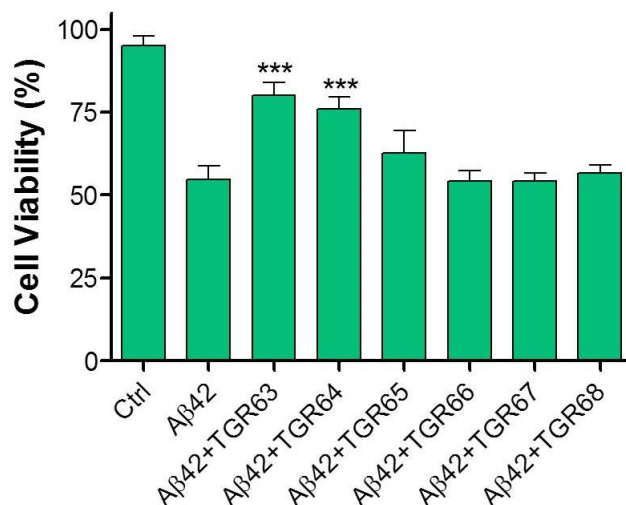


Figure 11. Cell viability observed after incubation (24 h) with Aβ42 (20 μM) and TGR63 (40 μM) or TGR64 (40 μM) or TGR65 (40 μM) TGR66 (40 μM) or TGR67 (40 μM) or TGR68 (40 μM), independently. Each experiment was repeated three times (n = 3), and error bars represent the standard deviation (SD).

4.13 TGR63 and TGR64 as therapeutic agents in Parkinson disease

PD is a neuronal disorder, mainly affect the motor system. α -Syn is a presynaptic neuronal protein that is linked neuropathologically to PD and play a vital role in the pathogenesis in number of ways.³⁷ Self-aggregation of α -Syn to form fibrillar aggregates and these toxic species mediates disruption of cellular homeostasis and cause neuronal death.³⁸ These toxic aggregates

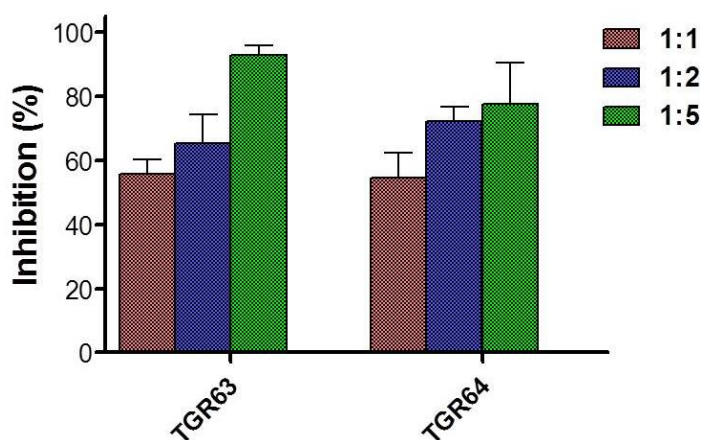


Figure 12. ThT binding assay to study α -Syn aggregation inhibition in presence of TGR63 and TGR64. Each experiment was repeated three times (n = 3). Error bars represent the standard deviation (SD) of the fluorescence measurement.

affect various intracellular targets, especially synaptic function. In this context, we employed our NMI derivatives to study the possible modulation of α -Syn aggregation. The effect of NMI derivatives (TGR63 and TGR64) on α -Syn (100 μ M) aggregation inhibition was studied through ThT binding assay. Experiments were performed at stoichiometric ratios (α -Syn:inhibitor) of 1:1, 1:2, and 1:5 with the fixed concentration of α -Syn of 100 μ M. The inhibition experiments demonstrated that TGR63 and TGR64 are capable of inhibiting α -Syn aggregation (Figure 12). TGR63 and TGR64 have shown a concentration-dependent inhibition. At 1:1 ratio, inhibitors (TGR63 and TGR64) showed ~54 % decrease in the formation of α -Syn aggregates. Further increase in the concentration of inhibitors with 1:2 and 1:5 ratio have effectively decreased α -Syn aggregation to 65% and 93% in TGR63 and 72% and 77% in TGR64. Therefore, TGR63 and TGR64 are new class of molecules for modulating A β and α -Syn aggregation involved in AD and PD, respectively.

4.14 Conclusion

In conclusion, we have synthesized a series of hydrophobic NMI derivatives to target hydrophobic interactions involved in amyloid aggregation. Among the designed molecules, TGR63 and TGR64 were found to be promising lead candidates for modulating amyloid toxicity observed in AD and PD. ThT binding and cell viability assay clearly shown that TGR63 and TGR64 could efficiently modulate the amyloid toxicity with enhanced cellular viability. Cell viability assay also suggests that TGR63 and TGR64 are involved in modulating various other cellular pathways in addition to the amyloid aggregation inhibition, for rescuing neuronal cells from amyloid toxicity. Further, studies towards understanding and identifying the molecular pathways effected by TGR63 and TGR64 for enhancing cell viability are under progress.

Chapter 4C

Non-toxic berberine derivative to rescue cells from multifactorial A β toxicity

In the last few decades, various classes of molecules like peptides, peptidomimetics, natural products, and small synthetic molecules have been developed and tested to identify therapeutic candidates for the AD. However, most of these efforts failed, as they were not capable of inhibiting multifaceted A β toxicity.² Moreover, series of failure of several synthetic drug candidates in clinical trials have forced scientific community to search for novel ways of developing therapeutic agents targeting AD. Among them natural products or plant extracts have shown promising results.³⁹ Natural products, such as curcumin, resveratrol, and epigallocatechin-3-gallate (EGCG) have been shown to reduce the A β toxicity through their antioxidant and aggregation inhibition properties.^{11,17,18} EGCG, bioactive ingredient of green tea is a polyphenolic antioxidant flavonoid with aggregation modulation, anti-inflammatory and neuroprotective properties.⁴⁰ Similarly other natural products like brazilin, rosmarinic acid, luteolin, tanshinone and apigenin have shown to effectively modulate A β toxicity in the AD.³⁹ Among the natural products berberine (Ber) is a well-known alkaloid used in Chinese medicine to treat various disease conditions such as anti-diarrhoea, anti-hypertension, anti-inflammatory and anti-tumour.⁴¹ Ber is also shown to be a potential candidate for the possible treatment of various neurodegenerative diseases, especially in case of the AD.⁴² However, cytotoxicity of Ber has hindered its use as a lead drug candidate. Herein, we have synthetically modified the Ber to the polyphenolic, non-toxic and efficient modulator of multifaceted A β toxicity in the AD.

4.15 Synthesis and comparative cytotoxicity of berberine derivative

Berberine has shown therapeutic implications in various diseases including neurodegeneration.⁴³ Unfortunately, the cytotoxicity exhibited by Ber has restricted its use as a drug candidate for the AD. The exact molecular mechanism of cytotoxicity exhibited by Ber is not understood. Herein, we sought of synthetically modifying the Ber, to reduce the cytotoxicity. The Ber structurally

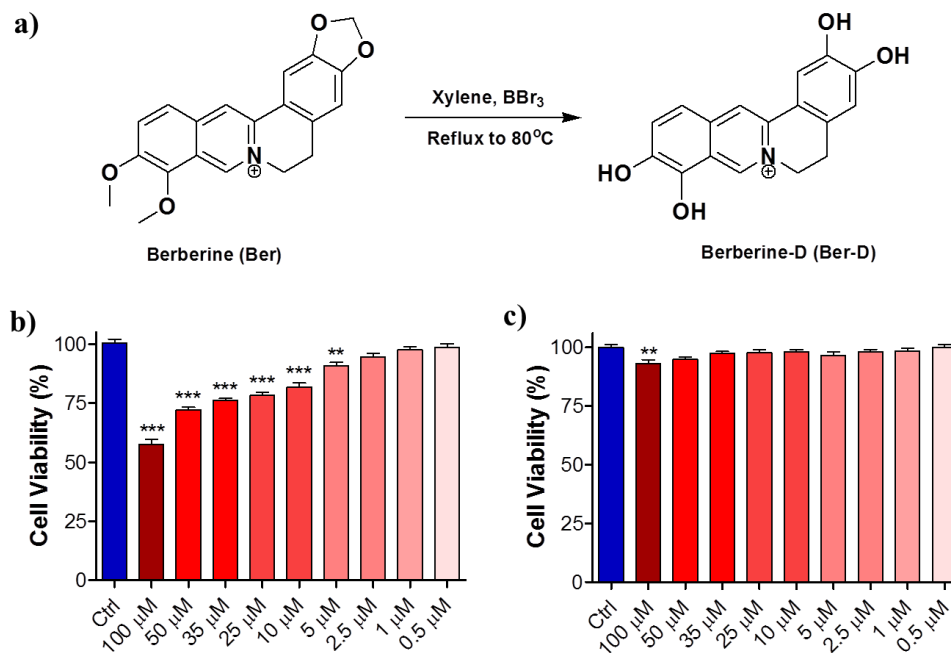


Figure 13. a) Preparation of Ber-D. b) The cellular viability of Ber and Ber-D in PC12 cells analyzed through MTT assay.

has four protected hydroxyl groups deprotecting (Berberine deprotected = Ber-D) them would lead to four phenolic hydroxyl groups, which structurally resemble polyphenolic antioxidant molecules. Generating free hydroxyl groups in Ber, which would enhance the antioxidant property, and the change in structure could modulate cytotoxicity. The Ber-D was prepared from Ber through a simple high yielding synthetic procedure shown in Figure 13. Ber was dissolved in xylene and refluxed in the presence of boron tribromide (BBr_3) to obtain Ber-D in good yield (70%). First, we determined the cellular viability of Ber-D in comparison with Ber through cell viability assay (MTT assay) in PC12 cells (neuronal cell line). Surprisingly, Ber-D was found to be nontoxic to cells when compared to parent Ber. Ber-D was non-toxic to cells up to 50 μM , only slight decrease (7%) in cell viability was observed at 100 μM . Whereas, Ber exhibited a decrease in cell viability at 5 μM (80%) and a further increase in concentration has drastically decreased the cell viability. Therefore, synthetic modification (Ber-D) has successfully enhanced

the cellular viability over the parent molecule Ber. Next, we studied the effect of Ber-D in modulating multifaceted A β toxicity in comparison to Ber.

4.16 Inhibition of metal independent and dependent A β aggregation

Thioflavin (ThT) binding assay was performed to evaluate the inhibition of A β 42 aggregation by the Ber-D in comparison with parent molecule Ber. The A β 42 (10 μ M) was incubated alone and independently with 100 μ M of Ber and Ber-D at 37 °C for 48 h in PBS (pH 7.4, 10 mM). Then, ThT (10 μ M) was added, and the fluorescence was monitored at 485 nm (Figure 14a). The Ber-D exhibited ~60% inhibition of A β 42 aggregation compared to control Ber which showed ~17% inhibition. Ber-D showed a concentration-dependent A β 42 aggregation inhibition property, 10 μ M, 20 μ M and 50 μ M of Ber-D showed inhibition of 20%, 27% and 39%, respectively. To further validate the aggregation inhibition data we performed dot blot analysis of the same samples used in ThT binding assay. We employed A β 42 aggregates specific antibody (OC) to determine the extent of aggregation inhibition (Figure 14b and 14c). In agreement with data from ThT binding assay Ber-D exhibited maximum aggregation inhibition efficiency over Ber (Figure 14b). Next, we evaluated the effect of Ber-D on metal-induced A β aggregation through ThT binding assay. The A β 42 (10 μ M) with Cu²⁺ (10 μ M) was incubated in the presence or absence of Ber-D and Ber at 37 °C for 24 h in PBS (pH 7.4, 10 mM) and then ThT was added, and the fluorescence was measured at 485 nm (Figure 14c). The Ber-D exhibited ~61% inhibition of metal-mediated A β 42 aggregation compared to control Ber which showed ~12% inhibition. Ber-D showed a concentration-dependent A β 42 aggregation inhibition property, 10 μ M, 20 μ M and 50 μ M of Ber-D showed inhibition of 25%, 39% and 37%, respectively. This signifies that Ber-D could modulate both the metal-dependent and independent A β 42 aggregation significantly compared to control.

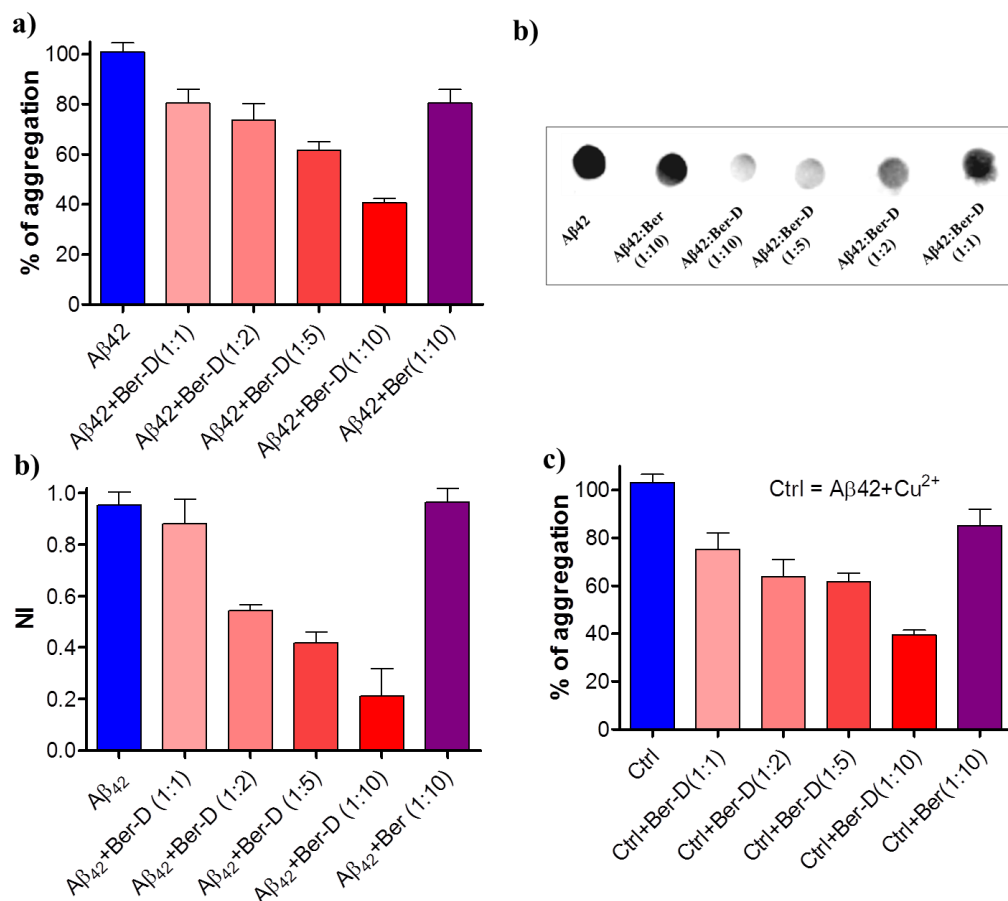


Figure 14. Inhibition of A β 42 aggregation studied by ThT binding assay and dot blot analysis a) A β 42 (10 μ M) was incubated alone and independently with Ber-D (1:1, 1:2, 1:5 and 1:10 stoichiometry) and Ber (1:10). Aggregation inhibition was quantified through normalized fluorescence intensity (NFI) of ThT at 485 nm. (b) Dot blot analysis of A β 42 (10 μ M) peptide incubated independently with 50 μ M Ber-D and Ber. OC (1:3000) is used as primary antibody followed by secondary antibody (HRP conjugated anti-mouse antibody, 1:10000). Chemiluminescence was recorded by treating blots with ECL reagent for 2 min, and the intensity is quantified (c). (d) A β 42 (10 μ M) and Cu²⁺ was incubated alone and independently with Ber-D (1:1, 1:2, 1:5 and 1:10 stoichiometry) and Ber (1:10). Aggregation inhibition was quantified by ThT assay. Each experiment was repeated minimum three times (n = 3), and error bars represent the standard deviation (SD) of the NFI.

4.17 Molecular docking studies

Ber and Ber-D bind to both core and surface sites of A β protofibril.⁴⁴ Most of the amyloid binding molecules, binds to the core site of A β protofibril.⁴⁴ However, in the case of Ber and Ber-D the entry cleft site was the one associated with larger binding affinity followed by the core-2 site (Figure 15). Surface site and core-1 site were associated with not so stronger binding

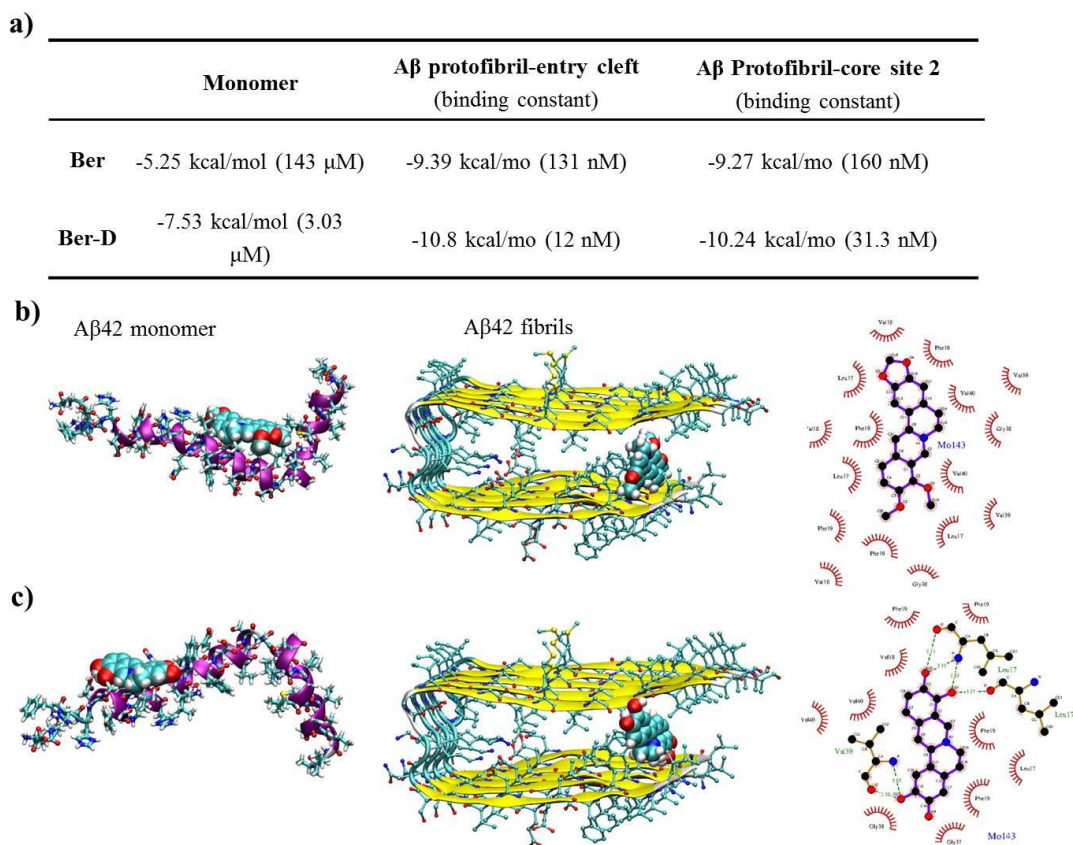


Figure 15. a) Summary of molecular docking studies for Ber-D and Ber towards A β 42 monomer and aggregates. b) Docking mode of Ber-D and Ber with A β monomer and aggregates. Indicate different binding sites in figure, core 1 , core 2 etc

affinity. The binding affinity and binding energy values for Ber and Ber-D with A β monomer and fibrils were obtained from molecular docking (Figure 15a). Both have a smaller binding affinity (in the micromolar range) towards the monomer than the fibril (in the nanomolar range). In addition, Ber-D has 5-10 fold larger binding affinity towards fibril than the Ber in both the core sites (Figure 15b). The relatively larger binding affinity of Ber-D with amyloid aggregates compared to Ber has significantly helped in improved inhibition of A β 42 aggregation as shown by ThT binding assay. The most stable complex of Ber with the monomer is stabilized by two hydrogen bonds formed between the Ber and His6 and His14 residues while for the Ber-D two hydrogen bonds are formed with the Asp7 residue of the monomer. Using the LigPLOT program

the interaction of Ber and Ber-D with different amino acids of A β 42 in amyloid fibril and nature of interactions was investigated. As can be seen in Figure 15b the interaction of Ber with fibril is mostly hydrophobic in nature (dominated by van der Waals than electrostatic). However, in the case of Ber-D, the interaction between the Ber-D and fibril is also mediated by the hydrogen bonding interactions. This may be the reason why Ber-D interacts strongly with fibril than the Ber and show aggregation inhibition properties.

4.18 Metal independent antioxidant assays

We studied the effect of Ber-D on ROS generated through the metal-independent mechanism. A series of antioxidant assays were performed to prove the antioxidant property of Ber-D. First, we performed DPPH (2,2-diphenyl-1-picrylhydrazyl) assay, where DPPH is an organic compound with stable free radical and predominantly absorb at 517 nm.²⁴ The presence of scavengers quenches the radicals and causes a reduction in the absorption intensity at 517 nm, which is correlated to scavenging or antioxidant property of compounds under study. In this assay, DPPH (50 μ M) was added to the solutions of Ber or Ber-D (50 μ M) in methanol and absorption was recorded at 517 nm after 30 min of incubation (Figure 16a). The control Ber showed only ~32% of antioxidant capacity (AC), whereas compounds Ber-D exhibited AC efficiency of 97%. The enhanced AC is attributed to the four hydroxyl groups present in Ber-D. Ber-D exhibits a concentration-dependent improvement in the AC, where 5 μ M, 10 μ M and 25 μ M of Ber-D showed AC of 10%, 62% and 81%, respectively. Further, we performed ABTS (2,2'-azino-bis(3-ethylbenzothiazoline-6-sulphonic acid)) assay.⁴⁵ In the presence of H₂O₂, radical cation from of ABTS is generated (ABTS \cdot^+) with characteristic absorption at 735 nm. The absorption at 735 nm represents the presence of ABTS \cdot^+ , the addition of antioxidant molecule would quench the radical leading to decrease in the absorption intensity. This particular property can be used to

determine the AC of antioxidants. $ABTS^{\cdot+}$ is incubated with ascorbate (100 μM , positive control), Ber-D (50 μM) or Ber (50 μM) for 15 min in dark followed by absorption measurement at 735 nm (Figure 16b). Ber-D exhibited AC of 100%, which is slightly higher than the ascorbate indicating the efficient antioxidant nature of Ber-D, whereas Ber showed AC of only 29%. The results obtained are in coherence with DPPH assay. Further, antioxidant activity of Ber-D and Ber were evaluated by the oxygen radical absorbance capacity assay method using fluorescein

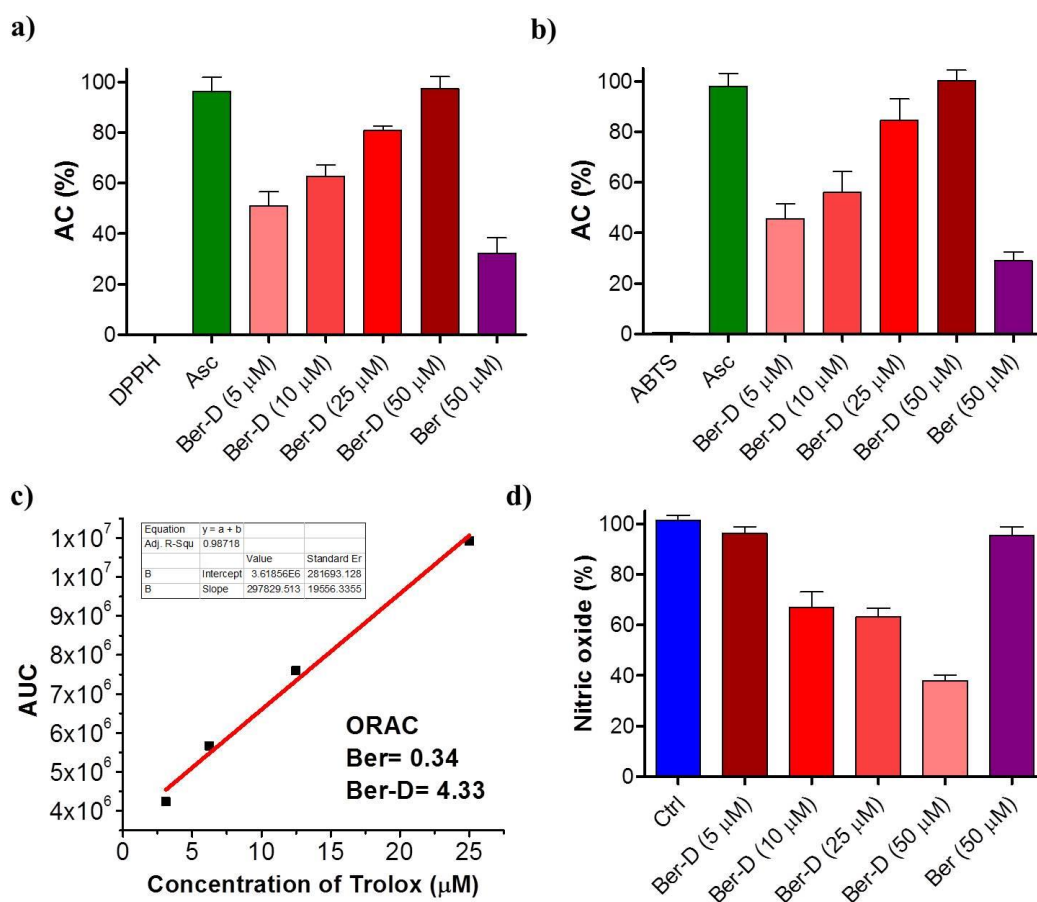


Figure 16. Metal independent antioxidant assays a) DPPH assay for Ber-D (5 μM , 10 μM , 25 μM and 50 μM) or Ber (50 μM) was analyzed and plotted as their percentage of antioxidant capacity (% of AC). b) ABTS radical cation scavenging property of Ber-D (5 μM , 10 μM , 25 μM and 50 μM) or Ber (100 μM) was analyzed and plotted as their percentage of antioxidant capacity (% of AC). c) Known concentrations of Trolox is used to obtain a standard curve and the ORAC activity of Ber-D and Ber is calculated as Trolox equivalents. d) Nitric oxide scavenging property of Ber-D (5 μM , 10 μM , 25 μM and 50 μM) or Ber (50 μM) was analyzed and plotted as their percentage of antioxidant capacity (% of AC).

(ORAC-FL) (Figure 16c).⁴⁶ The vitamin E analogue Trolox was used as an internal standard. Ber-D showed an ORAC-FL value of 4.33 Trolox equivalents, whereas Ber exhibited 0.34 Trolox equivalents. Ber-D has four times the efficiency in quenching the radical species when compared to Trolox implicating the efficient and improved antioxidant property of Ber-D over Ber. Next, we evaluated the antioxidant property of Ber-D towards reactive nitrogen species (RNS). We have used nitric oxide as a mimic for RNS and was generated from sodium nitroprusside.⁴⁷ Sodium nitroprusside in aqueous solution (pH = 7.4) spontaneously generates nitric oxide and interacts with oxygen to produce nitrite ions which can be further estimated by Greiss reagent. To a solution of sodium nitroprusside (5 mM) in ethanol, Ber or Ber-D (50 μ M) was added, and absorption was recorded at 546 nm after 100 min of incubation at 25 °C (Figure 16d). The control Ber showed only 5% decrease in NO production, which is comparable to the untreated sample. Interestingly, Ber-D exhibited 78% decrease in NO production. Moreover, Ber-D exhibited a concentration-dependent decrease in NO production where 5 μ M, 10 μ M and 25 μ M of Ber-D showed a decrease in NO production of 3%, 33% and 37%, respectively. DPPH, ABTS, ORAC and nitric oxide assay clearly showed that the presence of phenolic hydroxyl groups enhances the antioxidant property of Ber-D over its parent molecule Ber.

4.19 Metal-dependent antioxidant assays

The redox cycle of Cu^{2+} in $\text{A}\beta\text{-Cu}^{2+}$ complex generates ROS through Fenton-type reaction. Effective silencing of copper redox cycle in the $\text{A}\beta\text{-Cu}^{2+}$ complex is crucial to modulate ROS generation. To evaluate the redox silencing property of Ber-D, ascorbate assay was performed.⁹ To PBS (10 mM, pH = 7.4) solutions containing Cu^{2+} (5 μ M) and 3-CCA (50 μ M), Ber (50 μ M) or Ber-D (50 μ M) were added independently and the fluorescence at 450 nm was monitored upon addition of ascorbate (150 μ M) at 70 min (Figure 17a). Ber-D treated solution showed only

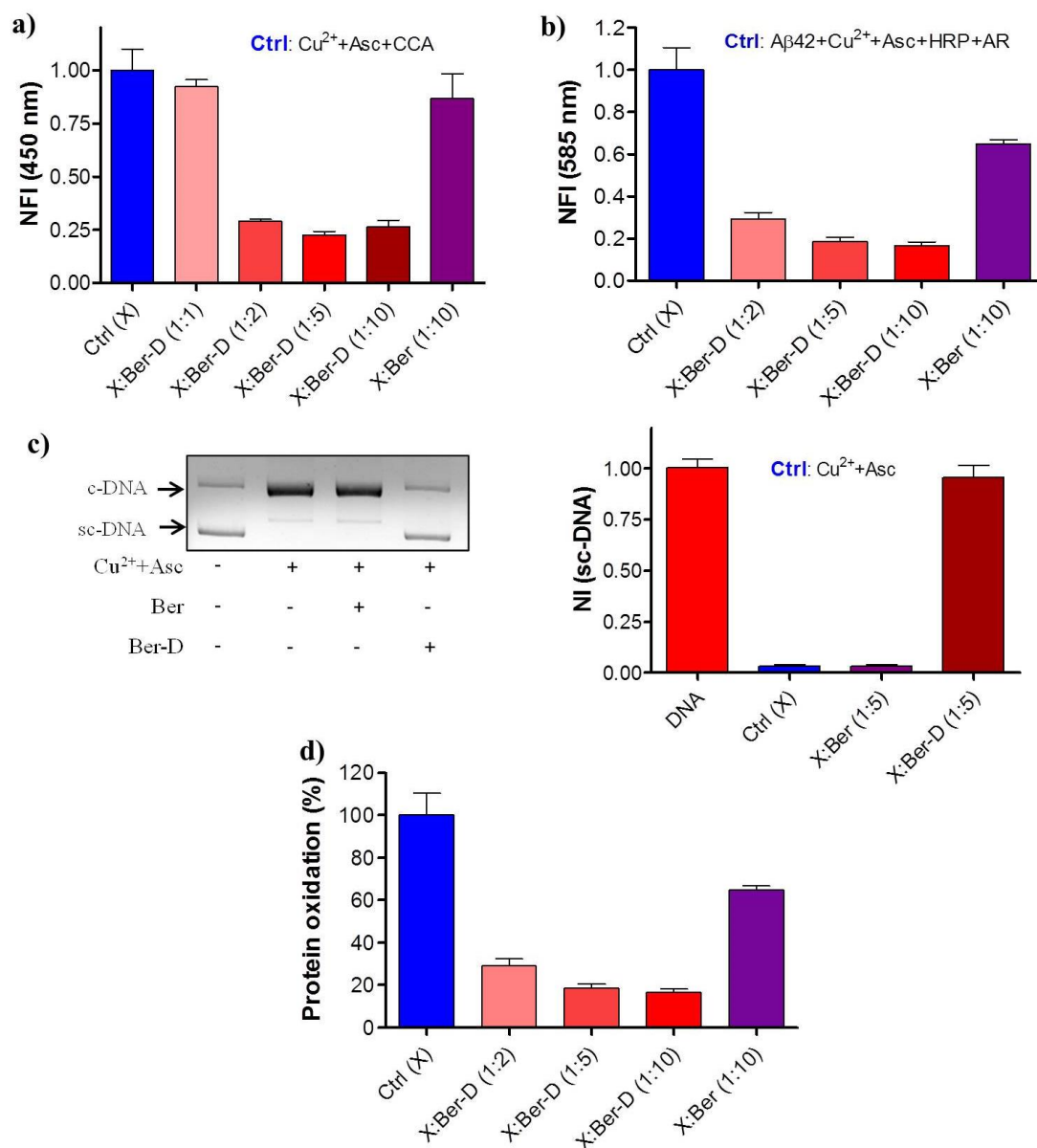


Figure 17. Metal-dependent antioxidant assays a) Fluorescence intensity (452 nm) of 7-OH-CCA generated with Cu^{2+} (5 μM) and ascorbate (150 μM) in the presence of Ber-D (5 μM , 10 μM , 25 μM and 50 μM) or Ber (50 μM) after 70 min of incubation at 37 $^{\circ}\text{C}$. c) Resorufin fluorescence intensity (585 nm) measured in solutions of $\text{A}\beta_{42}$ (5.1), Cu^{2+} (5 μM), ascorbate (150 μM) HRP and amplex red (10 μM) in the presence of Ber-D (5 μM , 10 μM , 25 μM and 50 μM) or Ber (50 μM) after 60 min of incubation at 37 $^{\circ}\text{C}$. c) DNA damage. Agarose gel electrophoresis of plasmid DNA (pBR322, 2 $\mu\text{g}/\text{mL}$ or 0.75 $\mu\text{g}/\text{mL}$) treated with Ber-D or Ber and Cu^{2+} (5 μM) in the presence of ascorbate (150 μM). d) BSA (1mg/mL), Cu^{2+} (0.1 mM) and H_2O_2 (2.5 mM), Ber-D or Ber (1 mM) are added independently, the percentage of the protein or BSA oxidation was analyzed and quantified through DNPH absorption at 370 nm. Supercoiled DNA (sc-DNA), circular DNA (c-DNA). Each experiment was repeated three times ($n = 3$), and error bars represent the standard deviation (SD) of the normalized fluorescence intensity (NFI).

25% of fluorescence indicating that the Ber-D binds to Cu^{2+} and maintain it in redox-state. On the other hand, the solution treated with Ber showed 86% increase in fluorescence indicating its minimal interference in the redox cycle of Cu^{2+} and generation of $\cdot\text{OH}$ radicals (Figure 17a). Therefore, Ber-D prevented the generation of hydroxyl radicals by binding and suppressing the redox cycle of Cu^{2+} . $\text{A}\beta_{42}\text{-Cu}^{2+}$ generates hydrogen peroxide (H_2O_2) that subsequently converts to hydroxyl radicals; this scenario of H_2O_2 production *in vitro* was studied by the hydrogen peroxide assay.⁹ To a solution containing $\text{A}\beta_{42}$ (5.1 μM), Cu^{2+} (5 μM), HRP and Amplex Red (10 μM) in PBS buffer (10 mM, pH = 7.4) Ber-D (50 μM) or Ber (50 μM) were added. Then the samples were incubated for 10 min followed by the addition of ascorbate (150 μM), and fluorescence was recorded at 585 nm ($\lambda_{\text{ex}} = 571$ nm) after 1 h. Ber-D exhibited 84% decrease in the H_2O_2 generation, whereas Ber showed negligible effects (Figure 17b). This study confirmed that Ber-D efficiently sequestered the metal ion from the $\text{A}\beta_{42}\text{-Cu}^{2+}$ and transformed it into a redox-dormant state thereby preventing the generation of ROS.

4.20 DNA damage and protein oxidation

The ROS generated by $\text{A}\beta\text{-Cu}^{2+}$ triggers neuronal toxicity through pathways that include DNA damage and protein oxidations among others.⁴⁸ A simple *in vitro* experiment was performed to demonstrate the ability of Ber-D to prevent DNA damage from ROS generated by the $\text{A}\beta_{42}\text{-Cu}^{2+}$ complex. Plasmid DNA (pDNA) was used as a model for cellular DNA to assess the ROS-induced damage. DNA was subjected to *in-situ* generated ROS in the absence and presence of Ber-D followed by the analysis of structural stability and integrity of DNA through agarose gel electrophoresis. To PBS (10 mM, pH = 7.4) solutions containing Cu^{2+} (5 μM), pDNA (pBR322, 2 $\mu\text{g/mL}$) and Ber-D or Ber (25 μM), ascorbate (150 μM) was added and the samples were incubated for 3 min at 37 °C followed by agarose gel electrophoresis (Figure 17c). The presence

of Ber-D showed protection of pDNA (as indicated by the intact and stable supercoiled band) in the presence of copper ascorbate system, whereas Ber failed to prevent the pDNA damage (as indicated by disappearance of a supercoiled band of pDNA) (Figure 17c). This is a clear indication that Ber-D binds to Cu^{2+} and prevent the production of hydroxyl radicals, whereas Ber is not capable of complexing Cu^{2+} and as a consequence it failed to prevent the pDNA damage. The ROS generated by $\text{A}\beta$ aggregates in the presence of Cu^{2+} cause oxidation of biomacromolecules such as proteins, which further leads to the neuronal death. The protein oxidation leads to the formation of protein carbonyls and the measurement of carbonyls give reasonable approximation of the extent of oxidation. The protein carbonyls can be measured and quantified using 2,4-dinitrophenylhydrazine (DNPH).²⁶ DNPH reacts with carbonyls in protein backbone to form hydrazones which can be detected spectroscopically by monitoring the absorption intensity at 370 nm. We performed a simplified version of protein oxidation, where the $\text{Cu}^{2+}+\text{H}_2\text{O}_2$ system was used to generate ROS and bovine serum albumin (BSA) employed as a protein target to assess the extent of oxidation. Ber-D or Ber (1 mM) were independently added to PBS buffer (pH = 7.4, 10 mM) solutions containing BSA (1mg/mL), Cu^{2+} (0.1 mM) and H_2O_2 (2.5 mM) (Figure 17d). The samples were incubated at 37 °C for 24 h in the dark followed by the addition of DNPH (5 mM). After incubation of the samples for 10 min absorption was recorded at 370 nm to determine the percentage of protein oxidation. In the presence of Ber, protein oxidation of ~64% was observed, whereas Ber-D exhibited a significant reduction in the protein oxidation to 16%. Moreover, Ber-D exhibited a concentration-dependent reduction in the protein oxidation (29% at 0.2 mM and 18% at 0.5 mM). These results clearly suggest that Ber-D with a polyphenolic groups effectively quench the ROS generated and, prevent the DNA damage and protein oxidation.

4.21 Cellular toxicity

After demonstrating the potential of Ber-D as an effective inhibitor of multifaceted A β toxicity (modulating metal dependant and independent A β aggregation and modulating metal dependant and independent ROS generation to reduce oxidative stress) further study was conducted to determine the efficiency of Ber-D in reducing multifaceted A β toxicity in a cellular context. All experiments were performed in low serum media (2% FBS, RPMI) to minimize the interference

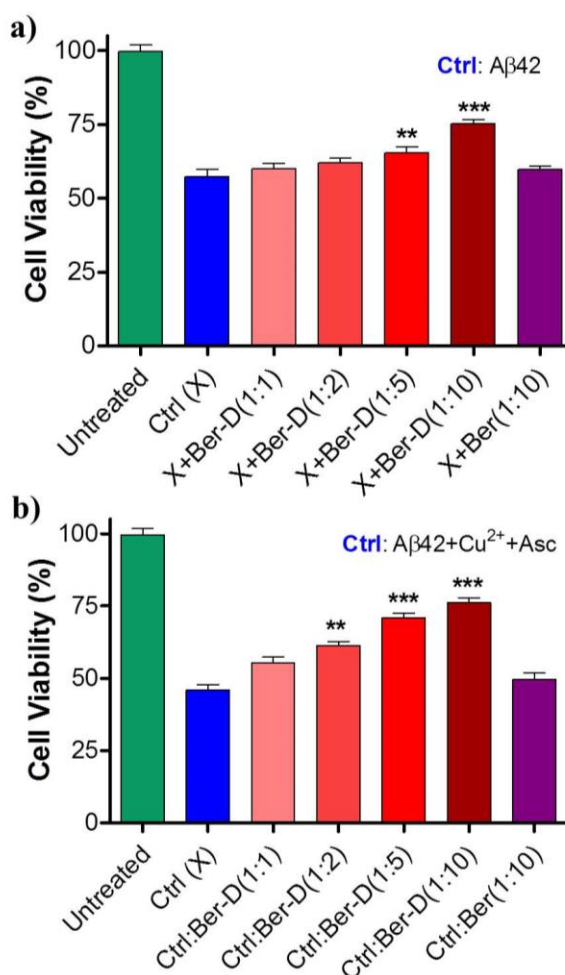


Figure 18. Modulating A β toxicity in PC12 cells a) PC12 cell viability observed after incubation (24 h) with A β 42 (10 μ M), and with Ber-D (10 μ M, 20 μ M, 50 μ M and 100 μ M) or Ber (100 μ M) independently. b) PC12 cell viability observed after incubation (24 h) with A β 42 (10 μ M), Cu²⁺ (10 μ M), ascorbate (200 μ M), and with Ber-D (10 μ M, 20 μ M, 50 μ M and 100 μ M) or Ber (100 μ M) independently. Each experiment was repeated three times (n = 3), and error bars represent the standard deviation (SD).

of BSA. The ability of Ber-D to rescue PC12 cells from toxicity induced from A β 42 was studied through MTT assay. A β 42 (10 μ M) treated PC12 cells were incubated independently with Ber (100 μ M) and Ber-D (100 μ M). The A β 42 (10 μ M) alone exhibited 43% reduction in cell viability (57% viable cells) compared with the untreated cells showing 100% cell viability (Figure 18a). The PC12 cells treated with Ber (100 μ M) showed negligible protection (59% viable cells) from A β 42 toxicity. Remarkably, Ber-D (100 μ M) treated cells showed significant improvement in the cell viability (75%) from A β 42 induced toxicity. Ber-D exhibited concentration-dependent improvement in cellular viability (10 μ M - 59%, 20 μ M - 61% and 50 μ M - 65%). Next, we evaluated the ability of Ber-D to rescue PC12 cells from toxicity induced from the A β 42-Cu²⁺ complex. A β 42-Cu²⁺ (10 μ M) with ascorbate (200 μ M) treated PC12 cells were incubated independently with Ber (100 μ M) and Ber-D (100 μ M). A β 42-Cu²⁺ (10 μ M) with ascorbate (200 μ M) exhibited 55% reduction in cell viability (45% viable cells) compared to untreated cells showing 100% cell viability (Figure 18b). The PC12 cells treated with Ber showed negligible protection from the A β 42-Cu²⁺ toxicity. Interestingly, Ber-D (100 μ M) treated cells showed significant improvement in cell viability from A β 42-Cu²⁺ induced toxicity (76% viability). Ber-D exhibited significant protection of cells from A β 42-Cu²⁺ toxicity even at relatively low concentrations (61% at 20 μ M: and 71% at 50 μ M). These results signify that Ber-D can effectively protect the neuronal cells from both metal-dependent and independent A β 42 toxicity. These results are in good agreement with the *in vitro* antioxidant assays. Overall, the nontoxic and multifunctional nature of Ber-D, inhibition of A β aggregation and prevention metal-induced toxicity, makes it a potential modulator of multifaceted A β toxicity.

4.22 Molecular pathway for protection of neuronal cell from A β toxicity

The A β -mediated mitochondrial dysfunctioning in the neuronal cells is an important pathway in

contributing to multifaceted toxicity in AD.²⁹ The preliminary changes observed during mitochondrial damage is the reduction in mitochondrial membrane potential (MMP) and generation of ROS.³² The changes in MMP can be directly correlated to the actual functioning of the mitochondria.⁴⁹ Thus, the effectiveness of Ber-D in preventing the mitochondrial damage caused by the A β in PC12 cells was evaluated by measuring the MMP using Rhodamine 123 (Rho123). PC12 cells treated with A β 42 (10 μ M) were incubated independently with Ber-D or Ber (50 μ M) for 12 h, followed by the addition of Rho123 (500 nM) and monitoring fluorescence emission at 534 nm (Figure 19a). The cells treated with A β 42 showed ~28% reduction in the MMP compared to untreated cells (100%). The cells incubated with Ber showed significant protection from A β 42 toxicity with MMP of 44%. Interestingly, Ber-D treated cells (affected by A β 42 toxicity) showed MMP of 75% (increase of 47% in MMP compared to the Ber

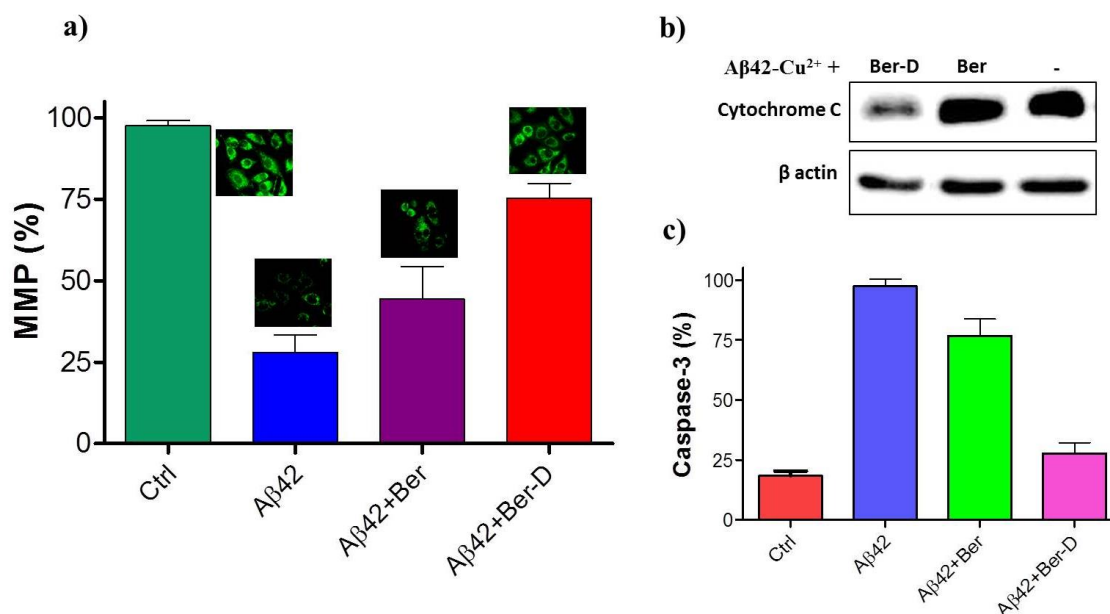


Figure 19. a) Quantification of MMP through Rho123 fluorescence at 534 nm (λ_{ex} = 511 nm) in PC12 cells treated with Rho123, observed after incubation (12 h) with A β 42 (10 μ M) and Ber-D or Ber (50 μ M). Inset: corresponding microscopic images b) Western blot analysis of cytochrome C levels observed in PC 12 cells treated with A β 42 (10 μ M) and Ber-D or Ber (50 μ M). c) Caspase-3 levels observed in PC 12 cells treated with A β 42 (10 μ M) and Ber-D or Ber (50 μ M). Each experiment was repeated three times ($n = 3$), and error bars represent the standard deviation (SD).

treated cells) indicating that Ber-D can prevent the interaction of A β with mitochondria and hence prevent its damage. The prevention of mitochondrial damage from A β peptide by Ber-D could be the possible mechanistic pathway for the observed protection of neuronal cells. To further strengthen our assumption we have measured the cytochrome C levels of PC12 cells treated with A β 42 in presence and absence of Ber-D or Ber (50 μ M) through immunoblotting. A significant enhancement of the cytochrome C release in the cytosol was observed in cells treated with A β 42 (10 μ M) (Figure 19b). Interestingly, Ber-D treated cells showed a significant decrease in the levels of cytochrome C in the cytosol. However, Ber (50 μ M) showed cytochrome C levels comparable to A β 42 treated cells, indicating the protective nature of Ber-D (50 μ M) over Ber from A β 42 toxicity possibly through prevention of mitochondrial damage. The activation of various caspases is involved during mitochondrial damage leading to apoptotic cell death.^{49, 50} Caspases play a major role in activating and regulating the apoptosis process. A β 42 treated cells exhibited increased activity of caspase 3 (Figure 19c). In contrast, cells treated with Ber-D (50 μ M) showed a significant decrease in the caspase-3 activity (27%) compared to cells treated with A β 42 (10 μ M, 97%). The decrease in the levels cytochrome C and caspase-3 by Ber-D in A β 42-Cu²⁺ treated cells, clearly imply that Ber-D prevent the mitochondria damage and this could be the possible mechanistic pathway for protection of cells from A β toxicity.

4.23 Conclusion

In summary, we successfully prepared a non-toxic synthetic analogue of Ber, viz., Ber-D to efficiently target multifaceted A β toxicity of AD. Ber-D inhibited metal independent and dependent A β aggregation (ThT binding assay and dot blot analysis). DPPH, ABTS, ORAC and nitric oxide assay clearly showed that Ber-D is an efficient antioxidant. Further, Ber-D efficiently prevented ROS generated by Cu²⁺ in reduced condition and from A β 42-Cu²⁺ complex.

Furthermore, the DNA and protein damage induced by the H_2O_2 and Cu^{2+} was efficiently protected by Ber-D. Ber-D exhibited high cellular viability at elevated concentrations when compared to Ber. *In vitro* inhibition of multifaceted $\text{A}\beta$ toxicity was further verified *in cellulo* conditions. The PC 12 cells were rescued from $\text{A}\beta_{42}\text{-Cu}^{2+}$ induced multifaceted toxicity by Ber-D. The protective nature of Ber-D to PC12 from $\text{A}\beta$ toxicity is possibly through its interaction and prevention of $\text{A}\beta$ aggregation, quenching ROS generation and antioxidant effect and averting mitochondrial damage. Overall, the multifunctional properties suggest that Ber-D is a potential candidate to develop therapeutic agents for treating AD.

4.24 Experimental methods

General methods. All reagents and solvents were procured from Sigma Aldrich and used without any further purification unless mentioned. All the air and moisture sensitive reactions were carried out under argon or N_2 atmosphere. Absorption and fluorescence spectra were recorded with Agilent Cary series UV-Vis-NIR absorption and Agilent Cary eclipse fluorescence spectrophotometers, respectively. Data was plotted and analyzed in origin 8.5 or prism 5. ^1H NMR and ^{13}C NMR were performed using Bruker AV-400 spectrometer with chemical shifts reported in parts per million (tetramethylsilane used as internal standard). Mass spectra were obtained from Agilent 6538 UHD HRMS/Q-TOF high-resolution spectrometer.

4.24.1 Synthesis of HMMs derivatives. To a solution of Clq or 5-chloroquinolin-8-ol or quinolin-8-ol (1 mmol) in acetone K_2CO_3 (3 mmol) and tert-butyl 2-bromoethylcarbamate (1.2 mmol) was added refluxed ($56\text{ }^\circ\text{C}$) for 6h. The reaction mixture was filtered and the filtrate was dried to obtain the product. The crude product was treated with TFA:DCM (1:1) for 3h. Then ice-cold ether was added to the reaction mixture to obtain 2-(quinoline-8-yloxy)ethanamine derivatives. To a solution of 2-(quinolin-8-yloxy)ethanamine derivatives (1 mmol) in DMF,

HBTU (1.2 mmol) followed by HOBt (1.2 mmol) was added at 0 °C under argon atmosphere. The reaction mixture was stirred till a clear solution was obtained, and then 3,4,5-trihydroxybenzoic acid was added (1.1 mmol). Using a syringe DIPEA (3 mmol) was slowly added in portions to the reaction mixture, and the reaction was stirred for 5–6 h at room temperature. The reaction was monitored by thin layer chromatography, on completion of the reaction and the reaction mixture was poured into water. The organic layer was separated, dried (Na_2SO_4) and evacuated. The crude product was purified by silica gel column chromatography.

Synthesis of TGR88. Eluted with 5% methanol in chloroform and obtained as light brownish powder; yield 53%. ^1H NMR ($\text{DMSO } d_6$, 400 MHz) δ 8.56-8.98 (m, 1H), 8.35-8.33 (m, 1H), 7.77-7.70 (m, 2H), 7.33-7.30 (m, 1H), 6.86 (s, 2H), 4.33-4.30 (m, 5H), 3.70-3.66 (m, 2H); ^{13}C NMR ($\text{DMSO } d_6$, 100 MHz) δ 166.6, 153.4, 149.5, 145.4, 139.7, 136.3, 132.7, 127, 126.2, 124.5, 123, 120.9, 110.4, 106.7, 67.3; HRMS (ESI-MS): found 500.9690, calcd. for $\text{C}_{18}\text{H}_{15}\text{ClIN}_2\text{O}_5$ $[\text{M}+\text{H}]^+$ $m/z = 500.9714$.

Synthesis of TGR87. Eluted with 3.5% methanol in chloroform and obtained as yellowish powder; yield 48%. ^1H NMR (CD_3OD , 400 MHz) δ 9.06-9.05 (m, 1H), 8.93-8.90 (m, 1H), 7.92-7.89 (m, 1H), 7.77-7.75 (m, 1H), 6.91 (s, 2H), 4.42 (t, $J = 5.2$ Hz, 2H), 3.96 (t, $J = 5.2$ Hz, 2H); ^{13}C NMR (CD_3OD , 100 MHz) δ 170.6, 153.1, 149.2, 146.7, 138, 129.3, 128.6, 125.9, 124.2, 123.6, 111.8, 107.9, 69.8, 40.8; HRMS (ESI-MS): found 375.0728, calcd. for $\text{C}_{18}\text{H}_{16}\text{ClN}_2\text{O}_5$ $[\text{M}+\text{H}]^+$ $m/z = 375.0748$.

Synthesis of TGR86. Eluted with 3.5% methanol in chloroform and obtained as yellowish powder; yield 62%. ^1H NMR ($\text{DMSO } d_6$, 400 MHz) δ 8.805 (s, 1H), 8.32-8.30 (m, 1H), 7.55-7.50 (m, 3H), 7.29-7.27 (m, 1H), 7.23 (s, 2H), 4.35 (t, $J = 12$ Hz, 2H), 3.78-3.74 (m, 2H); ^{13}C NMR ($\text{DMSO } d_6$, 100 MHz) δ 166, 154.2, 148.8, 139.9, 139.7, 135.8, 129.4, 129, 126.8, 121.8,

119.9, 109.9, 104.8, 66.9; HRMS (ESI-MS): found 341.1118, calcd. for $C_{18}H_{17}N_2O_5$ $[M+H]^+$ m/z = 341.1137.

4.24.2 Synthesis of NMI derivatives

4.24.2.1 Synthesis of 4-((4-*N,N* dimethylaniline)ethynyl)-1,8-naphthalic anhydride (1). To a solution of 4-bromo-1,8-naphthalic anhydride (200 mg, 0.72 mmol) in a mixture of DMF/Et₃N (1 : 1) under argon, Pd(PPh₃)₄ (27 mg, 0.023 mmol), sodium ascorbate (10 mg, 50 μmol), copper (II) sulfate (2 mg, 8 μmol) and 4-ethynylanisole (93.6 μL, 0.72 mmol) were added. The reaction mixture was stirred for 4 h at 80 °C. After completion of the reaction monitored by TLC, the reaction mixture was extracted with ethyl acetate, washed with NH₄Cl and brine, and dried over Na₂SO₄. The product was dissolved in ethyl acetate, precipitated with diethyl ether and collected by filtration. The compound was obtained as dark red coloured solid in 68% yield. ¹H NMR (CDCl₃, 400 MHz) δ 8.65 (d, 2H, *J* = 6.4), 8.64 (d, 2H, *J* = 4.2), 8.55 (d, 2H, *J* = 8), 7.92 (d, 2H, *J* = 7.6), 7.89 (t, 2H, *J* = 15), 7.55 (d, 2H, *J* = 4.2), 6.73 (d, 2H, *J* = 6.4), 3.06 (s, 6H); ¹³C NMR (CDCl₃, 100 MHz) δ 163.8, 151, 134.2, 133.6, 132.7, 131.5, 130.7, 130.4, 130, 127.4, 116.5, 111.7, 108, 40.1; HRMS (ESI-MS): found 342.1145, calcd. for $C_{22}H_{16}NO_3$ $[M+H]^+$ m/z = 342.1112.

4.24.2.2 Synthesis of TGR63. To a solution of 1 (200 mg, 0.58 mmol) dispersed in isopropanol (IPA) DIPEA (31 mL, 1.7 mmol) and 2-amino-*N,N,N*-trimethylethanaminium (60 mg, 0.58 mmol) was added and refluxed (80 °C) for 6 h. the reaction mixture was extracted with ethyl acetate, washed with brine, and dried over Na₂SO₄. The crude product was purified using column chromatography on silica gel using 1% MeOH in CHCl₃ as an eluent to afford a red coloured solid in good yield (75%). ¹H NMR (DMSO *d*₆, 400 MHz) δ 8.60 (d, 1H, *J* = 0.8), 8.58 (d, 1H, *J* = 1.2), 8.48 (d, 1H, *J* = 7.6), 8.03 (d, 2H, *J* = 4.4), 8.01 (t, 2H, *J* = 4.8), 7.61 (d, 2H, *J* = 2), 6.80 (d, 2H, *J* = 8.8), 4.48 (t, 2H, *J* = 13.6), 3.65 (t, 2H, *J* = 14.8), 3.21 (s, 9H), 3.01 (s, 6H); ¹³C

NMR (DMSO d_6 , 100 MHz) δ 163.3, 163, 158, 150.9, 133.2, 132.5, 131.3, 130.6, 130.4, 129.7, 128, 127.6, 122.4, 120.5, 111.8, 106.9, 102.3, 85.9, 52.4, 33.6; HRMS (ESI-MS): found 426.2176, calcd. for $C_{27}H_{28}N_3O_2$ $[M]^+$ $m/z = 426.2176$.

4.24.2.3 Synthesis of TGR64. To a solution of 1 (200 mg, 0.58 mmol) dispersed in isopropanol DIPEA (31 μ L, 1.7 mmol) and tert-butyl 2-aminoethylcarbamate (39 mg, 0.58 mmol) was added and refluxed (80 °C) for 6 h. the reaction mixture was extracted with ethyl acetate, washed with brine, and dried over Na_2SO_4 . The crude product was purified using column chromatography on silica gel using 0.25% MeOH in $CHCl_3$ as an eluent to afford a red coloured solid. Then the compound is deprotected using TFA (95% TFA, 4.5% DCM and 0.5% TIPS) and precipitate to obtain pure product in good yield (68%). 1H NMR (DMSO d_6 , 400 MHz) δ 8.77 (d, 1H, $J = 1.8$), 8.56 (d, 1H, $J = 3.6$), 8.45 (d, 1H, $J = 3.8$), 8.00 (d, 2H, $J = 3$), 7.97 (d, 2H, $J = 8.8$), 7.59 (d, 2H, $J = 3.3$), 6.74 (d, 2H, $J = 3.8$), 4.33 (t, 2H, $J = 11.6$), 3.17 (s, 2H), 3.01 (s, 6H); ^{13}C NMR (DMSO d_6 , 100 MHz) δ 163.8, 163.5, 150.8, 133.2, 132.2, 131.1, 130.5, 130.1, 129.7, 127.9, 127.7, 122.7, 120.8, 111.8, 107, 102, 85, 37.6, 37.5; HRMS (ESI-MS): found 383.1767, calcd. for $C_{24}H_{21}N_3O_2$ $[M]^+$ $m/z = 383.1634$.

4.24.2.4 Synthesis of TGR65. To a solution of 1 (200 mg, 0.58 mmol) dispersed in isopropanol DIPEA (31 μ L, 1.7 mmol) and 2-(2-aminoethoxy)ethanol (22 mL, 0.58 mmol) was added and refluxed (80 °C) for 6 h. the reaction mixture was extracted with ethyl acetate, washed with brine, and dried over Na_2SO_4 . The crude product was purified using column chromatography on silica gel $CHCl_3$ as an eluent to afford a red coloured solid in good yield (72%). 1H NMR (DMSO d_6 , 400 MHz) δ 8.76 (d, 1H, $J = 8.4$), 8.55 (d, 1H, $J = 7.2$), 8.43 (d, 1H, $J = 7.6$), 7.98 (d, 2H, $J = 8$), 7.95 (t, 2H, $J = 1.6$), 7.59 (d, 2H, $J = 8.8$), 6.79 (d, 2H, $J = 8.8$), 4.25 (t, 2H, $J = 12.8$), 3.67 (t, 2H, $J = 12.8$), 3.47 (s, 4H), 3.31 (s, 4H), 3.00 (s, 6H); ^{13}C NMR (DMSO d_6 , 100 MHz) 163.2,

162.9, 133.2, 132.1, 131.1, 130.5, 130.2, 129.7, 127.9, 127.6, 127.5, 122.4, 120.6, 111.8, 107, 101.8, 85, 72, 66.8, 60.1, 28.9; HRMS (ESI-MS): found 429.1803, calcd. for $C_{26}H_{25}N_2O_4$ $[M+H]^+$ $m/z = 429.1814$.

4.24.2.5 Synthesis of TGR66. To a solution of naphthalic anhydride (114 mg, 0.58 mmol) dispersed in isopropanol DIPEA (31 μ L, 1.7 mmol) and 2-amino-*N,N,N*-trimethylethanaminium (60 mg, 0.58 mmol) was added and refluxed (80 °C) for 6 h. the reaction mixture was extracted with $CHCl_3$, washed with brine, and dried over Na_2SO_4 . The crude product was purified using column chromatography on silica gel using 2% MeOH in $CHCl_3$ as an eluent to afford a white solid in good yield (88%). 1H NMR (DMSO d_6 , 400 MHz) δ 8.54-8.50 (m, 4H), 7.93-7.89 (m, 2H), 4.49 (t, 2H, $J = 14.4$), 3.66 (t, 2H, $J = 14.4$), 3.23 (s, 9H); ^{13}C NMR (DMSO d_6 , 100 MHz) δ 163.4, 134.7, 131.3, 130.9, 127.4, 127.3, 121, 89, 61.9, 52.5, 33.6; HRMS (ESI-MS): found 283.1439, calcd. for $C_{17}H_{19}N_2O_2$ $[M]^+$ $m/z = 283.1441$.

4.24.2.6 Synthesis of TGR67. To a solution of 4-dimethylamine-1,8-naphthalic anhydride (139 mg, 0.58 mmol) dispersed in isopropanol DIPEA (31 μ L, 1.7 mmol) and 2-amino-*N,N,N*-trimethylethanaminium (60 mg, 0.58 mmol) was added and refluxed (80 °C) for 6 h. the reaction mixture was extracted with $CHCl_3$, washed with brine, and dried over Na_2SO_4 . The crude product was purified using column chromatography on silica gel using 3.5% MeOH in $CHCl_3$ as an eluent to afford a yellow solid in appropriate yield (54%). 1H NMR (DMSO d_6 , 400 MHz) δ 8.50 (d, 1H, $J = 6.4$), 8.49 (d, 1H, $J = 4.2$), 8.38 (d, 1H, $J = 8.4$), 7.80 (d, 1H, $J = 7.2$), 7.78 (d, 1H, $J = 7.2$), 7.24 (d, 1H, $J = 4.2$), 4.96 (t, 2H, $J = 14$), 3.64 (t, 2H, $J = 14$), 3.20 (s, 9H), 3.12 (s, 6H); ^{13}C NMR (DMSO d_6 , 100 MHz) 163.7, 162.9, 156.9, 132.6, 132.1, 130.8, 124.9, 124, 122, 112.8, 112.5, 52.4, 44.3, 33.4; HRMS (ESI-MS): found 326.1864, calcd. for $C_{19}H_{24}N_3O_2$ $[M]^+$ $m/z = 326.1863$.

4.24.2.7 Synthesis of TGR68. To a solution of 4-(benzylethynyl)-1,8-naphthalic anhydride (172 mg, 0.58 mmol) dispersed in isopropanol DIPEA (31 μ L, 1.7 mmol) and 2-amino-N,N,N-trimethylethanaminium (60 mg, 0.58 mmol) was added and refluxed for 6 h. the reaction mixture was extracted with CHCl_3 , washed with brine, and dried over Na_2SO_4 . The crude product was purified using column chromatography on silica gel using in CHCl_3 as an eluent to afford a yellow solid in good yield (74%).

^1H NMR ($\text{DMSO } d_6$, 400 MHz) δ 8.83 (d, 1H, $J = 8.4$), 8.61 (d, 1H, $J = 7.2$), 8.51 (d, 1H, $J = 7.6$), 8.13 (d, 1H, $J = 7.6$), 8.05 (t, 1H, $J = 15.6$), 7.81-7.78 (m, 2H), 7.54-7.52 (m, 3H), 4.49 (t, 2H, $J = 14.4$), 3.67 (t, 2H, $J = 14.4$), 3.24 (s, 9H); ^{13}C NMR ($\text{DMSO } d_6$, 100 MHz) 163.2, 162.9, 132.3, 131.9, 131.4, 131, 130.9, 130.2, 129.9, 128.9, 128.4, 127.4,5, 126.5, 122.5, 121.8, 121.2, 99, 86.0, 61.9, 54.8, 52.4, 33.7; HRMS (ESI-MS): found 384.1693, calcd. for $\text{C}_{25}\text{H}_{23}\text{N}_2\text{O}_2$ $[\text{M}]^+$ $m/z = 384.1854$.

4.24.3 Preparation of Ber-D. To a solution of Berberine hydrochloride (1g, 2.6 mmol) in xylene (20 mL), boron tribromide (13.44 mL, 78 mmol) was added and refluxed at 100 $^\circ\text{C}$. The reaction mixture was washed with dichloromethane for 3 times, followed by dropwise addition of ice cold water, then stir the solution for 1h. The solution was filtered, and the precipitate was washed with water dried, at 40 $^\circ\text{C}$ in a vacuum oven for 4h to obtain Ber-D in 69.46% yield. ^1H NMR ($\text{DMSO } d_6$, 400 MHz) δ 10.63 (b, 1H), 9.96 (b, 1H), 9.74 (s, 1H), 9.25 (b, 1H), 8.59 (s, 1H), 7.78-7.45 (m, 3H), 6.79 (s, 1H), 4.85 (t, 2H, $J = 6$), 3.10 (t, 2H, $J = 6$); ^{13}C NMR ($\text{DMSO } d_6$, 100 MHz) δ 148.6, 145.4, 144.5, 143.2, 141.2, 136.6, 132.2, 129.8, 126.8, 118.8, 118.8, 118.1, 118.1, 118.0, 114.8, 112.5, 55.1, 25.8; HRMS (ESI-MS): found 296.1001, calcd. for $\text{C}_{17}\text{H}_{14}\text{NO}_4$ $[\text{M}]^+$ $m/z = 296.1023$.

4.24.4 A β inhibition assays. A β 42 peptide (0.25 mg) (Merck, calbiochem) was dissolved in the

hexafluoro-2-propanol (HFIP, 0.2 mL) and incubated at room temperature for 1 h. HFIP was then removed by a flow of nitrogen and further dried under vacuum. HFIP-treated A β 42 was then dissolved in DMSO to a final concentration of 1 mM and diluted to 200 μ M with 10 mM PBS (pH 7.4). The solution was incubated at 37 °C for 48 h with gentle and constant shaking. The formation of A β 42 fibrils was confirmed by Thioflavin T (ThT) assay. For the oligomer preparation, A β 42 was dissolved in DMSO to a final concentration of 1 mM and diluted to 100 μ M in PBS buffer (10 mM, pH 7.4). The solution was incubated at 37 °C for 1 h, after which the sample was incubated for 24 h at 4 °C for 1 h. The obtained sample was centrifuged, and the supernatant with oligomers was used for further experiments.

4.24.5 α -Synuclein fibril inhibition assay. All the NMA derivatives (TGR63, TGR64 and TGR65) were dissolved in TBS buffer (pH 7.4). Then they are added individually to a freshly prepared α -Syn (20 μ M) sample in TBS buffer. Then the solution is incubated at 37 °C for 3-5 days with the constant shaking of 150 rpm. The fibrils remaining intact were assayed using ThT assay.

4.24.6 Fluorescence spectroscopy. Fluorescence spectral measurements were carried out using Cary eclipse fluorescence spectrophotometer (Agilent technologies). ThT was added at the end of the experiment, and its fluorescence was recorded with excitation and emission wavelengths set at 450 and 483 nm, respectively. ThT concentration of 5-10 μ M was used for amyloid inhibition assay based on the A β 42 fibrillar concentration.

4.24.7 Dot blot analysis. PVDF membranes (Sigma Aldrich) were activated by incubating them in methanol solution for 5 min followed by washing with 10 mM PBS buffer (3X). Samples were spotted on the membranes (in triplicate), and non-specific sites were blocked by soaking in 5% BSA in PBS buffer and skim milk (0.5-1 hour, RT). Then membranes were incubated with either

primary antibody A11 (1:3000) for oligomer or Anti-beta-amyloid 1-42 antibody (Merck millipore) for A β 42 fibrillar aggregates at 4 °C for overnight and then washed with PBS buffer (3 x 5 min). These membranes were further incubated with the anti-mouse secondary antibody (1:10000) conjugated with horseradish peroxidase (HRP) for 30 min at RT. These membranes were washed with PBS buffer (3 x 5 min), incubated with enhanced chemiluminescence (ECL) reagent for 1 min and recorded the chemiluminescence in SYNGENE G-box. The signals from the unknown samples were compared to that of standard and concentration was estimated

4.24.8 Molecular docking of Clq derivatives. Docking study was carried out using Autodock vina.⁵¹ All the ligand structures were energy minimized with MMFF94 force field using Avogadro and Gasteiger partial charges were added using Autodock tools.⁵² The NMR structure for A β 42 fibril has been retrieved from RCSB PDB data bank (PDB ID 5KK3).³⁶ Polar Hydrogen added to the protein using MGT autodock tools. Precise Docking has been done in each part of the protein to know the most probable binding sites. The grid dimension has been assigned to 25x30x30 Å. The Lamarckian Genetic Algorithm was used for the process. All other parameters were set as default. Docking Results were analysed using Discovery Studio 3.5. The docking poses were captured using VMD tools.

4.24.9 Molecular docking for Ber-D. The molecular structure of Ber and Ber-D compounds were built using modern software and optimized at B3LYP/6-31G(d) by employing gaussian09 software.^X Further the frequency calculations were carried out to assure that the optimized structure corresponds to minimum energy. Molecular docking calculations have been carried out for both the compounds with monomeric and fibrillar structures of amyloid beta proteins using autodock software.^x In particular, the structure of the monomer of amyloid beta protein is from NMR measurements as reported (The PDB reference ID is 1Z0Q) while the protofibril structure

used is based on the solid-state NMR structure with reference ID 2BEG.X For the docking both conformers 1 and 8 of the 10 reported NMR structures were used since the conformer 8 was necessary to locate an additional core site for the molecules investigated. For the monomer, the docking box dimensions were set to 120, 90, 170 Å while for the protofibril the dimensions were 160, 110, 100 Å. In particular, the grid box dimensions were chosen so that even the surface binding sites for Ber, Ber-D can be identified. The binding affinities for the most stable complex structures were used for further analysis. The binding mode and pose as in the most stable complex structure has been used to prepare the input for the subsequent molecular dynamics simulations for these complexes. In the case of the fibril, there are many possible binding sites for the molecules. In particular, we have reported at least three high-affinity binding sites, and two surface sites in the protofibril and our previous studies showed that core-2 site is the site associated with larger binding affinity.

4.24.10 Ascorbate assay. To a solution of Cu^{2+} , 3-CCA and the Clq or HMMs or Ber-D in PBS buffer (10 mM, pH = 7.4), ascorbate was added and incubated at 37 °C. Non-fluorescent dye 3-CCA reacts with $\cdot\text{OH}$ generated by redox cycling of Cu^{2+} to form a fluorescent 7-OH-CCA ($\lambda_{\text{ex}}=395$ nm and $\lambda_{\text{em}}=452$ nm). The fluorescence intensity at 452 nm was measured using microplate reader.²³

4.24.11 Hydrogen peroxide assay. To a solution of A β 16, Cu^{2+} , 3-CCA and Clq or HMMs or Ber-D, in PBS (10 mM, pH = 7.4) ascorbate was added, and the sample was incubated at 37 °C for 90 min. Then 7-OH-CCA ($\lambda_{\text{ex}}=395$ nm and $\lambda_{\text{em}}=452$ nm) emission was measured using microplate reader.

4.24.12 DPPH assay. DPPH stock in methanol was added into transparent 96-well microplate and the compound stock solution made in methanol was added. The final concentrations of DPPH and HMMs in the assays were 50 and 10 μM , respectively. The microplate was incubated

in the dark at 37 °C for 30 min. The decrease in DPPH absorption at 517 nm was measured in a microplate reader at 30 min. The percent antioxidant capacity was calculated using the equation $[(\text{Abs} - \text{Abs C})/\text{Abs}] \times 100$, where Abs is the absorption of the DPPH alone, and Abs C is the absorption measured in the presence of the HMMs or Ber-D.

4.24.13 ABTS assay. ABTS^{•+} radical cation was formed by mixing 3.5 mM ABTS with 1.22 mM H₂O₂ and incubating for 6 h in the dark at RT. The ABTS^{•+} solution was diluted with ethanol to obtain an absorbance of ~0.7 at 734 nm. For the ABTS assay, ABTS^{•+} solution was added to Ber-D or Ber and incubated for 15 min followed by measurement at 735 nm. The AC was determined with respect to the ascorbate.

4.24.14 ORAC assay. The fluorescein (FL) was diluted with 75 mM PBS (pH 7.4) to 0.117 μM. The solution of Trolox was diluted with the same buffer to 3.1, 6.25, 12.5 and 10 μM. 40 mM of 2,2'-azobis(amidinopropane)dihydrochloride (AAPH) was prepared in 75 mM phosphate buffer (pH 7.4). The mixture of the Ber-D or Ber (10 μL) and FL (120 μL, 70 nM) were preincubated for 10 min at 37 °C, and then 60 μL of the AAPH solution was added. The fluorescence was recorded every minute for 120 min ($\lambda_{\text{ex}} = 485 \text{ nm}$, $\lambda_{\text{em}} = 520 \text{ nm}$). A blank using phosphate buffer was also carried out. The antioxidant curves (fluorescence versus time) was normalized to the blank curve. The area under the fluorescence decay curve (AUC) was calculated using following equation:

$$\text{AUC} = 1 + \sum_{i=1}^{i=120} (f_i / f_0)$$

f_0 = initial fluorescence reading at 0 min
 f_i = fluorescence reading at time i

The net AUC was determined by the expression $\text{AUC}_{\text{sample}} - \text{AUC}_{\text{blank}}$. Regression equations between AUC and Trolox concentrations were determined. ORAC-FL value for each Ber-D and Ber was calculated by using the standard curve.

4.24.15 Nitric oxide assay. Sodium nitroprusside (5 mM) in PBS (10 mM, pH = 7.4) was mixed with different concentrations of Ber-D dissolved in ethanol and incubated at 25 °C for 100 min. Sample (0.5 mL) from the incubation solution was removed and diluted with 0.5 mL of Griess reagent (1% sulphanilamide, 2% H₃PO₄ and 0.1% naphthylethylenediamine dihydrochloride). The absorbance of the chromophore formed during diazotization of nitrite with sulphanilamide and subsequent coupling with naphthylethylenediamine was read at 546 nm and referred to the absorbance of standard solutions of nitrite-treated in the same way with Griess reagent.

4.24.16 Protein oxidation. BSA protein (1 mg/Kg), 0.1 mM Cu²⁺, and 2.5 mM H₂O₂ in PBS buffer (pH 7.4, 50 mM) were incubated with Clq or HMMs (10 μM) (TGR86, TGR87, TGR88, Ber and Ber-D) independently for 24 h at 37 °C. The carbonyl groups quantification was performed using DNPH. Briefly, 500 μL of the sample solution was mixed with 500 μL of DNPH (10 mM in 0.5 M H₃PO₄), and incubated in the dark for 15 min. Then 250 μL of trichloroacetic acid (50% w/v) added and incubated at 20 °C. Centrifuge the sample for 5 min, discarded the supernatant without disturbing the pellet and washed with 1 mL (3X) of ethanol/ethylacetate (1/1; v/v). The pellet was re-suspended in 6 M guanidine-HCl and absorbance measured at 370 nm. The percent of protein oxidation was calculated using the equation [(Abs C- Abs)/Abs C] ×100, where Abs is the absorption of the DNPH alone, and Abs C is the absorption measured in the presence of the HMMs or Ber-D.

4.24.17 Cell viability assay. For the MTT assay, PC12 cells were seeded in a 96-well plate at a density of 12,000 cells/well in RPMI (Roswell Park Memorial Institute) medium (Gibco, Invitrogen) with horse serum (HS, 5%), foetal bovine serum (FBS, 10%) and antibiotic (pen-strep, 1 %) at 37 °C in an atmosphere of 5 % CO₂. After 24 h the media in the plates was replaced with low serum media (RPMI, 2% serum) and incubated with freshly prepared Aβ42-

Cu²⁺ (10 μM) in the presence of CLQ or HMMs or NMI derivatives or Ber-D independently with ascorbate (100 μM). Then 5 μL of MTT (10 mg/mL solution in PBS) was added to each well and incubated for 3 h. Subsequently, the media was discarded and 100 μL of 1:1 (DMSO: methanol) solution was added; the reduced MTT was measured by recording absorption at 570 nm (significance was determined by one-way ANOVA from GraphPad prism).

4.24.18 Measuring ROS levels. To study the effects of HMMs on oxidative stress induced Aβ42-Cu²⁺ complex in PC12 cells on treatment with, DCFDA assay was performed. PC12 cells were seeded in a 96-well plate, and after 24 h, media is replaced with RPMI, followed by an incubation for 4 h. Then the cells were washed with PBS and incubated with DCFDA (Invitrogen) for 30 min. The cells were washed and incubated Aβ42-Cu²⁺ (10 μM) in the presence of CLQ or HMMs independently with ascorbate (100 μM) for 40 min at 37 °C. The cells were washed, and the fluorescence intensity was measured at 529 nm ($\lambda_{\text{ex}} = 495 \text{ nm}$) using microplate reader (significance was determined by one-way ANOVA from GraphPad prism).

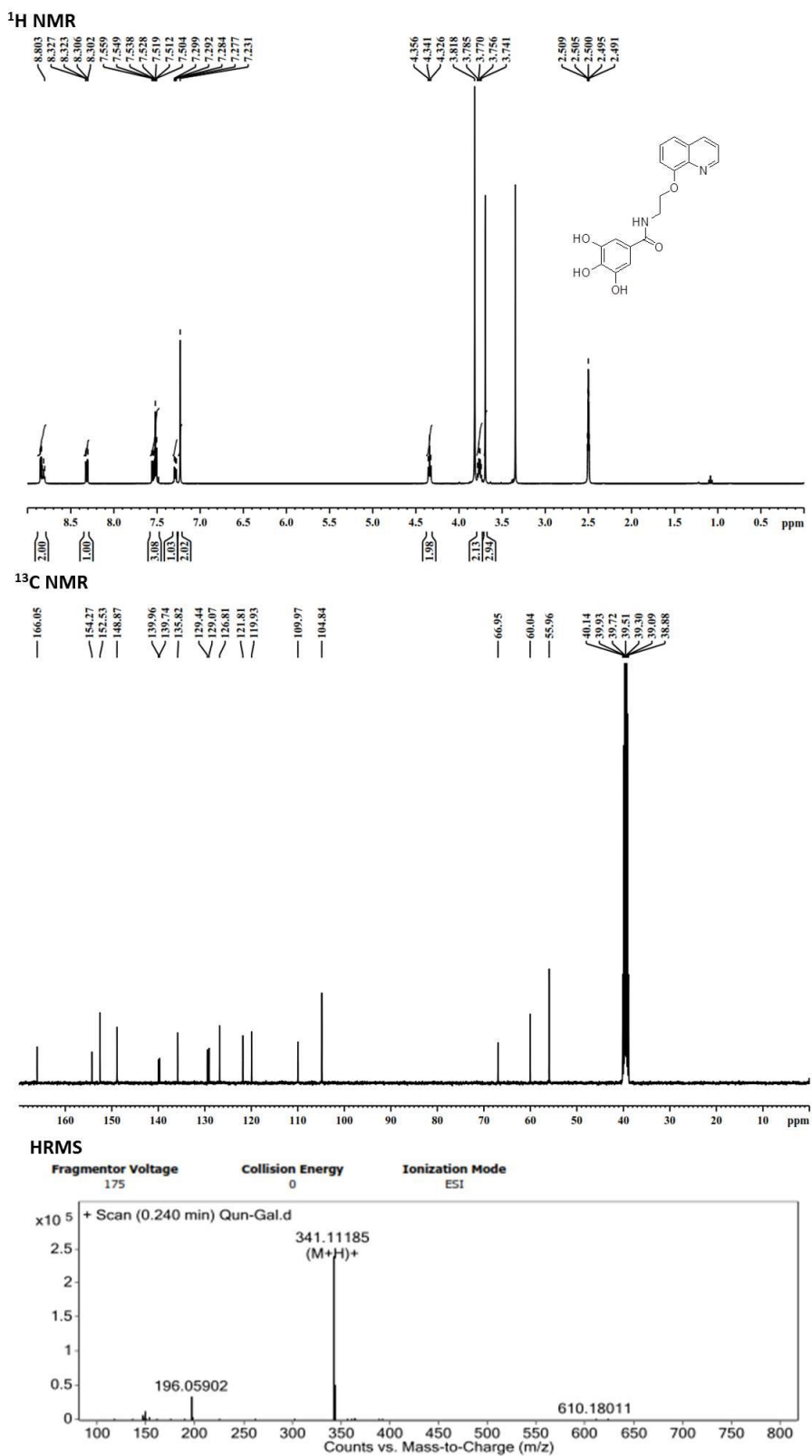
4.24.19 MMP measurement. PC12 cells were seeded in a 96-well plate at a density of 12,000 cells/well in RPMI medium (10% HS, 5% FBS and 1% PS) at 37 °C. After 24 h the media in the plates was replaced with serum-free media and incubated with freshly prepared Aβ42-Cu²⁺ (10 μM) in the presence of Clq or HMMs or Ber-D independently with ascorbate (200 μM) for 12h at 37 °C. Then the cells are washed with PBS buffer and incubated with Rho123 (0.5 μM) for 20 min. Then cells are thoroughly washed with PBS buffer (3X), and fresh RPMI media is added. The PC12 cells are imaged under a fluorescence microscope, and the fluorescence intensity at 534 nm is measured and quantified through microplate reader ($\lambda_{\text{ex}} = 511 \text{ nm}$).

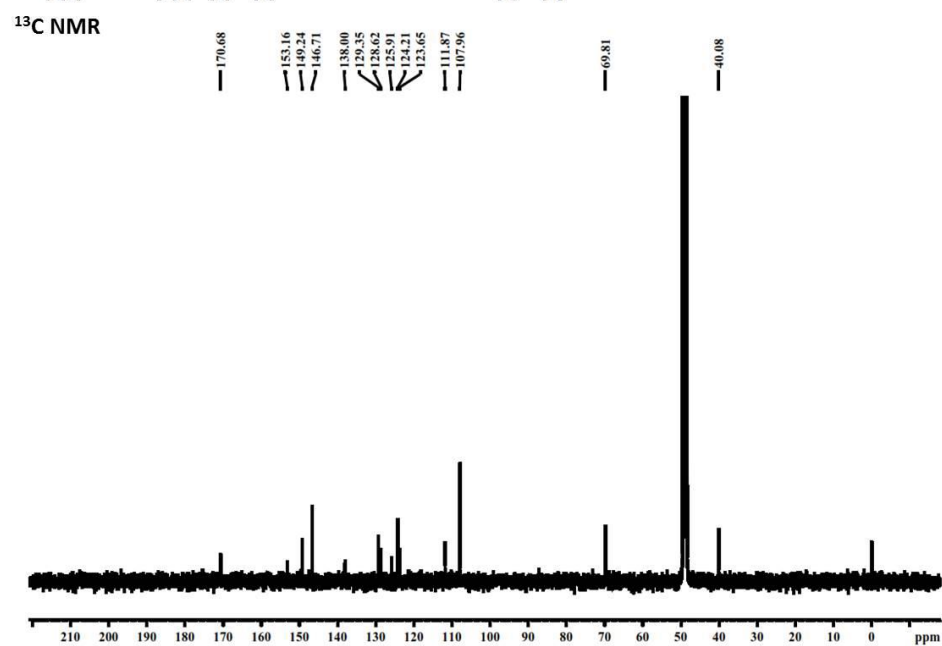
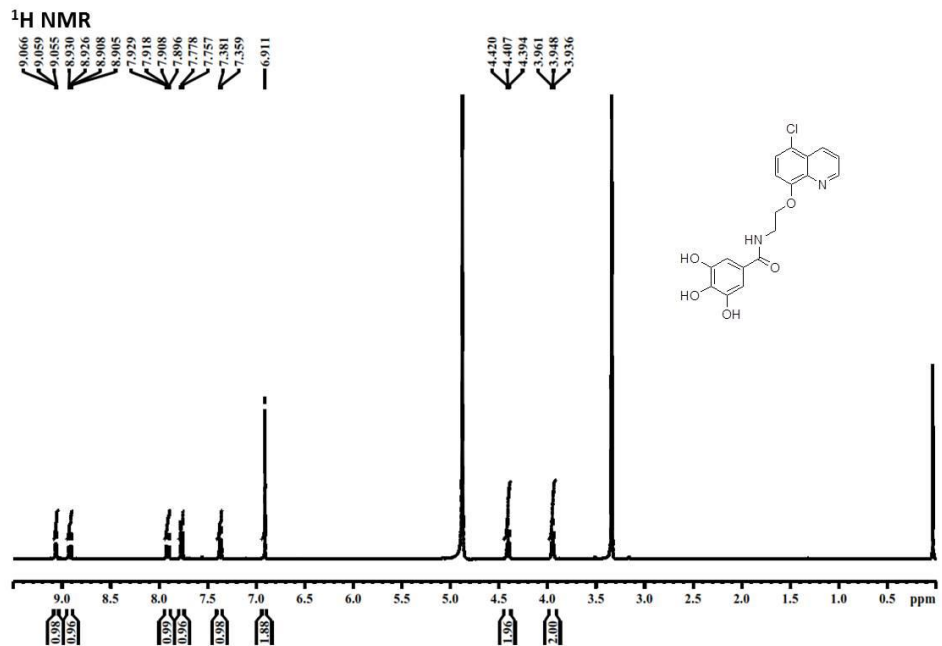
4.24.20 Cytochrome C. PC12 cells were seeded in petridish with RPMI medium (10% HS, 5% FBS and 1% PS) at 37 °C. After 24 h the media in the plates was replaced with serum-free media

and incubated with freshly prepared A β 42-Cu²⁺ (10 μ M) in the presence of Ber-D or Ber independently with ascorbate (200 μ M) for 12 h at 37 °C. The cells were lysed using RIPA buffer with a protease inhibitor. The cell lysate was centrifuged, and the supernatant was collected. The obtained samples were electrophoresed in a sodium dodecyl sulphate-polyacrylamide gel (SDS-PAGE) and then transferred to an activated PVDF membrane. The blot was blocked using BSA, washed, and incubated with cytochrome C antibody (Invitrogen, Thermo fisher) at 1:1000 dilution. The filter was then incubated with a secondary antibody that was conjugated with horseradish peroxidase. Finally, the blot was treated with ECL reagent and imaged under gel documentation system (chemiDoc MP, Bio-Rad).

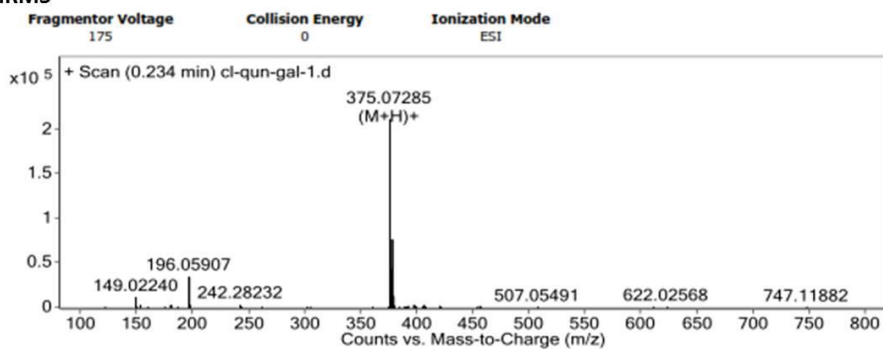
4.24.21 Caspase-3 assay. PC12 cells were seeded in petridish with RPMI medium (10% HS, 5% FBS and 1% PS) at 37 °C. After 24 h the media in the plates was replaced with serum-free media and incubated with freshly prepared A β 42-Cu²⁺ (10 μ M) in the presence of Ber-D or Ber independently with ascorbate (200 μ M) for 12 h at 37 °C. The cells were lysed using RIPA buffer with a protease inhibitor. The cell lysate was centrifuged, and the supernatant was collected. The supernatant was analysed using caspase-3 detection kit (Invitrogen, Thermo fisher) using microplate reader (SpectraMax i3x, Molecular devices).

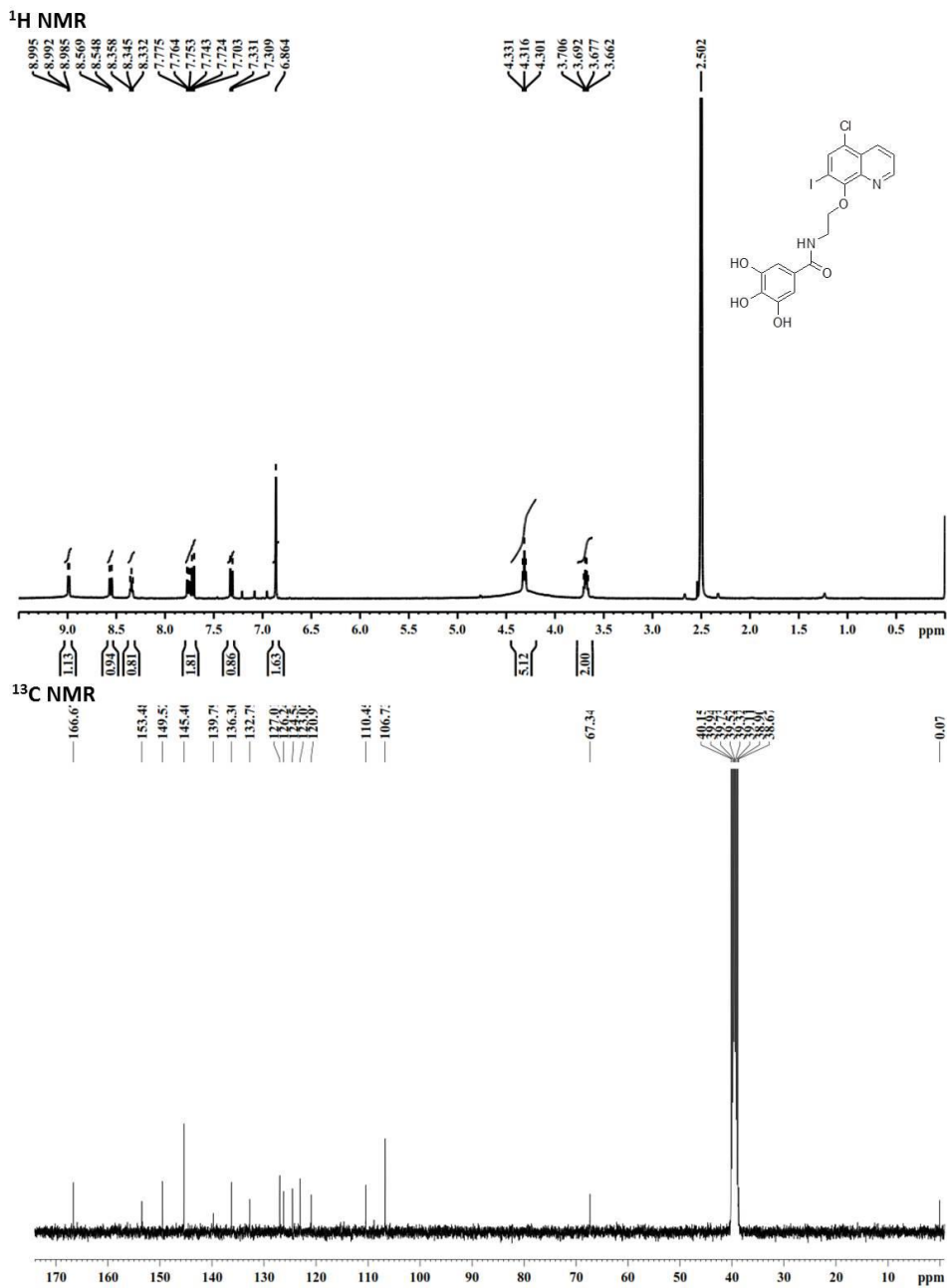
4.24.22 NMR and HRMS data



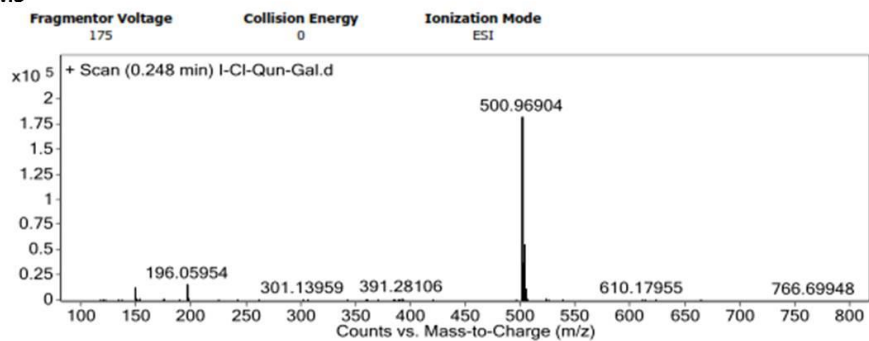


HRMS

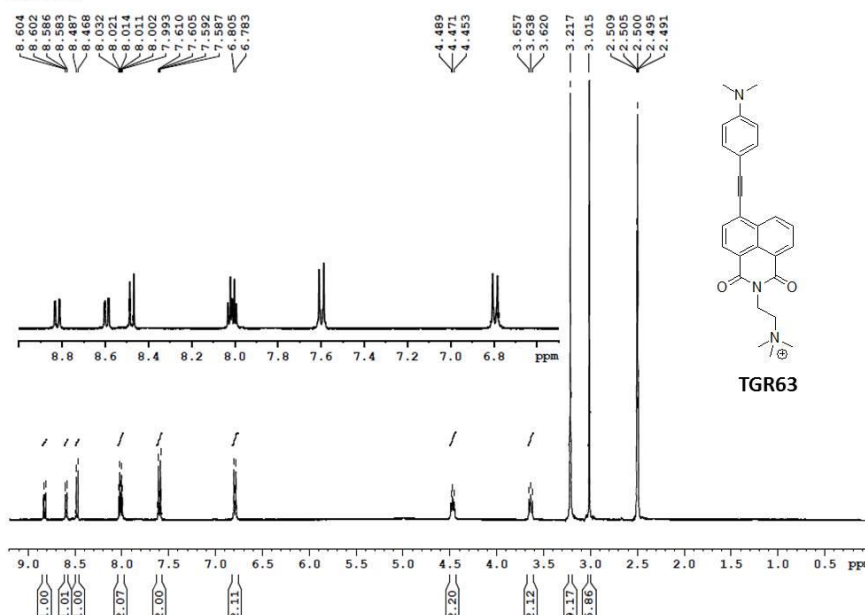




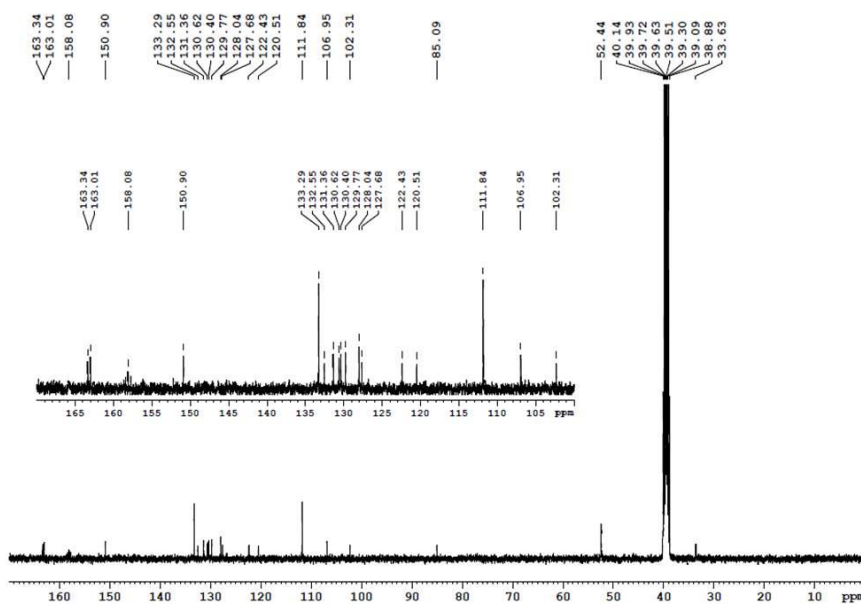
HRMS



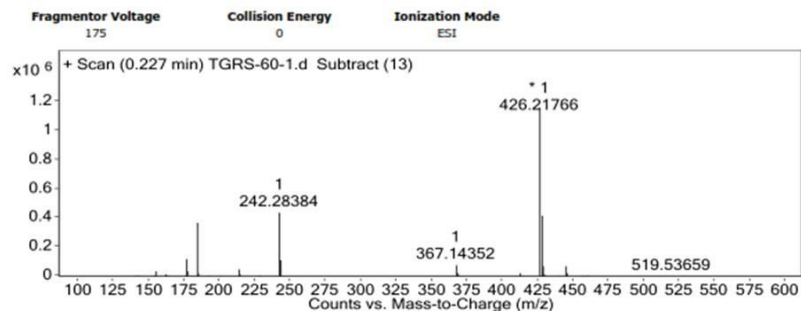
¹H NMR



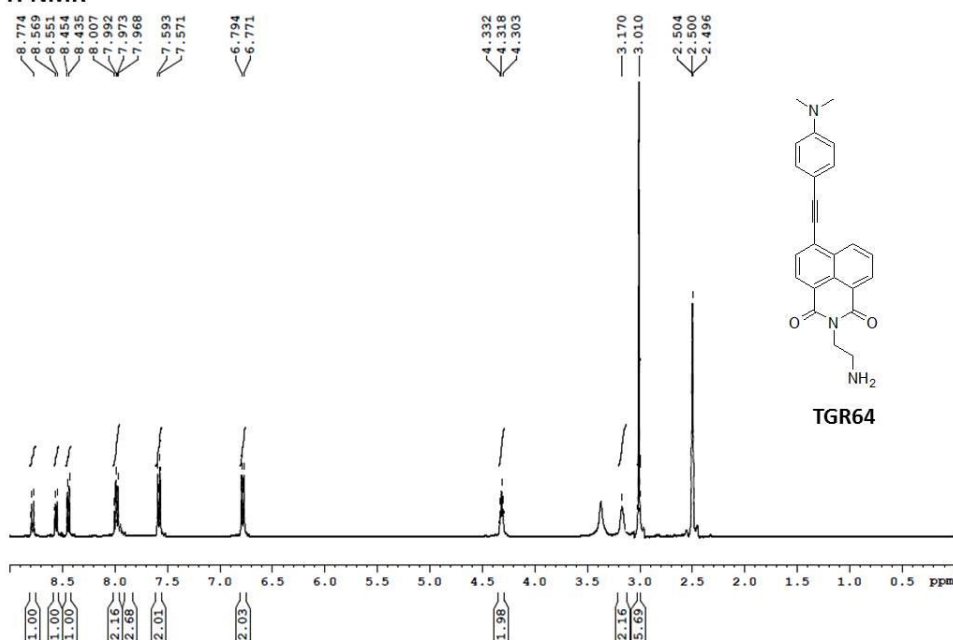
¹³C NMR



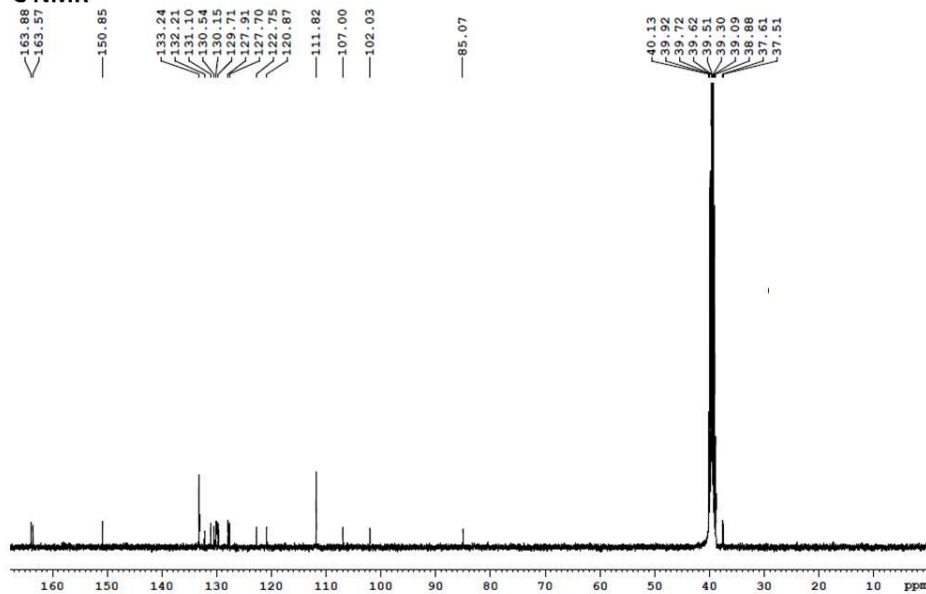
HRMS



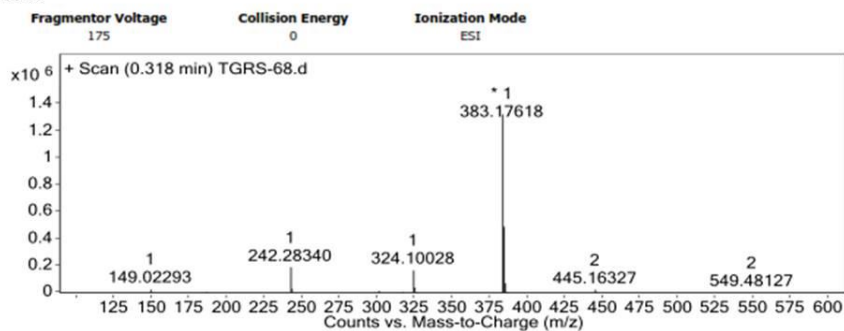
¹H NMR

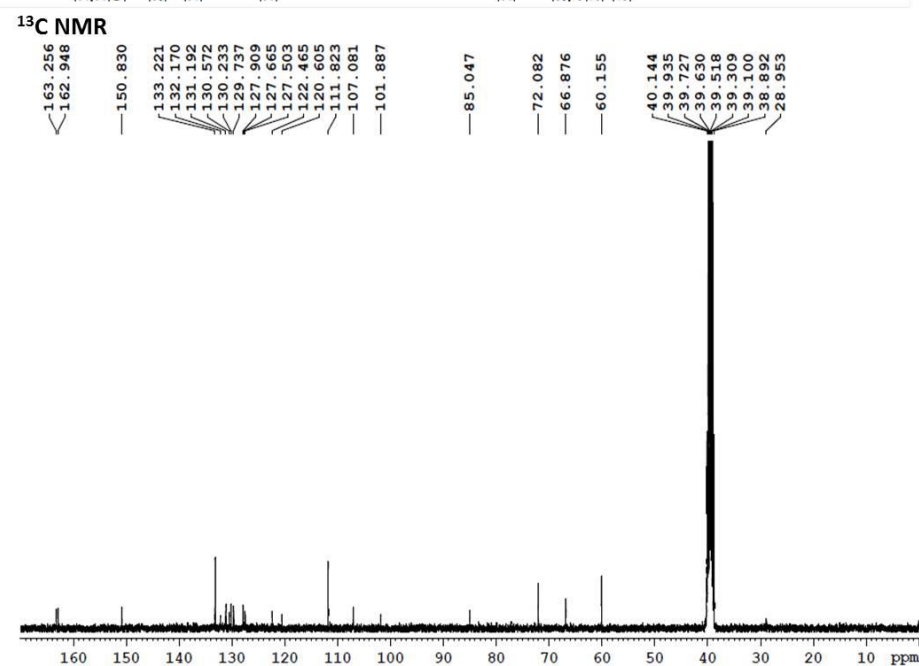
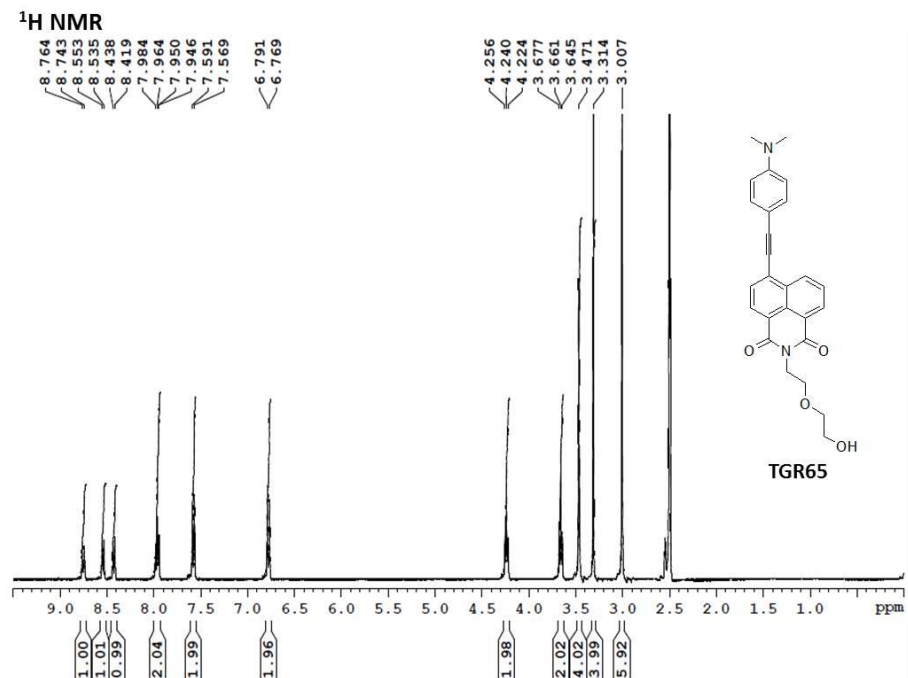


¹³C NMR

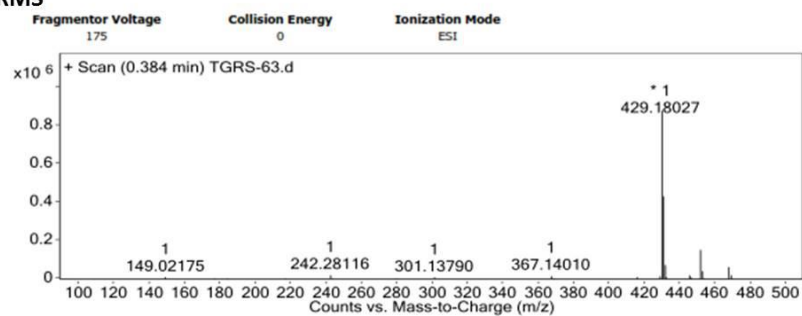


HRMS

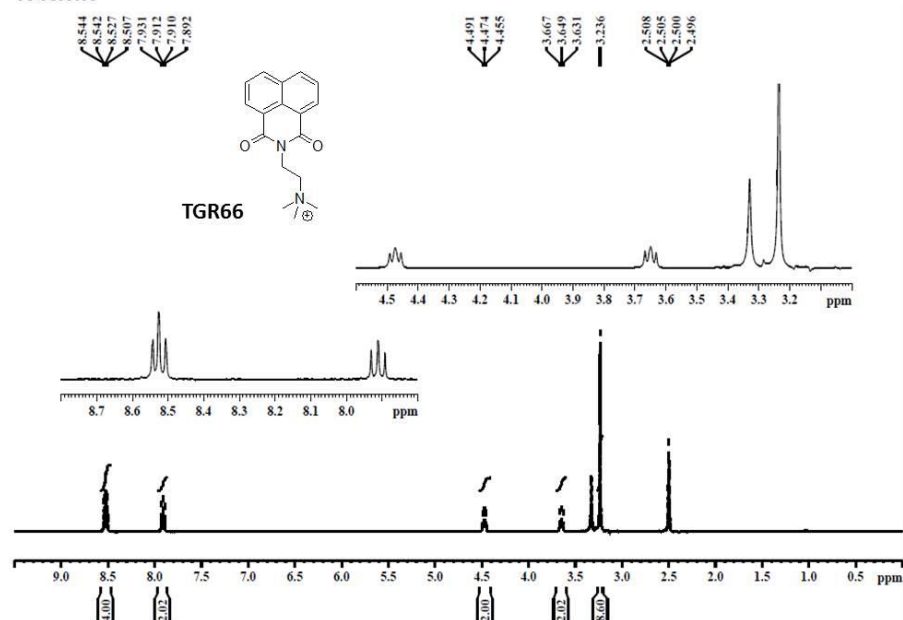




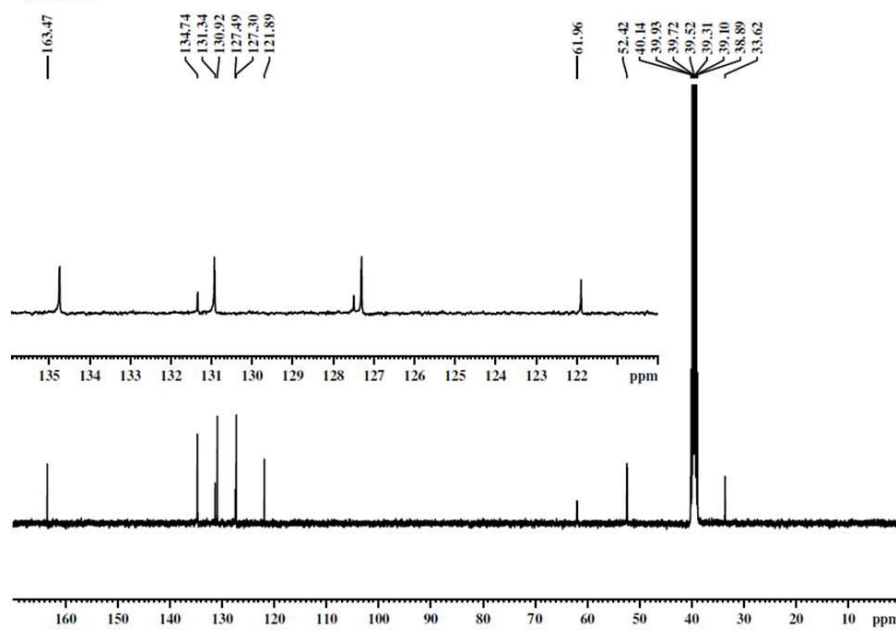
HRMS



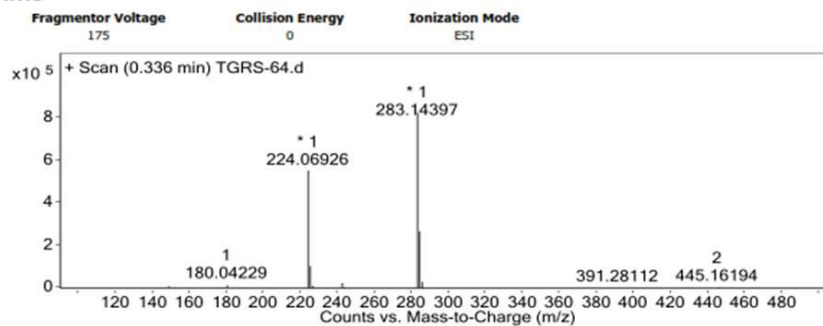
¹H NMR

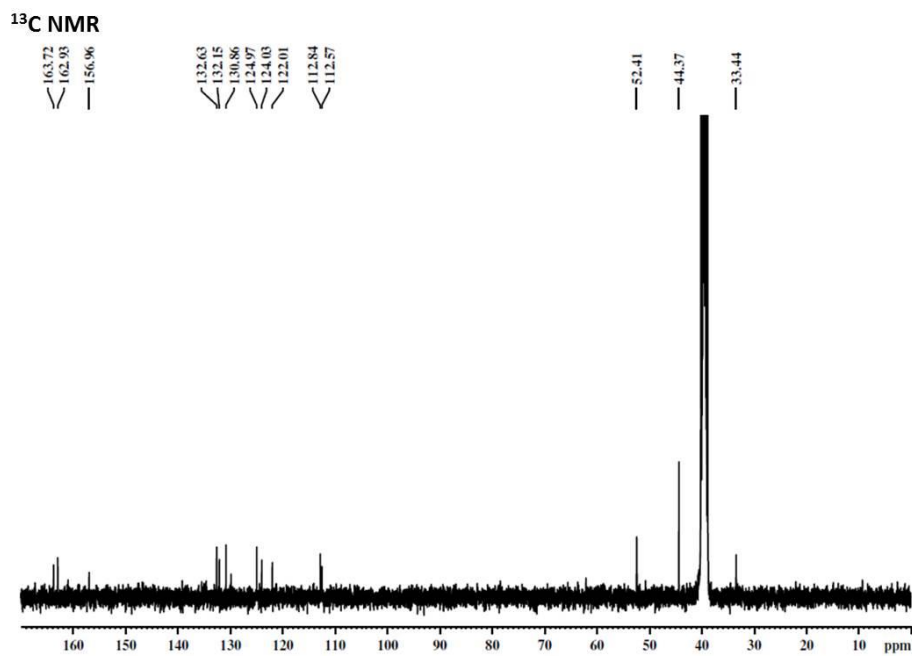
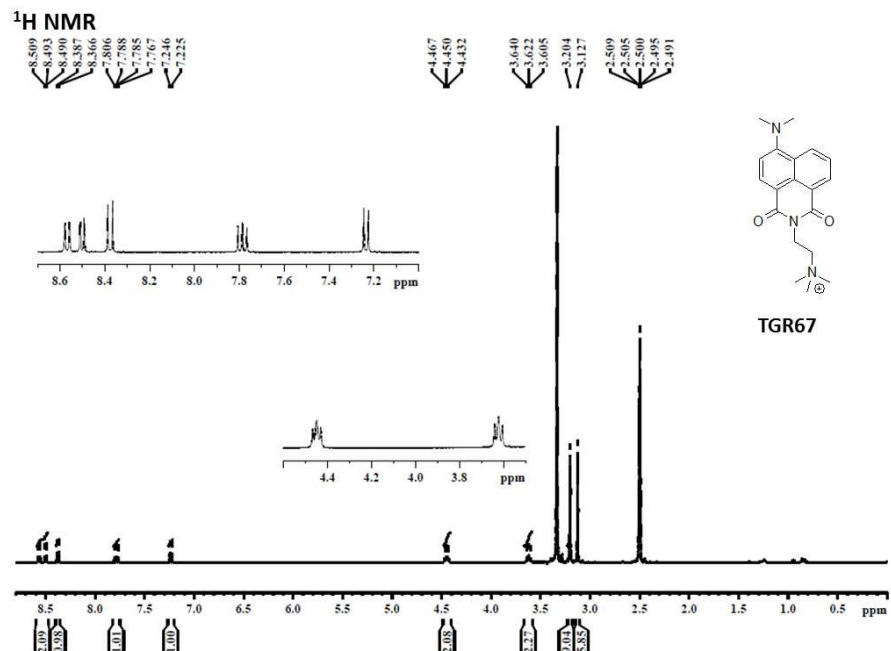
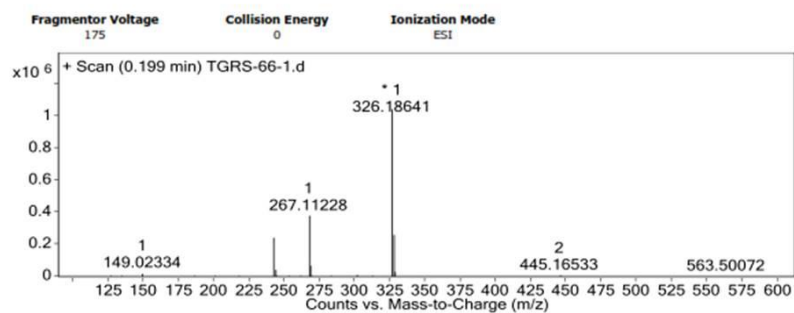


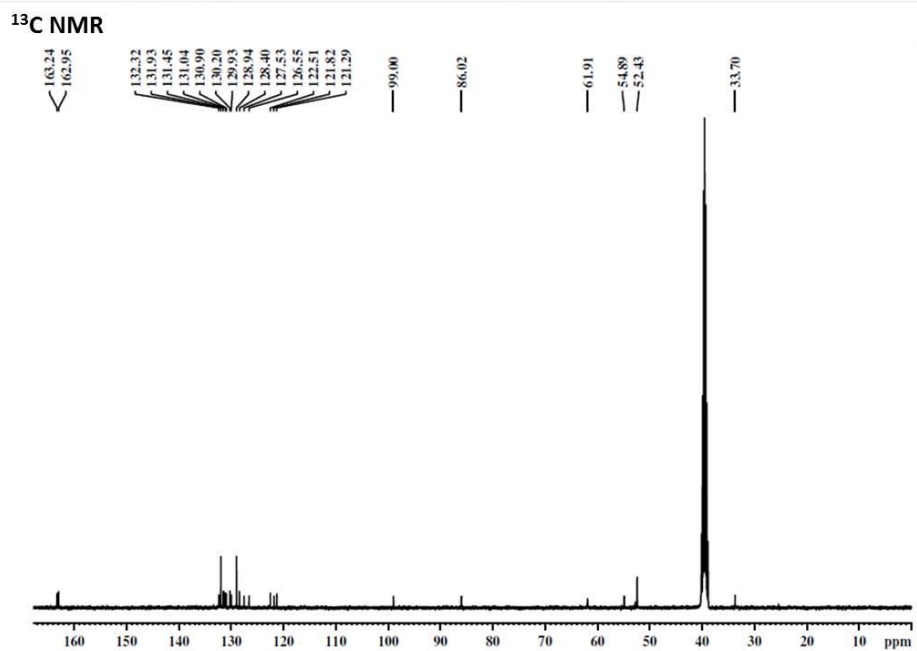
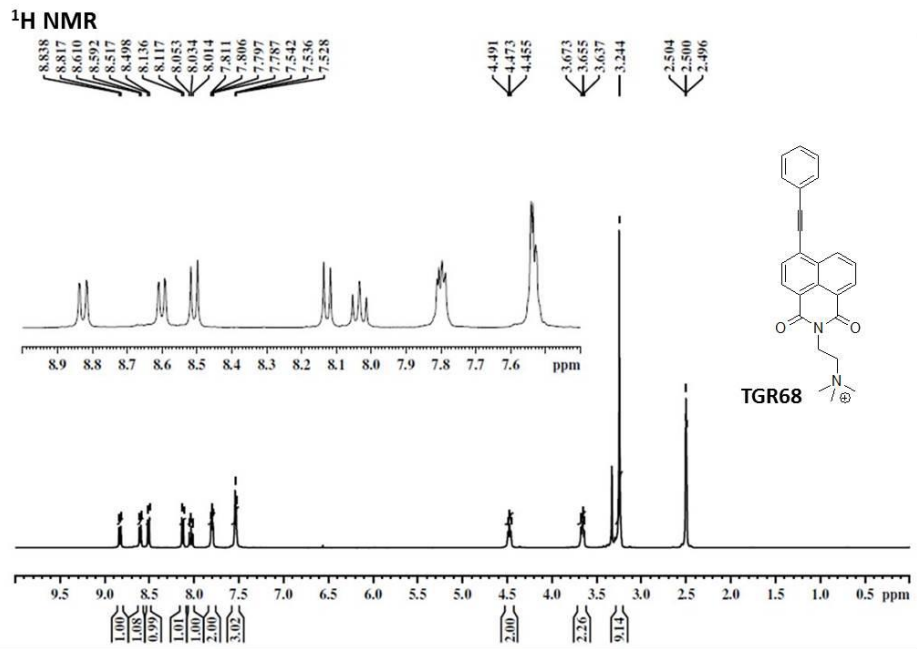
¹³C NMR



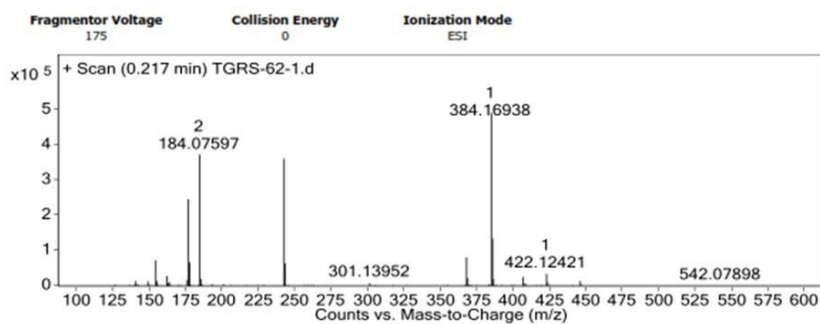
HRMS

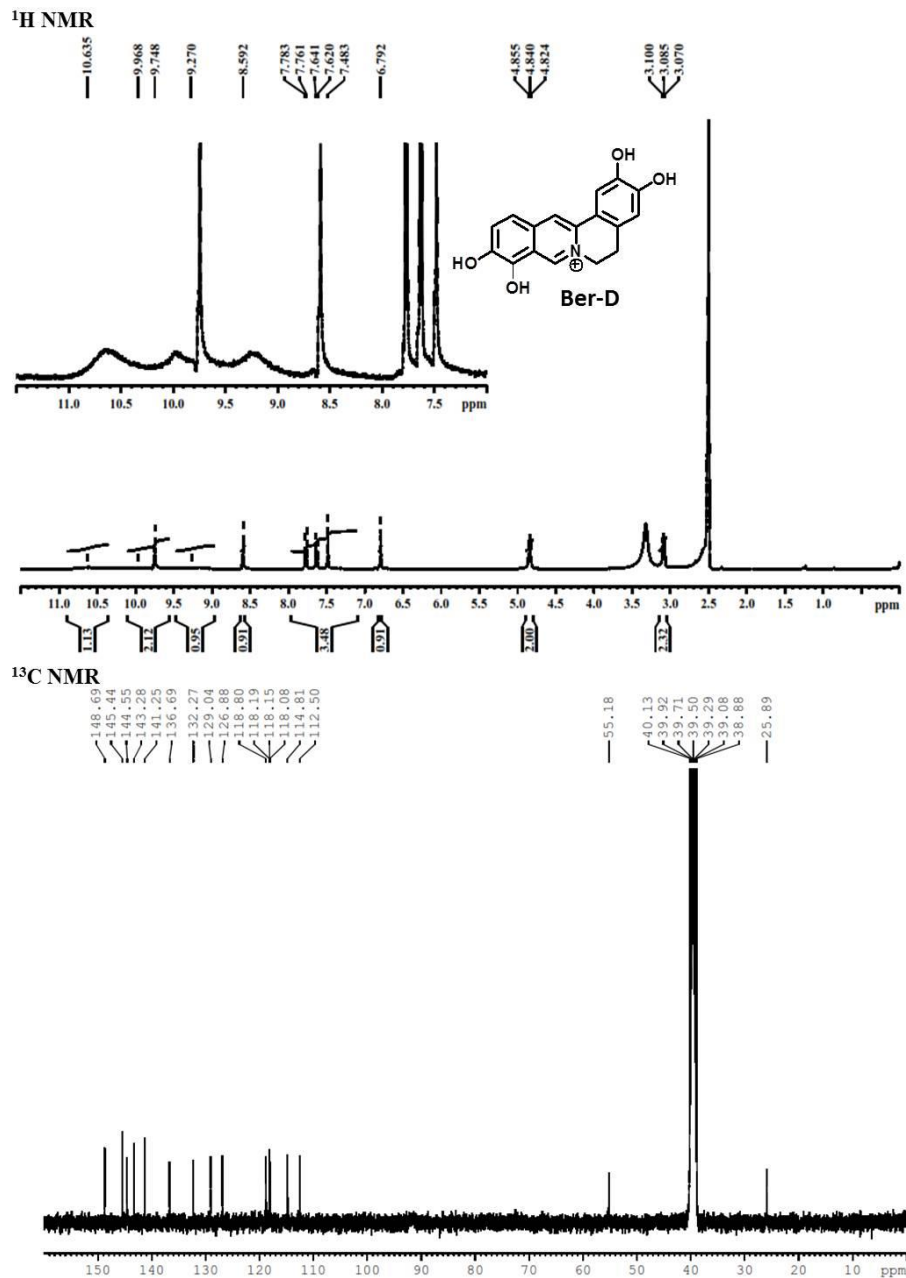


**HRMS**

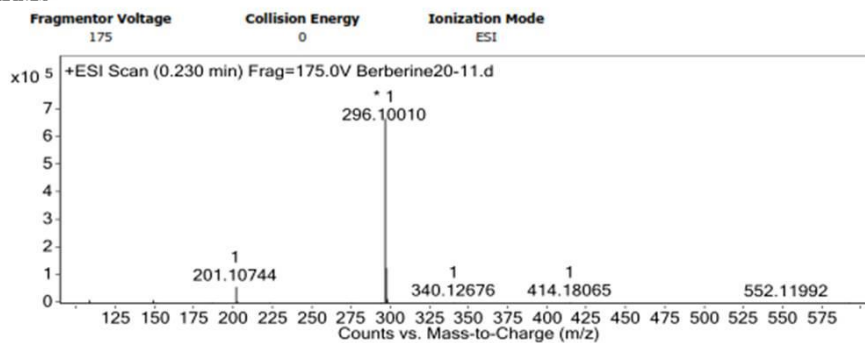


HRMS





HRMS



4.25 References

1. Knowles, T. P. J.; Vendruscolo, M.; Dobson, C. M., The amyloid state and its association with protein misfolding diseases. *Nat. Rev. Mol. Cell Biol.* **2014**, *15*, 384-396.
2. Karran, E.; Mercken, M.; Strooper, B. D., The amyloid cascade hypothesis for Alzheimer's disease: an appraisal for the development of therapeutics. *Nat. Rev. Drug Discov.* **2011**, *10*, 698-712.
3. Kaffy, J.; Brinet, D.; Soulier, J.-L.; Correia, I.; Tonali, N.; Fera, K. F.; Iacone, Y.; Hoffmann, A. R. F.; Khemtémourian, L.; Crousse, B.; Taylor, M.; Allsop, D.; Taverna, M.; Lequin, O.; Ongeri, S., Designed glycopeptidomimetics disrupt protein-protein interactions mediating amyloid β -peptide aggregation and restore neuroblastoma cell viability. *J. Med. Chem.* **2016**, *59*, 2025-2040.
4. Rajasekhar, K.; Suresh, S. N.; Manjithaya, R.; Govindaraju, T., Rationally designed peptidomimetic modulators of A β toxicity in alzheimer's disease. *Sci. Rep.* **2015**, *5*, 8139.
5. Folch, J.; Petrov, D.; Ettcheto, M.; Abad, S.; Sánchez-López, E.; Garcia, M. L.; Olloquequi, J.; Beas-Zarate, C.; Auladell, C.; Camins, A., Current research therapeutic strategies for Alzheimer's disease treatment. *Neural Plast.* **2016**, *2016*, 15.
6. Savelieff, M. G.; Lee, S.; Liu, Y.; Lim, M. H., Untangling amyloid- β , Tau, and metals in Alzheimer's disease. *ACS Chem. Biol.* **2013**, *8*, 856-865.
7. Savelieff, M. G.; DeToma, A. S.; Derrick, J. S.; Lim, M. H., The ongoing search for small molecules to study metal-associated amyloid- β species in Alzheimer's disease. *Acc. Chem. Res.* **2014**, *47*, 2475-2482.
8. Robert, A.; Liu, Y.; Nguyen, M.; Meunier, B., Regulation of copper and iron homeostasis by metal chelators: A possible chemotherapy for Alzheimer's disease. *Acc. Chem. Res.* **2015**, *48*, 1332-1339.
9. Rajasekhar, K.; Madhu, C.; Govindaraju, T., Natural tripeptide-based inhibitor of multifaceted amyloid β toxicity. *ACS Chem. Neurosci.* **2016**, *7*, 1300-1310.
10. Sharma, A. K.; Pavlova, S. T.; Kim, J.; Finkelstein, D.; Hawco, N. J.; Rath, N. P.; Kim, J.; Mirica, L. M., Bifunctional compounds for controlling metal-mediated aggregation of the A β 42 peptide. *J. Am. Chem. Soc.* **2012**, *134*, 6625-6636.
11. Lu, C.; Guo, Y.; Yan, J.; Luo, Z.; Luo, H.-B.; Yan, M.; Huang, L.; Li, X., Design, synthesis, and evaluation of multitarget-directed resveratrol derivatives for the treatment of Alzheimer's disease. *J. Med. Chem.* **2013**, *56*, 5843-5859.
12. Geng, J.; Li, M.; Wu, L.; Ren, J.; Qu, X., Liberation of copper from amyloid plaques: Making a risk factor useful for Alzheimer's disease treatment. *J. Med. Chem.* **2012**, *55*, 9146-9155.
13. Caballero, A. B.; Terol-Ordaz, L.; Espargaró, A.; Vázquez, G.; Nicolás, E.; Sabaté, R.; Gamez, P., Histidine-rich oligopeptides to lessen copper-mediated amyloid- β toxicity. *Chem. Eur. J.* **2016**, *22*, 7268-7280.

14. Jacobson, S. A.; Sabbagh, M. N., Investigational drugs for the treatment of AD: what can we learn from negative trials? *Alzheimer's Res. Ther.* **2011**, *3*, 14.
15. Matlack, K. E. S.; Tardiff, D. F.; Narayan, P.; Hamamichi, S.; Caldwell, K. A.; Caldwell, G. A.; Lindquist, S., Clioquinol promotes the degradation of metal-dependent amyloid- β (A β) oligomers to restore endocytosis and ameliorate A β toxicity. *Proc. Natl. Acad. Sci.* **2014**, *111*, 4013-4018.
16. Prachayasittikul, V.; Prachayasittikul, S.; Ruchirawat, S.; Prachayasittikul, V., 8-Hydroxyquinolines: a review of their metal chelating properties and medicinal applications. *Drug Des. Devel. Ther.* **2013**, *7*, 1157-1178.
17. Hyung, S.-J.; DeToma, A. S.; Brender, J. R.; Lee, S.; Vivekanandan, S.; Kochi, A.; Choi, J.-S.; Ramamoorthy, A.; Ruotolo, B. T.; Lim, M. H., Insights into antiamyloidogenic properties of the green tea extract (-)-epigallocatechin-3-gallate toward metal-associated amyloid- β species. *Proc. Natl. Acad. Sci.* **2013**, *110*, 3743-3748.
18. Rao, P. P. N.; Mohamed, T.; Teckwani, K.; Tin, G., Curcumin binding to beta amyloid: A computational study. *Chem. Biol. Drug Des.* **2015**, *86*, 813-820.
19. Berhanu, W. M.; Hansmann, U. H. E., Structure and Dynamics of Amyloid- β segmental polymorphisms. *PLOS ONE* **2012**, *7*, e41479.
20. Mithu, V. S.; Sarkar, B.; Bhowmik, D.; Das, A. K.; Chandrakesan, M.; Maiti, S.; Madhu, P. K., Curcumin alters the salt bridge-containing turn region in amyloid β (1-42) aggregates. *J. Biol. Chem.* **2014**, *289*, 11122-11131.
21. Di Vaira, M.; Bazzicalupi, C.; Orioli, P.; Messori, L.; Bruni, B.; Zatta, P., Clioquinol, a Drug for Alzheimer's disease specifically interfering with brain metal metabolism: structural characterization of its zinc(II) and copper(II) complexes. *Inorg. Chem.* **2004**, *43*, 3795-3797.
22. Gella, A.; Durany, N., Oxidative stress in Alzheimer disease. *Cell Adh. Migr.* **2009**, *3*, 88-93.
23. Guilloreau, L.; Combalbert, S.; Sournia-Saquet, A.; Mazarguil, H.; Faller, P., Redox chemistry of copper-amyloid- β : The generation of hydroxyl radical in the presence of ascorbate is linked to redox-potentials and aggregation state. *ChemBioChem* **2007**, *8*, 1317-1325.
24. Xu, W.; Wang, X.-B.; Wang, Z.-M.; Wu, J.-J.; Li, F.; Wang, J.; Kong, L.-Y., Synthesis and evaluation of donepezil-ferulic acid hybrids as multi-target-directed ligands against Alzheimer's disease. *MedChemComm* **2016**, *7*, 990-998.
25. Schieber, M.; Chandel, Navdeep S., ROS function in redox signaling and oxidative stress. *Curr. Biol.* **2014**, *24*, R453-R462.
26. Mesquita, C. S.; Oliveira, R.; Bento, F.; Geraldo, D.; Rodrigues, J. V.; Marcos, J. C., Simplified 2,4-dinitrophenylhydrazine spectrophotometric assay for quantification of carbonyls in oxidized proteins. *Anal. Biochem.* **2014**, *458*, 69-71.

27. Huang, S.-H.; Ke, S.-C.; Lin, T.-H.; Huang, H.-B.; Chen, Y.-C., Effect of C-terminal residues of A β on copper binding affinity, structural conversion and aggregation. *PLoS ONE* **2014**, *9*, e90385.
28. Eruslanov, E.; Kusmartsev, S., Identification of ROS using oxidized DCFDA and flow-cytometry. In *Advanced protocols in oxidative stress II*, Armstrong, D., Ed. Humana Press: Totowa, NJ, 2010; pp 57-72.
29. Pagani, L.; Eckert, A., Amyloid-beta interaction with mitochondria. *Int. J. Alzheimers Dis.* **2011**, *2011*.
30. Eckert, A.; Schmitt, K.; Götz, J., Mitochondrial dysfunction - the beginning of the end in Alzheimer's disease? Separate and synergistic modes of tau and amyloid- β toxicity. *Alzheimer's Res. Ther.* **2011**, *3*, 15.
31. Brand, Martin D.; Nicholls, David G., Assessing mitochondrial dysfunction in cells. *Biochem. J.* **2011**, *435*, 297-312.
32. Scaduto, R. C.; Grotyohann, L. W., Measurement of mitochondrial membrane potential using fluorescent rhodamine derivatives. *Biophys. J.* **1999**, *76*, 469-477.
33. Palop, J. J.; Chin, J.; Mucke, L., A network dysfunction perspective on neurodegenerative diseases. *Nature* **2006**, *443*, 768-773.
34. Sweeney, P.; Park, H.; Baumann, M.; Dunlop, J.; Frydman, J.; Kopito, R.; McCampbell, A.; Leblanc, G.; Venkateswaran, A.; Nurmi, A.; Hodgson, R., Protein misfolding in neurodegenerative diseases: implications and strategies. *Transl. Neurodegener.* **2017**, *6*, 6.
35. Eisele, Y. S.; Monteiro, C.; Fearn, C.; Encalada, S. E.; Wiseman, R. L.; Powers, E. T.; Kelly, J. W., Targeting protein aggregation for the treatment of degenerative diseases. *Nat. Rev. Drug Discov.* **2015**, *14*, 759-780.
36. Colvin, M. T.; Silvers, R.; Ni, Q. Z.; Can, T. V.; Sergeev, I.; Rosay, M.; Donovan, K. J.; Michael, B.; Wall, J.; Linse, S.; Griffin, R. G., Atomic resolution structure of monomeric A β 42 amyloid fibrils. *J. Am. Chem. Soc.* **2016**, *138*, 9663-9674.
37. Stefanis, L., α -Synuclein in Parkinson's disease. *Cold Spring Harb. Perspect. Med.* **2012**, *2*, a009399.
38. Recchia, A.; Debetto, P.; Negro, A.; Guidolin, D.; Skaper, S. D.; Giusti, P., α -Synuclein and Parkinson's disease. *FASEB J.* **2004**, *18*, 617-626.
39. Bui Thanh, T.; Nguyen Thanh, H., Natural product for the treatment of Alzheimer's disease. In *J. Basic Clin. Physiol. Pharmacol.*, 2017; Vol. 28, p 413.
40. Ehrnhoefer, D. E.; Bieschke, J.; Boeddrich, A.; Herbst, M.; Masino, L.; Lurz, R.; Engemann, S.; Pastore, A.; Wanker, E. E., EGCG redirects amyloidogenic polypeptides into unstructured, off-pathway oligomers. **2008**, *15*, 558.

41. Cicero, A. F. G.; Baggioni, A., Berberine and its role in chronic disease. In *Anti-inflammatory nutraceuticals and chronic diseases*, Gupta, S. C.; Prasad, S.; Aggarwal, B. B., Eds. Springer International Publishing: Cham, 2016; pp 27-45.
42. Cai, Z.; Wang, C.; Yang, W., Role of berberine in Alzheimer's disease. *Neuropsychiatr. Dis. Treat.* **2016**, *12*, 2509-2520.
43. Kysenius, K.; Brunello, C. A.; Huttunen, H. J., Mitochondria and NMDA Receptor-dependent toxicity of berberine sensitizes neurons to glutamate and rotenone injury. *PLOS ONE* **2014**, *9*, e107129.
44. Murugan, N. A.; Halldin, C.; Nordberg, A.; Långström, B.; Ågren, H., The culprit is in the cave: The core sites explain the binding profiles of amyloid-specific tracers. *J. Phys. Chem. Lett.* **2016**, *7*, 3313-3321.
45. Re, R.; Pellegrini, N.; Proteggente, A.; Pannala, A.; Yang, M.; Rice-Evans, C., Antioxidant activity applying an improved ABTS radical cation decolorization assay. *Free Radic. Biol. Med.* **1999**, *26*, 1231-1237.
46. Roy, M. K.; Koide, M.; Rao, T. P.; Okubo, T.; Ogasawara, Y.; Juneja, L. R., ORAC and DPPH assay comparison to assess antioxidant capacity of tea infusions: Relationship between total polyphenol and individual catechin content. *Int. J. Food Sci. Nutr.* **2010**, *61*, 109-124.
47. Sreejayan; Rao, M. N. A., Nitric oxide scavenging by curcuminoids. *J. Pharm. Pharmacol.* **1997**, *49*, 105-107.
48. Dizdaroglu, M.; Jaruga, P., Mechanisms of free radical-induced damage to DNA. *Free Radic. Res.* **2012**, *46*, 382-419.
49. Cha, M.-Y.; Han, S.-H.; Son, S. M.; Hong, H.-S.; Choi, Y.-J.; Byun, J.; Mook-Jung, I., Mitochondria-specific accumulation of amyloid β induces mitochondrial dysfunction leading to apoptotic cell death. *PLOS ONE* **2012**, *7*, e34929.
50. Guo, C.; Sun, L.; Chen, X.; Zhang, D., Oxidative stress, mitochondrial damage and neurodegenerative diseases. *Neural Regen. Res.* **2013**, *8*, 2003-2014.
51. Trott, O.; Olson, A. J., AutoDock Vina: Improving the speed and accuracy of docking with a new scoring function, efficient optimization, and multithreading. *J. Comput. Chem.* **2010**, *31*, 455-461.
52. Morris, G. M.; Huey, R.; Lindstrom, W.; Sanner, M. F.; Belew, R. K.; Goodsell, D. S.; Olson, A. J., AutoDock4 and AutoDockTools4: Automated docking with selective receptor flexibility. *J. Comput. Chem.* **2009**, *30*, 2785-2791.

Chapter 5

The cellular localization of A β 16 and implications in A β toxicity

The hydrophobic A β 42 peptide generated from APP, a transmembrane protein is released as a monomer into the extracellular matrix.¹ A β 42 undergoes a spontaneous aggregation into various polymorphic species namely oligomers, protofibrils, and fully grown fibrillar aggregates.² Several studies have suggested the reuptake of extracellular A β 42 into neuronal cells and resulting in the formation of intracellular aggregates, causing neuronal damage and cell death.³ Endocytosis of disease-causing misfolded proteins has also been observed in various cellular models of the tau protein, α -synuclein and huntingtin disease.⁴ The studies on internalization of A β 42 and its relation with the observed cytotoxicity is not fully understood.⁵ A β peptide can be broadly divided into two fragments based on their aggregation capabilities. A β 16 is an unstructured fragment of A β 42 fibrillar aggregates, whereas A β (17-42) is involved in the formation of a β -sheet structure which is predominantly observed in A β 42 fibrillar aggregates. A β (17-42) exhibit high cytotoxicity in the neuronal cells, however, the cytotoxicity exhibited by A β 42 is significantly higher than A β (17-42), indicating that A β 16 has a specific role in inducing cytotoxicity.⁶ While A β 16 has a limited role to play in the A β 42 aggregation, many reports indicate that A β 16 is involved in redox metal chelation and stabilizing oligomeric species. However, in the presence of metal ions, the cytotoxicity of A β 16 is predominantly enhanced indicating its role in redox cycling of metal ions to generate ROS.⁷ Herein, we sought to understand the role of A β 16 in enhancing the cellular toxicity of A β 42.

5.1 Design and synthesis

Fluorescence microscopy is extremely useful visualization tool.⁸ A β 42 has been shown to possess a close relation with mitochondria and subsequently causing toxicity.⁹ Moreover, a recent report by jung *et al.* have shown that A β 42 accumulates in mitochondria and cause mitochondrial dysfunction leading to apoptotic cell death.¹⁰ It is speculated that accumulation of

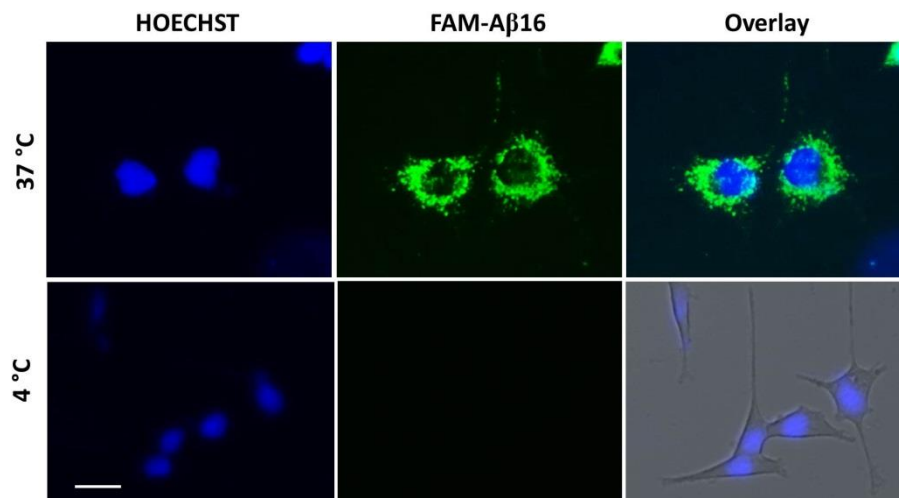


Figure 2. FAM-A β 16 (50 μ M) internalization into the PC12 cells at 37 $^{\circ}$ C and 4 $^{\circ}$ C. Scale bar = 15 μ M

Endocytosis is the prime mechanism of A β 42 internalization, to check the uptake process involved in FAM-A β 16 we performed a temperature dependent uptake studies.^{14, 15} If the uptake is energy dependent (endocytosis), then there will be no intake of FAM-A β 16 at lower temperature (4 $^{\circ}$ C) (Figure 2).¹⁶ FAM-A β 16 could not internalize into the cells at 4 $^{\circ}$ C indicating the uptake of FAM-A β 16 is through endocytosis.

5.3 A β 16 cellular localization

We studied the specific localization of FAM-A β 16 inside the live cells. Initially, we treated the MDA-MB-231 cells with FAM-A β 16 and Hoechst dye (nuclear staining dye) (Figure 3). Minimum colocalization was observed for FAM-A β 16 and Hoechst, indicating that FAM-A β 16 is predominantly localized in the cytoplasm. Mitochondria are considered the prime target for the A β 42 toxicity; we envision investigate the role of A β 16 in driving A β 42 towards mitochondria.^{9, 17-19} We treated MDA-MB-231 cells with FAM-A β 16 for 3 h, followed by staining the cells with mitotracker (Figure 3). There was no colocalization of FAM-A β 16 with mitochondrial region. Further, we performed a time-dependent live cell imaging of FAM-A β 16 and mitotracker live stained cells. With time there were no signs of interactions between the mitochondria and FAM-

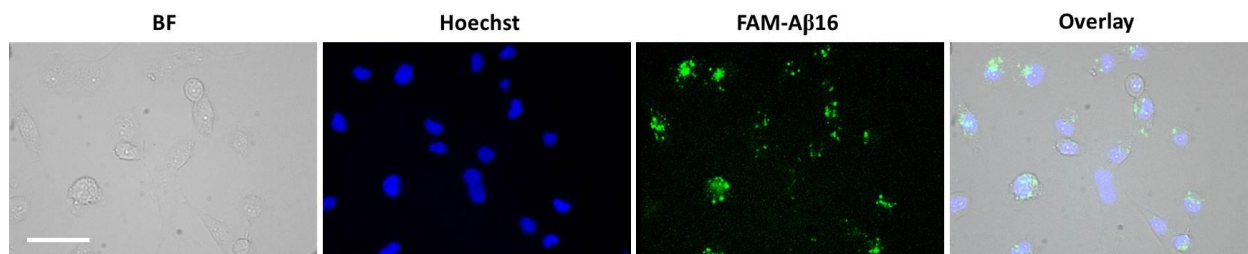


Figure 3. Fluorescence microscopy images of FAM-A β 16 (10 μ M) and Hoechst treated MDA-MB-231 cells. Scale bar = 15 μ M

A β 16, which indicate that A β 16 has no role in driving A β 42 towards mitochondria and its cytotoxicity (Figure 5). Next, we evaluated the localization of the FAM-A β 16 with lysosomes. MDA-MB-231 cells were incubated with FAM-A β 16 for 3 h, followed by staining the cells with lysotracker (Figure 4).²⁰ During normal endocytosis, the endosomes are either convert to lysosomes or fuse with lysosomes to form endolysosomes. The absence of FAM-A β 16 colocalization with lysosomes rule out the above process for endocytosis. Therefore, A β 16 is possibly internalized through receptor-based endocytosis similar to A β 42 peptide.¹⁵

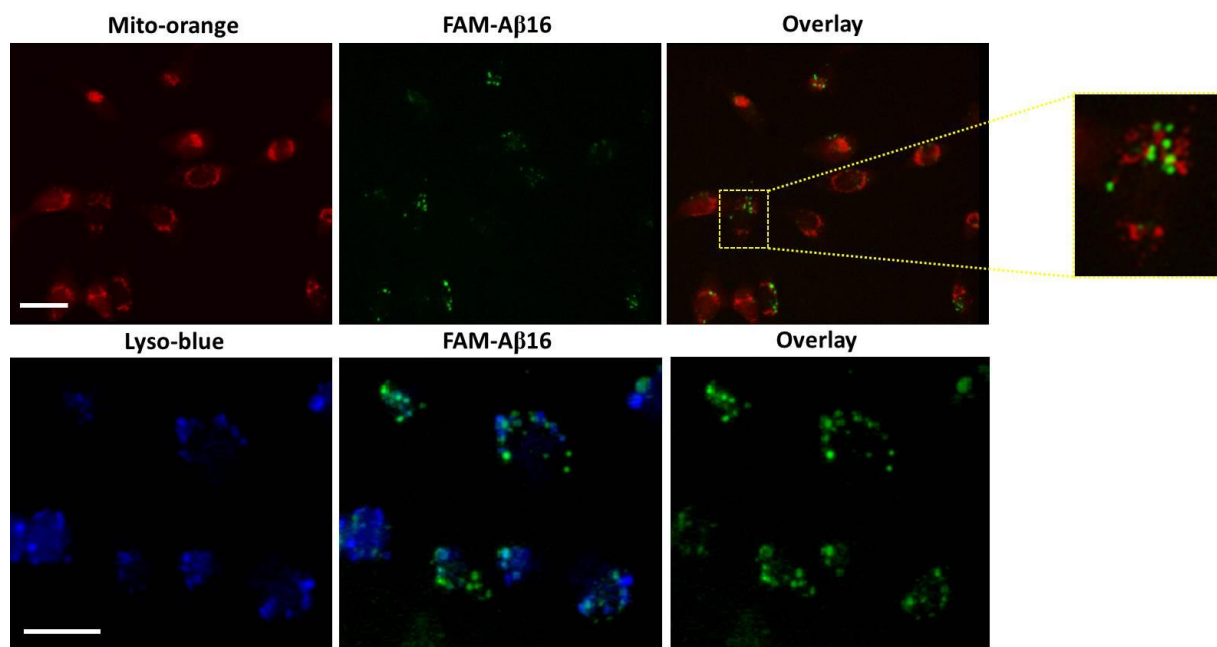


Figure 4. Fluorescence microscopy images of FAM-A β 16 (10 μ M) and mitotracker-orange or lysotracker-blue treated MDA-MB-231 cells. Scale bar = 15 μ M

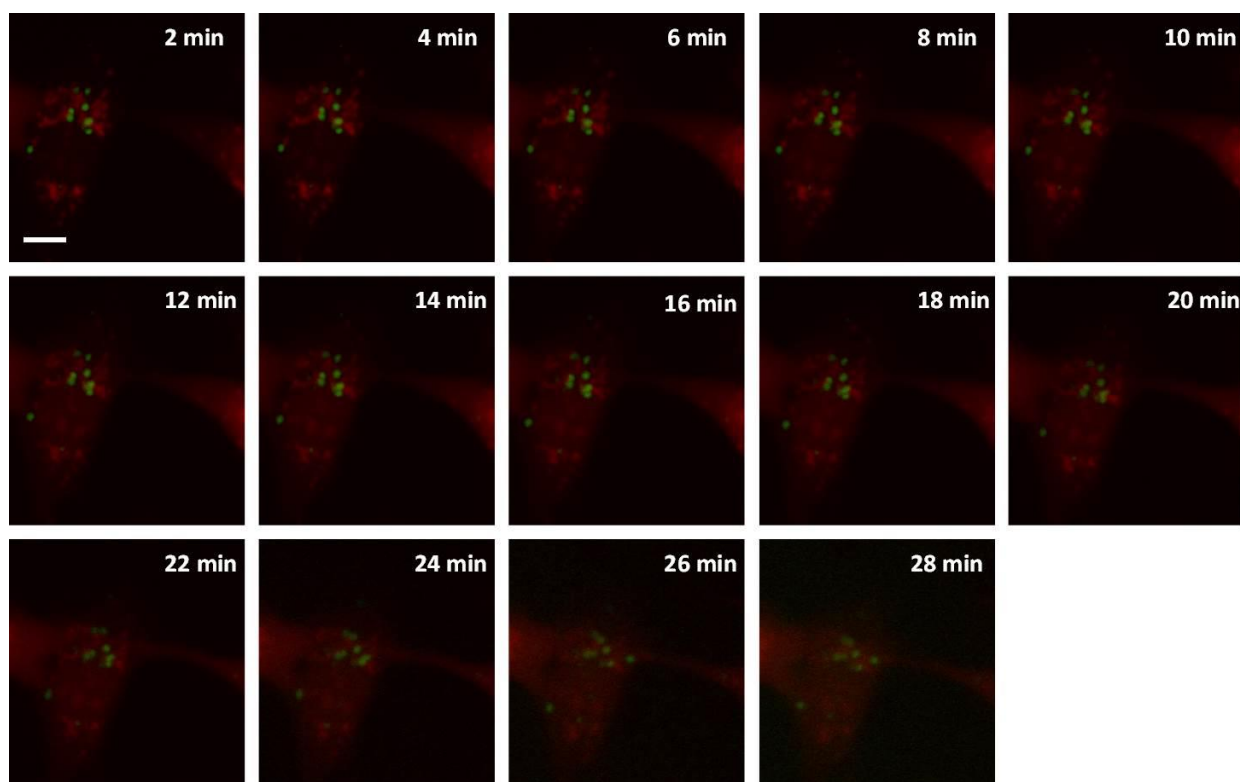


Figure 5. Time dependent fluorescence microscopy images of FAM-A β 16 (10 μ M) and mitotracker-orange treated MDA-MB-231 cells. Scale bar = 5 μ M

5.4 Conclusion

In conclusion, we have studied and understood that A β 16 has no role in driving A β 42 to mitochondria. A β 16 enters the cell through endocytosis and probably through receptor-mediated endocytosis similar to A β 42. Further, we are working on studying other fragments of A β 42 in combination with A β 16 and perform similar studies to understand the exact role of A β 16 in the cytotoxicity of A β 42.

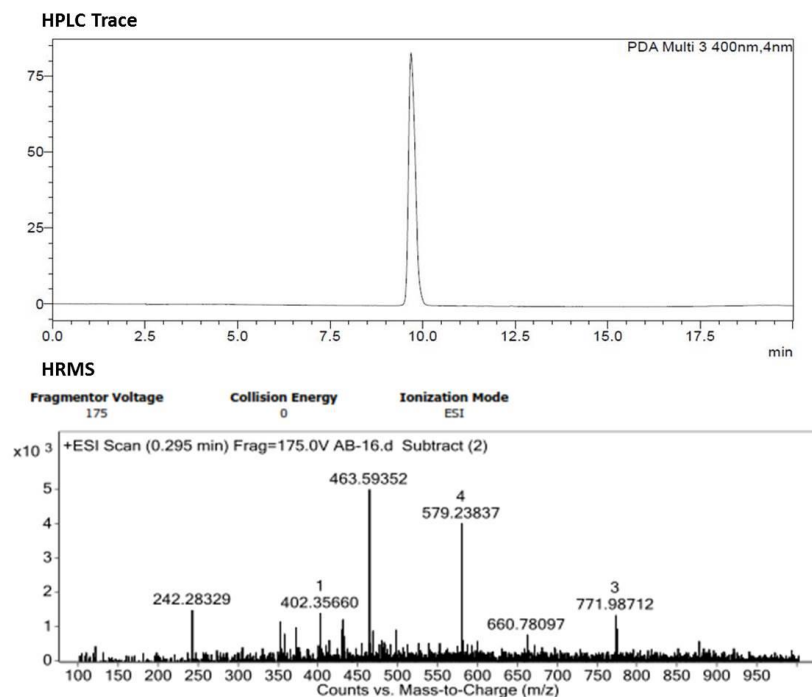
5.5 Experimental methods

5.5.1 Synthesis of A β 16-FAM. Peptide was synthesised using manual solid phase peptide synthesis protocols. We used Fmoc chemistry on Rink amide resin as a solid support for synthesis of peptide protected amino acids were used to prevent oligomerization and undesired

product formation during the course of peptide synthesis, the side chain functional groups present in amino acids were protected by different orthogonal protection groups. The resin was taken in reaction vessel and soaked in DCM for swelling (2 h) with optimal vortexing. Once the swelling was completed, resin was washed with DMF, followed by addition of 20% piperidine in DMF to deprotect Fmoc-group to obtain reactive free $-NH_2$ group on the resin. The first amino acid (4 equivalents) was coupled to the resin using coupling reagent HBTU, HOBt and non-nucleophilic base, DIPEA for 1 h with periodic vortexing. Unreacted reagents were washed off by multiple washing cycles (3 X DMF and 3 X DCM). The next amino acid was deprotected (Fmoc-deprotection) with 20% piperidine in DMF, for 15 min. Cycles of coupling and deprotection were continued till the last amino acid. Then FAM was coupled to the N-terminal of the peptide through HBTU coupling for 6 h. Once A β 16-FAM was synthesized, it was cleaved from the resin using a cocktail made up of 95% TFA, 2% TIPS in DCM. Cleaving cocktail cleaves the peptide from the resin and also deprotect all the side chain protecting groups of amino acids to obtain the desired free peptide sequence. The resin was separated from cocktail solution through filtration and cold diethyl ether was added followed by incubation at 0 °C for 1 h. The peptide suspension was centrifuged, the supernatant was decanted and the crude product was collected. The peptide was purified through HPLC (Shimadzu) and characterized through LCMS (shimadzu, LCMS 2020) and HRMS (Agilent Technologies 6538 UHD Accurate-Mass Q-TOF).

5.5.2 Cellular uptake studies. Cellular uptake studies were carried out in MDA-MB-231 cells employing fluorescence microscopy (Leica, DMi8). For imaging, cells were seeded into 35 mm glass bottom petridish in DMEM complete medium and incubated for 24 h. The cells were treated with FAM-A β 16 at 10 μ M for 3 h in DMEM medium (with serum). After 4 h incubation,

cells were washed with serum-free DMEM, incubate with fresh DMEM media and performed live imaging using Tokai hit live cell imaging system.



5.6 References

1. Rajasekhar, K.; Chakrabarti, M.; Govindaraju, T., Function and toxicity of amyloid beta and recent therapeutic interventions targeting amyloid beta in Alzheimer's disease. *Chem. Commun.* **2015**, *51*, 13434-13450.
2. Vandersteen, A.; Hubin, E.; Sarroukh, R.; De Baets, G.; Schymkowitz, J.; Rousseau, F.; Subramaniam, V.; Raussens, V.; Wenschuh, H.; Wildemann, D.; Broersen, K., A comparative analysis of the aggregation behavior of amyloid- β peptide variants. *FEBS Lett.* **2012**, *586*, 4088-4093.
3. Friedrich, R. P.; Tepper, K.; Rönicke, R.; Soom, M.; Westermann, M.; Reymann, K.; Kaether, C.; Fändrich, M., Mechanism of amyloid plaque formation suggests an intracellular basis of A β pathogenicity. *Proc. Natl. Acad. Sci.* **2010**, *107*, 1942-1947.
4. Yu, C.; Nwabuisi-Heath, E.; Laxton, K.; LaDu, M. J., Endocytic pathways mediating oligomeric A β 42 neurotoxicity. *Mol. Neurodegener.* **2010**, *5*, 19.
5. Jin, S.; Kedia, N.; Illes-Toth, E.; Haralampiev, I.; Prisner, S.; Herrmann, A.; Wanker, E. E.; Bieschke, J., Amyloid- β (1-42) aggregation initiates its cellular uptake and cytotoxicity. *J. Biol. Chem.* **2016**, *291*, 19590-19606.

6. Jensen, M.; Canning, A.; Chiha, S.; Bouquerel, P.; Pedersen, J. T.; Østergaard, J.; Cuvillier, O.; Sasaki, I.; Hureau, C.; Faller, P., Inhibition of Cu-amyloid- β by using bifunctional peptides with β -Sheet breaker and chelator moieties. *Chem. Eur. J.* **2012**, *18*, 4836-4839.
7. Faller, P.; Hureau, C.; La Penna, G., Metal ions and intrinsically disordered proteins and peptides: From Cu/Zn amyloid- β to general principles. *Acc. Chem. Res.* **2014**, *47*, 2252-2259.
8. Thorn, K., A quick guide to light microscopy in cell biology. *Mol. Biol. Cell.* **2016**, *27*, 219-222.
9. Reddy, P. H.; Beal, M. F., Amyloid beta, mitochondrial dysfunction and synaptic damage: Implications for cognitive decline in aging and Alzheimer's disease. *Trends Mol. Med.* **2008**, *14*, 45-53.
10. Cha, M.-Y.; Han, S.-H.; Son, S. M.; Hong, H.-S.; Choi, Y.-J.; Byun, J.; Mook-Jung, I., Mitochondria-specific accumulation of amyloid β induces mitochondrial dysfunction leading to apoptotic cell death. *PLOS ONE* **2012**, *7*, e34929.
11. Clementi, M. E.; Marini, S.; Coletta, M.; Orsini, F.; Giardina, B.; Misiti, F., A β (31–35) and A β (25–35) fragments of amyloid beta-protein induce cellular death through apoptotic signals: Role of the redox state of methionine-35. *FEBS Lett.* **2005**, *579*, 2913-2918.
12. Hughes, E.; Burke, R. M.; Doig, A. J., Inhibition of toxicity in the β -amyloid peptide fragment β -(25–35) using N-methylated derivatives: A general strategy to prevent amyloid formation. *J. Biol. Chem.* **2000**, *275*, 25109-25115.
13. Coin, I.; Beyermann, M.; Bienert, M., Solid-phase peptide synthesis: From standard procedures to the synthesis of difficult sequences. *Nat. Protocols* **2007**, *2*, 3247-3256.
14. Treusch, S.; Hamamichi, S.; Goodman, J. L.; Matlack, K. E. S.; Chung, C. Y.; Baru, V.; Shulman, J. M.; Parrado, A.; Bevis, B. J.; Valastyan, J. S.; Han, H.; Lindhagen-Persson, M.; Reiman, E. M.; Evans, D. A.; Bennett, D. A.; Olofsson, A.; DeJager, P. L.; Tanzi, R. E.; Caldwell, K. A.; Caldwell, G. A.; Lindquist, S., Functional links between A β toxicity, endocytic trafficking and Alzheimer's Disease risk factors in yeast. *Science* **2011**, *334*, 1241-1245.
15. Wesén, E.; Jeffries, G. D. M.; Matson Dzebo, M.; Esbjörner, E. K., Endocytic uptake of monomeric amyloid- β peptides is clathrin- and dynamin-independent and results in selective accumulation of A β (1–42) compared to A β (1–40). *Sci. Rep.* **2017**, *7*, 2021.
16. Jones, R., From amyloid- β to receptor endocytosis. *Nat. Rev. Neurosci.* **2005**, *6*, 669-668.
17. Lin, M. T.; Beal, M. F., Alzheimer's APP mangles mitochondria. *Nat. Med.* **2006**, *12*, 1241-1243.
18. Hansson Petersen, C. A.; Alikhani, N.; Behbahani, H.; Wiehager, B.; Pavlov, P. F.; Alafuzoff, I.; Leinonen, V.; Ito, A.; Winblad, B.; Glaser, E.; Ankarcrona, M., The amyloid β -peptide is imported into mitochondria via the TOM import machinery and localized to mitochondrial cristae. *Proc. Natl. Acad. Sci.* **2008**, *105*, 13145-13150.

19. Boczonadi, V.; Horvath, R., Amyloid- β in mitochondrial disease: Mutation in a human metallopeptidase links amyloidotic neurodegeneration with mitochondrial processing. *EMBO Mol. Med.* **2016**, *8*, 173–175.
20. Helmfors, L.; Boman, A.; Civitelli, L.; Nath, S.; Sandin, L.; Janefjord, C.; McCann, H.; Zetterberg, H.; Blennow, K.; Halliday, G.; Brorsson, A.-C.; Kågedal, K., Protective properties of lysozyme on β -amyloid pathology: Implications for Alzheimer disease. *Neurobiol. Dis.* **2015**, *83*, 122-133.

List of Publications

Publications included in Ph.D thesis

- Rajasekhar, K.; Narayanaswamy, N.; Piyush, M.; Suresh, S. N.; Manjithaya R.; Govindaraju, T. *ChemPlusChem.*, **2014**, 79, 25.
- Rajasekhar, K.; Suresh, S. N.; Manjithaya, R.; Govindaraju, T. *Sci. Rep.* **2015**, 5, 8139.
- Rajasekhar, K.; Chakrabartia, M.; Govindaraju, T. *Chem. Comm.* **2015**, 51, 13434.
- Rajasekhar, K.; Narayanaswamy, N.; Murugan, N. A.; Kuang, G.; Agren, H.; Govindaraju, T. *Sci. Rep.* **2016**, 6, 23668.
- Rajasekhar, K.; Madhu, C; Govindaraju, T. *ACS Chem. Neurosci.* **2016**, 7, 1300.
- Rajasekhar, K.; Narayanaswamy, N.; Murugan, N. A.; Viccaro, K.; Lee, H. G.; Shah, k.; Govindaraju, T. *Biosens. Bioelectron.* **2017**, 98, 54.
- Rajasekhar, K.; Kapil, M; Govindaraju, T. 2017 (To be communicated).
- Rajasekhar, K.; Suresh, S. N.; Manjithaya, R.; Govindaraju, T. 2017 (Under preparation).
- Rajasekhar, K.; Vardhaman, B.; Sourav, S.; Govindaraju, T. 2017 (To be communicated).

Miscellaneous - Publication

- Rajasekhar, K.; Chaithra. J. A.; Govindaraju, T. *Org. Biomol. Chem.*, 2017,15, 1584.
- Chilakapati, M.; Chandrashekhar, V.; Rajasekhar, K.; Govindaraju, T. *Org. Biomol. Chem.*, 2017,15, 3170.
- Rajasekhar, K.; Vardhaman, B.; Govindaraju, T. 2017 (Under preparation).
- Sourav, S.; Rajasekhar, K.; Vardhaman, B.; Govindaraju, T. 2017 (Under preparation).
- Pandeewar, M.; Chandra Shekar, V.; K.; Khare, H.; Rajasekhar, K.; Ramakumar, S.; Govindaraju, T. (To be communicated).

Patents

- Hybrid Cyclic Peptoids, Synthesis And Applications Thereof (**Indian Patent Application No.: 3712/CHE/2013**)
- Small molecular probes, processes and use thereof (**International Patent Appl. No. PCT/IB2015/052463, CA2944763A1, EP3126357A2, US20170137418, WO2015151071A3**)

